Brancazio
Cameron

Infrared Astronomy

Editors:
Peter J. Brancazio
Brooklyn College, the City University of New York and
Belfer Graduate School of Science, Yeshiva University

A. G. W. Cameron
Belfer Graduate School of Science, Yeshiva University and
Institute for Space Studies, Goddard Space Flight Center, NASA

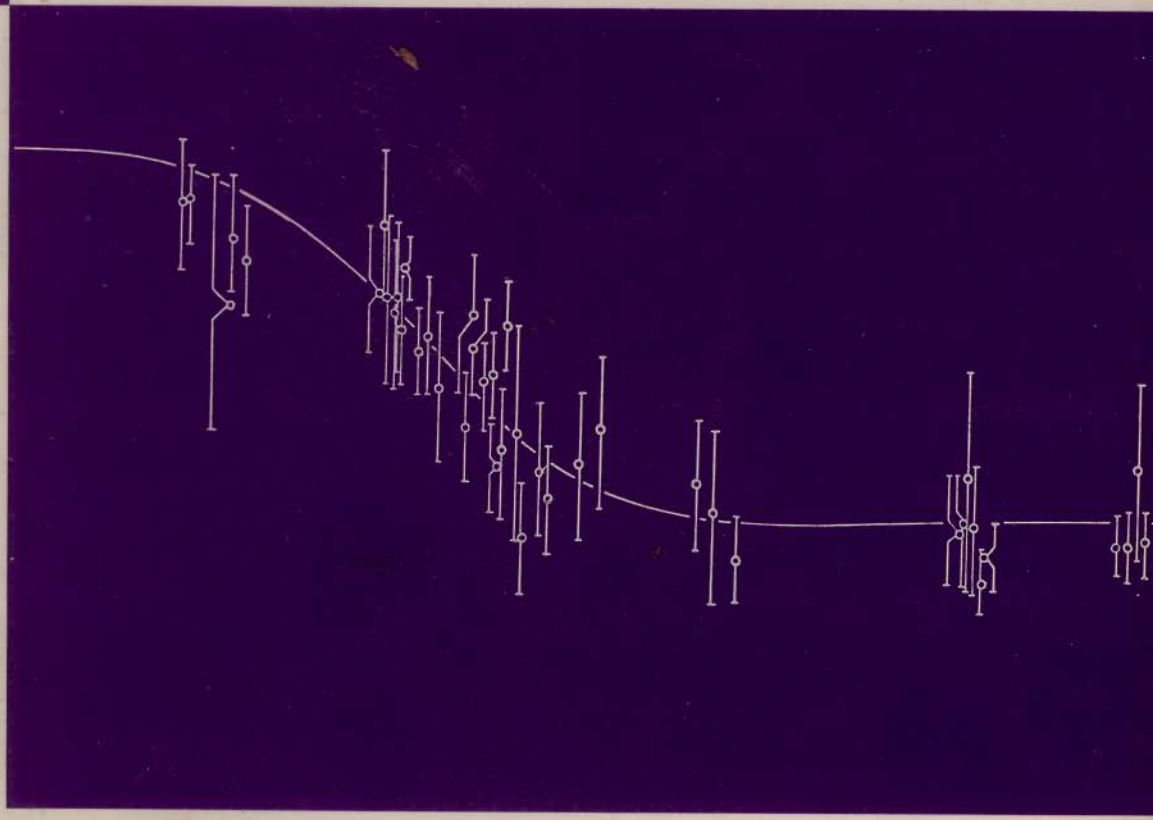

Infrared Astronomy

523.
015
012
INF

GORDON AND BREACH

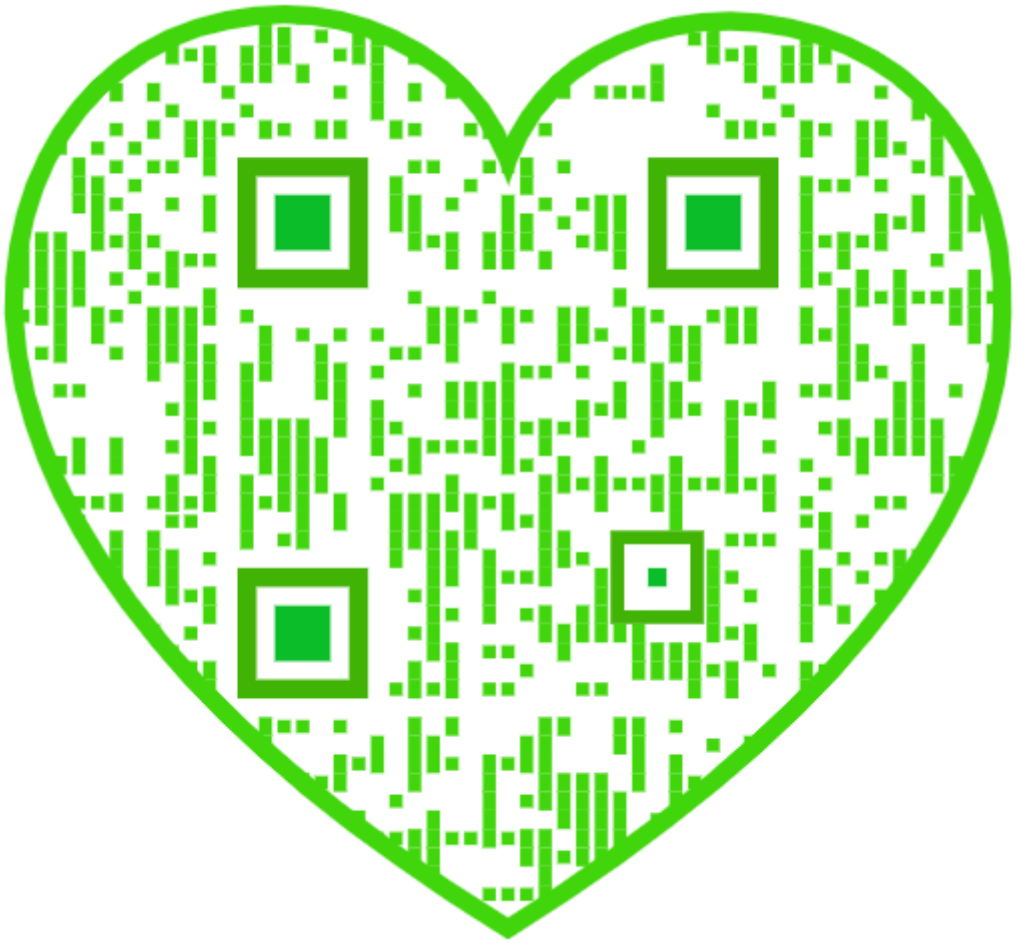

INFRARED ASTRONOMY

Edited by

PETER J. BRANCAZIO
Brooklyn College, the City University of New York
and Belfer Graduate School of Science, Yeshiva University

and

A. G. W. CAMERON
Belfer Graduate School of Science, Yeshiva University
and Institute for Space Studies,
Goddard Space Flight Center, NASA

GORDON AND BREACH, SCIENCE PUBLISHERS
New York • London • Paris

Copyright © 1968 by GORDON AND BREACH, Science Publishers, Inc., 150 Fifth Avenue, New York, N.Y. 10011

Library of Congress Catalog Card No. 68-19544

Editorial office for Great Britain:

Gordon and Breach, Science Publishers Ltd.
8 Bloomsbury Way
London, W.C.1

Editorial office for France:

Gordon & Breach
7-9 rue Emile Dubois
Paris 14e

Distributed in Canada by:

The Ryerson Press
249 Queen Street West
Toronto 2B, Canada

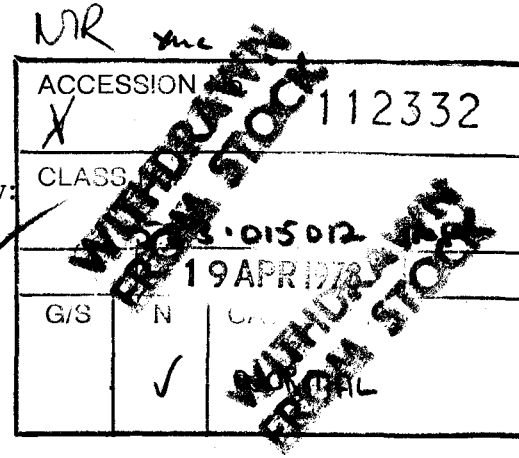

Reproduction in whole or in part by the U. S. Government or any department thereof is permitted.

Printed in the United States of America

PREFACE

On April 1-2, 1966, the Institute for Space Studies of the Goddard Space Flight Center, National Aeronautics and Space Administration, was host to an international group of astronomers and physicists at a conference on infrared astronomy. This was the eighth in a continuing series of interdisciplinary meetings on topics in space physics held at the Institute. The conference was organized by N.J. Woolf, W.F. Hoffmann, and A.G.W. Cameron, all of whom were then staff members of the Institute for Space Studies.

The previous Institute conferences were generally concerned with discussion of a specific area of space science which could be investigated by various techniques. In the present case the discussion was concerned with many areas of space science which can be investigated by infrared observations. This difference in approach was stimulated by the establishment of an experimental program in infrared astronomy at the Institute for Space Studies.

Some of the most stimulating discoveries in astrophysics made during the last 20 years have arisen from the development of radio astronomy, which has exploited a window of the electromagnetic spectrum open to study from the ground. The techniques of space research have so far allowed preliminary crude studies to be made above the atmosphere in the x-ray, gamma-ray, ultraviolet, and long wavelength radio regions of the spectrum. Many extremely important results have come from these experiments, and it is expected that astronomy will derive an enormous benefit from the full exploitation of these wavelength regions.

In contrast, there have been no infrared astronomy space experiments, and there have been only a few infrared astronomy balloon flights. This state of affairs has resulted in part from the lower sensitivity of infrared detectors and the necessity for cryogenic cooling, and in part because of the existence of several narrow infrared windows which can be explored by observations on the ground and in the atmosphere. There is a general feeling that these windows should be exploited before extensive plans are made for infrared astronomy spacecraft, since the discoveries made on the ground may influence the optimum design of infrared

observatories in space. With recent important improvements in infrared detectors, such ground-based studies have now begun.

The papers presented at this conference cover a number of different fields. The conference opened with an important report by J. Borgman on interstellar extinction in the infrared. There followed reports on infrared observations of stars and quasars, together with accounts of their spectral properties in the near infrared. M. Harwit and P. Thaddeus reported on the background radiation in the far infrared. This led naturally into a discussion of infrared emission from the interstellar medium. The final part of the conference dealt with solar system objects; namely, comets and planets. It is clear that much valuable work can be done in all these areas of study by infrared observations.

The conference was tape recorded and a transcript was subsequently prepared. From this transcript, first drafts of the papers were prepared and sent to the authors, who then had the opportunity to revise and update their papers as they wished. We thank them for their cooperation. The conference secretary was Mrs. Enid Silva, who handled very capably the arrangements for the meeting and participated extensively in the preparation of this proceedings volume. We express our special thanks to her. Mr. George Goodstadt, Mr. Nicholas Panagakos, Mr. Larry Stein, and several other staff members of the Institute for Space Studies gave valuable assistance in the organization of the conference, and we wish to thank them for their help in making it a success. This conference was the first function held in a newly-renovated building occupied by the Institute in the spring of 1966, and we wish to thank Dr. Robert Jastrow and Dr. Arthur Levine, Director and Executive Officer of the Institute, for their untiring efforts in making sure that the facilities would be ready in time.

P.J. Brancazio
A.G.W. Cameron

LIST OF CONTRIBUTORS

B. Basu, University of California, Berkeley, California
E.E. Becklin, California Institute of Technology, Pasadena, California
J. Borgman, Kapteyn Sterrewacht, Roden, The Netherlands
A.G.W. Cameron, Belfer Graduate School of Science, Yeshiva University, New York and Institute for Space Studies, Goddard Space Flight Center, NASA, New York
J. Connes, Observatoire de Meudon, France
P. Connes, Centre Nationale de la Recherche Scientifique, Bellevue, France
R.E. Danielson, Princeton University Observatory, Princeton, New Jersey
G.B. Field, University of California, Berkeley, California
Owen Gingerich, Smithsonian Astrophysical Observatory, Cambridge, Massachusetts
R.J. Gould, University of California, La Jolla, California
Martin Harwit, Cornell-Sydney University Astronomy Center, Cornell University, Ithaca, New York
F.J. Low, Lunar and Planetary Laboratory, University of Arizona, Tucson, Arizona and Department of Space Science, Rice University, Houston, Texas
D.P. McNutt, Cornell-Sydney University Astronomy Center, Cornell University, Ithaca, New York
G. Neugebauer, California Institute of Technology, Pasadena, California
R.W. Noyes, Smithsonian Astrophysical Observatory, Cambridge, Massachusetts
S. Orszag, Institute for Advanced Study, Princeton, New Jersey
James P. Pollack, Smithsonian Astrophysical Observatory, Cambridge, Massachusetts and Harvard College Observatory, Cambridge, Massachusetts
J.G. Rather, University of California, Berkeley, California
C. Sagan, Harvard University, Cambridge, Massachusetts and Smithsonian Astrophysical Observatory, Cambridge, Massa-Massachusetts
B.D. Savage, Princeton University Observatory, Princeton, New Jersey
K. Shivanandan, Cornell-Sydney University Astronomy Center, Cornell University, Ithaca, New York

W.M. Sinton, Lowell Observatory, Flagstaff, Arizona
Philip M. Solomon, Columbia University, New York
Hyron Spinrad, University of California, Berkeley, California
Patrick Thaddeus, Institute for Space Studies, Goddard Space Flight Center, NASA, New York
J.A. Westphal, California Institute of Technology, Pasadena, California
Robert F. Wing, University of California, Berkeley, California
B.J. Zajac, E.O. Hulburt Center for Space Research, Naval Research Laboratory, Washington, D.C.

CONTENTS

Preface v
List of Contributors vii

1. INTERSTELLAR EXTINCTION IN THE INFRARED, J. Borgman 1
2. A SURVEY AT 2-2.5 MICRONS, G. Neugebauer 13
3. OBSERVATIONS OF QUASARS AND COOL STARS, F.J. Low. 41
4. STELLAR SPECTRA, W.M. Sinton 55
5. SPECTRA OF COOL STARS, Hyron Spinrad and Robert F. Wing 63
6. INFRARED INTENSITY DISTRIBUTION AT THE SOLAR LIMB IN THE 20-MICRON REGION, R.W. Noyes 77
7. MODEL ATMOSPHERES FOR COOL STARS, Owen Gingerich 83
8. INFRARED ROCKET OBSERVATIONS, Martin Harwit, D.P. McNutt, K. Shivanandan and B.J. Zajac. 91
9. MEASUREMENT OF THE COSMIC MICROWAVE BACKGROUND WITH INTERSTELLAR MOLECULES, Patrick Thaddeus 101
10. EMISSION LINE OBJECTS, R.J. Gould. 109
11. THE INFRARED SPECTRUM OF INTERSTELLAR SHOCK WAVES, G.B. Field, B. Basu, J.G. Rather and S. Orszag. 115
12. PROTOSTARS, A.G.W. Cameron. 129
13. INFRARED OBSERVATIONS OF COMET 1965f, E.E. Becklin and J.A. Westphal 145
14. THE DRY MASSIVE MODEL OF THE ATMOSPHERE OF VENUS, P. Thaddeus 163
15. OPACITY OF THE VENUS ATMOSPHERE, P.M. Solomon. 171
16. A MODEL OF THE CLOUDS AND ATMOSPHERE OF VENUS, C. Sagan and B. Pollack. 181
17. INTERFEROMETRIC SPECTRA OF PLANETS, J. Connes and P. Connes. 191
18. MODELS OF THE ATMOSPHERE OF JUPITER, B.D. Savage and R.E. Danielson 209

Index 243

1

INTERSTELLAR EXTINCTION IN THE INFRARED

J. Borgman

There is considerable effort now being made in infrared astronomy to establish the infrared characteristics of interstellar extinction. There are two reasons for doing so. The first one is that we are interested in establishing the nature of the interstellar grains, e. g., their dimensions, chemical composition, etc. The second reason is that we would like to know more about the characteristics of the extinction properties themselves, so that the correction of photometric distances for interstellar extinction can be made more accurately.

The methods for investigating interstellar extinction are well known. We will review these methods so as to get some idea of the reliability of the results. As most of the material pertaining to infrared interstellar extinction has been discussed in relation to UBV data we will illustrate this review by making reference to colors and color excesses on the B-V scale.

I. THE COLOR DIFFERENCE METHOD

Fundamentally, the method is to observe two stars, one reddened and one unreddened, and see how their energy

distributions compare. We consider stars 1 and 2, the first of which is separated from the observer by a cloud of interstellar material. Then we determine the apparent magnitude $m_{1,\lambda}$ of star 1 as a function of wavelength and compare it with the apparent magnitude $m_{2,\lambda}$ of star 2. The difference is the absorption A_λ at the wavelength λ, plus a constant: tion A at the wavelength λ, plus a constant:

$$m_{1,\lambda} - m_{2,\lambda} = A_\lambda + C \qquad (1)$$

The constant C reflects primarily the different distances of the two stars. Normally the distances are not well known, so it is not possible to determine C with sufficient accuracy.

Nevertheless, we obtain an extinction curve (see Fig. 1) by plotting the observed quantity

$$\Delta m_\lambda = m_{1,\lambda} - m_{2,\lambda} = A_\lambda + C$$

as a function of the reciprocal wavelength. Reliable data on early type stars are available in the infrared as far as the 3.4μ atmospheric window. However, the extrapolation of the curve to $\lambda^{-1} = 0$ is uncertain. Extrapolation has been performed for some time simply by trying to match the observed curve with theoretical extinction curves, particularly those computed by Van de Hulst (1949) on the basis of ice grains. This was considered to be a successful procedure; it was thought that at long wavelengths the extinction should be very minor anyway. This would make the extrapolation relatively independent of the extinction model, provided the observations extend into the wavelength region where the extinction is expected to be small. Direct observational evidence that this is the case is difficult to obtain; the reddened O and B stars do not produce much radiation in the infrared. Neutral extinction escapes attention altogether with the color difference method.

Where it is important to correct a photometric distance for interstellar extinction it is common to use a parameter $R = A_V/E_{B-V}$, the ratio of the visual extinction A_V to the color excess $E_{B-V} = A_B - A_V$. The value of R can be obtained from an extinction curve which is based on

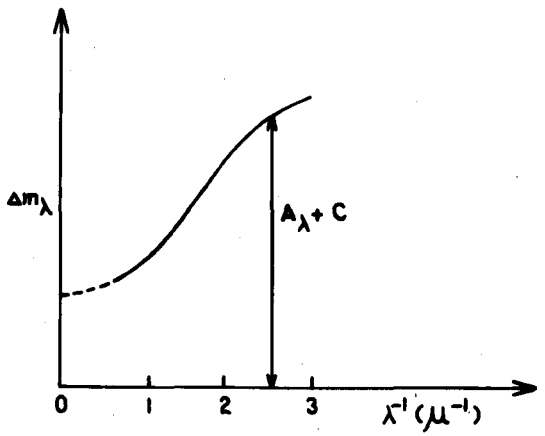

Fig. 1. The extinction curve as presented by the magnitude difference between a reddened and an unreddened star.

(a) observations in the BV system; (b) one or more observations in the infrared; (c) the extrapolated section of the curve between $1/\lambda = 0$ and the observation at the longest wavelength. The procedure is illustrated in Figure 2, where the extinction curve has been normalized to zero at the V effective wavelength and to 1 for the B effective wavelength. The result of this normalization is that the extrapolated value of the ordinate, at $1/\lambda = 0$, is equal to -R.

This technique has been applied to various regions in the Milky Way, with the result that in nearly all regions outside young galactic clusters the value of R obtained is approximately 3. It has become a tradition to apply this value almost universally, and to assume that it could not deviate greatly. However, there are exceptions in some young open clusters. In the case of the Orion Trapezium region, it turns out that the normalization procedure leads to a value for R of approximately 7 (Johnson and Borgman, 1963; Johnson, 1965). This result does not seem a priori unreasonable, since Van de Hulst's computations have shown that to obtain R = 7 requires that the grains be only about

30% larger than for the case of R = 3. However, the uncertainty of the extrapolation procedure should be kept in mind when assessing the reliability of these determinations. There is some evidence that this is not the correct procedure. Before considering this evidence in detail, we will describe two other methods for measuring interstellar extinction. One is called the variable extinction method, and the other is an older approach known as the cluster diameter method.

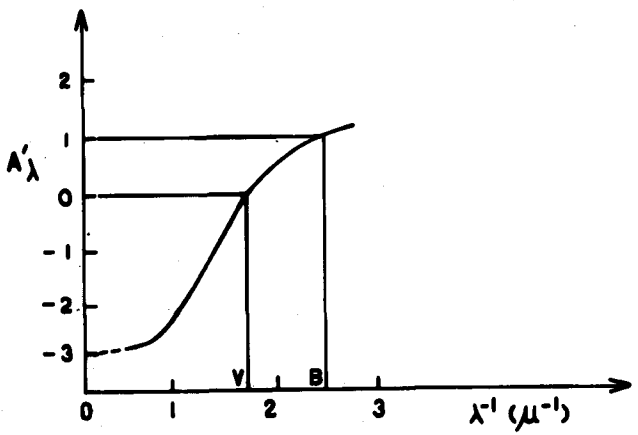

Fig. 2. The normalized extinction curve; $A'(\lambda)$ is obtained by multiplying the ordinates of Fig. 1 with a factor which makes the color excess $E_{B-V} = A'(B) - A'(V) = 1$ mag. and shifting the ordinate in order to make $A'(V) = 0$.

II. THE CLUSTER DIAMETER METHOD

We begin with the definition of the absolute visual magnitude, M_V:

$$M_V = V + 5 - 5\log r - A_V \qquad (2)$$

where V is the apparent visual magnitude, r is the distance, and A_V is the visual absorption. We rewrite Eq. (2) in the form

$$-5 + 5\log r = V - M_V - A_V. \qquad (3)$$

In the case of a star cluster an estimate of the distance can be made by measuring the angular diameter of the cluster and assuming that all clusters have the same linear dimensions. This was first done by Trumpler (1930). Once the distance to the cluster is determined in this manner, we can immediately calculate the lefthand side of Eq. (3), and if $V - M_V$ is known for individual stars on the basis of photometry and spectral classifications, we can then determine A_V. We note here that we have directly determined the extinction, rather than R or some other parameter. However, the photometric measurements and spectral classifications will also yield the color excess E_{B-V} for the star in question, so that R can be calculated.

III. THE VARIABLE EXTINCTION METHOD

We rewrite Eq. (2) as follows:

$$V - M_V = -5 + 5\log r + RE_{B-V} \qquad (4)$$

If we find a cluster for which we can plot $V - M_V$ against E_{B-V} and the value of R is the same for all stars in the cluster, we can then determine R from the slope of the curve. However, the determination is based only on that portion of the extinction that is variable. That is, if there is an irregular interstellar cloud between the cluster and the observer, then we will see the variable extinction across the cluster and can plot a curve to determine R for that particular cloud, but if there were an additional cloud with no variable extinction, it would escape our attention. In such a case the cluster will exhibit a certain value of R, but this pertains to a particular portion of the extinction only. The actual value of R could be either larger or smaller.

IV. SOME RESULTS

Values of R have been determined by methods II and III and the results are not always in agreement with those obtained from the extrapolated extinction curves. This is not surprising in view of the assumptions which have to be made in each of the three methods and which are not necessarily valid. We will illustrate our discussion of techniques by a few examples. For a more complete discussion the reader is referred to a paper by Johnson (1965); for the purpose of the present paper we will restrict ourselves to a discussion of the Cepheus, Perseus and Orion Sword regions.

In the case of Cepheus, both the cluster diameter method and the variable extinction method give values of R of approximately 5, whereas we would expect the value to be about 3 on the basis of the extinction curves of O and B type stars. For Perseus, the value obtained by the variable extinction method and the color difference method is in good agreement with the "normal" value of 3. However, the cluster diameter method gives about 5. In the case of the Orion Sword region, the variable extinction method gives R = 5, whereas the extrapolated extinction curve points to R = 7; these determinations, however, have relatively low weight because of the small extinction values.

V. M STARS

Extinction measurements have often been restricted to O and B stars. The nearly featureless spectra of these stars seem to be quite suitable for this purpose. However, substantial data below $1/\lambda = 0.3\mu^{-1}$ have hitherto not been obtained. One would like to fill the gap between $1/\lambda = 0.3\mu^{-1}$ and zero with some additional information. But B stars and O stars simply do not produce enough light to allow these measurements to be made reliably.

In an attempt to solve this problem, Johnson has turned to M stars. In the case of Cepheus, he has gone as far as $1/\lambda = 0.1\mu^{-1}$, by using the star μ Cephei. This is the only star so far which exhibits some extinction and which

has been observed to 10μ. The extinction curve for Cepheus is shown in Fig. 3. The long wavelength points represent the observations on μ Cephei as compared with Betelgeuse. The dotted line shows a theoretical curve of Van de Hulst, which extrapolates to 3. The intuitive extrapolation of the observations, including the μ Cephei measurements indicates a value of R = 5 in agreement with the cluster diameter method. The data for Perseus, shown in Fig. 4, give some indication of a similar situation. There are no stars available equivalent to μ Cephei, but there are some M stars in the double cluster of Perseus which have been observed to about

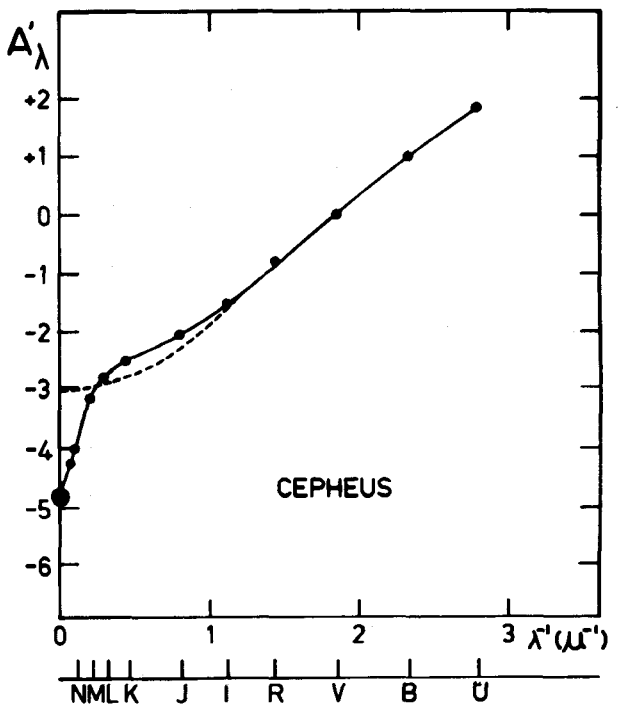

Fig. 3. The normalized extinction curve in Cepheus. Dots designate data from the color-difference method; the circle at $\lambda^{-1} = 0$ designates the value of -R as derived from cluster diameters. The value agrees well with the trend shown by the N and M data of μ Cephei.

5 microns. An extrapolation to R = 5 is indicated, in agreement with the value obtained from the cluster diameter method. It should be noted that the fully-drawn extinction curves in Figs. 3 and 4 cannot be matched by any of the suggested theoretical extinction models.

There is some additional information available which indicates that these curves might be correct. Evidence has been presented by Neckel (1965) who has pointed out that

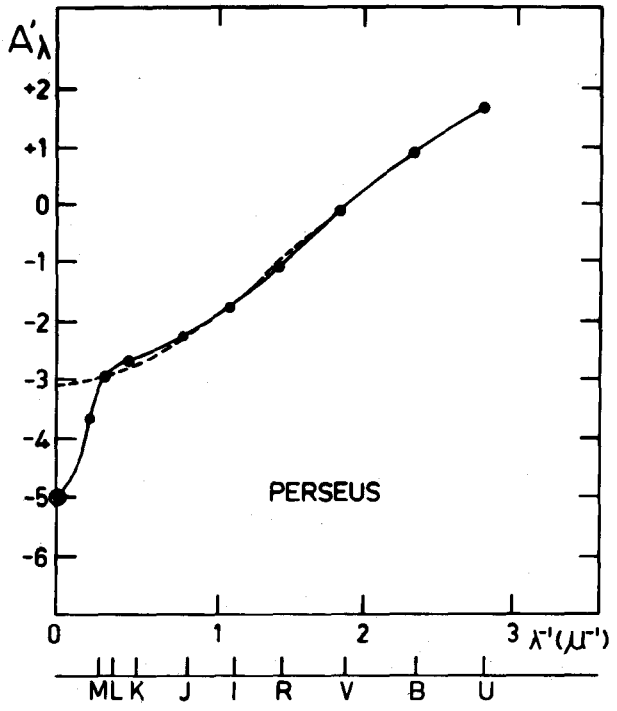

Fig. 4. The normalized extinction curve in Perseus. Dots designate data from the color-difference method; the circle at $\lambda^{-1} = 0$ designates the value of -R as derived from cluster diameters. A value of R equal to 3 would be compatible with the observations of early type stars (which do not include the M data) but the M data on the M stars in the double cluster indicate a larger value.

the value of the photographic absorption in the direction of the galactic pole is very close to about half a magnitude rather than the quarter of a magnitude which always had been assumed. This leads to a value of R of about 6 or 7, presumably caused by a significant "neutral" component of the extinction; a similar conclusion can be reached from Arp's (1962) study of the extinction as determined from counts of galaxies.

In connection with the use of M stars, one point should be raised. It has recently been found that at least some long-period, variable M stars show some polarization (Serkowski, 1966). Some of them exhibit high polarization, even at high galactic latitudes where there is no suspicion of interstellar extinction. This effect might indicate that these M stars are surrounded by an envelope of small particles. If this is so, then it might be argued that what we are observing here represents properties of such particles, or of an envelope around the M stars, rather than the interstellar extinction itself (Donn et al., 1966).

VI. CONCLUSION

There is considerable evidence that the wavelength dependence of interstellar extinction is characterized by values of R which are sometimes larger than the traditional value of 3. It appears that with regard to the galactic system the observations point to a value of R of approximately 3.5 in the direction towards the galactic center, whereas in the opposite direction, the value might be considerably larger—perhaps close to about 5. This would mean, for example, that the Perseus double cluster is at a much closer distance than we have hitherto assumed; it may even be in our own arm of the galaxy. Secondly, the galactic nucleus, because of the value of R = 3.5, moves much closer to the sun and we come back to the traditional value of about 8 kpc. The value of the Oort constant, expressed in km/sec/kpc, will move up again to about 20, which is also a traditional value. The galaxy as a whole would shrink to about 70% of its size as based on the assumption that R = 3.0.

There is clearly a need for really substantial photometric data, especially in the infrared region. These measurements should be made for O and B stars, because one has some justifiable suspicion in connection with M stars. However, even when using O and B stars caution is required; observational and theoretical studies on the existence and photometric significance of circumstellar envelopes should be undertaken to give assurance that the deduced information actually pertains to the interstellar medium.

REFERENCES

Arp, H. C., Astrophys. J. **135**, 971 (1962).
Donn, B., Stecher, T. P., Wickramasinghe, N. C., and Williams, A. D., Astrophys. J. **145**, 949 (1966).
Johnson, H. L. and Borgman, J., Bull. Astron. Inst. Neth. **17**, 115 (1963).
Johnson, H. L., Astrophys. J. **141**, 923 (1965).
Neckel, H., Z. Astrophys. **62**, 180 (1965).
Serkowski, K., Astrophys. J. **144**, 857 (1966).
Trumpler, R. J., Lick Obs. Bull. No. 420 (1930).
Van de Hulst, H. C., Rech. Astr. de l'Obs. d'Utrecht. **11** (part 2), 1 (1949).

DISCUSSION

R. M. Goody: One should be careful about making comparisons between stars such as μ Cephei and Betelgeuse, because there are distinct differences between the spectra of these stars in the near infrared.

J. Borgman: These differences pertain mostly to the water vapor bands, and the filters have been specified to avoid these water vapor bands as much as possible. However, this is a rather difficult point because the filters do not cut off completely at the water vapor bands.

H. Spinrad: Isn't it more likely to explain the stronger water lines in the spectra of μ Cephei by assuming that it is a cooler star than Betelgeuse? μ Cephei is more luminous,

so that to get the same band strengths to classify the two stars, μ Cephei has to be cooler.

J. Borgman: I agree with you that using M stars leads to questions of this nature. However, there is not much else that can be done. There just are no good stars for comparison. I might add that this point which was brought out about intrinsic differences has also been discussed in connection with the Orion stars. These certainly are not normal, and one cannot easily decide how to compare them. Johnson tends now to disregard some of the points in the infrared. He does this mainly because there are quite a number of faint red stars in the Orion Trapezium, and since the data pertain to the whole Trapezium, quite a number of red stars are being observed simultaneously. The Orion results should then be interpreted as partly due to some red companions, and partly to the reddening characteristics themselves.

M. Harwit: It is fairly important that we obtain accurate extinction factors in the two-to-three micron region, because there is some hope that one might be able to see, from above the atmosphere, the galactic nucleus and the distribution of at least the infrared stars on the far side of the galaxy. We could then get a crude map which would correspond in accuracy to the early radio maps of the galaxy. I think it is the one chance that one has of getting some kind of map of our own galaxy as far as stellar distributions, as contrasted to gaseous distributions. A factor of about one magnitude of uncertainty in the extinction coefficient at these wavelengths is significant because of the exponential relationship between the extinction and the distance.

2

A SURVEY AT 2-2.5 MICRONS*

G. Neugebauer

I. OBSERVATIONS OF EXTREMELY COOL STARS

As one part of a program of infrared astronomy carried on at the California Institute of Technology, a survey of the sky in two infrared spectral ranges, 0.68-0.92 μ and 2.01-2.41 μ, is being carried out. The motivation for such a survey is to obtain an unbiased census of objects that emit in the 2.0-2.5-μ atmospheric window; this will, of course, include many ordinary stars, but it might also reveal many potentially interesting objects that would not be included in an a priori selection of objects to be measured. In fact, a number

*Editor's Note: In lieu of the paper presented at the conference which was an interim report on work in progress, we have substituted three articles by Dr. Neugebauer and co-workers which include some more recent results. The articles are as follows: (I) Observations of Extremely Cool Stars, by G. Neugebauer, D. E. Martz, and R. B. Leighton (Astrophys. J. **142**, 399, 1965); (II) Further Observations of Extremely Cool Stars by B. T. Ulrich, G. Neugebauer, D. McCammon, R. B. Leighton, E. E. Hughes, and E. Becklin (Astrophys. J. **146**, 288, 1966); (III) Infrared Spectra of Low-Temperature Stars, by D. McCammon, G. Munch, and G. Neugebauer (Astrophys. J. **147**, 575, 1967). These articles are reprinted with the permission of the Astrophysical Journal.

of strikingly red stars have already been found. Since most of these "superred" stars occur in the Milky Way, interstellar reddening may be of some consequence; but in at least a few cases the stars seem to be intrinsically extremely red. These preliminary results seem of sufficient interest to merit brief description at this time.

The survey instrument consists essentially of a 62-inch, f/1 aluminized plastic mirror capable of 2' resolution. The entire mirror is vibrated sinusoidally at 20 c/s so as to move images across a detector system composed of a liquid-nitrogen-cooled, eight-element array of PbS detectors, arranged in a north-south line of four "push-pull" pairs, and a silicon photodetector. Each pair of PbS detectors spans a declination range of 10' so that 40' is spanned by the entire array. The Si detector spans a 20' declination range coinciding with that of the central two pairs of PbS detectors, and is located about 15' west of the PbS array. The telescope is normally swept in R. A. at 15 or 30 times sidereal rate in a raster pattern one hour of R. A. in "length" with 15' declination steps. In this way, a strip of sky 3° or 6° wide in declination is covered each night, each point of sky being covered at least twice.

A comparison of PbS signals with the K magnitudes of a number of stars listed by Johnson (1962, 1964) and of the Si detector signals with I magnitudes listed by Kron, White, and Gascoigne (1953) shows agreement within about ±0.2 mag. over a wide range of spectral types. The sensitivity is such that minimum detectable sources have infrared apparent magnitudes of approximately $I \approx 9$ and $K \approx 5$. From results obtained to date, it is estimated that ultimately several thousand objects bright enough at 2.0-2.5 μ to be measured within about ±0.2 mag. will be detected. Positions can be measured within about 1' in declination and 0^m1 in R. A. Although the system is preferentially sensitive to "point" sources, it is calculated that a 450°K black-body radiator with a 10' radius would give a signal-to-noise ratio of at least 10:1.

To get a preliminary idea of the relative numbers of stars of various colors being detected in the survey, the infrared color indices I - K for about 350 objects in a certain limited part of the sky that includes part of the Milky Way in the

Aur-Tau region have been tabulated. The objects were selected to have a K magnitude brighter than about 2 to assure that I - K could be measured sufficiently accurately for all objects. The distribution of measured I - K-values shows a steep decline in the relative number of stars per unit magnitude difference beyond I - K ≈ 4, and it becomes essentially zero at a value I - K ≈ 6, except for a few stragglers which amount to about 1 per cent of the total.

A study of the latter objects plus a few similar ones that have been found in other areas of the sky has indicated the stragglers have the following properties:

a) They are not just a little redder than the main group, but seem instead to be well separated in I - K from the rest. In fact, there is a suggestion of homogeneity in this group, the value I - K ≈ 7.5 being a typical color index. Approximately ten such extremely red objects have been observed so far. Of these only one, TX Cam, has been found listed in a catalogue of stars or variable stars.

b) They appear to occur mostly near the plane of the galaxy, but one has also been found near the north galactic pole.

c) The objects observed so far have K apparent magnitudes between 0 and 2; the latter limit is set by the minimum detectable 0.8-μ signal. Those few objects bright enough to appear on the red plates of the 48-inch Schmidt survey have been identified with faint stellar images—generally fainter than about magnitude 16. Only the brightest of them has yet been seen visually, and it is a difficult visual object even at the 200-inch telescope.

d) An estimate of the temperature of the extremely red objects can be obtained if one assumes the data are representative of a Planck blackbody distribution. The color index I - K = 7.5 corresponds roughly to the distribution of radiation emitted by a 1000°K black body. Near-infrared spectra of two of the brightest objects, as well as photometry in the 2.0-2.5- and 3.2-4.1-μ spectral ranges, confirm that a blackbody radiation temperature on the order of 1000°K is appropriate (J. D. Scargle, private communication; E. E. Becklin, private communication).

e) On the assumption that a star radiates as a black

body, one can estimate its angular diameter from its apparent magnitude. A 1000°K black body of apparent magnitude K = 0.0 should have an angular radius of approximately 0.''04, or about 10 $R_\odot$ per parsec distance. If the apparent tendency toward occurrence near the plane of the galaxy is real, this would imply large distances and huge sizes for these objects.

The approximate positions and preliminary magnitude estimates for two of the brightest of the infrared objects are as follows:

α (1965)	δ (1965)	I	K
$3^h 51^m.5$	+11°18'	7	0
20 45.2	+39 59	8	1

Portions of the red and blue plates of the 48-Schmidt camera survey showing the sources in Taurus and Cygnus are given in Figs. 1 and 2.

Further information concerning the numbers, positions, and other properties of these infrared stars will be published as it becomes available in the course of the reduction of the sky-survey data now under way.

We gratefully acknowledge the able assistance of Dr. Bruce T. Ulrich, E. E. Becklin, G. Fitzpatrick, E. Hughes, Mrs. P. Kuhi, D. McCammon, J. E. Nelson, and J. Westphal in the construction and operation of the survey system.

II. FURTHER OBSERVATIONS OF EXTREMELY COOL STARS

During the past year a group at the California Institute of Technology has continued a survey of the sky for objects which emit in the 2.0-2.5-μ atmospheric window. In this note we list some further bright and red sources to provide other observers with the coordinates of potentially interesting objects. The normal data reduction process of the survey has been bypassed to facilitate the quick selection of individual sources; no attempt has been made to insure the completeness of the list.

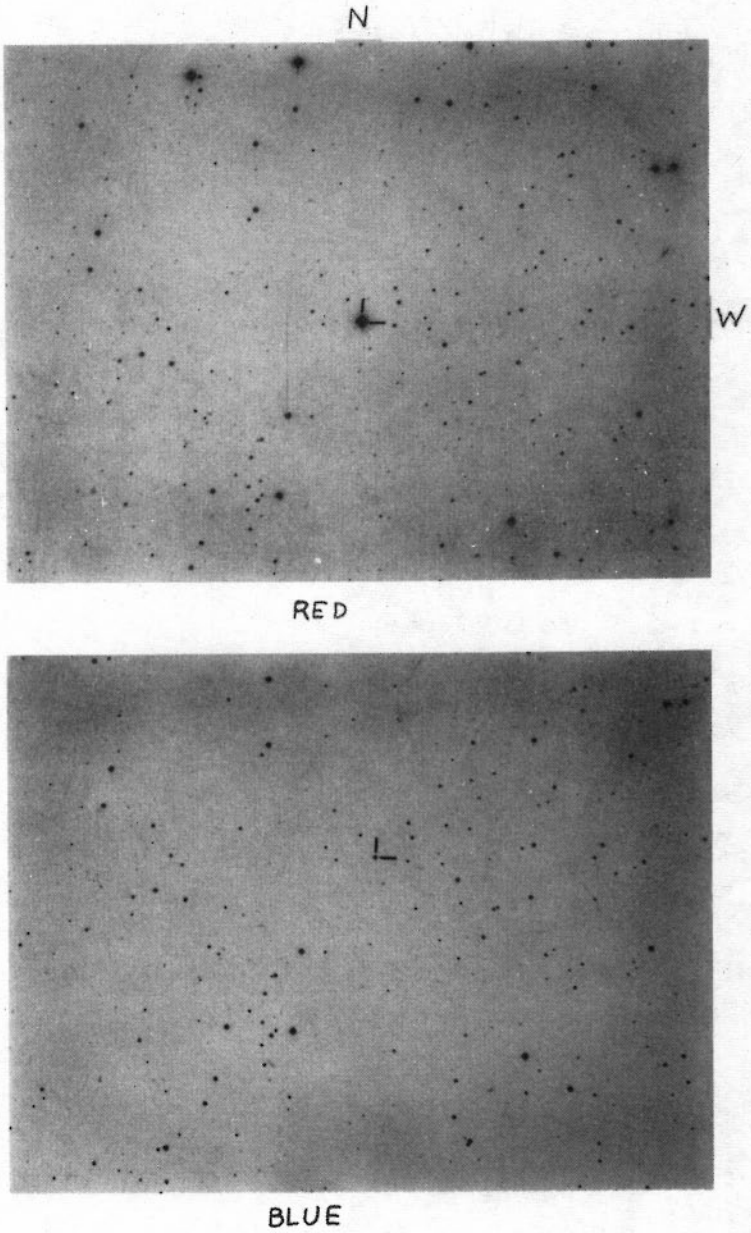

Fig. 1. Taurus Source

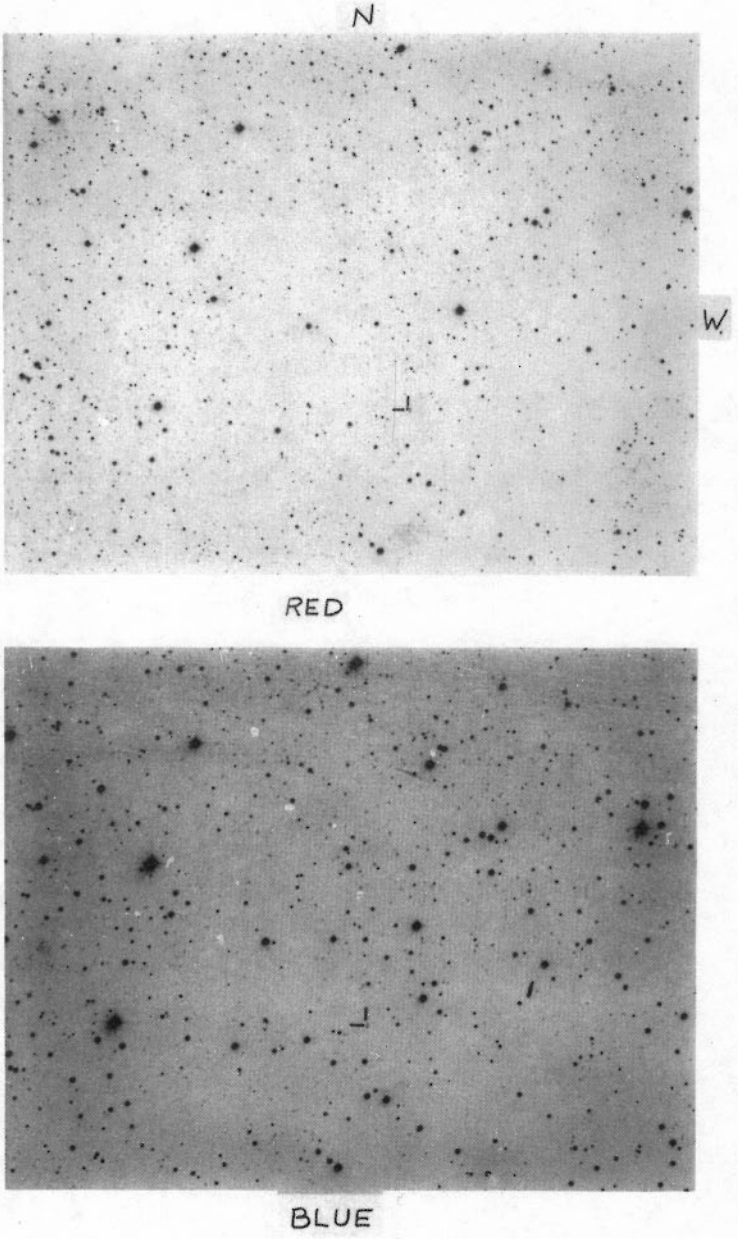

Fig. 2. Cygnus Source

As described previously, observations are made with a 62-inch telescope at both 2.0-2.4 μ (K) and 0.7-0.9 μ (I), and a strip of sky 3° wide in declination is scanned each night. At the present time, the region between -33° and +81° declination has been surveyed although the data have not been fully reduced. Typically between 200 and 500 sources brighter than K-magnitude 4.0 are recorded each night.

Table I includes magnitudes and coordinates of fourteen stars brighter than K $\sim$ 3 and having infrared color index I - K $\sim$ 6. Some additional magnitude measurements, obtained with the 62-inch telescope on nights when the regular survey was not being carried out, are also included. For each star of Table I, except for stars 3 and 10, an image was found which was significantly brighter on the E($\sim$0.65 μ) than on the O($\sim$0.4 μ) plate of the National Geographic Society-Palomar Observatory Sky Survey.

The K-magnitudes listed are accurate to about ±0.2 mag., and the error in each I magnitude is indicated in the table. The K-magnitudes are measured with a filter and detector system which closely resembles that of Johnson (1964), and thus these data can be compared directly with Johnson's data even for quite red sources. For stars earlier than about spectral type K, the I-magnitude values derived from our survey agree within 0.03 mag. with those of Kron, White, and Gascoigne (1953). However, the I-magnitudes in this survey are measured with a Si photodetector whose wavelength response differs from that of Johnson's (1965) photomultiplier, causing a discrepancy which increases with decreasing temperature and makes the survey I-magnitudes as much as 1-2 mag. fainter than Johnson's for the reddest objects.

Since a large fraction of red stars are variables, all sources in Table I were searched for in the General Catalogue of Variable Stars (Kukarkin, Parenago, Efremov, and Gol'opov 1958). As indicated, five can be identified with known variables. There is also definite evidence of variability both in I - K and K for some of the other stars that have been observed over a period of time.

Measurements of the relative flux received from five of the stars in the wavelength intervals 0.78-1.00 μ, 1.5-1.8 μ,

TABLE I

Red Star Data

Star	Identification	1950.0 R.A.	1950.0 Decl.	K	I	Date
1		$00^h\,04^m.3$	+42°48'	+2.4	> 10.5	Nov. 6, 1965
				+2.4	> 10.5	Sept. 22, 1965
2	RW And	00 44.6	+32 25	+2.2	8.2 ± .1	Oct. 29, 1965
3		01 03.8	+12 20*	+1.3	> 10.0	Oct. 6, 1965
				+0.9	> 10.0	Jan. 9, 1966
4		02 31.7	+64 55	+2.3	8.8 ± .3	Sept. 8, 1965
5		03 23.2	+47 22	+2.0	8.2 ± .2	Sept. 9, 1965
				+1.7	8.5 ± .2	Oct. 2, 1965
6		10 13.3	+30 49	+0.5	9.4 ± .5	Feb. 10, 1965
				+1.6	> 10.3	Dec. 1, 1965
				+1.8	> 10.3	Dec. 16, 1965
				+1.6	> 10.3	Jan. 22, 1966
				+1.6	> 10.3	Feb. 16, 1966
				+1.5	> 10.3	Mar. 26, 1966
7	WX Ser	15 25.5	+19 44	+2.0	8.1 ± .1	June 17, 1965
				+2.3	8.3 ± .2	Feb. 20, 1966
8	RU Her	16 08.2	+25 12	+0.8	6.8 ± .1	May 3, 1965
				+0.4	5.2 ± .1	Sept. 8, 1965
				-0.1	4.4 ± .1	Feb. 20, 1966
9	MW Her	17 33.4	+15 37	+1.6	7.9 ± .2	Apr. 21, 1965
				+1.8	8.3 ± .2	Sept. 8, 1965
10		20 31.8	+38 29	+2.4	> 10.3	Sept. 15, 1965
11		20 37.7	+39 01	+1.7	> 8.5	July 23, 1965
				+1.7	> 8.5	Sept. 15, 1965
12	DG Cyg	20 41.6	+43 01	+1.4	7.5 ± .2	June 29, 1965
				+1.5	7.8 ± .2	Aug. 8, 1965
				+1.4	7.3 ± .2	Sept. 15, 1965
13		21 32.1	+38 51	+1.6	8.3 ± .5	Sept. 15, 1965
14		23 42.6	+43 39	+2.1	8.0 ± .2	Nov. 6, 1965

*Offset from 75 Psc to this source is $7^s \pm 1^s$ west, 21'20" ± 15" south.

2.0-2.4 μ, and 3.0-3.8 μ are shown in Fig. 3. The data were obtained in January, 1966, using a photometer on the 24-inch telescope at Mount Wilson. It is interesting to note that two of the reddest of these sources lie out of the galactic plane and away from the galactic center.

It should be re-emphasized that the selection of sources presented here is neither unbiased nor complete.

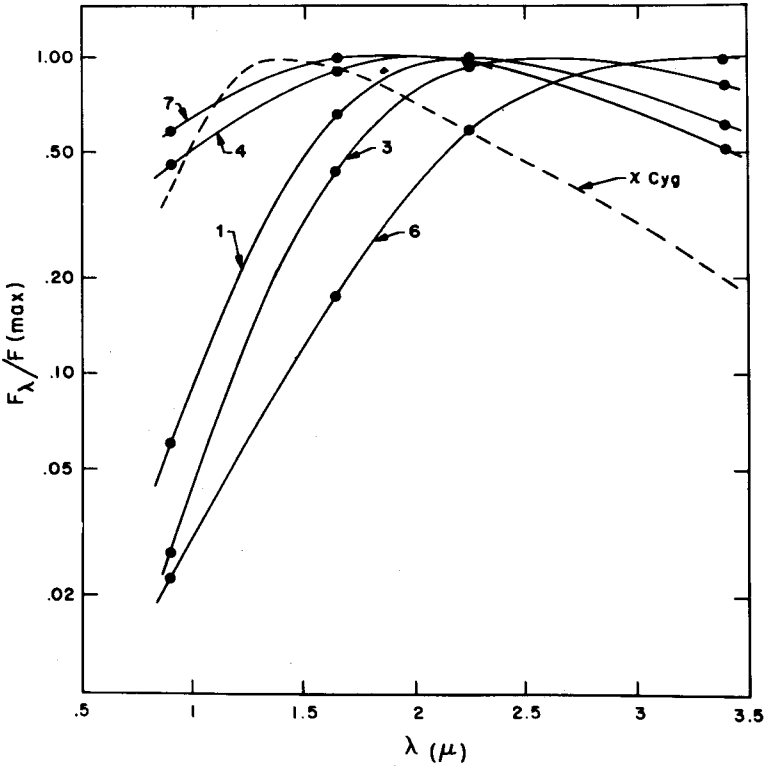

Fig. 3. The spectral-energy distribution of stars 1, 3, 4, 6, and 7. Also shown is χ Cyg at minimum (Johnson et al., 1965).

We acknowledge the able assistance of A. Dienes, G. Forrester, A. Gee, T. Hilgeman, P. Kuhi, A. Mackay, D. Martz, J. Nelson, T. Wesseling, and J. Westphal. We also express appreciation to R. G. Walker and A. P. D'Agati

for the magnetic-tape star catalogue used to calibrate telescope coordinates. We wish to thank Drs. F. Low and H. L. Johnson for pointing out an error in the identification of star 10.

III. INFRARED SPECTRA OF LOW-TEMPERATURE STARS

Introduction

The discovery of stars with extremely low color temperatures by the California Institute of Technology infrared sky survey has raised questions concerning the nature of their atmospheres. Since a large fraction of the energy radiated by these sources is in the infrared, their spectra in this region provide an observational approach to the study of this problem.

Stellar spectra at wavelengths between 1.2 and 2.5 μ have been obtained by Boyce and Sinton (1964), Sinton (1962, 1966), Kuiper (1962, 1963, 1964), Moroz (1966), and Mertz and Coleman (1966) with ground-based telescopes at resolutions on the order of 100. The Stratoscope II observations (Woolf, Schwarzschild, and Rose 1964) have also provided infrared stellar spectra under somewhat lower resolution, but with less telluric absorption. Observations in the regions $\lambda\lambda$1.5-1.8 and $\lambda\lambda$2.0-2.5μ appear to be most profitable, as they are relatively free of atmospheric absorption and also contain important spectral features of abundant molecules such as H_2O and CO.

In order to establish the relationship of the extremely red objects to known stars in the spectral sequence, a number of representative M, N, and S stars have been observed to complement measurements of the extremely red sources. To date only two of the latter sources have been observed, but the results obtained so far for the standard stars appear to be of sufficient interest to justify publication of a preliminary description of the spectra.

Instrumentation

The data were obtained with a 0.5-m-focal-length Ebert-Fastie spectrometer originally built for rocket flights. To adapt it for telescopic observations in the PbS infrared range, a 300 groove/mm grating has been installed, providing a dispersion of 31 Å/mm in the second order at $\lambda 1.6\ \mu$ and 65 Å/mm in the first order at $\lambda 2.2\ \mu$. The desired spectral order is isolated with interference filters. The original entrance slit has been replaced by a mirrored plate containing matched pairs of circular apertures of 0.5, 1.0, 1.5, and 2.0 mm diameter, any one of which can be selected to suit resolution and seeing requirements. Guiding is accomplished by viewing the light reflected from this plate through a small telescope. A 5 c/s mirrored chopper located immediately behind the entrance apertures alternately admits an f/16 beam of radiation from the star and a similar beam from a nearby area of the sky to the spectrometer. The radiation of that beam not entering the spectrometer during a given half of the chopping cycle is reflected to a wide-band ($\lambda\lambda 1.2$-$2.5\ \mu$) monitor detector.

Liquid-nitrogen-cooled PbS cells with f/1 field lenses are used to detect both the dispersed (signal) radiation and the monitor radiation. The noise-equivalent power of the $\frac{1}{2} \times \frac{1}{2}$ mm cell and 8-mm Si field lens combination used in the signal channel is about 5×10^{-14} watts at $2.2\ \mu$. Signals from both channels are synchronously demodulated and recorded on a single strip chart.

Although the entrance slits used are larger than the apparent stellar disk, seeing fluctuations and imperfections in guiding produce unavoidable variations in the amount of radiation entering the spectrometer. Spurious features arising from these variations are largely eliminated by dividing the signal channel amplitude by the amplitude of the monitor channel output at the corresponding time, thus normalizing the spectrum to constant total energy input.

The wavelength dependence of the response of the spectometer-detector system has been determined in the laboratory by scanning the radiation of a standard black body. The transmission curves obtained for the two spectral regions of

interest are given in Figs. 4 and 5, but they have not been incorporated in the stellar spectra presented here. These curves do not take into account atmospheric attenuation or possible nongray reflection losses at the telescope mirrors.

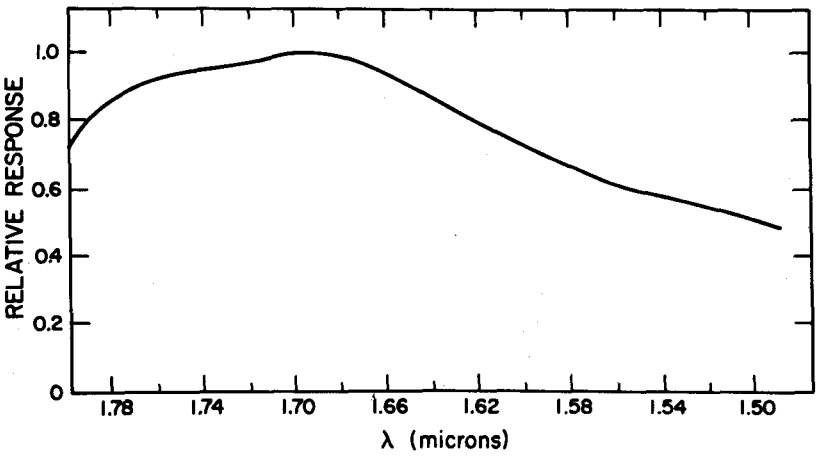

Fig. 4. Spectrometer system response. λλ1.5-1.8 μ

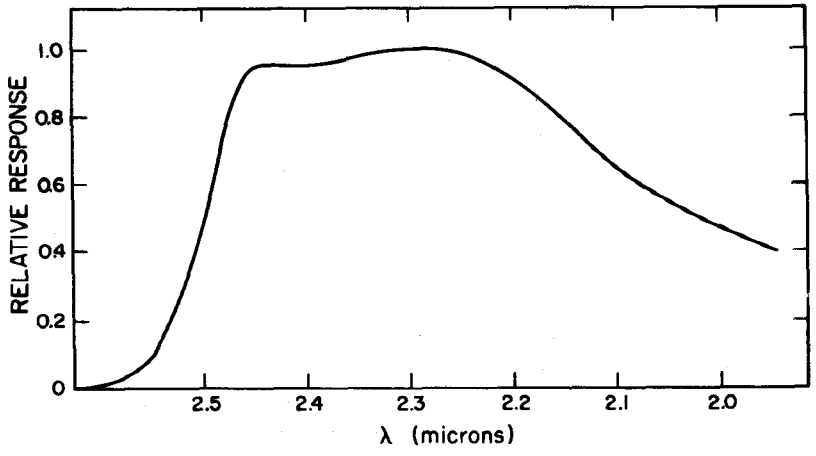

Fig. 5. Spectrometer system response. λλ2.0-2.6 μ

Observations

Spectra in regions λλ1.5-1.8 and λλ1.9-2.5 μ have been obtained with the spectrometer at the Cassegrain foci of the 24, 60, and 100-inch Mount Wilson reflectors and also at the east arm of the 200-inch Hale telescope at Mount Palomar between July, 1965, and April, 1966. From these observations spectra of twelve stars have been selected for this paper and are given in Figs. 6 to 11. Table II lists the observational details associated with each spectrum.

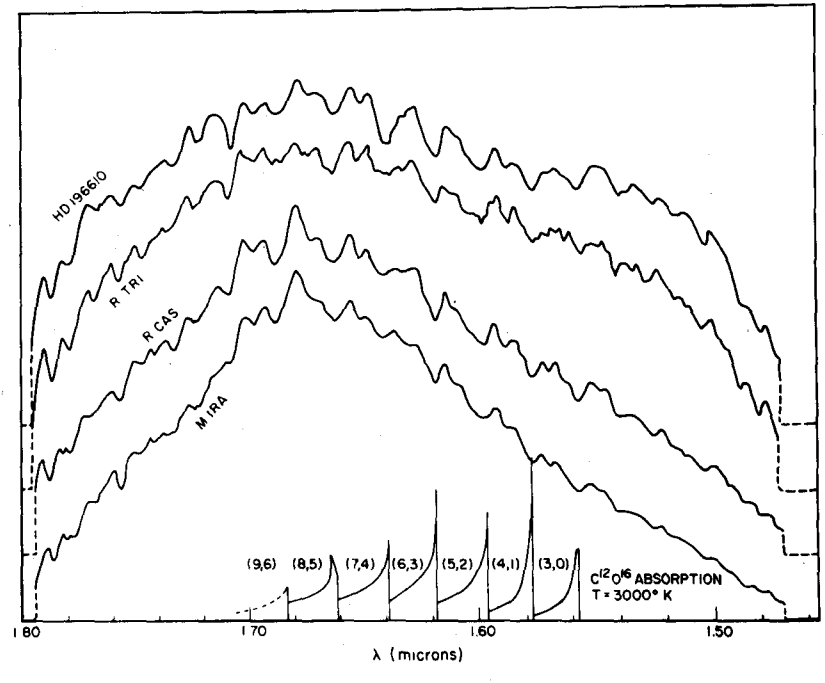

Fig. 6. Spectra of M-type stars in the interval 1.5-1.8 μ

Exit slit widths for the spectra were chosen to obtain the maximum resolution in a reasonable length of time while generally maintaining a signal-to-noise ratio of about 50. Although all spectra in this paper are single scans, each was repeated at least once. An example of the reproducibility generally obtained, as well as of the success of the

normalization procedure, is provided in Fig. 12, which shows two normalized scans of Y Canum Venaticorum along with the monitor channel records used to normalize them. This reproducibility is typical of the spectra shown except that of the NML (Neugebauer, Martz, and Leighton) Cygnus object in Fig. 10 which is of lower quality.

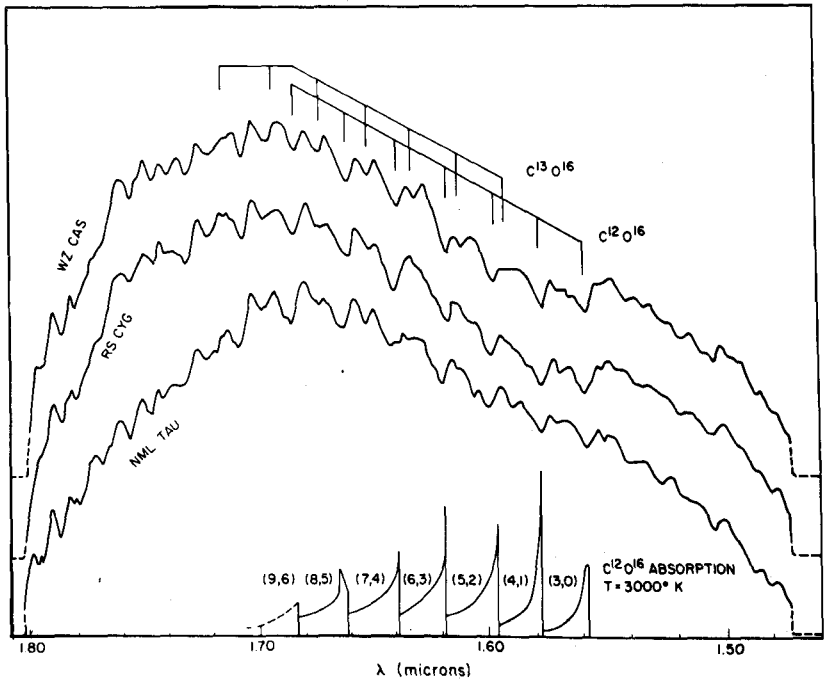

Fig. 7. Spectra of early carbon stars and of the NML Taurus source. λλ1.5-1.8 μ

An upper limit to the resolution obtainable in a spectral scan is set by the width of the exit slit, which defines the pass band for a fixed point source at the entrance aperture. In practice, accurate guiding is not always possible, and wandering of the stellar image in the entrance slit, which for spectra presented in this paper was 2 mm, may degrade the resolution. For the brighter stars the scanning rates were such that the resolution approached the limit set by the exit slit, whose width is given in the fifth column of Table II,

TABLE II

Journal of Observations

Object	Wavelength Range (μ)	Date	Telescope (inches)	Equiv. Exit Slit (Å)	RC Time Constant (sec)	Total Scan Time (min)	Scan Rate (Å/sec)	Air Mass
Fig. 3:								
HD 196610	1.5-1.8	Sept. 13, 1965	200	45	1.8	11	5	1.05
R Tri	1.5-1.8	Sept. 13, 1965	200	45	1.8	11	5	1.00
R Cas	1.5-1.8	Sept. 13, 1965	200	45	1.8	11	5	1.05
Mira	1.5-1.8	Sept. 13, 1965	200	45	1.8	11	5	1.26
Fig. 4:								
WZ Cas	1.5-1.8	Sept. 13, 1965	200	45	3.6	11	5	1.12
RS Cyg	1.5-1.8	Sept. 13, 1965	200	45	3.6	11	5	1.00
NML Tau	1.5-1.8	Sept. 12, 1965	200	45	1.8	11	5	1.10
Fig. 5:								
χ Cyg	1.5-1.8	Apr. 5, 1966	200	12	1.8	22	2.5	1.15
U Hyd	1.5-1.8	Apr. 5, 1966	200	12	1.8	22	2.5	1.50
Y CVn	1.5-1.8	Apr. 6, 1966	200	12	1.8	22	2.5	1.02
Fig. 6:								
Moon	1.9-2.5	Oct. 10, 1965	24	50	1.8	10	10	1.28
HD 196610	1.9-2.5	Sept. 13, 1965	200	95	1.8	10	10	1.09
R Tri	1.9-2.5	Sept. 13, 1965	200	95	1.8	10	10	1.02
R Cas	1.9-2.5	Sept. 11, 1965	200	95	3.6	10	10	1.05
Mira	1.9-2.5	Sept. 13, 1965	200	95	1.8	10	10	1.27
Fig. 7:								
NML Cyg	1.9-2.5	Sept. 23, 1965	100	95	11	40	2.5	1.07
RS Cyg	1.9-2.5	Sept. 13, 1965	200	95	3.6	10	10	1.00
NML Tau	1.9-2.5	Sept. 21, 1965	100	95	3.6	20	5	1.09
WZ Cas	1.9-2.5	Sept. 13, 1965	200	95	3.6	10	10	1.14
Fig. 8:								
α Ori	1.9-2.5	Sept. 20, 1965	60	25	1.8	20	5	1.41
χ Cyg	1.9-2.5	Apr. 5, 1965	200	25	1.8	20	5	1.09
U Hyd	1.9-2.5	Apr. 5, 1966	200	25	1.8	20	5	1.57
Y CVn	1.9-2.5	Apr. 4, 1966	200	25	1.8	10	10	1.03
Fig. 9:								
Y CVn-S1	1.5-1.8	Apr. 6, 1966	200	12	1.8	22	2.5	1.02
Y CVn-S2	1.5-1.8	Apr. 6, 1966	200	12	1.8	22	2.5	1.02
Fig. 10:								
α Lyr	1.5-1.8	Sept. 13, 1965	200	45	1.8	11	5	1.00
Fig. 11:								
α Lyr	1.9-2.5	Sept. 11, 1965	200	95	3.6	10	10	1.01

although a slight shift of features attributable to a slow drift of the stellar image in the entrance slit was sometimes observed over the length of a scan. In the NML Cygnus object, which cannot be observed visually, poorer guiding and slower scanning rates caused the resolution to be determined largely by the 2-mm entrance aperture.

Wavelength calibrations of the spectrometer were done in the laboratory by using emission lines of helium, argon, and mercury. The relative wavelength scale was found to be very stable over long periods of time, but slight shifts of the entire scale have been noted, making it necessary to identify some feature in each spectrum to establish a reference wavelength.

Spectra of α Lyrae, α Canis Majoris, and the Moon have been obtained in order to determine the influence of the terrestrial atmosphere. The features arising from atmospheric absorption are indicated in the spectrum of α Lyrae shown in Figs. 13 and 14. No attempt has been made to subtract the telluric features from the spectra given in this paper.

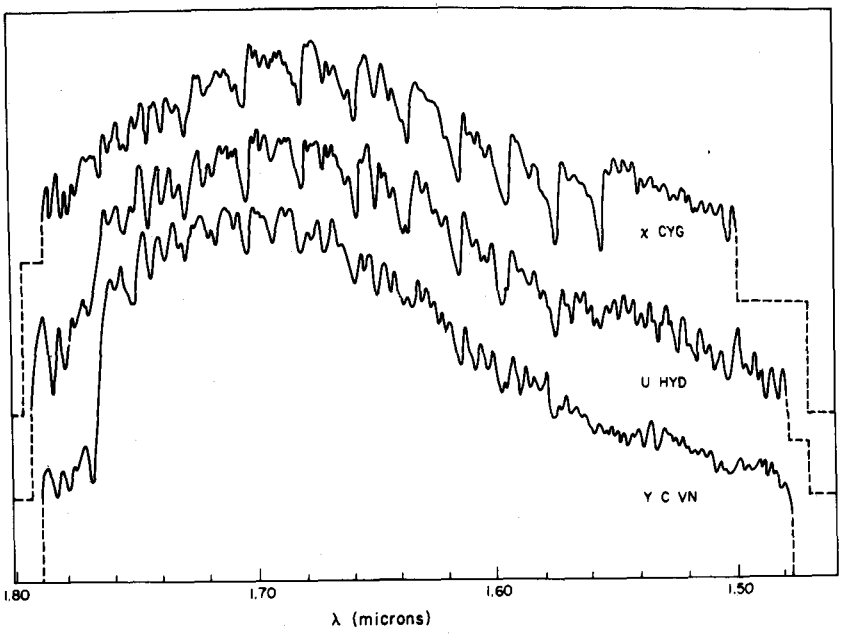

Fig. 8. Spectra of late carbon stars and χ Cygni. λλ1.5-1.8 μ

Description of the Spectra

1. REGION λλ1.5-1.8 μ: (a) M stars.—Spectra of the M-type stars in the region λλ1.5-1.8 μ are shown in Fig. 6 in a sequence of decreasing temperature from top to bottom. The most conspicuous feature of these spectra is the extended absorption of the λ1.4- and λ1.9-μ bands of stellar H_2O, which for lower temperatures has a deeper minimum around λ1.68 μ (Ferriso, Ludwig, and Thomson 1966). Thus the apparent maxima of the spectra around λ1.68 μ become more

pronounced. The observers of Stratoscope II (Woolf et al. 1964) have suggested that the peak at $\lambda 1.68\ \mu$ may be caused to some extent by the minimum value taken by the continuous absorption coefficient of H^- around this wavelength.

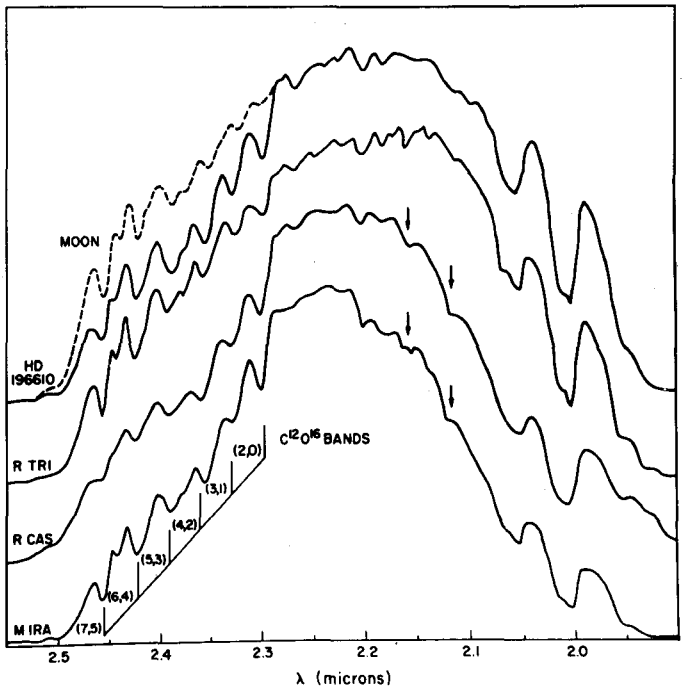

Fig. 9. Spectra of M-type stars in the interval $\lambda\lambda 1.9\text{-}2.5\ \mu$

A series of prominent band heads starting at $\lambda 1.56\ \mu$ is readily identified with the R-heads of the vibration-rotation bands of the third overtone of CO. The absorption coefficient of the CO molecule at a temperature of 3000°K, averaged over intervals of 10 Å, is plotted at the bottom of Fig. 6. The correspondence between the wavelengths of the stellar features and the calculated CO absorption from the (3,0) band up to the (9, 6) band at $\lambda 1.70\ \mu$ can be seen despite the overlap that exists among the higher bands in this sequence. Little can be inferred from either the apparent relative

intensities or the temperature dependence of these stellar features without more detailed study, since variations in the slope of the underlying stellar H_2O absorption with temperature and occasional coincidences with telluric or additional stellar features probably mask the actual band strengths. The 3000°K temperature was chosen only for convenience in plotting the CO absorption coefficient.

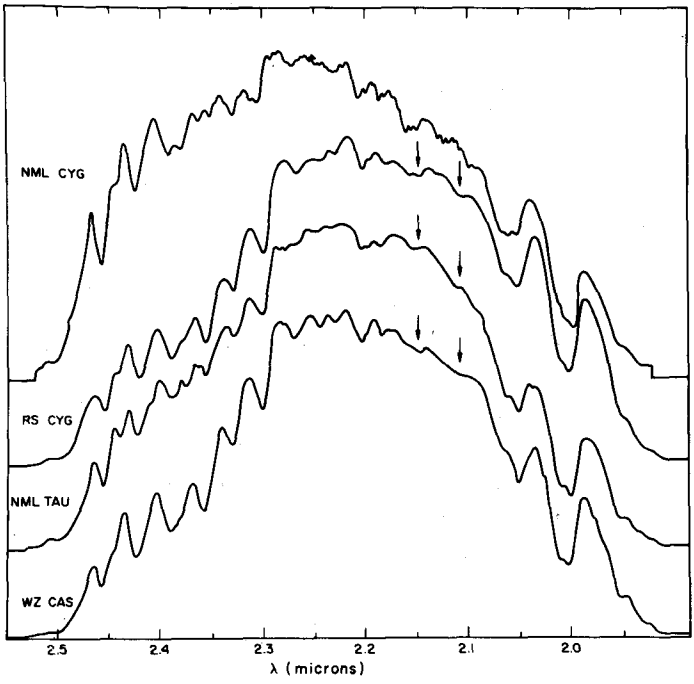

Fig. 10. Spectra of early carbon stars and of the NML Cygnus and Taurus sources. λλ1.9-2.5 μ

(b) N(R) and S stars.—The spectra of the carbon stars WZ Cassiopeiae and RS Cygni shown in Fig. 7 have a shape quite different from that of the M-type spectra. The absorption of the λ1.4 and λ1.9 μ H_2O bands is weaker, and consequently the intensity maximum at λ1.68 μ is more rounded than in the cooler M types. The onset of the CO absorption at λ1.56 μ, on the other hand, is more conspicuous; the

higher bands of the $\Delta\nu = 3$ sequence appear more clearly defined than in the M stars and seem to produce an appreciable depression in the apparent continuum. Again, this is probably due to the weakness of the H_2O absorption in this spectral region.

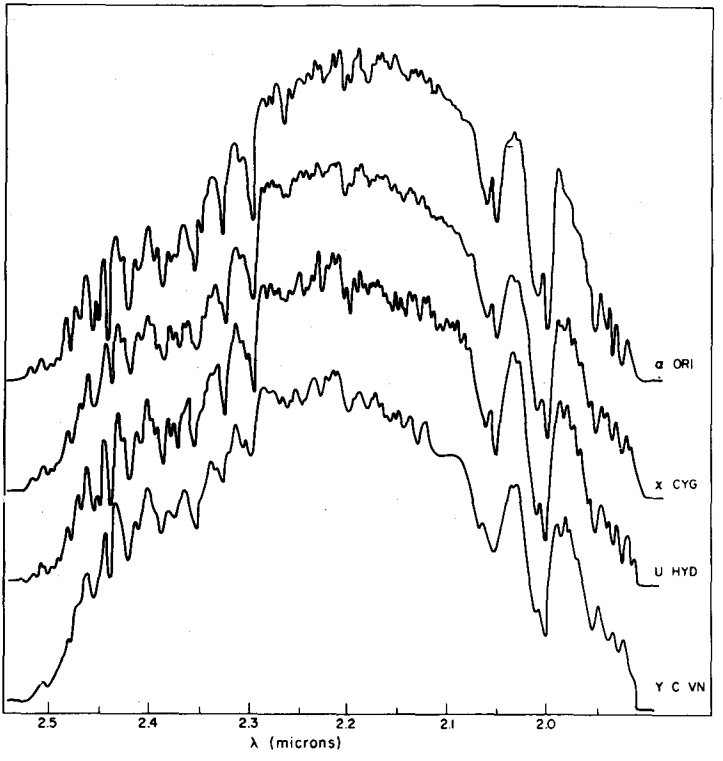

Fig. 11. Spectra of late carbon stars, α Orionis, and χ Cygni. $\lambda\lambda 1.9\text{-}2.5\ \mu$

In the star WZ Cas, known to be rich in C^{13} from the intensities of the isotopic Swan bands, features occur at wavelengths corresponding to the band heads of the $C^{13}O^{16}$ $\Delta\nu = 3$ band sequence which do not seem to be apparent in other stars.

The spectra of the later N-type stars Y Canum Venaticorum and U Hydrae are given in Fig. 8 with a resolution

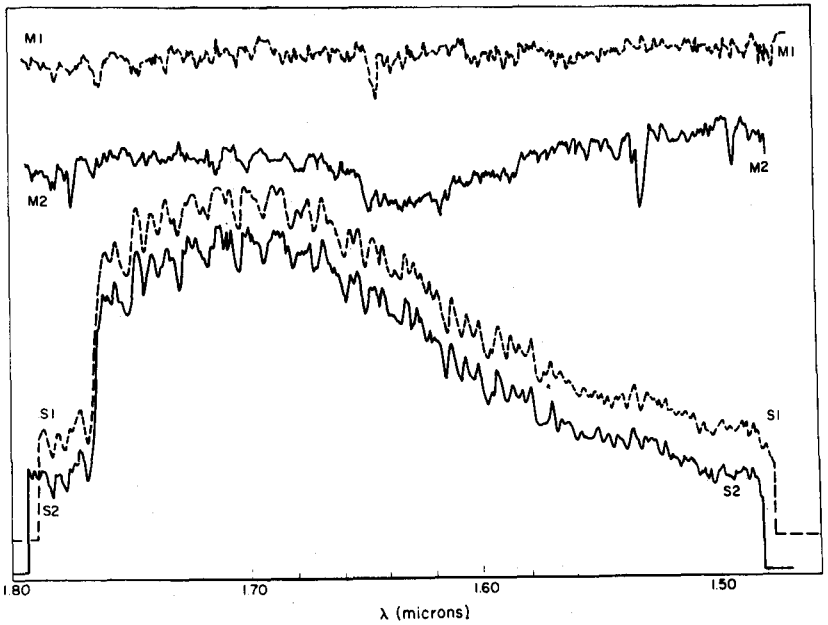

Fig. 12. Two normalized scans of Y Canum Venaticorum (S1, S2) and their respective monitor records (M1, M2).

about twice that typical of Figs. 6 and 7. The most remarkable feature of these spectra is the sharp discontinuity at $\lambda 1.76\ \mu$, which is not shown by any of the other carbon stars observed. The existence of a sudden decrease in intensity shortward of about $\lambda 4000$ Å in the spectrum of Y CVn and other N-type stars has been known for many years (Shajn and Struve 1947) and has been attributed to the absorption produced by C_3. The spectrum shortward of $\lambda 1.76\ \mu$ in Y CVn and U Hyd also shows marked differences from other stars. For comparison purposes a spectrum of χ Cygni with a comparable resolution is included in Fig. 8. The weakness of the $\Delta\nu = 3$ sequence of CO bands in the late N-type stars is quite obvious, and, in fact, the (3, 0) band of CO appears completely obliterated in Y CVn. Since, as seen in Fig. 11, the $\Delta\nu = 2$ band sequence of CO is not weakened in these same late N-type stars, and since there are no indications of strong H_2O

absorption, another source of absorption must be affecting the entire spectrum in this region. On the basis of the observed spectral characteristics of the late N-type stars in the photographic region, it would be logical to hypothesize that this absorption is produced by a polyatomic carbon compound, such as C_3 or SiC_2.

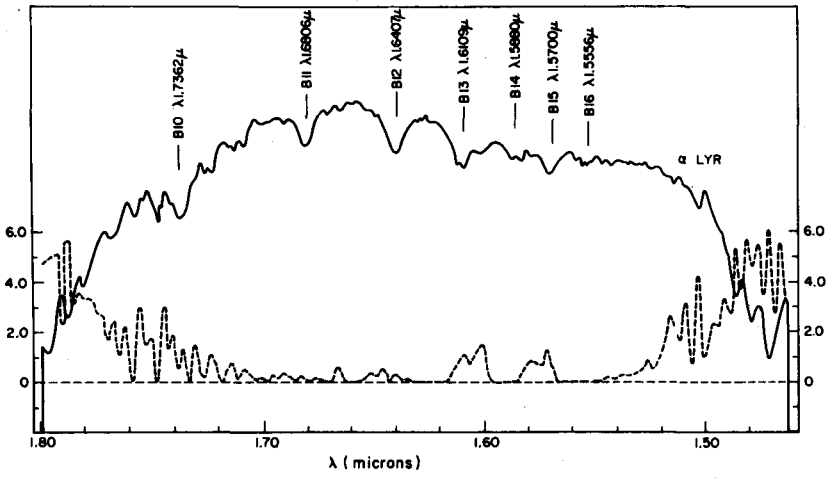

Fig. 13. α Lyrae, $\lambda\lambda$1.5-1.8 μ. Lines due to the Brackett series of atomic hydrogen are indicated. The absorption coefficient of the terrestrial atmosphere is plotted at the bottom of the figure.

The spectrum of the S star S Ursa Majoris, not reproduced in this paper, closely resembles that of χ Cyg, which is an intermediate object between S- and M-type stars. The $\Delta\nu = 3$ band sequence of CO appears as strong in χ Cyg as in the early carbon stars. The general shape of these spectra suggests the absence of the H_2O absorption apparent in the spectrum of Mira. This conclusion is in agreement with the findings of Wing, Spinrad, and Kuhi (1967) in the photographic region.

2. REGION $\lambda\lambda$1.9-2.5 μ: (a) M stars.—The appearance of the M-type stars in the $\lambda\lambda$1.9-2.5-μ region (Fig. 9) is

dominated by the H_2O absorption band at $\lambda 1.9\ \mu$, the wings of which extend further into the red as the temperature decreases. This absorption, combined with the shift of the energy peak to the red and the absorption of the $\Delta\nu = 2$ rotation-vibration bands of CO beyond $2.3\ \mu$, produces a sharper apparent maximum at around $\lambda 2.25\ \mu$ in the cooler stars. The head of the (2, 0) band of CO produces a discontinuity in the spectrum at $\lambda 2.30\ \mu$. The spectral region covered by the $\Delta\nu = 2$ sequence of CO bands is heavily affected by telluric absorption due to CH_4 and H_2O, as seen in the spectrum of the moon which has been superimposed on that of HD 196610 in Fig. 9. Nevertheless, these CO bands can be distinguished as has been reported by Boyce and Sinton (1964). The spectra of the cooler stars, Mira and R Cas, show two distinct shallow absorption features at $\lambda 2.13$ and $\lambda 2.16\ \mu$ which have not been identified. Sinton (1966) has observed similar features and attributed them to CH.

(b) N(R) and S stars.—As in the $\lambda\lambda 1.5$-1.8-μ region, the carbon stars shown in Fig. 10 are affected less than the M stars by stellar H_2O absorption and, as a consequence, their spectra are flatter. The $\Delta\nu = 2$ band sequence of CO is also prominent in the carbon stars, but it has a somewhat different appearance than in the M stars. In particular, the CO bands around $\lambda 2.4\ \mu$ are more distinct in the carbon than in the M stars; this probably is also an effect of the decrease in the underlying H_2O absorption. The spectrum of WZ Cas reproduced in Fig. 10 does not show any feature that can be identified with certainty with $C^{13}O^{16}$, possibly due to the lower resolution of these spectra. The unidentified features at $\lambda 2.13$ and $\lambda 2.16\ \mu$ noticed in the M stars are also present in WZ Cas and RS Cygni.

The spectra of two later N-type stars and of χ Cygni are shown in Fig. 11 at a resolution higher than that in the preceding figures. The spectrum of α Orionis, an M star, has been included for comparison purposes. As previously mentioned, the $\Delta\nu = 2$ CO bands are not weakened in the late N-type stars as the $\Delta\nu = 3$ bands were found to be. The unidentified features at $\lambda 2.11$ and $\lambda 2.16\ \mu$ seem to be stronger in the spectrum of the late N types.

3. THE NML STARS IN CYGNUS AND TAURUS: Since the main infrared spectral characteristics of the observed M-, N-, and S-type stars can be attributed to absorption bands of H_2O and CO, it is of interest to analyze the behavior of these features in the spectra of the NML stars in Cygnus and Taurus. The spectra of these objects in the $\lambda\lambda$1.9-2.5-μ region appear together with those of WZ Cas and RS Cyg in Fig. 10. The spectrum of the Cygnus object clearly is unique because of its high average energy around λ2.4 μ, a feature which might actually be a temperature effect or might be produced by heavy interstellar reddening. The flatness of the spectrum in the $\lambda\lambda$2.1-2.2-μ region indicates that the H_2O absorption due to the λ1.9-μ band is weak relative to that in the Mira-type variables. The weakness of the H_2O absorption is also indicated by the definition of the (7, 5) and (6, 4) CO bands. Thus, with regard to the H_2O absorption, the Cygnus object resembles a carbon star more than an M-type star. The spectrum of the Taurus source shows similar, although less pronounced, characteristics.

Because of the faintness of the Cygnus object in the

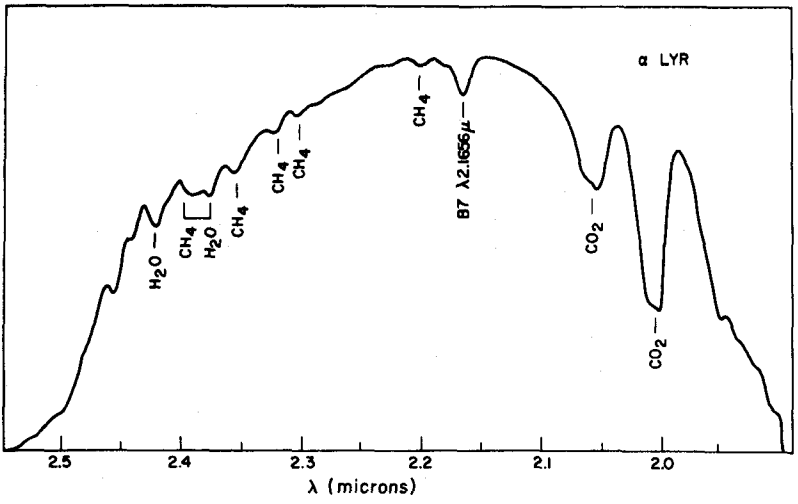

Fig. 14. α Lyrae, $\lambda\lambda$1.9-2.5 μ. Features due to terrestrial atmospheric absorption are indicated.

$\lambda\lambda$1.5-1.8-μ region, no spectrum of this source with a quality comparable to the other spectra in this paper has been obtained. However, the spectra available do not show any features strikingly different from those appearing in other stars. In particular, there is no sign of the unidentified absorption detected in the late N-type stars. The spectrum of the Taurus object in the $\lambda\lambda$1.5-1.8-μ region appears in Fig. 7, where its similarity to that of the carbon stars can be noticed. When the spectrum of the Taurus object is made to agree with that of an M star such as R Cas in the region $\lambda\lambda$1.6-1.7 μ, the spectrum of the Taurus object is somewhat higher than that of the M type around λ1.55 and λ1.75 μ. The weakness of the H_2O extended absorption is thus also apparent in this region. The low H_2O content of the Cygnus and Taurus objects and their consequent similarity to the carbon stars has been pointed out by Wing et al. (1967) on the basis of the appearance of the H_2O band at λ9400 Å.

Conclusions

The observations of low-temperature stars presented here have shown that their infrared spectral characteristics are primarily determined by the absorption due to H_2O. In the cooler M-type stars the H_2O absorption is very strong relative to that observed in the N- and S-type stars. The NML objects in Taurus and Cygnus in this respect resemble the carbon rather than the M-type stars.

The behavior of the H_2O absorption is readily understood in terms of variations in the C:O abundance ratio. In order to consider qualitatively the general features of stellar spectra in the infrared, the dissociation calculations of Tsuji (1964) for abundance ratios H:C:O:N corresponding to M stars and to carbon stars are shown in Fig. 15. The concentration of CO is seen to be about the same in both cases, but that of H_2O is drastically reduced in carbon stars.

The large concentration of some molecular species predicted at these temperatures is also interesting. In the M stars, for example, OH should be an abundant constituent. It has not been observed, however, even though the $\Delta\nu = 2$ band sequence of OH lies in the region $\lambda\lambda$1.5-1.8 μ

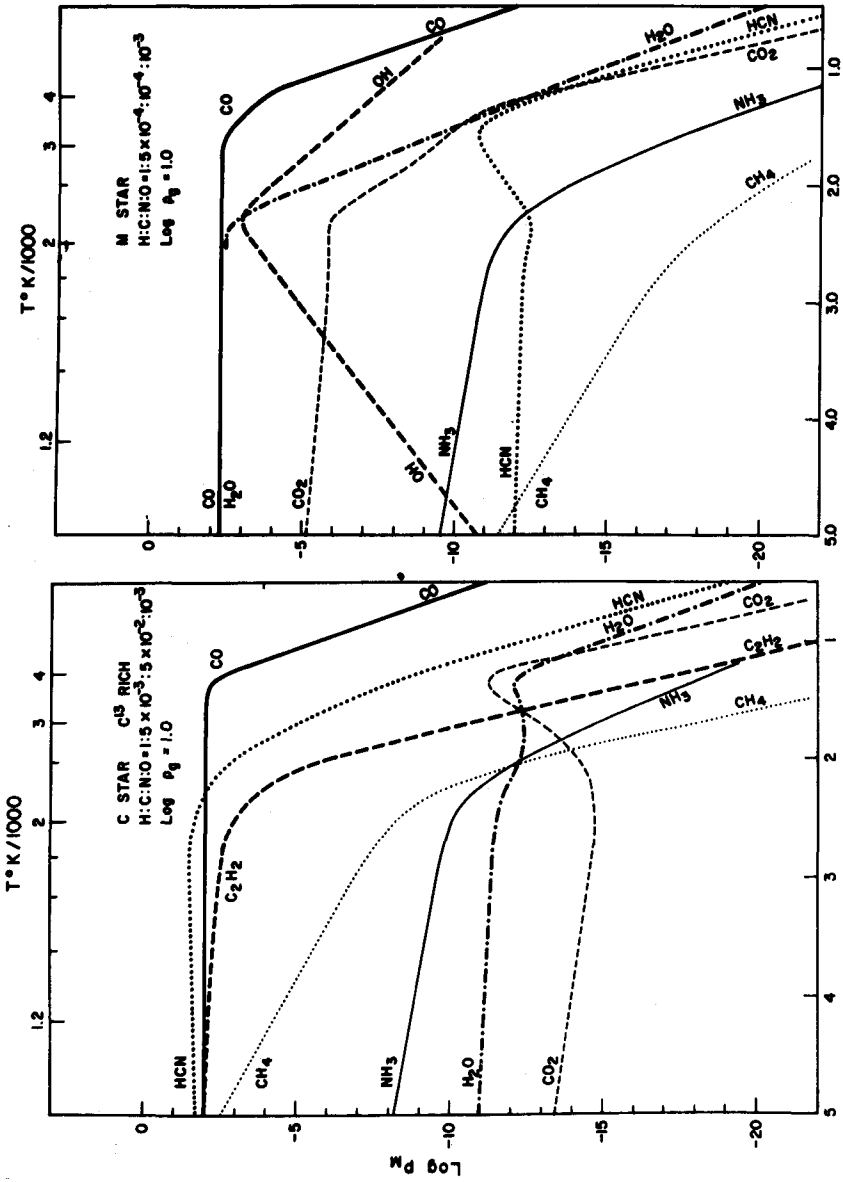

Fig. 15. Calculated molecular dissociation equilibria (after Tsuji, 1964).

(Chamberlain, 1961). The (9, 7) band has an origin at $\lambda 2.15$ μ, near the unidentified features noted above, but the very open structure of the OH bands and the fact that the unidentified features appear in carbon stars as well as in M-type stars rules out their identification with OH. Evidently, an attempt to detect OH will require higher resolving power than the one used here.

The large concentration of HCN and C_2H_2 predicted in carbon stars is also remarkable. The former molecule has bands at $\lambda 1.53$ and $\lambda 2.01$ μ, while the latter is known to have bands at $\lambda 1.54$, $\lambda 2.14$, and $\lambda 2.42$ μ. In the spectra available no features can be ascribed to either of these two molecules.

The observation of strong absorption features, presumably due to polyatomic molecules, in the spectra of late N-type stars brings up the question of why even cooler stars, such as the Cygnus object, do not also show very strong absorption features not identifiable with diatomic molecules. As Tsuji (1964) has pointed out, however, below 2200°K the partial pressure of free carbon exceeds the saturated vapor pressure of graphite, and thus it is possible that graphite particles can precipitate, producing a decrease in the concentration of other polyatomic carbon compounds.

A quantitative understanding of the energy curves of the low-temperature stars in the infrared and of their main spectral absorption features will have to be based on calculated model stellar atmospheres. We propose to return to this aspect of the problem at a later date.

The spectrometer has been loaned to us by the Space Sciences Division of the Jet Propulsion Laboratory. We thank all the members of the California Institute of Technology infrared astronomy group, but especially E. Becklin and C. Spencer, for their efforts supporting this work. We are indebted to Dr. Aert Schadee for calculating the absorption coefficient of the rotation-vibration bands of CO and to M. Katz for her help in reducing the data. We thank Dr. William S. Benedict for a helpful discussion.

REFERENCES

Boyce, P. B. and Sinton, W. M., Sky and Telescope **29**, 78 (1964).

Chamberlain, J. W. Physics of the Aurora and Airglow (Academic Press, New York, 1961), p. 368.

Ferriso, C. C., Ludwig, C. B., and Thomson, A. L. J. Quant. Spectr. Radiative Transfer, **6**, 241 (1966).

Johnson, H. L., Astrophys. J. **135**, 69 (1962).

Johnson, H. L., Bol. Obs. Tonantzintla y Tacubaya, **3**, 305 (1964).

_____ Astrophys. J., **141**, 923 (1965).

Johnson, H. L., Mendoza V., E. E., and Wisniewski, W. Z., Astrosphys. J., **142**, 1249 (1965).

Kron, G. E., White, H. S., and Gascoigne, S. C. B. Astrophys. J., **118**, 503 (1953).

Kuiper, G. P. Commun. Lunar and Planetary Lab., **1**, 179 (1962).

_____ ibid., **2**, 17 (1963).

_____ Mém. Soc. Ray, Sci. Liège, Ser. 5, **9**, 365 (1964) (12th Int. Astro. Col., Liège, 1963).

Kukarkin, B. V., Parenago, P. P., Efremov, Y. U. I., and Gol'opov, P. N., Acad. Sci., U. S. S. R. (Moscow, 1968), Vols. **1** and **2**.

Mertz, L., and Coleman, I., Astrophys. J. **143**, 1000 (1966).

Moroz, V. I. Astr. Tsirk, (Sternberg Institute) No. 368, **4**, April 1966.

Neugebauer, G., Martz, D. E., and Leighton, R. B., Astrophys. J., **142**, 399.

Shajn, G. and Struve, O., Astrophys. J., **106**, 86 (1947).

Sinton, W. M., Appl. Optics **1**, 105 (1962).

_____ Meeting of Am. Astr. Soc., Hampton, Virginia, March 1966.

Tsuji, T., Ann. Tokyo Astro. Obs. **9**, No. 1 (1964).

Wing, R. F., Spinrad, H., and Kuhi, L. V., Astrophys. J., **147**, 117 (1967).

Woolf, N. J., Schwarzschild, M., and Rose, W. K. Astrophys. J., **140**, 833 (1964).

3

OBSERVATIONS OF QUASARS AND COOL STARS

F. J. Low

I. INTRODUCTION

Infrared observations of the celebrated quasar, 3C273, show that the total flux of electromagnetic energy received at the earth in all wavelengths is at least 2×10^{-12} watts/cm^2. If the distance to this object is that inferred from the cosmological interpretation of its measured red shift, and if it is assumed to radiate isotropically, then its total power output is at least 1000 times the entire radiant output of our galaxy! Even before infrared observations were made quasars were known to be inexplicably luminous. The important points here are that the total luminosity of 3C273 is 10 times greater than known previously and that most of the energy is radiated at wavelengths between 1 and 30 microns. It has now been established that quasars are not unique in their characteristic of radiating chiefly in the infrared, and it appears that all quasars do not have this property. Perhaps the most outstanding problem in infrared astronomy today is the study of the non-thermal processes involved in quasars and related objects.

A series of equally intriguing investigations are in progress concerning the nature and origin of cool stars. The existence of exceptionally red or cool stars has been known

since their photographic discovery by Hetzler (1937). New objects added by the 2.2 micron sky survey at Mt. Wilson Neugebauer et al.(1965); Ulrich et al. (1966) and independently by Mendoza (1966), by Becklin and Neugebauer (1967), and by Kleinmann and Low (1967) have reawakened interest in the problem. We now know there is a sizable number of discrete sources which are observable in the range 1 to 25 microns but are virtually undetectable outside this range! The study of these new objects is both part of a general effort to understand stars found to have large infrared departures from the normal thermal spectral energy distribution, and an important source of information concerning the earliest stages of stellar formation.

In addition to these areas of investigation there are several other problems on which considerable progress could be reported if space permitted; i.e., the intensity and spectral distribution of planetary heat, the infrared transmission and radiation of interstellar dust, the continuum and line emission of HII regions, and the spectral energy distribution of galaxies.

In all these areas of interest there are common problems of instrumentation and experimental technique. The observational capabilities of ground based instruments at wavelengths between 1 and 25 microns are still being improved at a rapid pace; however, a brief description of current practice will help in discussing and evaluating the observational material.

II. INSTRUMENTATION FOR GROUND BASED OBSERVATIONS

The earth's atmosphere is relatively transparent for wavelengths between 1 and 25 microns. Beyond 25 microns there are no useful windows until we reach 1 mm. The special techniques developed for work at 1 mm are described elsewhere (Low, 1966); here we will discuss only the near infrared (1-4 microns) and the intermediate infrared (4-25 microns). The far-infrared (25-1000 microns) must await the development of telescopes carried above the atmos-

pheric water vapor by jet aircraft and other high altitude vehicles before significant progress will be obtained. Table I lists the photometric designation of the usable atmospheric

TABLE I

Photometric Designation	λ_{eff} (μ)	Absolute Flux, Mag = 0 $W/cm^2/\mu$	$W/m^2/Hz$	Limiting Magnitude
J	1.25	3.4×10^{-13}	1.77×10^{-23}	——
H	1.60	1.28×10^{-13}	1.09×10^{-23}	13.5
K	2.2	3.9×10^{-14}	6.3×10^{-24}	10.0
L	3.4	8.1×10^{-15}	3.1×10^{-24}	8.0
M	5.0	2.2×10^{-15}	1.8×10^{-24}	5.0
N	10.2	1.23×10^{-16}	4.3×10^{-25}	2.0
Q	22.0	7.7×10^{-18}*	1.02×10^{-25}*	0.0

*Provisional

windows, their effective wavelengths, the absolute fluxes corresponding to zero magnitude, and rough values for practical limiting magnitudes.

All of the large telescopes used for infrared work from the ground were designed for conventional optical use. No special attempt has been made to reduce or stabilize the thermal radiation of the telescope and no cooling below ambient is feasible. These constraints are not as serious as might be expected since the atmospheric contribution to the background is almost as large as that from the telescope and is far more variable.

One method of dealing with the background and its fluctuations is to employ the chopping arrangement shown in Fig. 1. The f/14 cone of starlight enters the photometer from the secondary of a Cassegrain telescope and is deflected by a small diagonal mirror moving back and forth at the chosen chopping rate of 10 cps. This mirror moves 2 mm, just far enough to shift the image in and out of the focal plane diaphragm. The result is that two beams are produced which traverse nearly identical paths through the telescope and atmosphere. Background cancellations of greater than 1000:1 are obtainable and fluctuations common to both beams

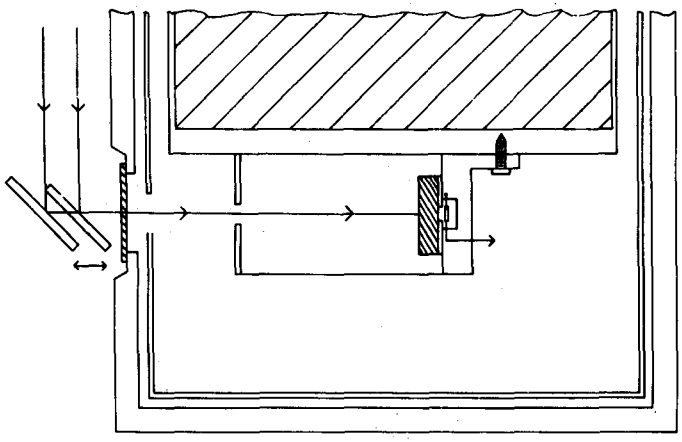

Fig. 1. Schematic representation of typical arrangement used with He cooled detectors. See text for description.

are cancelled. Other methods of "space filtering" are possible; for example, the star may be chopped by running the image rapidly in and out of focus, and more than one detector may be employed in different geometries. The sky noise component that is most difficult to cancel is associated with small scale atmospheric turbulence similar to the familiar "seeing" phenomenon. Were it not for "seeing" the telescope could be operated at the diffraction limit (about 2 arcsecond for a 60-inch at 10 microns) and much greater rejection of the background and sky noise could be achieved.

Since both beams are equivalent but 180° out of phase we observe a star by shifting it alternately between the two beams. This is accomplished by moving the telescope in declination after each 15 sec integration. Continous guiding is

necessary but no additional sky readings are needed and the signal-to-noise is doubled.

To limit the background on the detector we limit both its angular field and its spectral bandwidth. Figure 1 shows a cross section through a liquid helium dewar designed for our application, i.e. efficient cooling of detectors to 1.5 °K with no internal movement or vibration. Note the long cooled baffle and the cooled interference filters all inside the guard vacuum. The window may be placed at 45° to serve as a beam splitter sending the visible light to an eyepiece for setting and guiding.

The most important part of any infrared photometer or radiometer is the detector. At the University of Arizona there are 3 types of detectors currently in use: (a) commercially available PbS cells with noise equivalent power (N.E.P.) about 1×10^{-14} watt for 0.25×0.25 mm area; (b) low temperature germanium bolometers (Low, 1961) with N.E.P. between 2×10^{-14} and 2×10^{-13} for 0.5×0.5 mm areas, depending on background level; and (c) a new helium-cooled germanium photodetector (Low, to be published) for 1.6 microns with N.E.P. better than 1×10^{-14} watt for 1×1 mm area. The cooling requirements and spectral ranges of these detectors are quite different. PbS covers 1 to 4 microns and requires only liquid nitrogen (77°K). The germanium bolometer works about equally well from 2 to 1000 microns but must be cooled below 2°K for best sensitivity. The new germanium photodetector is sensitive between 1 and 1.7 microns and uses 4.2°K liquid helium. Fabry optics are employed when the detector is smaller than the focal plane diaphragm or to obtain very high optical throughputs.

In discussing the limiting performance of an infrared system we must start with a set of assumptions and definitions. Let us assume we are observing point sources and using a focal plane diaphragm large enough to keep guiding and seeing errors below 10 percent. We also assume a 60-inch telescope aperture and a 4-hour observing period. By our definition, a limiting magnitude star will produce a mean deflection 3 times its standard deviation (σ). As stated above, current results are given in Table I. At N and Q the sky noise completely dominates the bolometer noise. At M

sky and bolometer noise are frequently about equal. With PbS cells used at K and L, sky noise is rarely seen. At H the sky is dark and not noisy even without the cancellation of a dual beam chopper. Thus, if better limiting magnitudes are to be obtained, both improved "space filtering" and better detectors are needed.

Observing faint extended sources is more complicated and we will only indicate the state of the art. At M we have obtained a 2 σ measure at +2 mag in 2 hours with a 20 mm diameter field lens on a F/16 60" telescope.

Finally, we come to the absolute calibration procedures. Except for H and Q, all the photometric systems now in use at Arizona and their absolute calibrations have been discussed previously by Johnson (1965). At H a simple blackbody interpolation between J and K (1.25 and 2.2 microns) was carried out. At Q the provisional calibration is based on both stellar and planetary observations soon to be published in greater detail. In following these procedures we have purposely avoided two difficult problems, correction for atmospheric extinction and for telescope efficiency. Differential extinction corrections can generally be made quite accurately at all wavelengths, including 22 microns, where extinction variations are largest.

III. COOL STARS

Examining the H-R diagram showing the variation of stellar luminosity with temperature, we notice that extending the main sequence to temperatures below 2000 °K results in such low luminosities that the mere detection and identification of cool dwarf stars becomes quite difficult. However, the giant sequences run almost horizontally, indicating that luminous stars should be found down to some minimum temperature (~2000 °K) set by the requirement of maintaining hydrostatic equilibrium. Most stars found in this area of the H-R diagram are Mira variables. The coolest known example is probably NML Taurus, ~1200 °K at minimum (Wing et al. 1967). Presumably luminosity class I and II stars do not evolve into bright cool stars much below this

temperature. However, they are inherently the brightest stars we know in the near infrared. Both the photographic surveys at 0.8 micron (Haro and Chivara) and the 2.2 micron survey reveal the existence of numerous red giants, many of them heavily reddened by interstellar dust and most of them variable. There is no clear-cut indication of a piling up of such stars at very low temperatures as a result of aging.

In the earlier stages of stellar evolution, contracting clouds of gas and dust may radiate all or part of their energy in the infrared. In the discussion below several of the various possibilities are related to the observed properties of certain infrared stars. The fact that star formation, a common occurrence in the solar neighborhood, is not observed as a bright optical phenomenon has been explained, in part, on the basis that stars are born in private, behind opaque screens of interstellar dust clouds. It is a well-established property of these dust clouds that their optical opacity is high but that beyond about 2 microns they become transparent. Thus, save for radio observations, we are looking via the infrared for the first time into a volume of space where star formation must be occurring. But before examining our data for evidence of star formation let us seek to answer the question: what are the various mechanisms that can be expected to produce large infrared outputs in stars or protostars ?

One of the most obvious causes for an infrared excess is simply the occurrence of a cool companion with a hot star. A cool extended stellar atmosphere containing strong molecular absorptions will result in significant departures in the near infrared from the solar type of spectral energy distribution. This occurs, for example, in carbon stars. The sun is a good example of a star with no near or intermediate-infrared excess; in fact, because the H^- opacity increases with wavelength beyond 1.6 microns, the sun's spectral energy distribution drops well below the Planck curve for an effective temperature of 5900 °K. However, recent observations of the sun (Noyes, Beckers and Low, 1967) show that at some wavelength beyond 100 microns chromospheric opacity causes the brightness temperature to rise above the

boundary layer temperature of about 4500 °K. It has been pointed out by Noyes, Gingerich, and Goldberg (1966) that the chromospheric emission of stars with cool photospheres may become important at wavelengths as short as 10 microns.

The most general mechanism to be considered here is one in which circumstellar dust is heated by the star and reradiates in the infrared. Again considering the solar system, the interplanetary envelope and the planets absorb less than 10^{-6} of the sun's radiant energy. The energy absorbed and reradiated at longer wavelengths results in an infrared excess extending over a broad wavelength interval, 1 to 100 microns, so weak as to be virtually undetectable at great distances. If, however, the density of the interplanetary dust were increased by adding to it the mass contained in the planets, almost all the sun's energy would be degraded into the infrared by its circumstellar envelope. Significant amounts of dust may be maintained in circumstellar envelopes of different types. One of these is the preplanetary dust envelope discussed by Poveda (1965) and used by Low and Smith (1966) to explain the extended infrared continuum observed for R Monocerotis. Any star undergoing continuous mass ejection produces a constant supply of material which will condense to form grains as the temperature drops. These grains may account for the 22 micron excess observed in α Ori as shown in Fig. 2.

Johnson (1967) has pointed out several instances where the selective extinction of interstellar dust shifts the observed maximum of hot stars well into the near infrared. NML Cygnus, VI Cygni 12, and C.I.T. 11 are three dramatic examples. Thus we clearly cannot use the mere existence of a large infrared output as evidence for low temperatures.

Synchrotron emission associated with flares is a possible, but as yet unproven, source of infrared radiation in stars. Strong synchrotron radio outbursts have been detected from flare stars and, since much of the optical output of a flare is non-thermal, it would not be surprising to find synchrotron radiation in the infrared.

The next mechanism to be proposed here is equally conjectural: if a star produces large fluxes of particles which

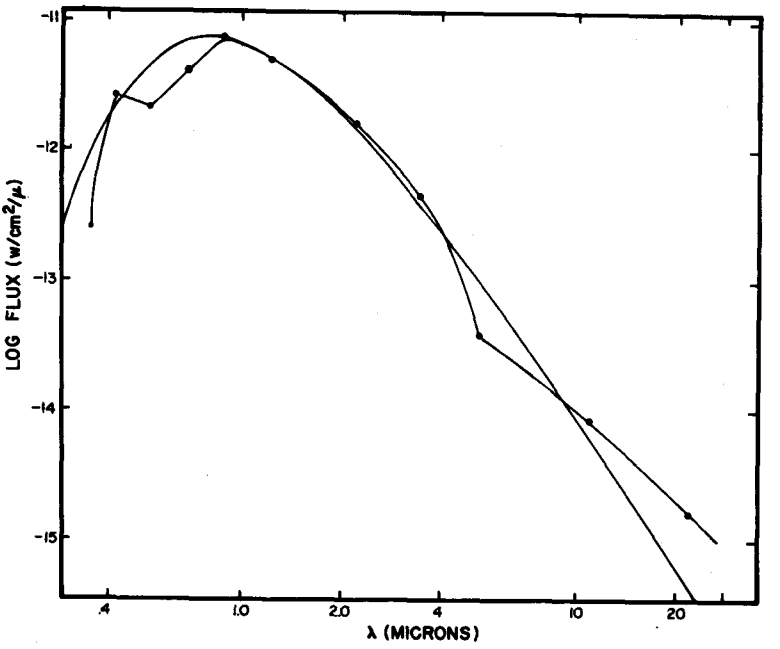

Fig. 2. Absolute flux versus wavelength for α Orionis. Smooth curve is a Planck distribution of 3400 °K. Note large excess at 22 microns.

are not contained by a magnetic field, some fraction of the energy released may be converted into infrared emission by the surrounding medium either by heating or by fluorescence. The fluorescence need not, of course, be confined to the infrared but may simply show up there because the star itself is so bright at shorter wavelengths.

In all the above cases the driving energy was thermonuclear. We should also consider those infrared objects which are heated entirely by gravitational contraction. Contracting interstellar dust clouds of all masses must be included as well as the numerous objects which contract with masses too low to form stars. The celebrated dark globules are likely candidates.

Turning now to observations which have already been

secured, we can see some of these mechanisms at work. Figure 2 shows the distribution of flux with wavelength for α Ori. In α Ori the excess at 22 microns may be chromospheric or be caused by circumstellar grains. If the latter is the case the diameter of the star at 22 microns should be much greater than at shorter wavelengths. Figure 3 shows the relative spectral energy distributions for a sequence of

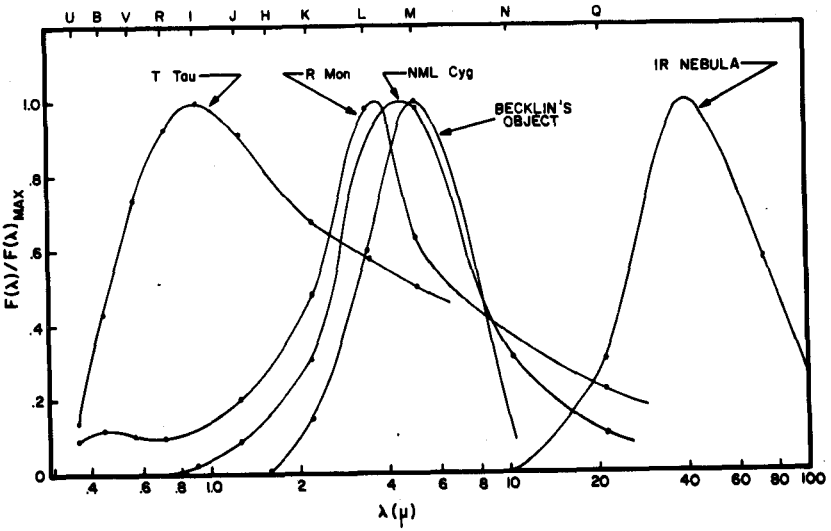

Fig. 3. Relative spectral energy distributions for 5 infrared objects.

infrared objects: (a) NML Cyg, a highly reddened late type super giant; (b) T Tauri, a protostar with most of the preplanetary material already consolidated; (c) R Mon, a protostar still embedded in its preplanetary envelope; (d) Becklin's object, possibly a very young protostar emitting no detectable light short of 1 micron; and (e) the extended infrared object in Orion, a large contracting mass fragment ing into stars.

Of these objects only NML Cygnus appears to be unrelated to the problem of star formation. Johnson (1967) finds

that this object has a most remarkable spectral energy distribution even after correcting for the enormous interstellar reddening. However, no observational evidence exists at present to suggest that the interpretation as a star of spectral type M6Ia is in error.

It now appears that the family of stars related to T Tauri form an evolutionary sequence starting with preplanetary systems such as R Mon and proceeding forward to the main sequence. Further studies of these objects should provide data concerning the early stages of planetary formation.

Becklin's object differs from the other known infrared stars in that it conforms very well to a Planck curve up to the peak near 5 microns but drops off rapidly beyond the peak. This is fundamentally different from NML Cygnus, which is an example of interstellar reddening, and from R Mon, which illustrates circumstellar reradiation. Its angular diameter computed from its 1-5 micron color temperature of 610°K[6] is 0.06 arcseconds, giving a linear diameter of 30 A.U. Its luminosity is 10^3 times the sun or about equal that of R Mon even though its linear diameter is almost 10 times smaller. The fact that no light from the central condensation penetrates the envelope and the close fit to a Planck curve from 1.6 to 5 microns suggests a much higher density than in the case of R Mon.

The discovery of the extended 20 micron source near Becklin's object confirms that we are indeed dealing with prestellar systems and suggests that further study will provide much needed observational data with which to test the numerous theories of stellar and planetary formation.

IV. QUASARS

The first infrared detection of a quasi-stellar object, 3C273B, was made by Johnson (1964) at a wavelength of 2.2 microns. Since that time we have observed this object at all infrared wavelengths available from the ground including 1 mm (Low and Johnson, 1965; Low, 1965). These data are presented in Fig. 4.

The rapid large scale outbursts found at millimeter and

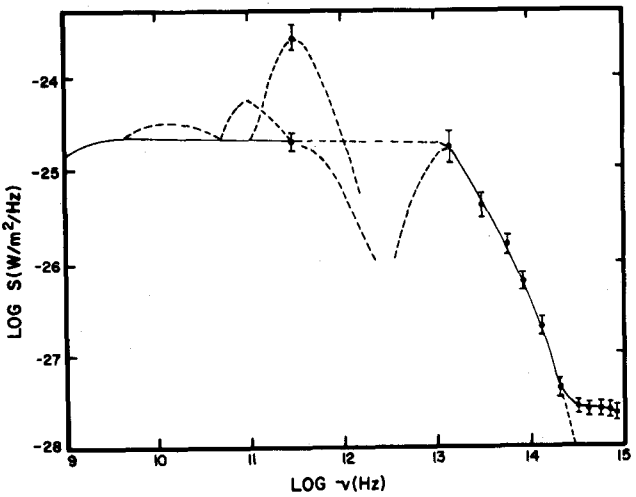

Fig. 4. Absolute flux versus frequency for 3C273B.

microwave frequencies have not been found in the range from 1 to 25 microns, where most of the energy is radiated. This fact alone implies a multiplicity of energy sources. No appreciable variations in the optical continuum have occurred during the period in which the infrared data were taken; therefore, we do not know if variations in the optical continuum are independent of or are caused by the principal energy source producing the infrared. Thus it is quite possible that the main energy source is constant or changing very slowly. Only recently have we secured 1.6 micron data of sufficient accuracy to test this point rigorously or to determine whether the steep part of the continuum is gradually decaying.

We have only a few solid facts concerning the infrared source in 3C273B. Its angular size is unknown. Whether it supplies the low energy electrons to the quiescent radio source is still quite uncertain despite our efforts to connect the two spectra. The infrared polarization of the object, if any, is unknown as is its distance and hence its true luminosity. Nor do we know if 3C273 is unique. New observations of other quasars at 1.6 microns are now being successfully

carried out. So far, we can only say that no other quasar yet observed has the steep rise between 1 and 1.6 microns shown by 3C273B.

In view of the large infrared contribution to the total luminosity of 3C273 and the complex relationships that must exist between the radio, infrared and optical sources, it is not surprising that efforts to correlate red shifts with radio or optical apparent luminosities have not been particularly successful. At present it is not even possible to state with any certainty the true range of apparent total luminosities involved.

The distance to 3C273B is highly disputed, but must fall, according to present ideas, between 10 and 500 megaparsecs. Even if the shortest distance is taken, its infrared luminosity is greater than the radiant output of many galaxies. It is interesting to note that perhaps the most energetic sources in the universe radiate most of their energy at wavelengths which fall in the least studied portion of the spectrum, just between the domains of conventional optical and radio astronomy.

It is a pleasure to acknowledge the support given this research by the National Science Foundation and the National Aeronautics and Space Administration.

REFERENCES

Becklin, E. E. and Neugebauer, G., Astrophys. J. **147**, 799 (1967).

Hetzler, C., Astrophys. J. **86**, 509 (1937).

Johnson, H. L., Astrophys. J. **139**, 1022 (1964).

Johnson, H. L., Commun. Lunar and Planetary Lab., No. 53 (1965).

Johnson, H. L., Astrophys. J. 149 (1967) (in press).

Kleinmann, D., and Low, F. J., Astrophys. J. Letters, July 1967.

Low, F. J., J. Opt. Soc. Am. **51**, 1300 (1961).

Low, F. J., Astrophys. J. **142**, 1287 (1965).

Low, F. J., Proc. IEEE **54**, 477 (1966).

Low, F. J. and Johnson, H. L., Astrophys. J. **141**, 336 (1965).

Low, F. J. and Smith, B. J., Nature **212**, 675 (1966).
Mendoza, E. E., Astrophys. J. **143**, 1010 (1966).
Neugebauer, G., Martz, D. E., and Leighton, R. B., Astrophys. J. **142**, 808 (1965).
Noyes, R. W., Beckers, J. M., and Low, F. J., Solar Phys., 1967 (in press).
Noyes, R. W., Gingerich, O., and Goldberg, W., Astrophys. J. **145**, 344 (1966).
Poveda, A., Bol. Obs. Tonantzintla y Tacubaya **4**, 15 (1965).
Ulrich, B. T., Neugebauer, G., McCammon, D., Leighton R. B., Hughes, E. E., and Becklin, E., Astrophys. J. **146**, 288 (1966).
Wing, R. F., Spinrad, H., and Kuhi, L. V., Astrophys. J. **147**, 117 (1967).

4

STELLAR SPECTRA

W. M. Sinton

For the past three years or so we have been making interferometric spectra of the stars. The experimental technique has been to record a two-beam interferogram digitally and obtain the spectrum by making a Fourier transform of the interferogram on a digital computer. The instrument is a birefringent interferometer using rutile and a brief description of it has been given (Boyce and Sinton, 1965). Altogether, over fifty stars have been observed with this equipment.

A sample of some of the spectra that we have observed is shown in Fig. 1. First of all, we note that there are three CO_2 bands from the terrestrial atmosphere that show up in these spectra. Also, the spectra are cut off at 1.9μ and 2.5μ by terrestrial water vapor bands. Many of the other features are also terrestrial in origin and are due to methane bands and water vapor. The first star shown, α Lyr, has as its only stellar feature the Brackett γ line of hydrogen. The other spectra are of progressively later type stars. The first overtone carbon monoxide bands can be seen in α Tau, β Peg, and α Her. These bands have heads in their R branches and, although there is considerable overlapping of the individual bands, the heads corresponding to different vibrational excitation form a well

resolved progression. The amount of absorption by CO as a function of spectral type is shown in Fig. 2. It is not until about KO that we begin to see absorption by carbon monoxide. At spectral type M6 the CO absorption appears to reach a plateau. The super-giants, shown by open circles, show considerably more carbon monoxide absorption than the giant stars of the same spectral type.

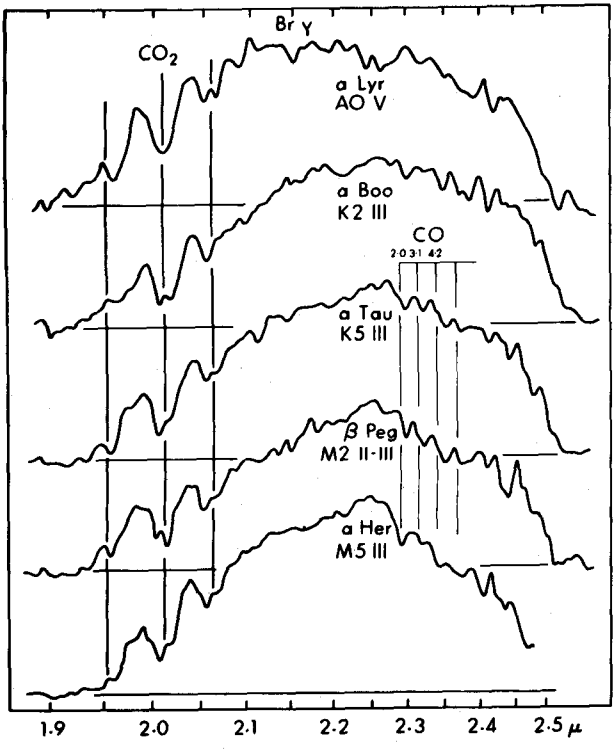

Fig. 1. Interferometric Spectra of α Lyr, α Boo, α Tau, β Peg and α Her. The carbon monoxide bands can be seen in α Tau and later type stars.

Spectra of the Mira-type variable star R Leo are shown in Fig. 3. We find that the CO absorption does not vary appreciably, while water vapor is considerably stronger at minimum. We have made measurements of the H_2O and CO absorption at different phases of the star; the results

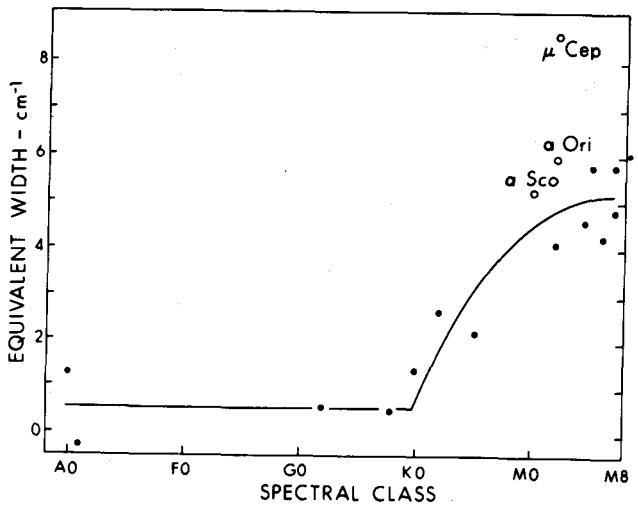

Fig. 2. The combined equivalent width of the 2-0 and 3-1 heads of the CO bands for stars of different spectral type. Carbon monoxide appears only beyond type KO.

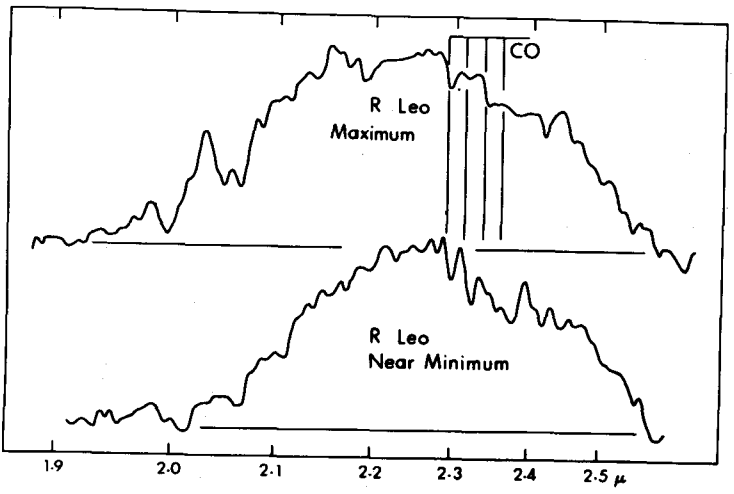

Fig. 3. Spectra of the Mira variable star R Leo at maximum light and just preceding minimum light.

are shown in Fig. 4. The water vapor shows a significant variation, with a minimum at maximum light; on the other hand the CO does not vary appreciably. Such behavior is to be expected since from calculations of the dissociation of molecules (Tsuji, 1964) the abundance of CO has reached a plateau for temperatures below 3000°K but the H_2O abundance depends on the temperature for temperatures above 2000°K.

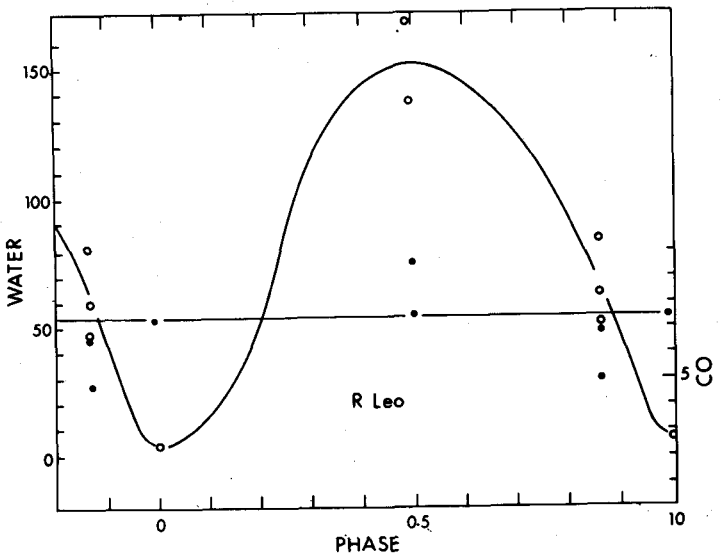

Fig. 4. Strengths of the water absorption and CO absorption with the phase variation for R Leo. The open circles are the strength of the water band and refer to the scale on the left. This scale gives the equivalent width of that part of the band between 4500 and 5000 cm^{-1} assuming that there is no water absorption at 4500 cm^{-1}. For determining this absorption the averaged spectra of stars of mean type MIII was used for an envelope with no stellar water. The filled circles show the CO equivalent widths and refer to the scale on the right. The units for both scales are cm^{-1}.

The spectrum of χ Cyg however, does show a variation of the CO absorption, as seen in Fig. 5. The upper spectrum, which shows the greatest amount of carbon monoxide, was taken somewhat before minimum light, while the lower spectrum, taken somewhat prior to maximum light, shows the least CO. The variation of the CO, as well as the variation of water, is shown as a function of the phase of the star in Fig. 6. We see that there apparently is a complementary relationship between the water vapor and the carbon monoxide as a function of the phase of the star. Maximum carbon monoxide and minimum water occur definitely before maximum light, and the reverse occurs before minimum light.

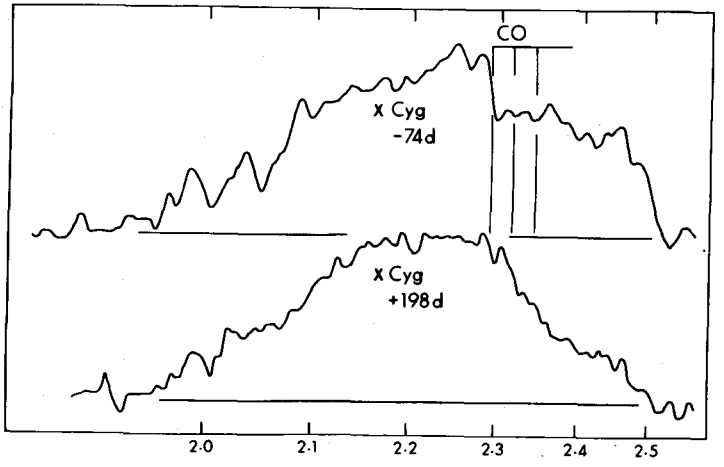

Fig. 5. Spectra of χ Cyg showing maximum CO absorption and minimum water absorption (upper spectrum) and minimum CO absorption and maximum water absorption (lower spectrum).

Of particular interest is the strength of the carbon monoxide bands in carbon stars. In Fig. 7 are spectra of UU Aur, T Lyr and RS Cyg. It can be seen that RS Cyg exhibits rather strong carbon monoxide absorption while in the other carbon stars the CO absorption is considerably weaker. We have also been looking for absorption by vibrational transitions in the CH molecule. The vibrational

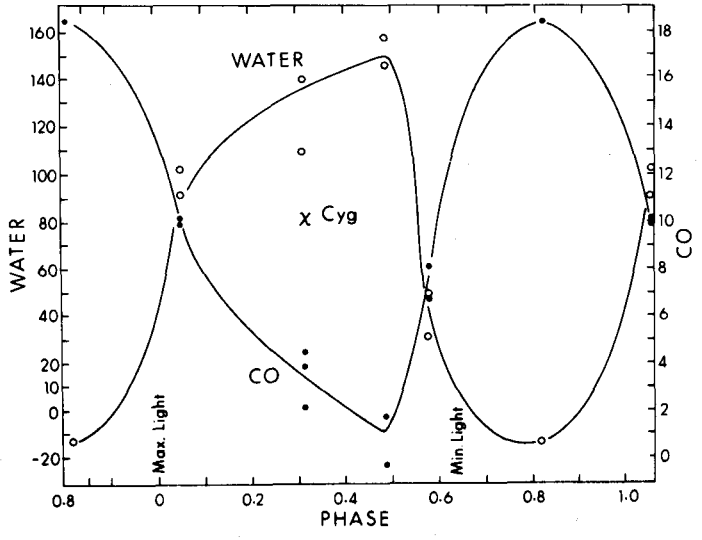

Fig. 6. The variation with the stellar cycle of water and carbon monoxide for the Mira variable χ Cyg. The meanings of the symbols and the units for equivalent widths are the same as for Fig. 4.

spectrum of this molecule has not been previously observed in the laboratory. We have computed the location of spectral lines on the basis of the molecular constants of the ground electronic state. The vibrational spectrum is an unusual one for a diatomic molecule in having Q branches. The existence of a net orbital angular momentum of the electrons about the internuclear axis in the electronic ground state makes $\Delta J = 0$ an allowed transition. The Q branches will be prominent features of the CH spectrum at the origin of the bands and they will occur at about 5080, 4825, 4570 and 4310 cm^{-1} for the 3-1, 4-2, 5-3, and 6-4 bands respectively. At our resolution individual lines of the branches will not be resolved, but the net effect of the clump of lines should be as noticeable as

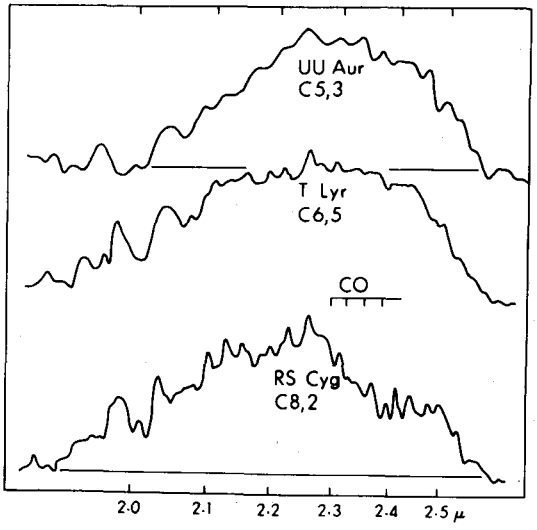

Fig. 7. Spectra of carbon stars UU Aur, T Lyr, and RS Cyg.

the R-branch heads which will be at 4965, 4696, and 4428^{-1} for the 4-2, 5-3, and 6-4 bands respectively. However, nothing definite is discernable at these locations.

REFERENCES

Boyce, P. B. and Sinton, W. M., Sky and Telescope **24**, 78 (1965).

Tsuji, T., Ann. Tokyo Astro. Obs. **9**, No. 1 (1964).

DISCUSSION

N. Woolf: It is quite difficult to obtain the abundances of any of these molecules from the strength of the band, because the band strength depends largely on the turbulent velocity in the atmosphere, and gives little information about the abundance.

W. M. Sinton: Do you think that effects of the turbulent velocity can explain the variations in χ Cygni?

N. Woolf: In that case we have a very different situation. Here one is really seeing the atmosphere blocking different molecules at different times. The very fact that there is a difference in the way the water vapor and the CO vary suggests that it is more than just a matter of turbulent velocity.

P. M. Solomon: The fact that you are seeing such strong CH bands indicates strong turbulent velocities in these stars. CH lines are normally very far apart; in order to have an effectively continuous opacity there must be very high turbulent velocities.

W. P. Bidelman: Is it at all possible to find out anything about CO_2 in these stars? Some of the variation in the CO absorption might be due to the formation of CO_2.

H. Spinrad: That kind of equilibrium would not explain these variations except at lower temperatures.

P. M. Solomon: With regard to CO absorption, at low temperatures the H_2O provides the dominant opacity even where the CO bands occur. Although you may have the same amount of CO in the atmosphere, it will not appear in the spectra because H_2O absorption is much stronger in that region.

W. M. Sinton: That is true, but then one has to explain the result for R Leo, where the H_2O opacity appears to vary while the CO opacity does not.

5

SPECTRA OF COOL STARS

Hyron Spinrad and Robert F. Wing

We have made some observations of cool stars in the near infrared spectral region. We will first describe high-dispersion photographic spectrograms obtained at the coudé focus of the Lick Observatory 120-inch telescope and then turn to lower resolution observations made with a photoelectric scanner.

A series of spectra of the variable star Mira is shown in Fig. 1. The original dispersion was 16 Å/mm in the one-micron region. Virtually all of the features seen are of terrestrial origin (spectra a and f are plates of Arcturus which show only the terrestrial water lines). However, one can also see in the Mira spectra the S(3) line of molecular hydrogen. This quadrupole transition has a very low f-value; the strength of the line indicates that the H_2 abundance is enormous. The calculated value is about 6×10^{26} molecules/cm^2 at minimum light. The strength of the line clearly varies with phase, with maximum strength occurring near minimum light. The shift in wavelength is the result of the orbital motion of the earth, which here we use to good advantage—the rest position of the H_2 line coincides with a strong set of terrestrial water lines. Figure 2 shows a spectral scan made by Münch shortly after spectrum d of Fig. 1 was obtained. The equivalent width is on the order

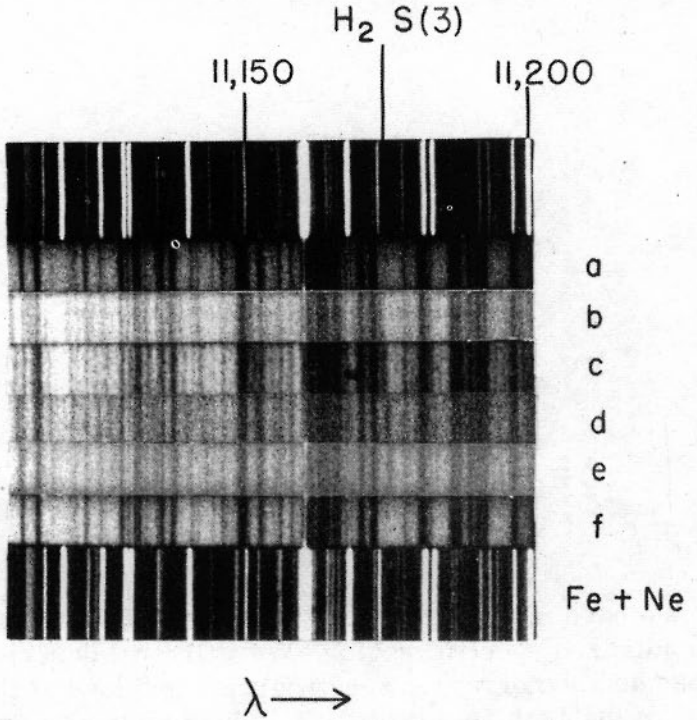

Fig. 1. A series of spectrograms of Mira (b-e) showing the S(3) line of molecular hydrogen. Spectra a and f are of Arcturus and serve to identify the terrestrial water lines. The change in the earth's orbital motion in the direction of Mira causes a progressive displacement of the H_2 line relative to terrestrial features from b to e. Plate c, on which the H_2 line is strongest, was taken near minimum light (Spinrad 1966).

of 0.6 Å, and it can be seen that the half width of the S(3) line at this phase is at least a little more than 1 Å. There is definitely a width to the line; this is probably the first time that a molecular hydrogen quadrupole line has been seen to be broadened. It is most probable that the line is broadened extrinsically by turbulence or stream motion in the atmosphere of Mira.

The existence of water vapor can be illustrated by making use of the large Doppler shift for Mira. Figure 3 shows a high-dispersion spectrum with four lines from the

high-excitation part of a water vapor band centered at 11,400 Å. The terrestrial and star lines are separated by the Doppler shift. However, this is an uneconomical way to learn about water vapor in stars because of the time required to obtain such spectrograms.

We are trying to use some of this data quantitatively. Line saturation is normally an annoying problem; however, we now have sufficient dispersion to measure the line profiles, so that it is not necessary to calculate them. We have determined the abundances to be used in molecular equilibria calculations from direct measurements of line widths. However, the water vapor lines in the spectra cannot be measured precisely because of the large turbulent velocities on

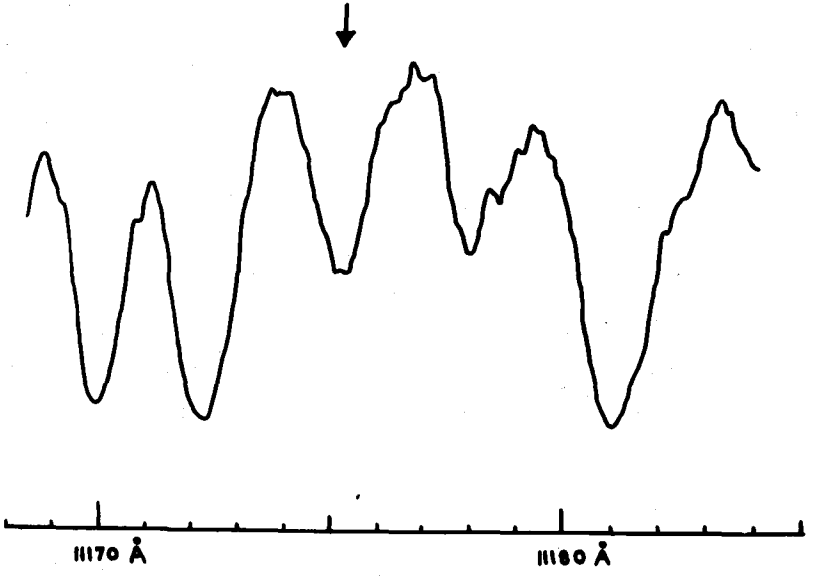

Fig. 2. A photoelectric scan of the post-minimum spectrum of Mira obtained by G. Münch at Mt. Wilson. The arrow indicates the molecular hydrogen S(3) line, which is broader than the instrumental resolution of 0.6 Å; the other features are due to water vapor (Spinrad 1966).

Mira. For the turbulent velocity we have derived a value of approximately 30 km/sec, which is well above the velocity of sound; perhaps we are looking at some kind of stream motion rather than macroturbulence in the atmosphere.

With absolute H_2O and H_2 abundances from the high-dispersion spectra, and using available data on CO, CN, TiO and ZrO, Spinrad and Vardya (1966) have attempted to establish a set of elemental abundances. In this way we avoid the pitfalls involved in pinning down atmospheric temperatures for these stars. We have found that the normal M stars, as exemplified by Mira, have a ratio O/C = 1.05, with an uncertainty of a few percent. The N/C ratio is not well established, but it is probably about 2. The O/H ratio can only be determined from CO observations. The CO abundance in Mira is perhaps a little less than α Orionis, so that O/H $\approx 10^{-3}$ to 10^{-4}, which is roughly consistent with the solar value. The most significant factor, however, is the ability to determine the ratio of oxygen to carbon with heretofore unobtainable precision.

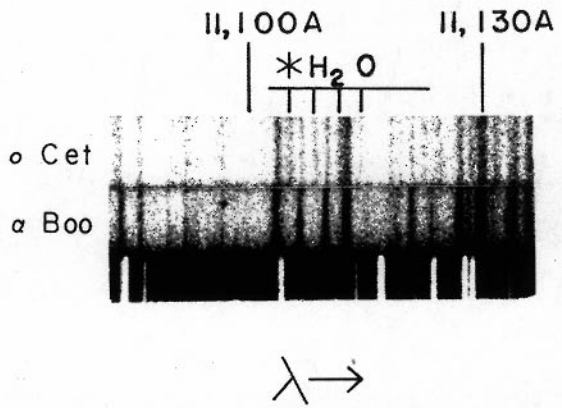

Fig. 3. This comparison of Mira (above) and Arcturus (below) demonstrates the presence of steam in the atmosphere of Mira. The large geocentric velocity of Mira separates these high-excitation water lines from their terrestrial counterparts. Mira was within two weeks of minimum light when this plate was taken on September 24, 1964. Original dispersion 16 Å/mm.

We will conclude our discussion of high-dispersion spectra with an examination of the first high-dispersion slit spectrogram of an infrared star, the Taurus source, taken at maximum light in August 1965 (Fig. 4). The dispersion in this case was 32 Å/mm. The exposure was set at an hour and a half, and the plate was overexposed by a factor of 3. No further spectrograms were obtained because the star was not visible at the coudé slit. We have compared the Taurus object spectrum with that of χ Cygni at an advanced phase. Both spectra exhibit atomic lines of neutral titanium and singly-ionized strontium. There are also vanadium oxide band heads near 10,500 Å which are weaker in Taurus than in χ Cygni. The latter is in fact a weak-banded star as compared to the oxygen-rich Mira variables of the same temperature. There is, however, a TiO band at 11,032 Å which can be seen in χ Cygni but is absent in the Taurus source. We also observe the Paschen γ emission line of hydrogen, which is a rather common feature of Mira variables at maximum and post-maximum phases. In fact the lines Pγ and Hδ exhibit the same behavior except that Pγ is very broad. For the Taurus spectrum, the width corresponds to a velocity of between 60 and 80 km/sec.

We will now consider some lower resolution results for fainter stars in the same part of the spectrum. The instrument used was a photoelectric scanning device designed by Wampler, mounted at the prime foci of the Lick

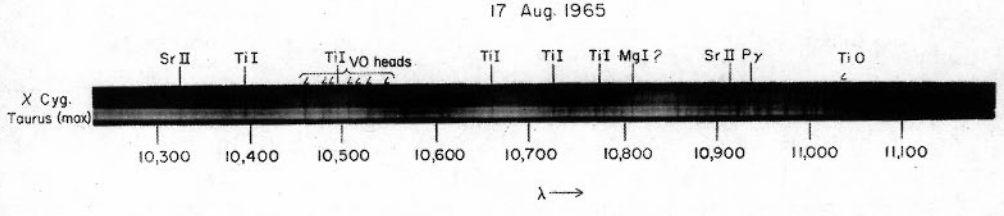

Fig. 4. Spectrograms of χ Cygni at phase +134^d (above) and the Taurus infrared star near maximum (below). The molecular band strengths yield spectral types of M9 for χ Cygni and M7 for the Taurus object. Note the emission at Pγ in the Taurus object (Wing, Spinrad and Kuhi 1967).

36-inch and 120-inch reflectors. Two typical scanner spectra are shown in Fig. 5. We observe at discrete wavelengths rather than continuously across the spectrum, and the continuum has been interpolated between the points. These stars are standards of types M3 and M7. The water is largely, if not entirely, of terrestrial origin in both spectra; CN and TiO are detectable at M3, TiO and VO at M7.

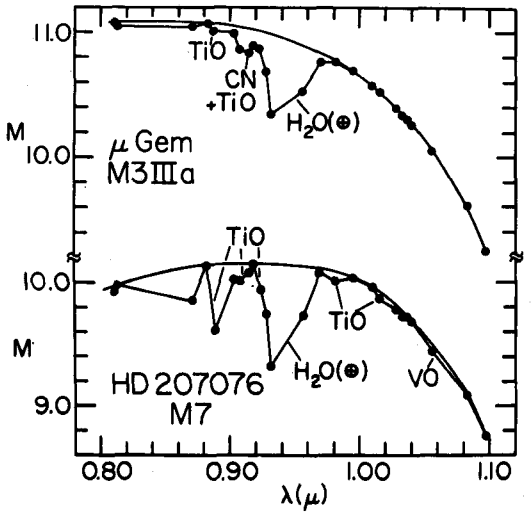

Fig. 5. Scanner spectra, on the instrumental system, for typical stars of types M3 and M7. A magnitude scale is used for the ordinate. Note the change in the strength of the TiO band near 0.88μ. The depression from 0.92 to 0.97μ is the ρ band of terrestrial water (Wing, Spinrad and Kuhi 1967).

Figure 6 compares the spectra of Mira at minimum light and the Taurus object near maximum. Mira exhibits very strong absorption by TiO and VO (spectral type M9), and rather substantial H_2O. The Taurus object, as one can judge from the curvature of the spectrum, is of the same temperature class as Mira. TiO, VO and H_2O are present in the spectrum but are weaker than in Mira, indicating spectral type M7. This scan of the Taurus object was made simultaneously with the coudé spectrogram shown in Fig. 4.

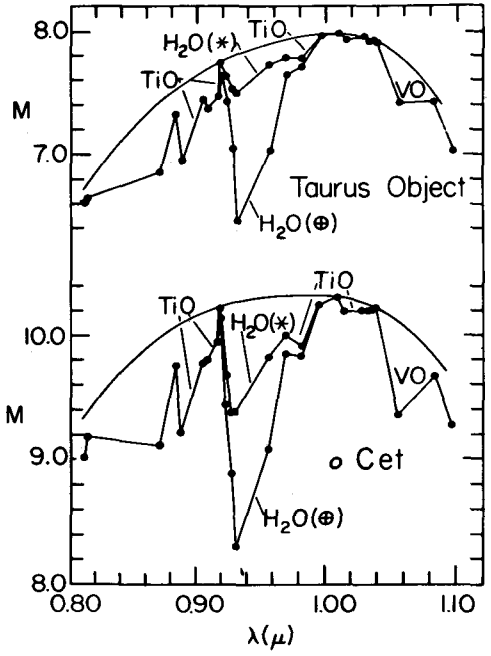

Fig. 6. Scanner spectra of Mira at minimum light and the Taurus infrared star near maximum, both obtained on August 17, 1965. Scans of control stars have been used to separate the terrestrial and stellar components of the water depression (Wing, Spinrad and Kuhi 1967).

A more recent scanner spectrum, taken as the Taurus object was approaching minimum light, is shown in Fig. 7. In this case the control star was the hot supergiant ϵ Orionis, which has been used to give a good measurement of the terrestrial H_2O. The Taurus object spectrum here shows large H_2O, TiO and VO depressions, corresponding to spectral type M9.5, and an energy distribution which is much redder than in the previous spectrum. We don't call a spectrum M10 unless its oxide bands are substantially stronger than those shown in Fig. 7. So far we have observed only five different stars which at minimum light meet our requirements for spectral type M10; these are the Taurus object

itself, R Cassiopeiae, W Andromedae, RU Herculis and TX Camelopardalis.

The Cygnus source is quite atypical (Fig. 8). Besides its extreme redness, it has surprisingly weak VO and TiO bands, corresponding to spectral type M6. No H_2O, CN or ZrO is visible.

To help us gain some insight into the properties of cool

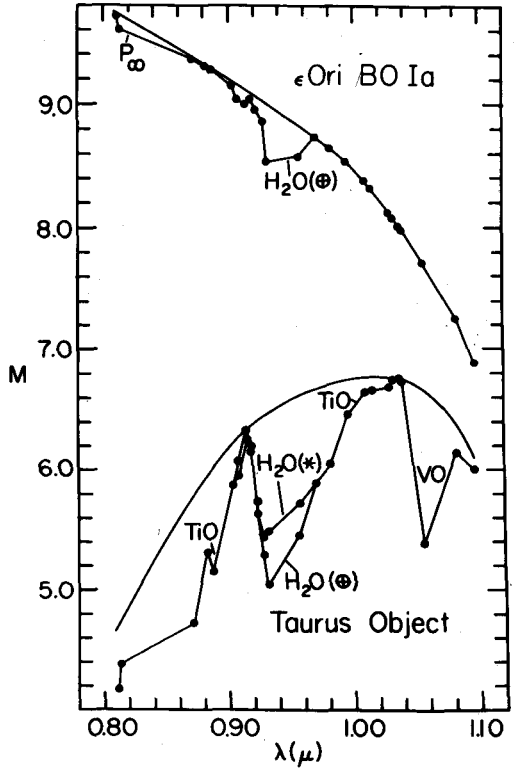

Fig. 7. Scanner spectra of the hot standard ϵ Orionis and the Taurus infrared star on February 9, 1966, an unusually dry night. The scans were made consecutively at identical zenith distances; the water depression in the Taurus spectrum is mostly stellar. The spectral type derived from this scan of the Taurus object is M9.5 (Wing, Spinrad and Kuhi 1967).

stars, we have prepared the diagram shown in Fig. 9. Stars have been plotted according to their temperature index and the band strength of the titanium and vanadium oxides. The band strength is determined by the depths of the bands and is measured in magnitude units with band strength increasing upwards. The scales have been normalized to spectral type AO. The near-infrared temperature index gives a distorted scale in which the difference between the late M types is much larger than the difference between spectral types A and early M.

First of all, we note that there is an M star sequence extending from W Andromedae and R Cassiopeiae, cool stars with very strong bands, down to the M2 stars, where the bands are just barely visible. There is not a great deal of scatter along this sequence, but the scatter that does exist is likely to be real. Variable stars will migrate up and down the sequence, according to their phase. R Andromedae, a well-known S star, clearly lies to the right of the M-star sequence; that is, for a given temperature index, the bands

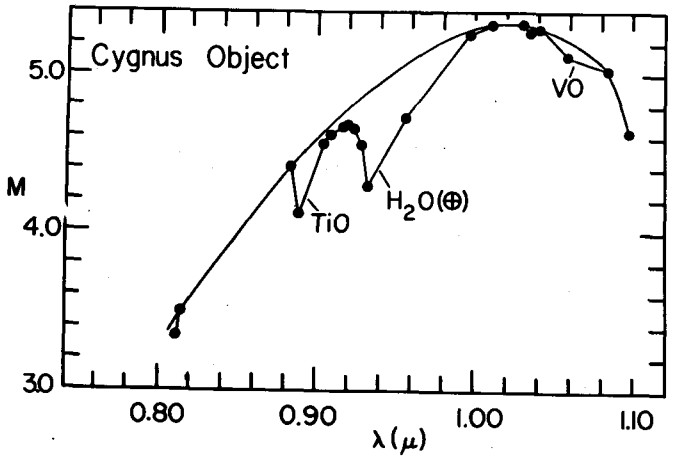

Fig. 8. The near-infrared spectrum of the infrared star in Cygnus. The star is obviously abnormal, with very weak oxide bands for the redness of its energy distribution (Wing, Spinrad and Kuhi 1967).

are far weaker than for a corresponding M star. At minimum light R Andromedae is as red as any normal M stars in the diagram, yet the band index corresponds only to M7.

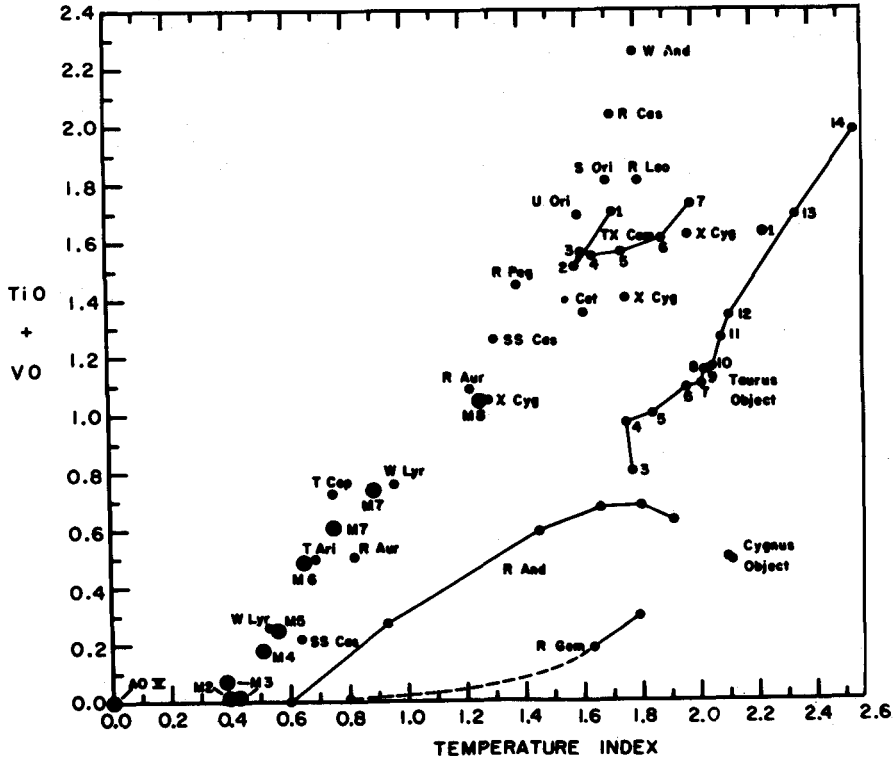

Fig. 9. The sum of the scanner indices of TiO and VO band strength is plotted against an index of the near-infrared continuous energy distribution. Both coordinates are on a magnitude scale, with the origin specified by spectral type AO V. Circled dots refer to standards of spectral classification. Most of the stars fall upon a well-defined and nearly linear sequence, while the S stars R Andromedae and R Geminorum and the infrared stars in Taurus and Cygnus fall well below it. Lines connect different observations of the same variables (Wing, Spinrad and Kuhi (1967).

Thus R Andromedae is very weak in the oxides; this is probably a result of the fact that the O/C ratio is very low—perhaps 1.02 or 1.03. Oxide formation is thus inhibited by the lack of free oxygen. R Geminorum, usually called a "pure" S star, is an even more extreme case. However, we should keep in mind that a large amount of interstellar reddening will also move stars horizontally to the right in this diagram.

The Cygnus object, which lies very far from the M sequence, has shown no significant variability in light, color or band strength. It therefore is not a Mira variable. On the basis of far-infrared photometry it is the reddest object in the sky that is known from spectroscopic observations to be a star. (The fact that the Taurus object at minimum light comes out even redder in our color index may simply mean that that we have underestimated the effect of blanketing on this index in the case of M10 stars). It has been suggested by Johnson that the Cygnus object is a very luminous star of type M6 which is very heavily reddened. On the other hand, it could be some kind of very cool source having a low O/C ratio. For example, it is clear from the diagram that a cooler version of R Geminorum would have the same characteristics as the Cygnus source. At present we have no way to choose between these possibilities; with either interpretation, the Cygnus object is unique.

The Taurus source is now fairly well understood. It is definitely a Mira variable; the temperature varies from the equivalent of an M9 star at maximum to a value of perhaps 1200°K at minimum. The band strength changes enormously, but at all phases it is well displaced from the M sequence in Fig. 9. This displacement alone indicates that the star either is reddened or has a low O/C ratio like the S stars. However, we also have a measurement of the H_2 abundance from the coudé spectrogram; when the Taurus object was at maximum light, the H_2 abundance was about the same as that of Mira at minimum. The infrared colors of Mira at minimum and the Taurus object at maximum are likewise about the same. Since the H_2 abundance should be a good index of temperature, there is no reason at all to

believe that the Taurus object is heavily reddened by interstellar or circumstellar material. We conclude that the Taurus object has an O/C ratio similar to that of R Andromedae.

It is becoming clear that observational studies of cool stars will rely more and more heavily upon measurements in their infrared spectra. Coudé spectrograms are useful for examining weak features in the brighter stars, especially features which can be seen only when a favorable geocentric radial velocity displaces them from terrestrial absorption lines, and for measuring line profiles; photoelectric scans can be used to provide color temperatures and molecular band strengths down to quite a faint magnitude limit. The infrared amplitudes of Mira variables are sufficiently small (typically 2 mag at one micron) that observations can be obtained almost as easily at minimum light as at maximum. Perhaps most important, infrared studies of cool stars provide information about several of the most abundant molecules in late-type atmospheres.

REFERENCES

Spinrad, H. Astrophys, J. **145**, 195 (1966).

Spinrad, H. and Vardya, M. S. Astrophys, J **146**, 399 (1966).

Wing, R. F., Spinrad, H., and Kuhi, L. V. Astrophys, J. **147**, 117 (1967).

DISCUSSION

F. J. Low: With regard to the Cygnus object, there is one other fairly essential point. The star VI Cygni No. 12 has a temperature of at least 10, 000°K and is about 3° from the Cygnus object. If you derive an extinction curve for this star, the curve is almost identical in every respect to the extinction curve you would need to put in front of an M6Ia star to make it look like the Cygnus object.

H. Spinrad: The Cygnus source would still be an unusual object, since it would be the only M6Ia star that we know of. However, if this interpretation is correct, it would be worthwhile to look at face-on galaxies where the reddening might not be too large. On an infrared photograph, possibly even at one micron, such stars might well be the outstanding objects of the spiral arms.

L. H. Aller: For what stars do you obtain an O/C ratio of 1.05?

H. Spinrad: We get this value for α Orionis, Mira and R Leonis. The last two are, as far as we know, typical of the pure M-type Mira variables.

6

INFRARED INTENSITY DISTRIBUTION AT THE SOLAR LIMB IN THE 20-MICRON REGION

R. W. Noyes

We have been studying limb darkening in the sun in an attempt to determine the position of the point at which the solar temperature goes through a minimum, as well as the details of the subsequent rise in the overlying chromosphere. The study of limb darkening has the advantage over making radiometric measurements of giving a relative measurement from center to limb. We can then obtain the slope of the temperature curve in the atmosphere directly, without having to resort to very careful calibration. Since the results are only relative, however, we cannot obtain the temperature itself.

There are well-known advantages to using the infrared to measure limb darkening. First, the opacity beyond 1.6μ varies as λ^2, where λ is the wavelength, so that the optical depth (say at 5000 Å) to which we see will decrease as $1/\lambda^2$. Then by the Eddington-Barbier relation, the value of cos θ for which we see radiation from a particular depth increases as λ^2. Furthermore, near the limb the distance in seconds of arc inside the limb at which we see to that depth varies as $\cos^2 \theta$, or as λ^4. For example, that level which is seen one second from the limb at 10 microns will be seen 40 seconds from the limb at 25 microns. Consequently the

requirements on spatial resolution are much less severe in the far infrared.

Most of the present information on the temperature structure near the minimum is derived from observations of the continuum in the visible part of the spectrum. The temperature distributions that we would expect to measure on the basis of two models are illustrated in Fig. 1. The temperature variation as a function of optical depth at 5000A is shown in Fig. 1(a); the Pagel (1961) model is characterized by a rather steep drop to a minimum temperature of about 4300°K, with a sharp rise to a plateau temperature of approximately 6000°K. The Utrecht reference model (Heintze et al., 1964) gives a much smoother curve with a broader, shallower tempeature minimum. Figure 1(b) shows the intensity distribution near the extreme solar limb expected at 25 microns for these two models. It can be seen that quite a bit of limb brightening is expected for both models. This is especially true for the Pagel model, for which the limb brightening is very large, reaching a value of 1.2 at one second of arc from the limb. The limb brightening results from the sharp temperature rise into the chromosphere, and would be visible at 25 microns as a bright ring at the limb. (Since the radius of the sun is about 1000 seconds of arc, Fig. 1b shows only the outer 5% or so of the solar disk.). The curves pass through a gradual flat minimum at about 200 to 300 seconds of arc inside the limb, so that the limb brightening should easily be visible if in fact either of these models is correct.

Recently, Beckers, Low and I began a program of measuring the limb intensity in the infrared; thus far we have made low resolution measurements at 24.3 microns and higher resolution measurements at 22.5 microns.

The 24.3μ observations were obtained in March, 1966 at the five-foot telescope of the University of Arizona's Lunar and Planetary Laboratory, using a germanium bolometer as detector. A chopper sampled light from two five-arc sec circles on the solar image separated by 18 arc sec; thus the resulting AC signal nearly corresponded to the spatial derivative of the solar intensity distribution. A layer of high quality black polyethylene was stretched over

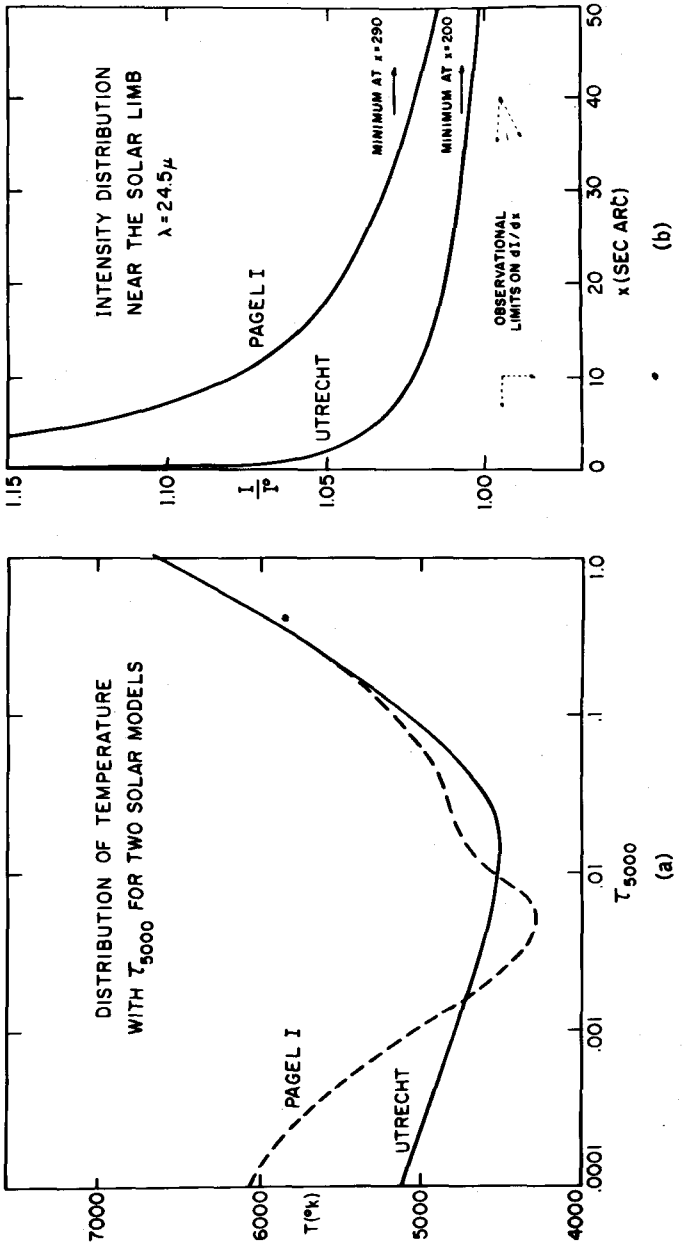
DISTRIBUTION OF TEMPERATURE
WITH τ_{5000} FOR TWO SOLAR MODELS
PAGEL I
UTRECHT
T(°K)
7000
6000
5000
4000
.0001
.001
.01
.1
1.0
τ_{5000}
(a)
INTENSITY DISTRIBUTION
NEAR THE SOLAR LIMB
λ = 24.5μ
PAGEL I
UTRECHT
$\frac{I}{I^0}$
1.15
1.10
1.05
1.00
MINIMUM AT x=290
MINIMUM AT x=200
OBSERVATIONAL
LIMITS ON dI/dx
0
10
20
30
40
50
x (SEC ARC)
(b)

Figure 1

the telescope to prevent excessive heating of the optics; scans of Venus with and without the polyethylene showed no noticeable degradation of the image. In principle we should have been able to unfold the data to yield a resolution of 5 arc sec, given by the size of the chopped aperture, but this was impossible, mainly due to the presence of considerable noise in the data. This noise was due to sky transparency fluctuations, which are not eliminated by this chopping system. At 40 arc sec inside the limb, we find the slope to be -.05% ± .07% per sec of arc. Closer to the limb, the broad instrumental profile prohibits our assigning a definite value to the slope; nevertheless, we can show from the direction of asymmetry of the derivative about the limb position that limb darkening persists at least to 10 arc sec from the limb. Such a result already seems in definite disagreement with each of the two models considered above.

We next tried to improve the precision of these results by carrying out a high spatial resolution infrared observation at the November, 1966 total eclipse of the sun. We set up a twelve-inch f/8 cassegrain telescope at a site on the center line of the eclipse north of Arequipa, Peru, at an altitude of 14,000 feet. The entrance aperture to the detector was now a slot, 1 arc min by 3 arc min, oriented parallel to the moon-sun line and perpendicular to the solar limb. Our filter was a broadband interference filter, cutting on sharply at 20.4 microns and peaking at 22.5 microns. We chopped alternately between a region including a slice of the solar crescent and a region on the dark surface of the moon. Unfortunately thin clouds were in front of the sun on the day of the eclipse, but we were nevertheless able to record the intensity decrease before second contact and increase after third contact well enough to improve considerably the resolution of our earlier observations. Preliminary analysis of these data indicate that the solar intensity distribution at 22.5 microns is essentially flat to within one or two arc sec of the limb. The data and their analysis will be discussed in more detail elsewhere.*

* Proceedings of the Utrecht Study Week in the Solar Photosphere, April 1967. To be published in Solar Physics, 1968.

It appears from our two sets of observations that the temperature minimum of the solar photosphere must be very much broader and extend higher than indicated in either of the two models discussed above. Two arc sec from the limb corresponds to $\cos \theta = 0.06$, so the same height is seen at the disk center at a wavelength $\lambda = 22.5\mu/\sqrt{.06} = 92$ microns. Therefore we do not expect to see the brightness temperature of the sun increase with wavelength for wavelengths less than 100μ. This result is in complete agreement with the findings of Beer that there is no minimum in the curve $T(\lambda)$ for wavelengths less than 50 microns.

REFERENCES

Heintze, J. R. W., Hubenet, H., and deJager, C., Bull. Astron. Inst. Neth. **17**, 442 (1964).

Pagel, B. E. J., Astrophys. J. **133**, 924 (1961).

7

MODEL ATMOSPHERES FOR COOL STARS*

Owen Gingerich

The first serious attempt to construct nongray model stellar atmospheres for cool stars took place a few years ago when Dr. Shiv Kumar and I produced a series of models in the effective temperature range 2500 to 4500°K (Kumar, 1964; Gingerich and Kumar, 1964). Our models, which did not include any sources of molecular opacity, showed an absorption window between the H^- bound-free and free-free at 1.65μ. Because this coincided approximately with the maximum of the blackbody curve for these low-temperature stars, predicted continua showed an unusually sharp peak at 1.65μ. The predictions of these models gave added incentive for the Stratoscope II project to observe the infrared spectra of a group of late-type stars (Woolf, 1965). Those observations showed dramatically the necessity for including absorption from water vapor in the models.

The molecular absorption is, however, only one of the serious problems in constructing these severely nongray models. Another is the treatment of the equation of state, which involves the solution of molecular equilibria as well as a consideration of various atomic contributors of free

*This progress report reviews work done jointly with David Latham and Jeffrey Linsky of the Smithsonian Astrophysical Observatory.

electrons. A further problem is the almost pathological scattering. At low temperatures, and especially for high gravities, virtually all hydrogen is driven into the molecular state. If H_2O and CO absorptions are not included, Rayleigh scattering from molecular hydrogen greatly predominates, and even at 10,000 Å we have virtually a pure scattering situation.

Still another problem is the convective instability, which reaches up to an optical depth of 0.1 (measured at 10,000 Å). The adiabatic gradient is low because of the molecular hydrogen, and becomes especially low as these molecules dissociate. Since at the present time we have not yet incorporated a treatment of convection, we must regard our work as an interesting theoretical experiment, paving the way for, but not yet achieving, realistic models. On the other hand, the gradient should very quickly become adiabatic within the zone of convective instability, and such an adiabatic model may be fairly easily constructed as a limiting case. Although we have not yet carried out this procedure, our previous experience indicates that we should encounter no difficulty in those calculations.

A few crude hand calculations suggest that if the models had adiabatic gradients instead of radiative ones, there would be little temperature change down to optical depth unity at 10,000 Å, and therefore we have reason to hope that the idealized models are not so bad as we might have thought initially.

I should now like to describe a few of the characteristics of the new models at 2500°K that have been constructed by David Latham, Jeffrey Linsky, and myself. These include a more sophisticated treatment of the equation of state and a more careful analysis of scattering than did the models reported 2 years ago. Since very little hydrogen is ionized, most of the electrons are contributed by easily ionized metals. These play an important role in the formation of H^-, which provides one of the chief opacity sources. Altogether 30 atoms have been individually considered as electron contributors; sodium, potassium, and calcium are the principal sources of electrons, but we discovered with surprise that in some regions rubidium is the

third most important source. It would appear that small changes in the metal abundances could affect the structure of these idealized models rather strongly.

For stars with solar abundances the composition of the atmosphere can be established by considering simply the formation of molecular hydrogen—that is, the other molecules have in comparison negligible abundance, although they could affect the structure radically through the opacity. If the water-vapor absorption is included, it is necessary to consider about 10 dissociation equations related to the formation of H_2O. These include, besides water and molecular hydrogen, OH, CO, CO_2, SiO, SiH, MgO, MgH, and TiO. The molecular abundances are found by iteration, and many iterations are required to establish the equilibrium. This part of the program is working, but it would be premature to state any conclusions at this time.

In our idealized case of a radiative model with no absorption from water vapor, with $T_{eff} = 2500°$ and $\log g = 5$, that is, a dwarf or subdwarf, there is a billion times more molecular hydrogen than neutral hydrogen. This means that the principal source of opacity is Rayleigh scattering from molecular hydrogen, and we must analyze the radiation in a highly scattering atmosphere. The scattering iterations become fairly formidable, but using a set of simultaneous linear integral equations as a first approximation, we can get a reasonably accurate solution in about 3 minutes on the IBM 7094. With about half a dozen such iterations with the Avrett-Krook temperature correction procedure, we can achieve a flux constancy of about 1 percent. (In scattering atmospheres it should, perhaps, be noted that the flux constancy is not necessarily a sensitive criterion for the accuracy of a model.)

Incidentally, the abrupt flux maximum at 1.65μ is completely absent in this $\log g = 5$ atmosphere. When the gravity is diminished to $\log g = 3$, the molecular hydrogen is only a thousand times more abundant than neutral hydrogen, and the maximum at 1.65μ is present but not especially pronounced. Consequently, the height of this radiation peak promises to be a sensitive luminosity indicator.

Let me now list somewhat more systematically the

opacity sources used in these models. The most important absorptions are from H^- and H_2^-. At wavelengths longer than 1μ, He^- plays an appreciable role, contributing as much as one third of the opacity at some depths. We are using a polynomial fit to the absorption coefficients obtained for He^- by Somerville (1965). In the ultraviolet, where there is too little flux to matter anyway, the bound-free continuous absorption from neutral metals predominates. As indicated previously, the absorption from all of these sources may be considerably less than the Rayleigh scattering from neutral or molecular hydrogen, or, near the surface, from electron scattering.

In addition to these continuous opacity sources that we have used, we ought to worry about absorption from lines or bands. Just because there is heavy blanketing in the visual region, especially from TiO, does not necessarily mean that the infrared region is strongly affected. Although the TiO does go on into the infrared, it probably does not have too serious an effect on the structure. On the other hand, the Stratoscope II observations have shown that molecular absorption from water vapor cannot be ignored in realistic models. Unfortunately, until now many of the astronomically relevant parameters have been lacking for the important bands at 1.4 and 1.9μ. The work of Auman (1966) at Princeton, where over two million individual lines are being considered, will eventually help to eliminate this gap in our present knowledge. His preliminary results show that the lines of water vapor are so numerous as to present a continuous absorption rising toward longer wavelengths beginning roughly at 1μ. When the absorption coefficients are considered as a harmonic mean, the principal bands produce variations of 1 or 2 orders of magnitude against the already high continuous background due to water vapor.

In examining our initial models, we see that for log $g = 5$ we have a gas pressure averaging 1 or 2 orders of magnitude more than at the surface of the earth, and for log $g = 3$ we get approximately atmospheric pressure. This means that the laboratory results obtained at atmospheric pressure for some of the water vapor bands are indeed

applicable to these models, and we conclude that the pressure broadening is sufficient to make the principal bands essentially opaque. There may be enough turbulence in a low-gravity supergiant star such as Mira to make the principal bands opaque there also.

Therefore, as an educated guess, we have simulated the water-vapor absorption by a series of infinite opacity blocks at the position of the bands, plus a general additional absorption source at other wavelengths in the infrared taken as proportional to the remaining absorption and scattering opacity. This was not an attempt to build a realistic model, but rather a scheme to learn something about what might be considered a limiting case with the molecular H_2O absorption present.

In the 2500°, log g = 5 model, the temperature more than doubled in the outer photospheric layers, with an enormous change in the molecular-to-neutral-hydrogen ratio, from 10^9 to 10^2. Consequently, the absorption from H^- replaced the scattering from H_2 as the principal opacity source. The gas pressure also decreased, although not enough to vitiate our assumption about the saturation of the principal bands. The shape of the continuum was considerably changed, and the flux maximum reappeared at 1.65μ. Unfortunately, the convective instability was unaffected, and so it is clear that both the problems of convective energy transport and the molecular absorptions must be solved before we can have models that can be confidently compared against observations.

REFERENCES

Auman, J. R., "Opacity of hot water vapor," Astron. J. **71**, 154 (1966).

Gingerich, O. and Kumar, S. S., "Calculations of low-temperature model stellar atmospheres," Astron. J. **69**, 139 (1964).

Kumar, S. S., "Model atmospheres for late-type stars," Inst. d'Astrophys. Liège, Collection in 8°, No. 472, pp. 476-478 (1964).

Somerville, W. B., "The continuous absorption coefficient of the negative hydrogen molecular ion," Astrophys. J. **139**, 192-197 (1964).

Woolf, N. J., "Infrared spectra of stars, planets and the moon from Stratoscope II," Astronomical Observations from Space Vehicles, I. A. U. Symposium No. 23, edited by J. L. Steinberg, pp. 267-273 (1965).

DISCUSSION

R. Weymann: What is the coolest effective temperature for which you can get reasonable models?

O. Gingerich: Using the idealized models without any simulated H_2O we can get down to 2000°K. In trying to get to lower temperatures, we ran into trouble with the opacity routine. I don't believe that there is any reason in principle why we cannot go to lower temperatures, but we have not been successful thus far. If we put in the water-vapor absorption in some fashion, then there is no trouble going down to 1500°K.

R. Weymann: You consider your models to be violently nongray. Have you made any comparisons to see what differences one finds if one assumes a simple gray mean opacity?

O. Gingerich: No we haven't done this simply because the program is set up to calculate everything with respect to the optical depth at 10,000Å, and we have not bothered to form means. It would probably be something worthwhile to look at.

L. H. Aller: In an M dwarf atmosphere with a temperature of about 2500°K, at what optical depth would the main opacity source change from Rayleigh scattering to H^-?

O. Gingerich: At 10,000Å, one would have to go to an optical depth of 1. At this point the opacity may still be 50% Rayleigh scattering. At visible wavelengths, there is even more scattering. For all ordinary purposes, as a rough approximation one can regard Rayleigh scattering as the main source of opacity in these objects—even for dwarf stars. But as soon as you begin to put in the

molecular bands, the temperature is raised sufficiently so that the opacity reverts to H^-.

P. Solomon: In the entire range from 1 to 5 microns, you can expect molecular bands to produce a continuous opacity, because of either the high pressures or turbulent velocities. The bands are completely connected, and you can practically forget about Rayleigh scattering, H^-, or He^-. It is not proper to try to simulate molecular bands by infinite blocks with windows on the side because it still gives a very low mean transmission on the average.

O. Gingerich: Right, but as a rough starting guess it is a reasonably decent assumption to use an infinite opacity block to simulate the band, which is so completely saturated. Furthermore, there are no regions that are completely transparent. In addition to the infinite opacity bands, we introduce in all other regions of the infrared an additional opacity source which is proportional to the remaining opacity.

8

INFRARED ROCKET OBSERVATIONS

Martin Harwit, D. P. McNutt,
K. Shivanandan and B. J. Zajac

When we began our program of rocket observations in the infrared, our first goal was to perform a simple astronomical observation. The simplest experiment would be to look at the sun or moon, which are bright enough so that one does not have to use cooled detectors. However, since we were more interested in sources outside the solar system, we decided that cooling could not be avoided. It became clear that we could not compete (at least in the early experiments) with ground-based stellar observations, so we decided we would concentrate on diffuse sources, which are very difficult to observe from the ground. There are many interesting problems in this category. We would like to make observations on the zodiacal light, for example, or interstellar clouds; eventually we would like to get spectra. At the present stage our aim is to send up a simple instrument which will send back astronomical information. The results will guide our future efforts.

To begin with, one would not include a pointing control in a first rocket experiment; a first generation device is usually fairly heavy, and so is a pointing control. If both are used, the rocket does not get up to suitable altitudes,

and there is a loss of observing time. At best, the Aerobee rockets that we have been flying provide about five minutes of useful observing time. We therefore decided to build a payload which would allow us a slow scan of the sky as the rocket rolled and precessed. Normally, the rocket is given an initial spin to stabilize it on the way up; weights attached to cables are thrown out and the rocket transfers its angular momentum to these weights and slows down. Consequently, there is some means of control on the final roll rate. We were aiming for a roll period of about ten seconds. That is about the best that one can hope to get with this method.

The next consideration is the kind of optical system to be used. It turns out that for diffuse sources, it is not important to have a large mirror. The limiting factor is the available detector size; one can obtain good quality detectors which are 3 to 5 mm in diameter at the largest. It is important to have a fast light-gathering system. We used a f/0.8, 5.5 inch diameter paraboloidal mirror, which for a 3 mm detector defines a ~3° field of view.

If one is going to look at infrared diffuse sources and also try to get absolute levels of background radiation in the sky, it is extremely important to compensate for the infrared radiation given off by the telescope itself and also for terrestrial radiation that may be scattered into the telescope. To protect against scattering it is necessary to carefully blacken the telescope. But once the telescope is blackened, it becomes an infrared (thermal) emitter and this must be compensated for. We decided that it would be easier to avoid an elaborate compensating system by just cooling the whole telescope down to cryogenic temperatures. The easiest coolant to use is liquid nitrogen, which has a high heat capacity, does not evaporate rapidly, and is very easy to handle. The detector that operates efficiently out to the longest wavelengths at liquid nitrogen temperatures is gold-doped germanium, sensitive out to about 7.5μ.

Figure 1 shows the optical configuration. We built a long telescope to discriminate against terrestrial radiation. The earth is a strong emitter in the wavelength range that we decided to look at (1 to 7.5μ). The amount of radiation that the earth emits in this range is of the order of a billion

times greater than what we expected our detector sensitivity to be. We had to be certain that we discriminated against all terrestrial emission up to one part in a billion; in fact we were able to get the required discrimination at 45° above the horizon. Ordinarily, a long telescope tube would necessitate looking along the rocket axis. It was much easier to have a telescope door on the side of the rocket and to use a diagonal mirror. Incident light is chopped at the entrance aperture by a stator-rotor combination. It is then reflected by the diagonal mirror to the paraboloid, and then focussed via a flat secondary mirror onto the dectectors. We used two detectors on the particular flight that we are describing here. One was an indium arsenide detector for the 1-3.05μ range. We have on a different flight also used an indium antimonide detector. The field of view of the detectors was about 3°. A cutaway diagram of the actual instrument can be seen in Fig. 2. At the entrance are a number of blackened beryllium-copper strips. These

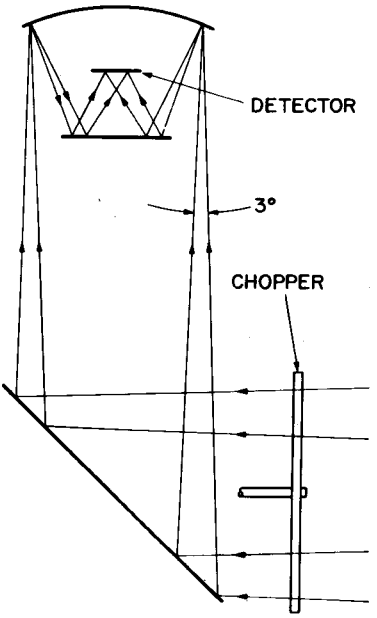

Fig. 1. Optics of telescope.

baffles are initially folded across the entrance aperture of the system, and are cooled down by contact with the liquid nitrogen. This permits a calibration on the ground of a completely dark, liquid nitrogen-cooled telescope. When the telescope door on the rocket is blown off, these baffles pop out to give an additional length of telescope tube to protect against terrestrial emission as well as radiation from the rocket tail fins. All edges on the chopper have been sharpened to knife edges, again to reduce any possible

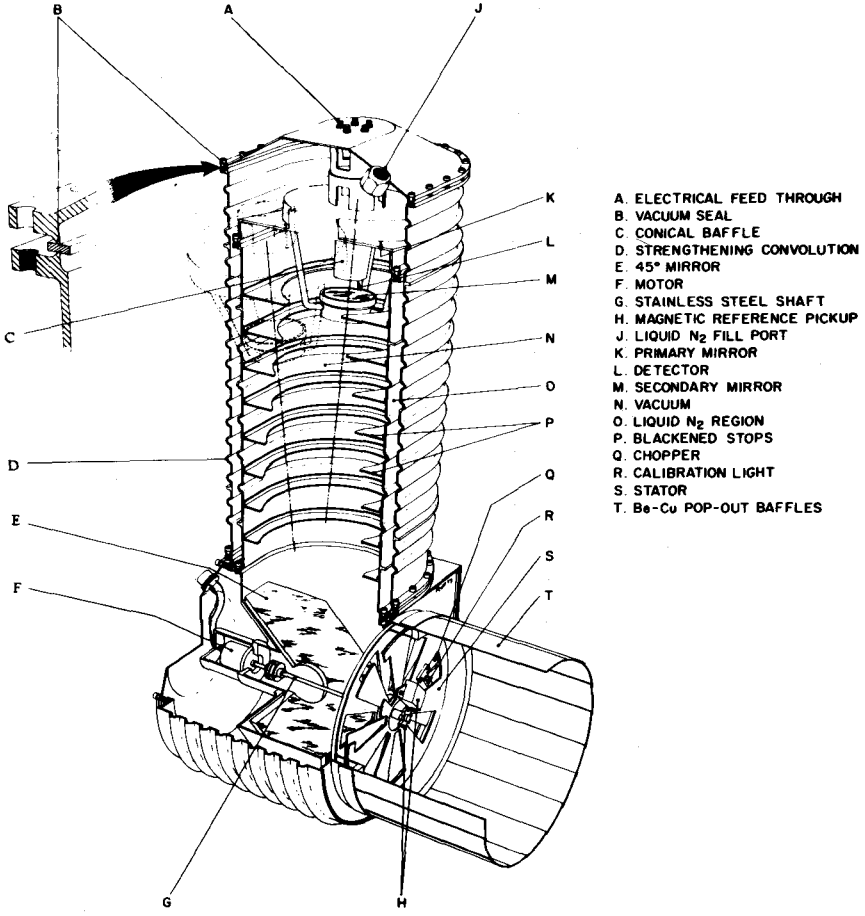

Fig. 2. Design of instrument.

scattering of earth radiation. The device is driven by a small motor which is run at 8000 rpm at liquid nitrogen temperatures. The motor requires special bearings, which were very kindly lubricated for us by Mr. Martin Devine of the Naval Air Research Center in Philadelphia. The bearings are lubricated with molybdenum disulfide. There is additional baffling all along the main telescope tube. This is needed to give the required factor of a billion in light discrimination.

Mounted on the stator is a magnetic pickup that gives a phase reference for the chopping frequency. There is a small calibration light which was turned on at 65-second intervals during flight. This light was used as a secondary calibration standard, to make sure that the detectors were operating properly. We had previously calibrated this light in comparison to a black body. The light operates at two different light levels, each one kept on for one second. This allows us to compensate for any nonlinearities in the detector-amplifier response. To calibrate the system we removed the baffles and put a copper disk blackened with paint across the entrance aperture, thus simulating a diffuse background. This disk was intitially filled with liquid nitrogen, and the detector saw virtually nothing. We would then remove the liquid nitrogen and warm the disk by passing cool gas through. When the disk warmed up to about 100°K the gold-doped germanium would start responding. Consequently, calibration in terms of the black body gave us an idea of the response of the whole system to diffuse radiation. This is, we believe, an effective method of calibration because it takes into account reflection losses, filter losses, detector losses, and so forth.

In Fig. 3 we see a photograph of the device. It is made of stainless steel; the corrugations allow us to build a much lighter structure. At the back (not shown in the figure) is a basket filled with zeolite, an agent which pumps very actively when cooled to liquid nitrogen temperatures. This meant that we were able to disconnect our instrument from any pump or other auxillary system and sustain a four-hour hold, being certain that everything would still be cold when the time for the flight came. The entire device

(Fig. 3) is covered with a section of the rocket made of corrugated aluminum. This provides a vacuum stystem.

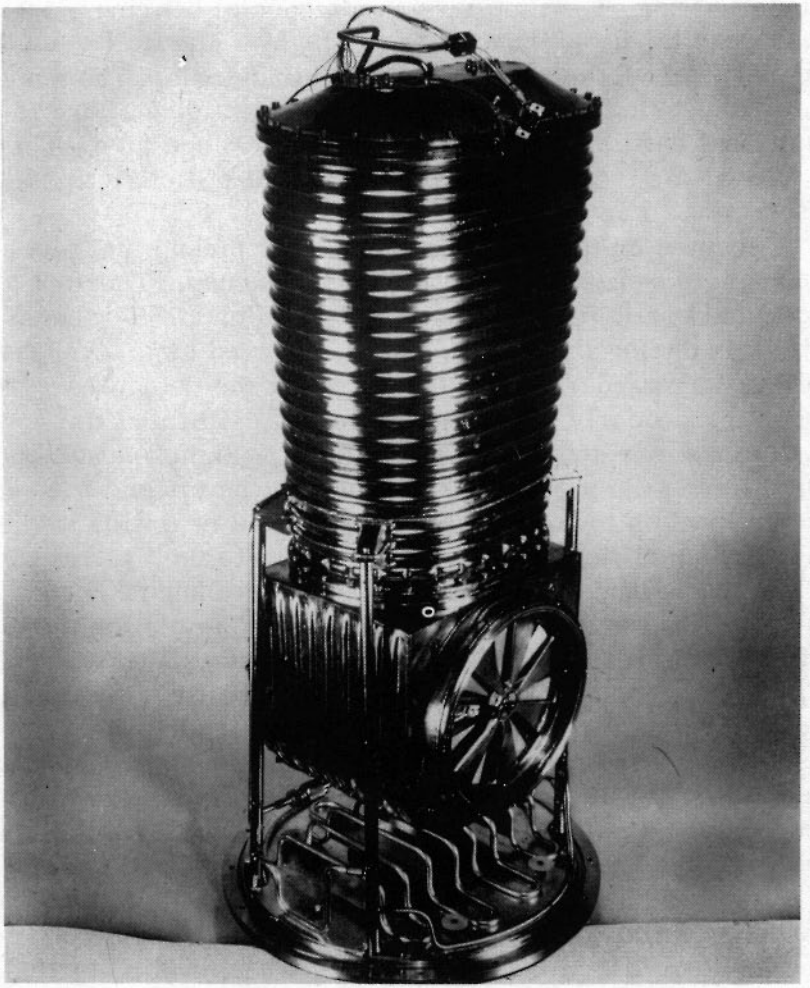

Fig. 3. Photograph showing complete telescope.

The electronics system (Fig. 4) is a phase-sensitive device with low-noise preamplifiers. We used a linear-logarithmic amplifier, through which the small signals expected from the sky were seen linearly, but we could still look down at the earth and obtain signals in the logarithmic range. This gave us some additional confidence that the detectors were operating the same way as before the flight.

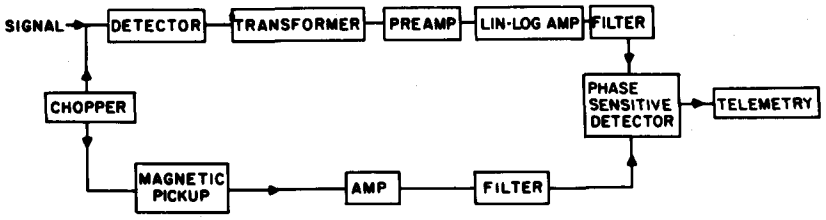

Fig. 4. Systematics of electronic design.

During the actual flight, the telescope made about 24 scans through the sky as the rocket rolled and precessed (Fig. 5). This gave us a reasonable amount of sky coverage. However, in the first flight we were only able to see the earth. The fact that we did not detect any stars is not very surprising in retrospect, because our roll rate was high. Rather than the ~10 sec roll period hoped for, we ended up with a 4 sec roll period. At this roll rate, the amount of time spent looking at any one given star is only about one-fifteenth of a second.

We are able from our data to give an upper limit to the total amount of radiation coming in from the universe. In the 1-3μ range, we obtain an upper limit to the energy density of 2×10^{-12} ergs/cm^3, which corresponds to a flux of about 10^{-9} watts/cm^2-sterad. The upper limit for the 3-7μ range is 2×10^{-11} ergs/cm^3. These values seem rather high as compared to the energy densities in the visible and milimeter ranges. We expect to be able to reduce these limits by a factor of 10 with improved sensitivity of our detectors.

This has been essentially a status report on the first stages of our project. We have described the apparatus in detail because it is quite different from what one uses for ground-based observations. Operation at liquid-nitrogen temperatures has several advantages, among which are additional sensitivity and the fact that there is no need for extensive compensation for background. There are many other observations that we can make, over a larger wavelength range, with more complicated equipment; the addition of pointing controls, for example, will enable us to

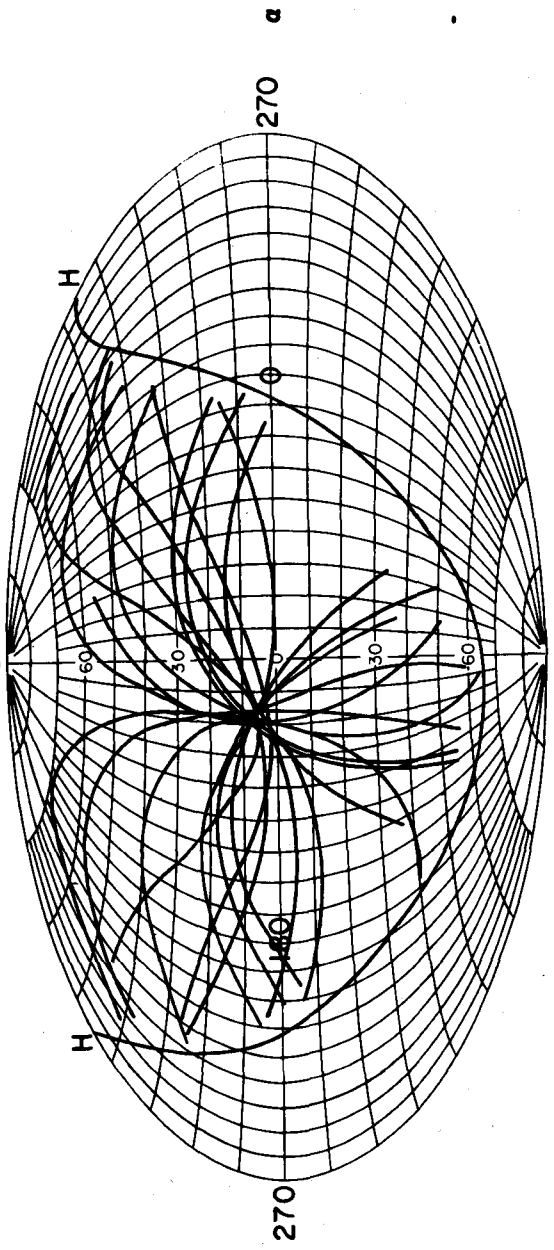

Fig. 5. Tracks of scans made by telescope on first flights.

attain better sensitivity and greater integrating times for more interesting regions of the sky.

Our work was supported by grants from the National Science Foundation, to Cornell University and to the E. O. Hulburt Center for Space Research at the Naval Research Laboratory. NRL was also supported by a contract from the Office of Naval Research.

DISCUSSION

L. H. Aller: Were you able to draw any conclusions about the zodiacal light from these results?

M. Harwit: Unfortunately, no. We fired at a time when we expected to be able to see the zodiacal light rather well—about 4:30 A.M. when the sun was well below the horizon. We did get a very strong signal in the neighborhood of the horizon, but it is not at all clear what we saw. Our observations are consistent with some of the models that predict very strong brightness concentration towards the sun, but on the other hand it could also be a sort of secondary scattering in the atmosphere. I believe that what one has to do is to make sure that the sun is at least 30° below the horizon to eliminate secondary scattering.

We did see the airglow, however; it appeared as a peak in the signal as we crossed the horizon. It is not uniform, however. We didn't get exactly the same thing everytime we crossed the horizon; sometimes the airglow appeared, and other times it did not.

G. Field: What is the point in going to such high altitudes?

M. Harwit: Mainly to avoid the water vapor. We also were afraid of the atmospheric OH emission, which occurs at 60 kilometers.

F. Low: One should be able to do at least as well at an altitude of about 40,000 feet. It is the turbulence in the atmosphere, causing variations in the radiation, and not the atmosphere itself that bothers us on the ground. If you are above the turbulence, you can readily tolerate

the remaining background as long as it is constant.

M. Harwit: This is true, but there are other factors. First of all, if one wants to get information anywhere around 6 microns, as we did with the 3 to 7 micron detector, then the 6.3-micron line is very bad even at balloon altitudes. Furthermore, at these altitudes it is not possible to make a measurement of the absolute amount of radiation coming in to the earth.

9

MEASUREMENT OF THE COSMIC MICROWAVE BACKGROUND WITH INTERSTELLAR MOLECULES

Patrick Thaddeus

Following the discovery by Penzias and Wilson (1965) of an unexpectedly intense and isotropic component of cosmic radio noise at $\lambda = 7.35$ cm, and Dicke's suggestion (1965) that this was the residual of the primordial fireball, we were interested in seeing whether infrared techniques being applied by Hoffmann and Woolf here at the Institute for Space Studies to a balloon sky survey in the vicinity of 300μ could be used to measure the background in the wavelength region 1-2 mm. If the cosmic background does in fact have a 3° Kelvin thermal spectrum this is the region where most of the energy lies, as can be seen in Fig. 1, and since on an extragalactic scale thermal radiation at this temperature possesses roughly one hundred times the energy density of starlight, this is the wavelength region where a measurement of the background intensity deals potentially the most damaging blow to the Steady State Theory. At the same time, due to the millimeter and submillimeter rotational lines of water vapor, the sky opacity is sufficiently high in this region to preclude measurement of the background from the earth's surface.

Since by far the greater part of the atmospheric water vapor lies in the troposphere, however, it is not necessary to ascend to extreme altitudes in order to perform the millimetric background measurement. Clauser and I have

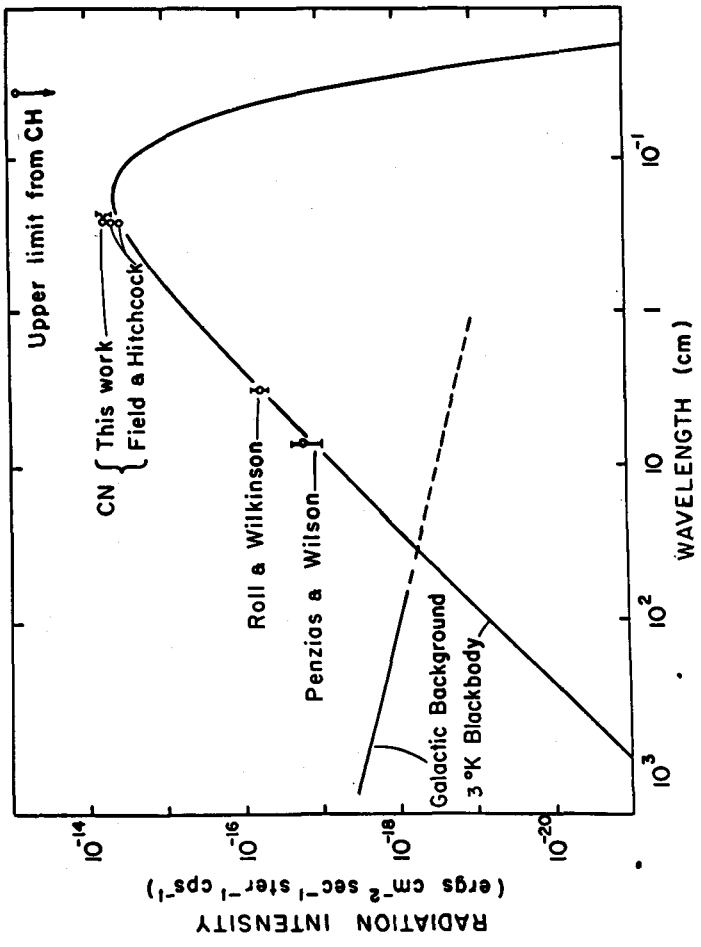

Fig. 1. Measurements to date of the cosmic microwave background.

calculated that even on the basis of pessimistic assumptions of the stratospheric water content such measurements are certainly possible from balloon altitudes (120,000 ft.), and might profitably be attempted from very high altitude aircraft (70,000 ft.). This is an important advantage since a measurement of very cold thermal radiation from an environment which lies near 300°K is inevitably plagued by a variety of small systematic uncertainties, due, for example, to the diffraction of hot thermal radiation into the system (backlobes in antenna terminology), or the emission from windows used to isolate the liquid-helium cooled radiometer from the atmosphere. The usual way, of course, to isolate such effects in laboratory work is to do the measurement under a variety of conditions, permuting optical components, choppers or microwave switches, etc.—a procedure virtually impossible with spacecraft or sounding rockets, and which at best is laborious and expensive with balloons. The frequent damage or misalignment on landing experienced by balloon instruments is a further difficulty.

The detector which Hoffmann and Woolf intend to use in their far infrared sky survey is a helium-cooled germanium bolometer, constructed by Low, and of the type used by him for astronomical observations from 10μ to 1 mm. While Clauser and I were considering the various problems associated with absolute flux measurements with such a detector, Woolf pointed out that the well known interstellar optical lines of CN, CH, and CH^+ already gave information about the density of radiation in space in the millimeter and submillimeter regions. It was his understanding that in all cases the observed lines were strictly resonance transitions, yielding a rotational temperature of 0°K to within the observational uncertainties, and implying in particular from CN that the cosmic background at $\lambda = 2.63$ mm was much less than 3° Kelvin (Figure 2). Since there are theoretical grounds for believing that the background must closely conform to a thermal spectrum if it is of cosmic origin (Weymann 1966), there seemed room for other interpretations than Dicke's of the Penzias and Wilson measurement.

It was at this time that we discovered in the literature

Adams' observation of the R(1) CN transition against ζ Ophiuchi, and McKellar's (1941) calculation of 2.3°K for the CN interstellar rotational temperature, based on Adams' visual estimate that the ratio of the R(0) to R(1) line intensities was 5 to 1. Little significance was attached to this remarkable observation when it was made a generation ago for the following reason: CN is the heaviest molecule observed in the interstellar medium, and its rotational structure is much more compact than that of the hydrides CH and CH^+. Due to the ν^{-3} dependence of the lifetime of electric dipole transitions, it is not unreasonable to assume that the lifetime of the first excited rotational state of CN is comparable in the interstellar medium to the characteristic time of collisional or optical excitation

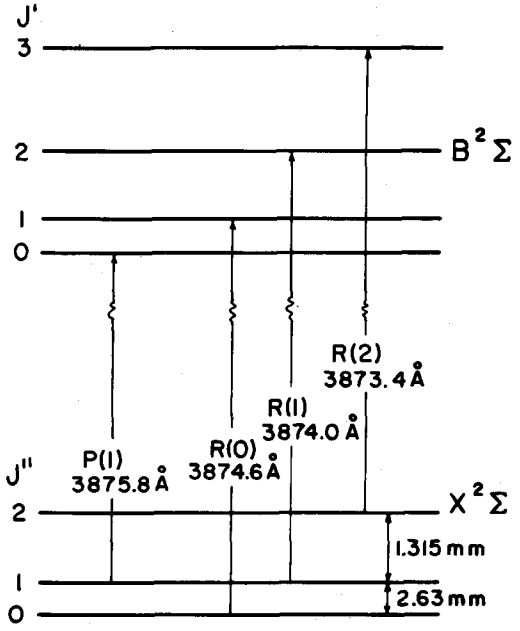

Fig. 2. Lower rotational levels of the CN $X^2\Sigma$ - $B^2\Sigma$ (0, 0) violet band. The doublet fine structure of these levels is too small to be resolved, and is not shown. For a Σ - Σ transition the selection rule $\Delta J = \pm 1$ holds.

of the molecule, which would result in appreciable population of this state.

When we examined this assumption in detail, however, we found that all processes in typical HI regions are in all likelihood at least three orders of magnitude too small to account for the observed CN excitation (Thaddeus and Clauser 1966). Field and Hitchcock (1966) arrived independently at the same conclusion at virtually the same time, as did Shklovsky and Slysh (1966) in the Soviet Union. The former authors in addition measured six excellent plates of ζ Ophiuchi taken by Herbig with the Coudé spectrograph of the 120 inch telescope, and found the CN rotational temperature to lie within the range 2.7-3.4°K. Subsequently Clauser and I also observed the interstellar CN lines of ζ Oph using the Kitt Peak solar telescope and an image intensifier system developed by Livingston and Lynds. The very high resolution grating spectrograph of this instrument makes it a favorable telescope for the study of sharp interstellar lines against bright stars. The result of adding together our two best plates is shown in Fig. 3. The rotational temperature is given in terms of the ratio r of the R(0) to R(1) line strengths, and the molecular rotation constant B, by

$$T_r = 2hB/k \ln(2r) \qquad (1)$$

From the trace shown in Fig. 3 we find $T_r = 3.75 \pm 0.50$°K, in reasonable agreement with the measurements of Field and Hitchcock.

There is one circumstance, however, which I think warrants considerably more observational work on this problem. Slow charged particles—particularly protons—are very effective in exciting the rotational levels of polar molecules, due to the long range of the Coulomb force. We have calculated, for example, that for protons at 10,000°K the cross section for excitation of the J = 1 level of CN is of the order of 10^4 Å^2, leading to the conclusion that this mechanism could be responsible for the observed CN rotational temperature if the molecules lie in typical HII regions (Thaddeus and Clauser 1966). It is worth remarking

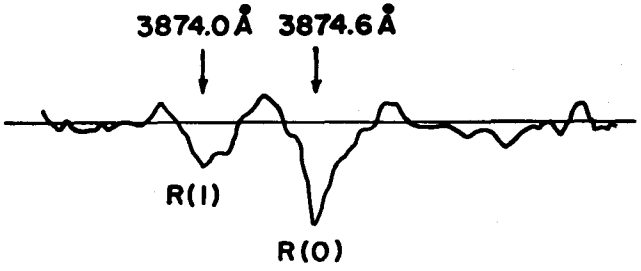

Fig. 3. The CN violet band in the interstellar medium observed against ζ Ophiuchi with the McMath solar telescope.

in this regard that in one instance Münch (1964) has been led to propose that CN molecules are actually being flashed off grains by an advancing ionization front. One way to dispel this possibility is to show that the CN rotational temperature is an invariant from star to star, but since CN is only seen against a handful of stars, (ζ Oph is the most favorable) and the lines are never strong, this would require a great deal of observation with the largest instruments. (It should be noted here that Field and Hitchcock (1966) have also been able to measure the CN rotational temperature against ζ Persei, and find $T_r = 3.0 \pm 0.6°K$) It would also be useful if a good correlation between CN and HI 21 cm velocities could be established.

(Note added in proof, August 1967) By digitizing and numerically synthesizing a number of high-resolution interstellar plates taken at Mt. Wilson, Lick, and Mt. Palomar over the past thirty years by Adams, Dunham, Münch, Herbig and other observers, we have now succeeded in measuring the rotational temperature of CN against a total of eight stars. The uncertainties vary from about 0.2° to as much as 1.0°K, but the result in each case is consistent with a temperature of 3°K. In particular, it should be stressed that in no case where the R(0) line is observed with sufficient strength is an absence of CN excitation found. It is our view that this invariance of the rotational temperature is the strongest evidence that no appreciable

CN excitation is due to charged particles. During the past few months we have also observed the 21 cm profile in the direction of these eight stars, using the 300 foot transit telescope at Green Bank, and find good correlation between the CN and HI velocities, which is consistent with the idea that the molecules are well embedded in an HI region.

The synthesis of all the available ζ Persei observations also seems to be revealing the R(2) CN transition which arises from the second excited rotational level. The signal strength of this line is very weak, but when compared to the R(1) strength it allows a crude estimate of $3.8 \pm 1.0°K$ for the brightness temperature of the background at $\lambda = 1.315$ mm. At still shorter wavelengths, the strong signal-to-noise (about 50:1) of the synthesized CH and CH^+ interstellar lines of ζ Ophiuchi allow the following upper limits to be placed on the background temperature: $T(560\mu) < 5.0°K$ (from the 4300 Å CH line), and $T(350\mu) < 10.7°K$ (from the 4232 Å CH^+ line).

REFERENCES

Adams, W. S., Astrophys. J. **93**, 11 (1941).
Field, G. B. and Hitchcock, J. L, Phys. Rev. Letters **16**, 817 (1966).
McKellar, A., Publ. Dominion Astrophys. Obs. **7**, 251 (1941).
Münch, G., Astrophys. J. **140**, 107 (1964).
Penzias, A. A. and Wilson, R. W., Astrophys. J. **142**, 419 (1965).
Shklovsky, I. S., Astronomical Circular No. 364, Academy of Sciences of the Soviet Union (1966).
Thaddeus, P. and Clauser, J. F., Phys. Rev. Letters **16**, 819 (1966).
Weymann, R., Astrophys. J. **145**, 560 (1966).

DISCUSSION

P. Solomon: It seems unlikely that there would be CN in

HII regions. It would dissociate in a matter of 500 or 1000 years, and unless there is a very rapid production mechanism CN wouldn't exist.

P. Thaddeus: On the other hand, from the recent OH radio observations there is some reason to believe that OH is associated with HII regions. Also Münch, looking at a CN region against a distant emission nebula, observed identical Doppler shifts for CN and helium lines in the nebula. Consequently, there is some suspicion in this case that CN, if it is not in the HII region, is at least close to the ionization front. The density associated with ionization fronts is also a serious problem, since there may be 10 to 100 hydrogen atoms/cm^3, and collisions will be significant.

P. Solomon: How do you account for Münch's observation in which lines originating in higher levels are observed?

P. Thaddeus: Münch indicated to me that those lines may be saturated. If this is the case, until you delve into the problems of saturation, you cannot accurately calculate the rotational temperature.

G. B. Field: I would agree with the last statement. First of all, Münch did not see the corresponding R branch, which should appear. Also, the R(0) line has an 80 mÅ equivalent width, which suggests a very high degree of saturation. I would also like to mention a fact that Woolf pointed out some time ago, namely, that these results, even if they are only considered as upper limits, fall below the dilute blackbody line for a higher temperature. In connection with Peebles' work, we should consider the possibility that the dilute blackbody radiation is from an earlier phase—possibly from the time of formation of galaxies. In other words, the radiation may peak in the micron rather than in the millimeter part of the spectrum.

P. Thaddeus: This is why the CH and CH^+ measurements are potentially interesting, even though they are not too sensitive, and it is also why the higher CN transitions are perhaps even more important.

10

EMISSION LINE OBJECTS

R. J. Gould

Several years ago, I made a summary (Gould, 1964) of the infrared lines which would be emitted from interstellar HII regions. These lines all result from transitions between fine structure levels of certain ions, in which the upper level is excited by electron collisions and is depopulated by a magnetic dipole radiative transition. The level separation is characteristically 10^{-2} to 10^{-1} ev.

There are many such lines, but the most important from the observational point of view are from Ne^{+} at 12.8 microns, S^{+3} at 10.5 microns, and Mg^{+3} at 4.49 microns. Each of these lines results from a $^2P_{3/2} - {}^2P_{1/2}$ transition, and the level separation is about 0.1 ev. The upper level will be depopulated primarily by the emission of radiation as long as the electron density is less than about 10^5 electrons/cm^3.

Actually, a considerable amount of energy is emitted from a galaxy in these lines, particularly in the Ne^{+} line since in HII regions neon is primarily in the singly ionized state. One can estimate the luminosity of the galaxy in this line; the value is about 10^{42} ergs/sec, which is on the order of a hundredth of the total luminosity of the galaxy. The intensity of the neon line is roughly equal to that of

the Hα line from ionized regions. However, the ratio of the line intensity to the continuum intensity is much greater for the neon line than for the Hα. This is why Sciama and I (1964) have suggested the possibility of measuring the background radiation in the neon line due to external galaxies out to the Hubble radius. This radiation would be smeared into a continuum by the differential red shift, and would provide a good way of testing cosmological models.

It now appears that the best opportunities for observing these infrared lines arise from observations of planetary nebulae. The flux from such a line is essentially proportional to the volume integral of the product of the electron and ion densities. The best way to actually estimate the total intensity in a given infrared line is to compare with the intensity of the Hα or Hβ lines, which is a measure of the product of the electron and proton densities. The temperature dependence for the production of the infrared lines is practically the same as for the Hα and Hβ lines, so that the main problem is to estimate the abundance of the particular ion relative to ionized hydrogen.

We can estimate the neon ion concentration for a planetary nebula such as IC418 by comparing with the observed helium ionization, since the first ionization potential of helium is almost the same as the first ionization potential in neon. On this basis, it was found that about 60% of the neon was singly ionized (Gould 1966). There are certain difficulties involved in estimating the neon ionization from the helium ionization, because it is not clear whether recombination to triplet states of helium actually contributes to the ionization balance; we are not certain that the 2^3S state of helium is not photoionized by the Lyman α radiation. In arriving at 60% ionization, it was assumed that recombination to the triplet state of helium did contribute to the ionization balance. If, on the other hand, it is assumed that there are only recombinations to singlet levels, it is found that about 25% of the neon is ionized. We use a Ne/H ration of 10^{-4}, as given by Aller (1961) for planetary nebulae. It should be noted that this ratio may differ by a factor of 2 from one planetary to another.

On the basis of these estimates, one obtains for IC 418 a flux in the neon line of about 0.6×10^{-16} watts/cm^2. This result can be compared with a preliminary observation made by Low on IC 418. He finds a flux of 10^{-15} watts/cm^2 in the region between 12.5 and 13.5 microns, so that this first preliminary observation agrees fairly well with the calculated value.

Insofar as there are other lines and other planetary nebulae, it appears that a likely object for observation is the high-excitation planetary NGC 7027. The most prominent lines should be those from sulphur and magnesium. It can be estimated that the magnesium line flux should be about 0.7×10^{-16} watts/cm^2, and for the sulphur line the flux should be from 3 to 10×10^{-16} watts/cm^2. Both values are certainly large enough to be observed.

REFERENCES

Aller, L. H., The Abundance of the Elements (Interscience Publishers, New York, 1961).

Gould, R. J., Ann. Astrophys. **27**, 815 (1964).

Gould, R. J. and Sciama, D. W., Astrophys. J. **140**, 1634 (1964).

Gould, R. J., Astrophys. J. **143**, 603 (1966).

DISCUSSION

G. B. Field: It seems to me that your estimates of the luminosity of the galaxy at 12.8 microns are optimistic. For example, the total radiation emitted by early type stars is less by one order of magnitude than what you calculate to be the total radiation coming out in this line. I don't see how you make up that discrepancy. It seems to me that you are assuming that nearly all of the radiation in the HII region is essentially coming out at this wavelength. I would estimate a factor of 100 less.

R. J. Gould: I would be surprised if it was a factor of 100

less. It is true that a high fraction of the energy that gets emitted from HII regions is in this neon line—at least 30% in some instances. (See note 2 below)

G. B. Field: It simply contradicts observations to have an HII region at the low temperature that you have claimed (Burbidge, Gould, and Pottasch, Ap. J. **138**, 945 (1963)). Observations suggest 9000°K. I think 5000°K can be ruled out.

L. H. Aller: I don't know offhand of any emission nebula having a reasonably high surface brightness that has a temperature as low as 5000°K. They all seem to have temperatures around 9000 or 10,000°K.

R. J. Gould: The actual equilibrium gas kinetic temperature, of course, depends on the temperature of the central star and the radiation field. But I don't think that any of these problems should be taken as pessimism against the main argument. For planetary nebulae, the theoretical temperatures based on the heating and cooling always seem to be lower than the observed ones, even without including cooling by these infrared lines.

E. P. Ney: How confident are you that what was observed in the spectrum of IC 418 was a neon line?

F. H. Low: Reasonably confident. The bandwidth was about half a micron, centered on the line. We do not know of any other reasonable explanation for it.

R. H. Beer: It is worthwhile making the point that the 12 micron window is at best only 90% transparent. To pick out an emission line one must have a resolution of the order of the line width; otherwise the line can be lost in the continuum.

G. B. Field: Then the only experimental claim is that there is something in that band, but it is not certain that it is a line?

R. J. Gould: Yes, but there is no other reasonable energy source that could produce the luminosity observed in this band.

J. A. Westphal: Did you look at an adjacent wavelength region to make sure there was no continuum there?

F. H. Low: Yes. We used three filters: a broad band filter which transmitted between 13.5 and 17μ; a filter

that cuts off below 11μ; and a filter that cuts off just below 12.5μ, just short of the line. The last two are cut off by the atmosphere very rapidly. If the flux had been due to a continuum spread out over the entire band, we would have seen a much larger signal that we did see with the broad band filter.

Notes Added in Proof February 1967

1. Since the conclusion of this symposium a detailed discussion of infrared line emission from planetary nebulae has been given in a paper by Delmer, Gould, and Ramsay (Ap. J. **149**, 495 (1967). In this paper improved estimates are made of the infrared line spectra of nine bright planetaries; eleven lines from various ionization states of the elements O, Ne, Mg, S, and A are considered. It should perhaps be mentioned that the Mg^{+3} line at 4.49μ is weaker than originally thought but a number of other lines from these nine planetaries have intensities in the range 10^{-18} to 10^{-16} watts/cm^2.

2. Concerning the first point raised by Dr. Field regarding the galactic luminosity in the 12.8μ line, the reader should be referred to my recent paper (Ap. J. **146**, 944 (1966)) which was stimulated by the above discussion.

3. Regarding the observations of electron temperature in HII regions, it might be mentioned that recent radio observations do indeed indicate lower temperatures in the neighborhood of 5000°K for some diffuse nebulae.

11

THE INFRARED SPECTRUM OF INTERSTELLAR SHOCK WAVES

G. B. Field, B. Basu, J. G. Rather, and S. Orszag

It has long been thought that interstellar turbulence should dissipate into infrared lines, none of which have ever been observed. It is worthwhile to calculate what kind of spectrum should be seen, especially because the state of our knowledge about interstellar matter is rather incomplete. If we were able to see the energy emitted in these lines, it would be a great step forward.

We will deal specifically with the neutral component of interstellar matter; that is, the neutral hydrogen regions which comprise roughly 90% of the mass of interstellar matter. Our knowledge of this subject comes primarily from studies of 21-cm radiation and the optical absorption lines due to elements such as calcium and sodium. On this basis, it has been possible to construct a rough picture of the physical state and motion of the material. As a rough approximation, one can say that it seems to be agglomerated into clouds having a density of the order of 10 atms/cm^3 and a harmonic mean temperature of about 100°K. The sound velocity in these clouds will be about 1 km/sec. The radius of a cloud is of the order of 5 pc, and the number of clouds per kpc along a line of sight taken in a random direction through the galaxy is thought to be about 7.

The clouds are moving with respect to one another; that is, one sees relative motions in profiles of various lines, corresponding to an rms velocity of approximately 10 km/sec. This is approximately Mach 10 with respect to the internal thermal velocity of the clouds. For this reason we expect the turbulence to be highly compressible and to give rise to shock waves and associated dissipation. This dissipated energy is of particular interest, since it will be emitted in the infrared. Kahn pointed out that one can approximate the dissipation by considering that clouds collide with one another with a mean collision time of 6×10^6 years. As a result of a collision, one would expect shock waves to be formed at the interface. That is, a shock wave will propagate into each of the two clouds in such a way as to bring the material to a halt, while compressing the material and heating it to a high temperature. It can be easily calculated that one should see 1 shock per kpc along a random line of sight. In some cases, the shock can be seen edge-on and will exhibit a relatively high brightness of infrared radiation. In other cases, it is being viewed at right angles, and a lower surface brightness is seen.

The total energy dissipated in such interstellar cloud collisions has been calculated to be 8×10^{39} ergs/sec, which is approximately 10^{-3} of the luminosity of the galaxy. It appears that a considerable amount of energy in the galaxy is being dissipated in this manner; hopefully it can be observed. Furthermore, because the collision time is rather short compared to the life of the galaxy, one has to explain how the kinetic energy of a cloud is being replenished when it is being dissipated on a very short time scale. In other words, if nothing were done to replace this energy, the clouds would essentially become cold and motionless after 10^7 years. This energy could possibly be supplied by HII regions, which can be thought of as explosions in which there is a high internal pressure and temperature produced by the heating of the gas by ultraviolet radiation emitted by the early-type stars imbedded in these regions. An HII region effectively acts as a spherical piston, compressing and accelerating the gas in the surrounding HI region. It is important to note, however, that energy flow from an HII region into an HI

region and then into the shock waves formed by the collision is conjectural, and has not been directly observed.

Our program, then, is to analyze a particular model of such a shock wave and determine what the infrared spectrum should be. We have made a number of simplifications, the main one being that we consider only steady shocks. After such a collision has taken place, the shock waves begin to propagate out into the clouds. Initially a steady state does not exist, but it can be shown that there is an almost-steady state solution to the problem, in which the individual shock waves propagate rather slowly out from the interface and the rest of the cloud moves into the interface in a steady, constant-velocity fashion. The problem then becomes one of following the motion of a gram of gas as it goes from the cool region ahead of the shock into the hot region behind the shock. For convenience, we assume two similar clouds, and the interface is taken to be the center of mass of the two clouds. We can effectively consider the interface to be a "brick wall," since this is the point of zero motion. The material approaches the interface with a velocity v. We assume a density $\rho_0 = 10$ atoms/cm^3 and a temperature $T_0 = 100°K$. A useful parameter is the Mach number of the shock, defined as the cloud velocity divided by the sound velocity in the unshocked gas.

The equations describing the interaction can be written in the shock frame; this is made possible by the assumption of steady motion. The first condition is the conservation of matter:

$$\rho v = \text{constant} \tag{1}$$

The conservation of momentum provides the second condition:

$$\rho v^2 + p = \text{constant} \tag{2}$$

The equation describing the conservation of energy is not as straightforward, since we cannot assume that the shock is adiabatic. In fact, it is much closer to being isothermal in the sense that nearly all of the energy generated by the shock goes into radiation. The equation can be written as follows:

$$dt = -\frac{p}{L}\, d \ln(T^{3/2}/\rho) \qquad (3)$$

In this equation L is the total energy radiated in ergs/cm^3-sec, and is in fact the infrared radiation generated by inelastic collisions between the various constituents of the medium. Typically an atom is raised to an excited state by an inelastic collision, and is de-excited by the emission of a photon. The simplifying feature is that this photon is in the infrared, for which the opacity is very small; thus it escapes without further interaction with the gas. Therefore we can consider L as a volume emissivity and integrate Eq. 3 without worrying about optical depth effects.

There are a number of different processes which contribute to L. The first process is the excitation of fine-structure levels by electron-ion collisions. The ions we are considering are not H ions; after all, we are concerned with HI regions. They are the ions of easily-ionized elements such as Fe, Si, and C (see Fig. 1). In interstellar space these rather common elements are easily ionized by starlight. The free electrons produced by the ionization of these elements then collide with the ions, resulting in excitation to higher levels. The cross sections used here are due to Seaton.

The next process to be considered is collisions between hydrogen atoms and the same ions. This has not been considered previously; cross sections were first calculated by Takayanagi. Although the hydrogen atom is uncharged, and one might therefore expect the cross section to be small compared to that for electron collisions, there is so much more hydrogen than electrons that in fact the hydrogen-ion collisions dominate over electron-ion collisions by a factor of 3 to 20. This result represents a significant change from previous work on the problem. We next take into account collisions between H atoms and other atoms. An atom of particular interest is oxygen. The cross section is relatively small because both constituents are neutral, but this interaction does contribute somewhat to the spectrum. The abundances adopted are as follows, relative to hydrogen:

$O = 7 \times 10^{-4}$, $C^+ = 3 \times 10^{-4}$, $Si^+ = 3 \times 10^{-5}$ and $Fe^+ = 8 \times 10^{-6}$.

It should be realized that the abundances in interstellar matter are not at all well known; there is also the possibility that some of these elements may be trapped in grains. Therefore our abundances might be overestimates.

Finally, we consider collisions between hydrogen atoms and hydrogen molecules, and excitation of the rotational levels J = 0, 2 ... . This is somewhat hypothetical, since H_2 has never been observed in interstellar space. There has been a good deal of theoretical work on the problem, but it is not decisive. Our calculations predict the infrared spectrum of H_2 that would be produced by a shock wave on the basis of various assumed abundances of H_2, and may provide a way to determine whether H_2 is in fact present in interstellar matter. There are very good cross section

COOLING LINES

Substance	Transition	λ(μ)	Log λ(μ)
C^+	$^2P_{3/2} - {}^2P_{1/2}$	156	2.193
O	$^3P_1 - {}^3P_2$	63	1.799
	$^3P_0 - {}^3P_1$	147	2.167
Si^+	$^2P_{3/2} - {}^2P_{1/2}$	35	1.544*
Fe^+	$^6D_{7/2} - {}^6D_{9/2}$	26	1.415
	$^6D_{5/2} - {}^6D_{7/2}$	35	1.544*
H_2	2 → 0	28	1.447
	4 → 2	12	1.079
	6 → 4	8.0	0.903
	8 → 6	6.1	0.785
	10 → 8	5.0	0.699
	12 → 10	4.4	0.643

*Same

Fig. 1. Infrared lines used in the cooling calculation.

calculations by Takayanagi, which were employed in a subroutine to find the distribution of H_2 molecules over the rotational levels. We consider only parahydrogen, with values of J = 0, 2, 4, ... 12. We take into account only the quadrupole transitions; i.e., $\Delta J = 2$. The wavelengths of the radiation resulting from these transitions are listed in Fig. 1.

We now substitute the collision rate calculations into Eq. 3; with the aid of Eqs. 1 and 2 and the ideal gas law, Eq. 3 can be solved to give the temperature as a function of time. Once we determine the temperature, density and pressure behind the shock front, we can evaluate the intensity of each individual line in ergs/cm^2-sec-ster for a line of sight normal to the shock front. We have performed the calculation for three values of the Mach number: M = 5, 10, and 15; the cooling curves are shown in Figs. 2, 3 and 4. The various curves are labeled according to the assumed fraction of H_2. It can be seen that the amount of H_2 has a significant effect on the cooling. The critical value of the H_2 abundance is about 10^{-3}. That is, if more than 0.1% of the medium is H_2, cooling will occur considerably more rapidly. This is also a critical value in terms of the infrared spectrum, since most of the energy would then be radiated in the hydrogen molecular spectrum. The observation of this spectrum would give direct information as to the amount of H_2 present.

We have calculated the intensities of the expected spectral lines. These are shown in Figs. 5, 6, and 7 for various values of the Mach number and H_2 abundance. First of all, it can be seen that the total intensity in all lines increases with the Mach number. In fact, it can be shown that the total intensity goes as M^3. Generally speaking then, observable radiation would tend to come from regions which are colliding with relatively high velocity. Since the total amount of energy to be dissipated is the same (for a given M) regardless of the H_2 abundance, it follows that when the H_2 abundance is large the amount of radiation in the lines other than H_2 is lessened, and vice versa. As previously stated, the turnover is at about 0.1% H_2 abundance; at this point the radiation shifts from the fine structure lines, which are at relatively long wavelengths, to the H_2 lines at shorter wavelengths.

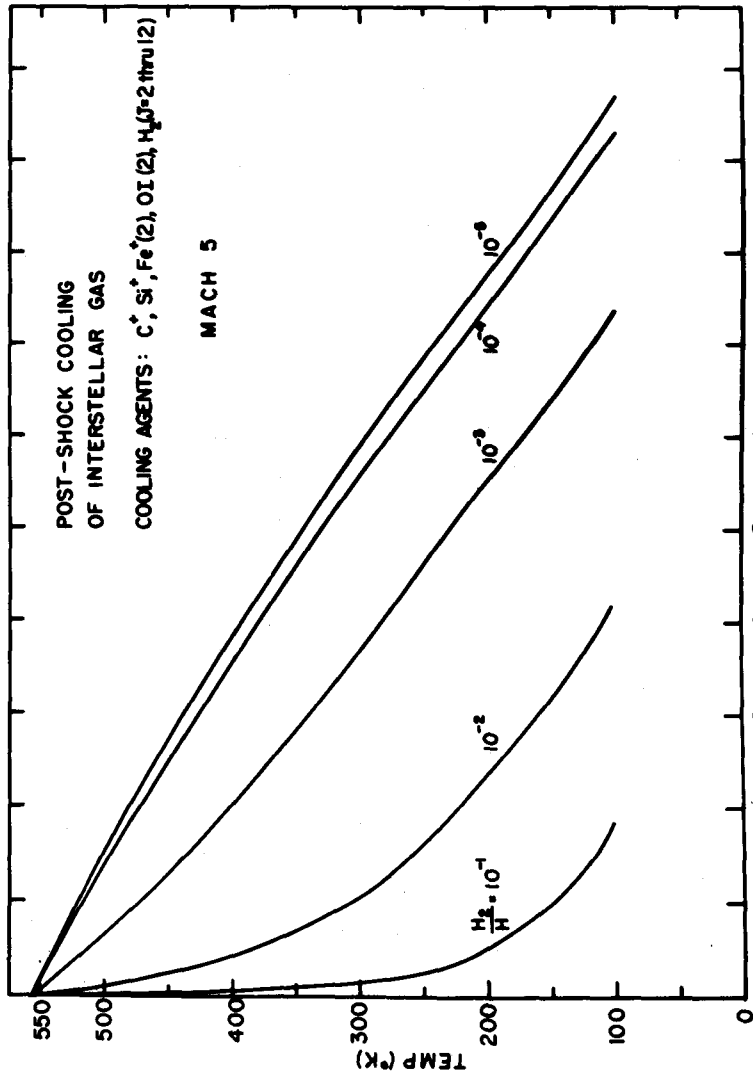

Fig. 2. Temperature history of matter which has passed through a shock of Mach 5 at t = 0.

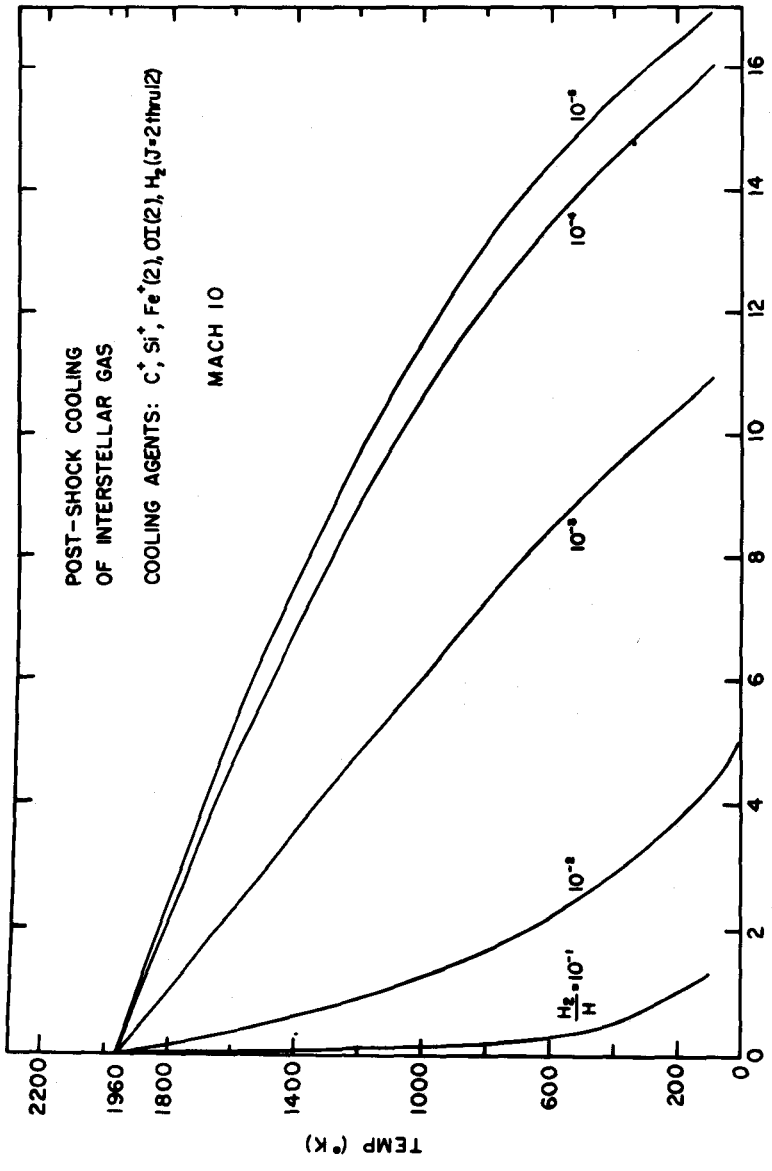

Fig. 3. Temperature history of matter which has passed through a shock of Mach 10 at t = 0.

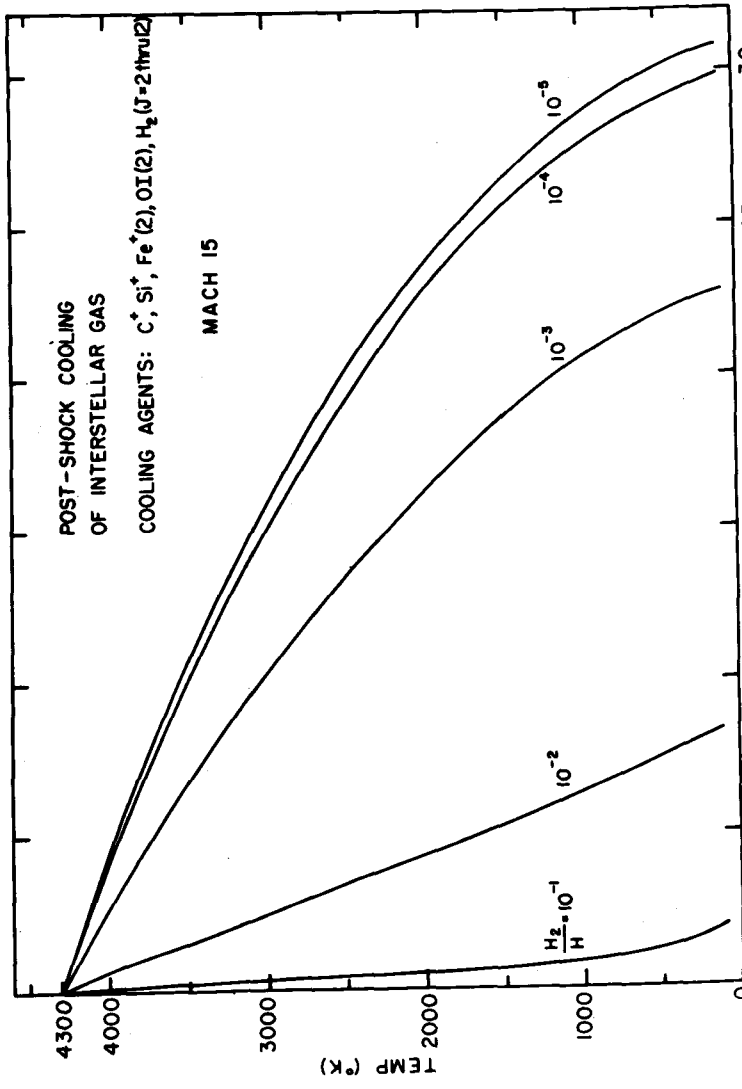

Fig. 4. Temperature history of matter which has passed through a shock of Mach 15 at t = 0.

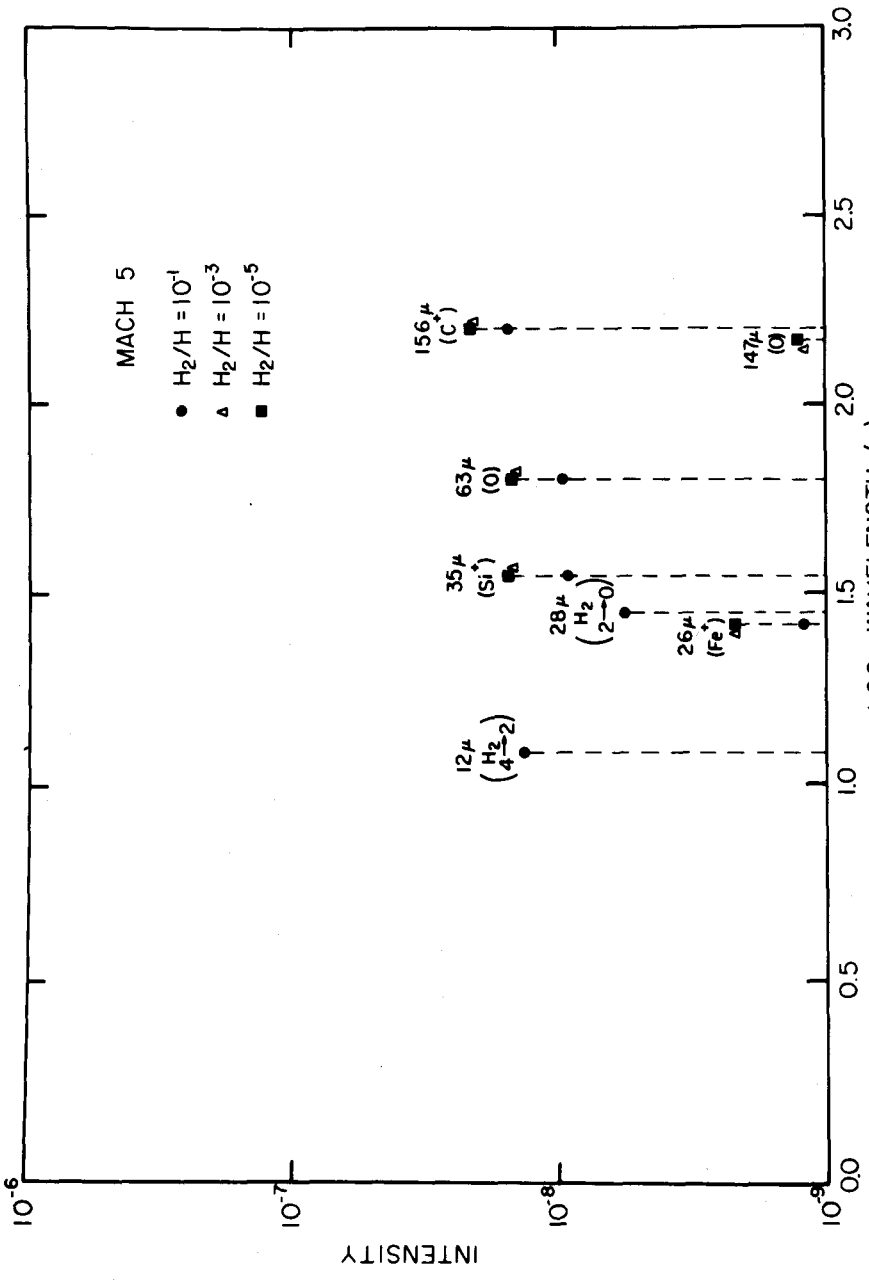

Fig. 5. Infrared line spectrum observed normal to Mach 5 shock. The temperatures are too low to excite much H_2 emission.

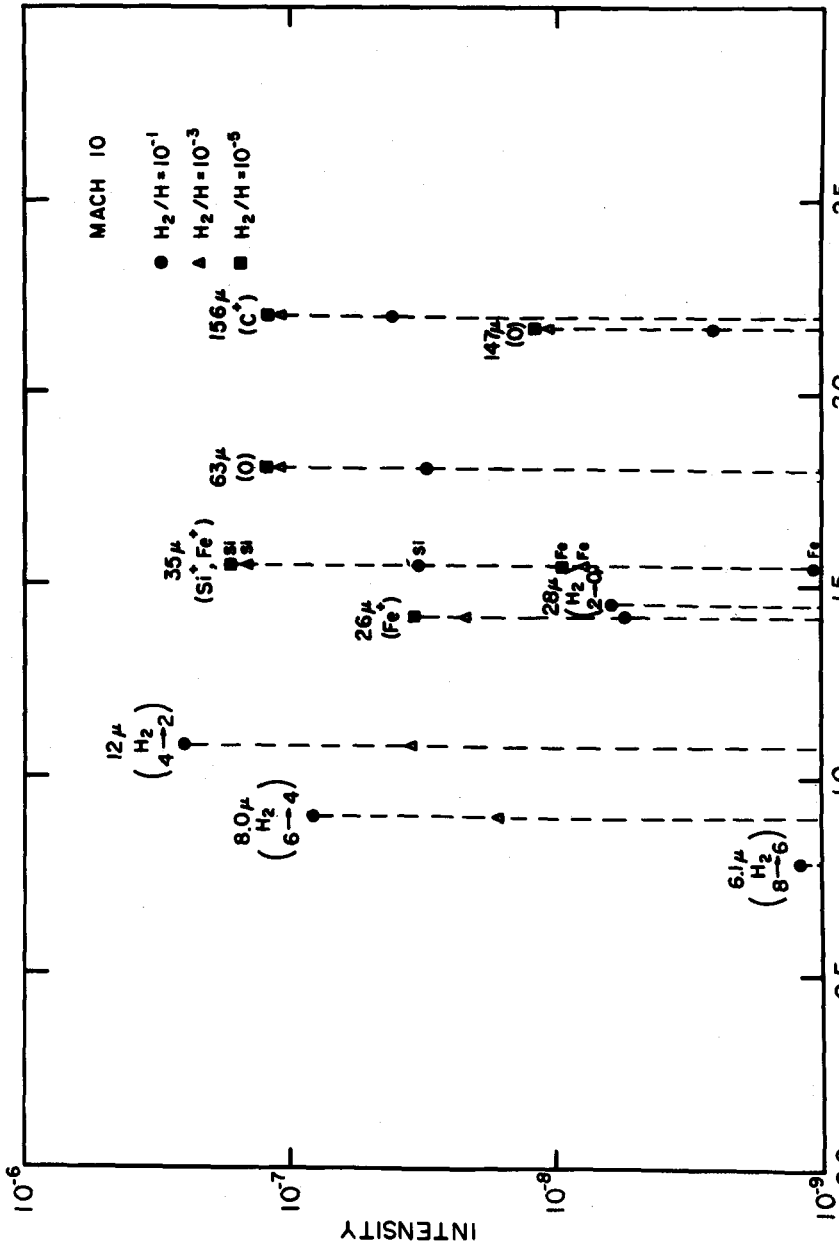

Fig. 6. Infrared line spectrum observed normal to Mach 10 shock.

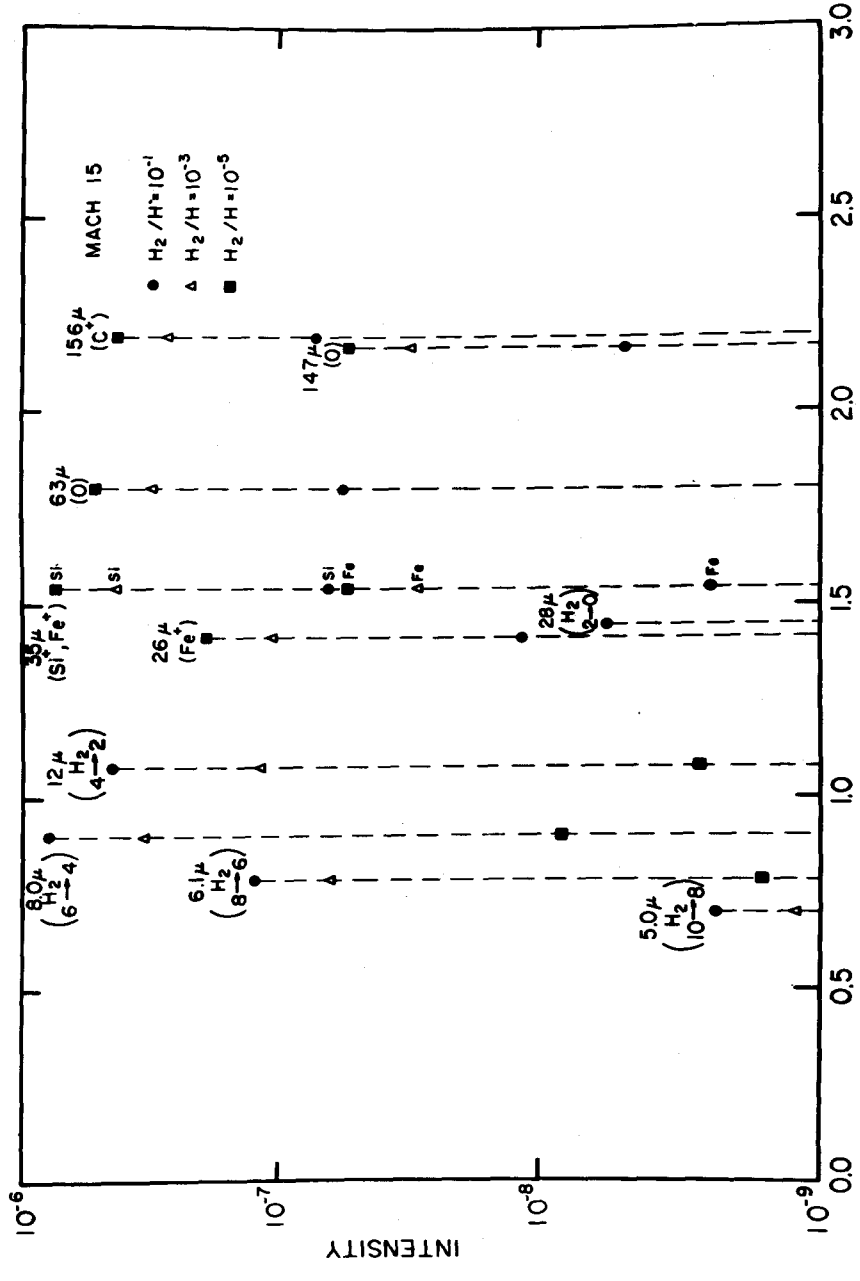

Fig. 7. Infrared line spectrum observed normal to Mach 15 shock. Note excitation of H_2 by much higher temperatures.

The silicon line at 35 microns seems to be a prominent feature. Finally, we note that the strongest hydrogen line in each case appears to be either the $J = 6 \rightarrow 4$ line at 8 microns or the $J = 4 \rightarrow 2$ line at 12 microns. This is a somewhat surprising result; as most previous estimates indicated that the $J = 2 \rightarrow 0$ line at 28 microns would be most readily excited. We believe this is a result of the fact that the high density behind the shock de-excites the $J = 2$ level collisionally, since the $2 \rightarrow 0$ transition is slow.

We have described the kind of radiation that one might hope to observe coming from shocks. The intensities of these lines at the earth would be on the order of 10^{-14} watts/cm^2-ster, which is close to the instrumental limit. It is possible that by looking in some directions, more than one shock front might be in the line of sight. There would probably not be more than ten in any particular direction.

DISCUSSION

A. G. W. Cameron: Wouldn't the intensities be considerably smaller if magnetic fields were taken into account?

G. B. Field: Yes. A magnetic field will tend to resist compression, so that the energy will not be so easily dissipated. Our results would apply only for shocks which lie essentially along the magnetic field. It seems reasonable to suppose that perhaps a third or a half of the material would satisfy this condition.

R. J. Weymann: How does the emission compare with that calculated by Gould for contracting stars?

R. J. Gould: I once made an estimate of the intensity of the 28-micron radiation in the galaxy due to star formation. The total flux is about 3×10^{-16} watts/cm^2 as seen at a distance of 10 kpc. This figure is based on the assumption that in star formation the protostar goes through a stage in which it suffers a collapse that is instigated by the 28-micron emission.

M. Harwit: There seems to be enough energy available to excite the first vibrational state. Is the collisional cross section for this interaction very small? These transitions

would be easy to observe, especially if they fall near 2 microns, where the atmosphere is very favorable.

G. B. Field: We followed Takayanagi and Nishimura in ignoring these transitions. It might be worthwhile for us to consider them, especially for the Mach 15 case.

R. J. Gould: What electron density did you use to calculate the electron-ion cooling?

G. B. Field: We assume an electron density of 3.8×10^{-4} H, where H is the hydrogen abundance. This is slightly more than the total metallic ion abundance.

R. J. Gould: The electron density could be much higher if there is a high flux of low-energy cosmic rays, producing additional ionization.

G. B. Field: A surprising result that emerged from our calculations was that the electrons do not contribute in any case. The atoms seem to dominate the situation.

R. J. Gould: What is the latest observational information as to the mean temperature in HI regions?

G. B. Field: We are able to determine a harmonic mean temperature, which seems to be around 120° K. The 21-cm absorption measurements give a value of about 60° K. The difference results from the fact that emission and absorption processes represent different kinds of clouds, since the low temperature clouds absorb more easily.

L. H. Aller: A likely place where one might see the radiation you have predicted would be something similar to 30 Doradus, where there is a tremendous HII region impinging on a tremendous HI cloud.

G. B. Field: In general, if our picture is correct, we would look for these effects in the neighborhood of HII regions, which is where the energy should be dissipated.

R. J. Gould: Our theoretical investigations as to the H_2 abundance (Gould, Gold and Salpeter, Ap. J. **139**, 408 (1963)) indicate that between 10 and 20% of the hydrogen is in molecular form. There is also some indirect evidence based on the amount of mass found in the plane of the galaxy that seems to support this figure.

G. B. Field: The major difficulty with having a high H_2 abundance is that the cooling is already extremely efficient even with only 1% H_2. It is difficult to explain

how the harmonic mean temperature could be 100° K. It is more likely to be about 20° K.

N. Woolf: It is worth mentioning that radio observations of OH occasionally show poor correlation with the 21-cm results, perhaps suggesting that there are large concentrations of molecular hydrogen.

G. B. Field: From the point of view of this conference, perhaps the point that we should stress is that we really are very ignorant in these areas, and therefore any observations are welcome.

12

PROTOSTARS

A. G. W. Cameron

There has been a great deal of debate on the question of how star formation is initiated. My own inclination is to adapt the model of the interstellar medium proposed by Parker (1966). If initially there is a magnetic field along a galactic spiral arm, it will be unstable for reasons somewhat related to the classical Rayleigh-Taylor instability, and any gas lying along the lines of force would tend to collect in pockets. The gas would be trapped in individual clouds, which would be essentially stable because of the magnetic boundary pressure together with the general gravitational forces.

A typical interstellar cloud will have a mass of the order of 1, 000 solar masses. It is of interest to determine the conditions under which it will become gravitationally unstable; this requires the internal energy to be low enough so that the gravitational compression can overcome it. It can be shown that the hydrogen number density at the threshold of gravitational instability is of the order of 1, 000 particles/cm^3. Such a density is very nearly equal to that of the densest clouds observed. This is probably not a mere coincidence; a cloud reaching a density of several hundred particles/cm^3 is likely to go into gravitational collapse. Typical cloud densities are of the order of 10 particles/cm^3, so

there is a question as to the manner by which higher densities are attained. The most likely process for this purpose is probably that the radiation from already-formed stars ionizes the lower-density gas near the cloud boundary, and the higher pressure thus induced tends to compress the gas along the lines of force until the threshold for gravitational instability is reached. Once gravitational instability sets in, the cloud starts to collapse and heat up; the same cooling mechanisms as those discussed by Field in the previous paper will then be operative, and many of the same lines will be produced. What is needed here (and has not yet been carried out) is a study of the hydrodynamics of such a collapse, giving the temperature of the gas as a function of time and compression.

The free-fall time for the collapse of the cloud is about 2 million years. Essentially, as the collapse proceeds, the temperature does not rise rapidly. The increasing density raises the efficiency of the cooling mechanisms; the rates of the various two-particle collision processes discussed by Field increase as the square of the particle number density. One can crudely describe the initial phase of the collapse of the cloud as being isothermal.

The later stages of collapse have been discussed by Gaustad (1963). The cloud has now become sufficiently dense that the interstellar grains begin to play a role. They will absorb the radiation emitted by the cloud, and then reradiate it, leading to a somewhat different problem with respect to infrared detectability. The radiation emitted by an interstellar grain depends on the internal temperature of the grain, which in turn is governed by the rate of absorption of energy. The internal temperature will in general be less than the gas kinetic temperatures of the particles which strike or are absorbed by the grain. Interstellar grains have interior temperatures of a few degrees Kelvin, and will not emit as black bodies because their dimensions are small compared to the typical wavelengths emitted by black bodies at such temperatures. At any rate, grains will basically emit infrared radiation of fairly long wavelength.

As the gas cloud becomes more and more compressed there will begin to be some trapping of radiation, and the rate

of collision of the ions and atoms with the grains themselves will become large enough for the grain temperatures to rise more toward equilbrium with the gas kinetic temperatures, although they would still be expected to lag below. At grain temperatures in the 100 to 200° K range, the ice constituent of the grains will sublime. At temperatures in the vicinity of 1000 to 1500° K, the metallic constituents of the grains will evaporate away. The opacity of the cloud becomes significant in the later stages of collapse because of absorption by the grains. When the temperature exceeds 1500° K, the opacity will be due mainly to hydrogen and will be correspondingly reduced.

One of Gaustad's principal contributions has been to show that the optical depth at the center of whatever fragments the cloud may have broken into remains quite small; therefore, in no sense will the fragments of the cloud be decelerated to rest. Kelvin-Helmholtz contraction will certainly not occur until the temperature exceeds 1800° K, at which point dissociation of H_2 is initiated. The dissociation of H_2 absorbs energy and prevents the temperature from increasing very rapidly until the dimensions of the cloud fragments are quite small. For example, a fragment of one solar mass would have to shrink down to a radius of about 100-200 a.u. This will only occur very near the end of the free-fall collapse. Consequently, virtually all during the 2 million years needed for collapse, the medium will be characterized by line emission processes similar to those described by Field.

It is clear that in order to describe adequately the process of star formation, one must somehow take angular momentum into account. It is worthwhile to consider first what happens to a star during the earliest stages of Kelvin-Helmholtz contraction if it has no angular momentum. We will start at the point where hydrogen molecules have been dissociated, hydrogen is ionized, and helium is largely doubly ionized. A star will first be quasi-stable, in the sense of hydrostatic equilibrium, when the gravitational energy release is sufficient to provide for the internal energy required for hydrostatic stability (which by the virial theorem is half of the released gravitational potential

energy) as well as for the ionization and dissociation processes which take place largely in the interior. We call this energy condition "the threshold of energy stability." When one considers stellar models of large stars with gravitational potential energy release as the sole energy source in the interior, we are faced with the famous condition pointed out by Hayashi; namely, that one can only get a suitable solution by looking at conditions in the matter at the photosphere, where the opacity will be suitably large.

The dependence of opacity on temperature and density is shown in Fig. 1. The opacity is high at temperatures in

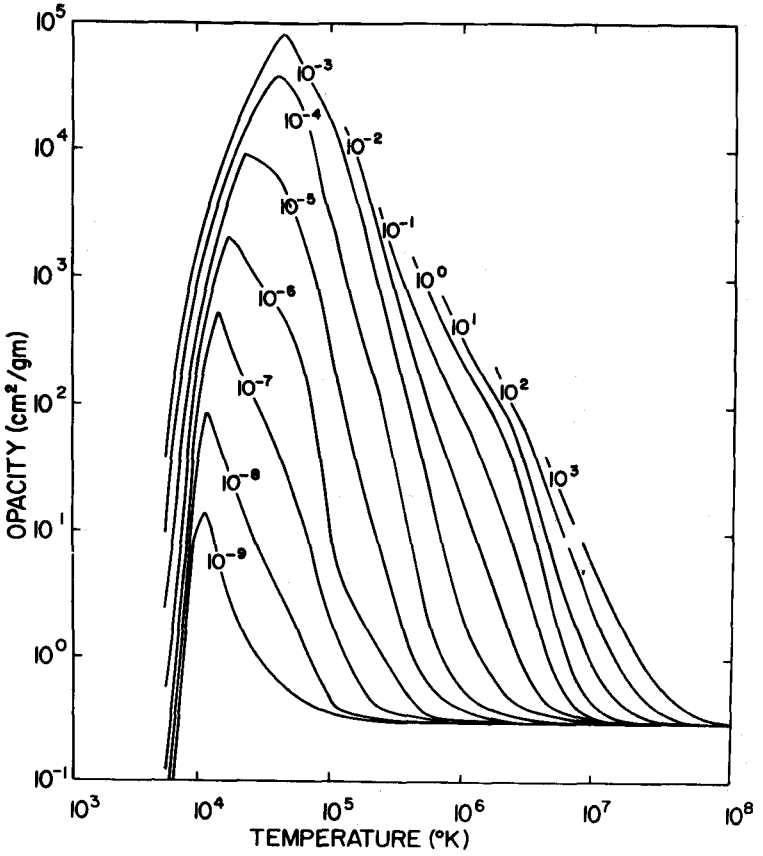

Fig. 1. Opacities for lines of indicated density (gm/cm^3) calculated as a function of temperature from the Los Alamos Opacity Code.

the 10^4 - 10^5 °K range because of bound-free and free-free transitions; there will be a large contribution from H^- as long as the electron densities are high. At temperatures below 10^4 °K the hydrogen is largely neutral, and we have to rely on the metals to supply the electrons. The opacity falls rapidly as the H^- abundance decreases. The opacities calculated at lower temperatures (Fig. 2) are undoubtedly too small, but could be improved by including molecular opacities. The main effect of the omission of sources of opacity is that the curves are shifted somewhat to the right. Consequently, the surface temperatures of the models that are

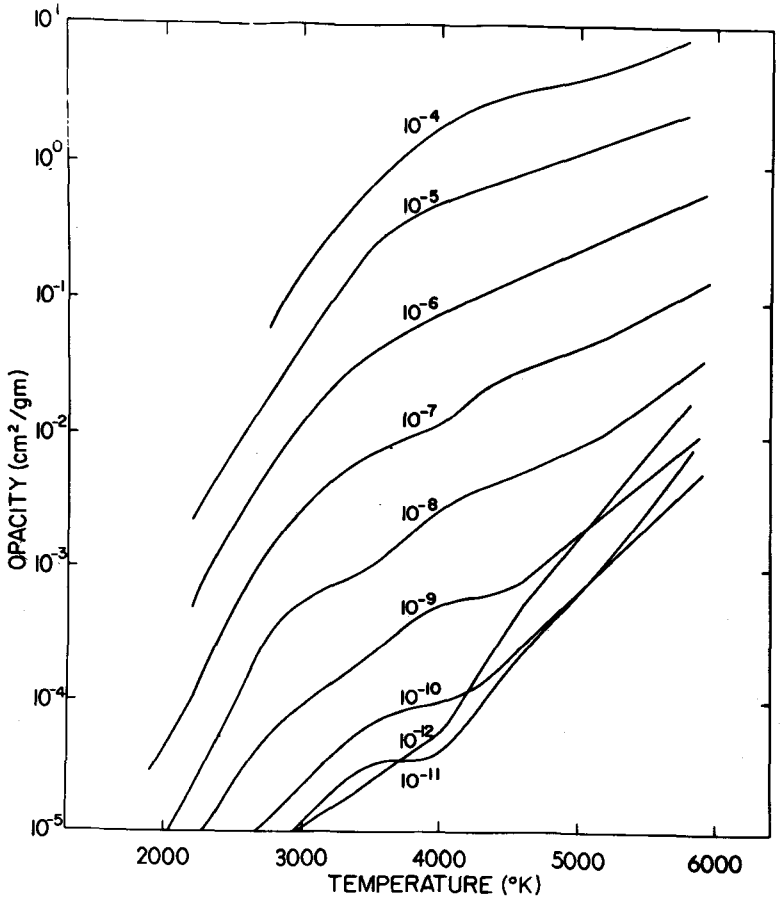

Fig. 2. Details of the opacities at low temperatures.

calculated assuming these opacities will be a little too high.

Ezer has calculated many stellar models for the early contraction phase. The results of the calculations for the sun are illustrated in Fig. 3. The evolutionary track begins at the threshold of energy stability for the sun. A star of 1 solar mass collapsing with no angular momentum would probably start close to the top of this track. The early contraction is rapid because of the high luminosity. The radius of the model is large, and the only energy source is gravitational potential energy release upon contraction. This is not a strong source as long as the radius is large, so that in the initial stages the rate of contraction is rather great. If deuterium burning occurs, it will take place when the luminosity is roughly ten times the present solar luminosity, when the sun is still completely convective. Deuterium burning, assuming the same D/H ratio as in the earth's oceans, would add about half a million years to the times shown on the diagram. The T-Tauri phase would occur after deuterium burning. The sun then evolves onto the main sequence with the beginning of hydrogen burning.

Similar evolutionary tracks have been calculated for a range of masses (Fig. 4). In each case the star has been taken from the threshold of energy stability on to the main sequence until the time at which half of the central hydrogen has been destroyed. It can be seen that the more massive stars have a longer horizontal contraction, but there is always a Hayashi phase. More important, the calculations show that the log of the effective temperature is never less than about 3.5. As a check, we have compared the results of our calculations with those of Iben (see Fig. 5). Although the masses being compared are not always quite the same, and Iben's calculations start somewhat further down from the threshold of energy stability, the calculations are in quite good agreement. The differences are readily understandable in view of the different opacity tables used in the two calculations. The main point is that there is agreement in expecting a lower limit to the temperatures of protostars.

Figure 6 shows the results of our calculations for

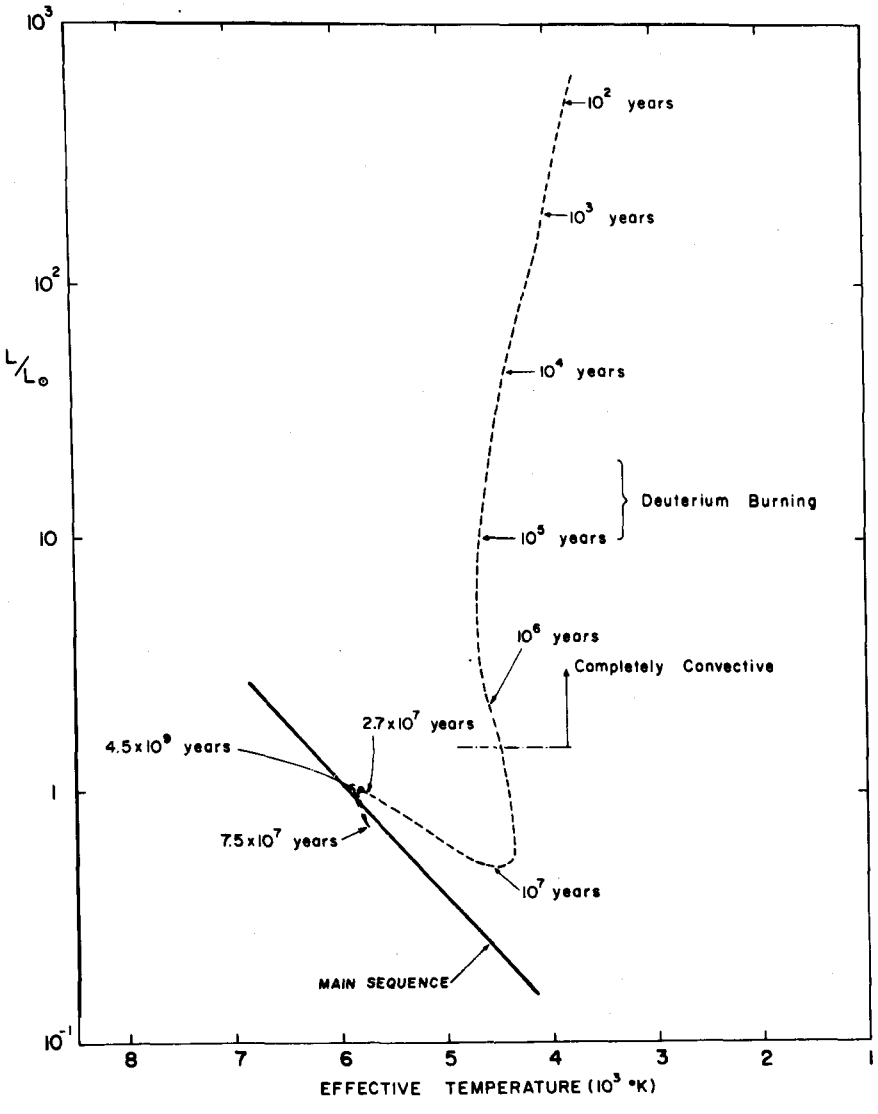

Fig. 3. The Hertzsprung-Russell diagram for the sun through the contraction up to its present main sequence position with a mixing-length equal to two pressure scale heights. The evolution times are indicated on the track at several positions.

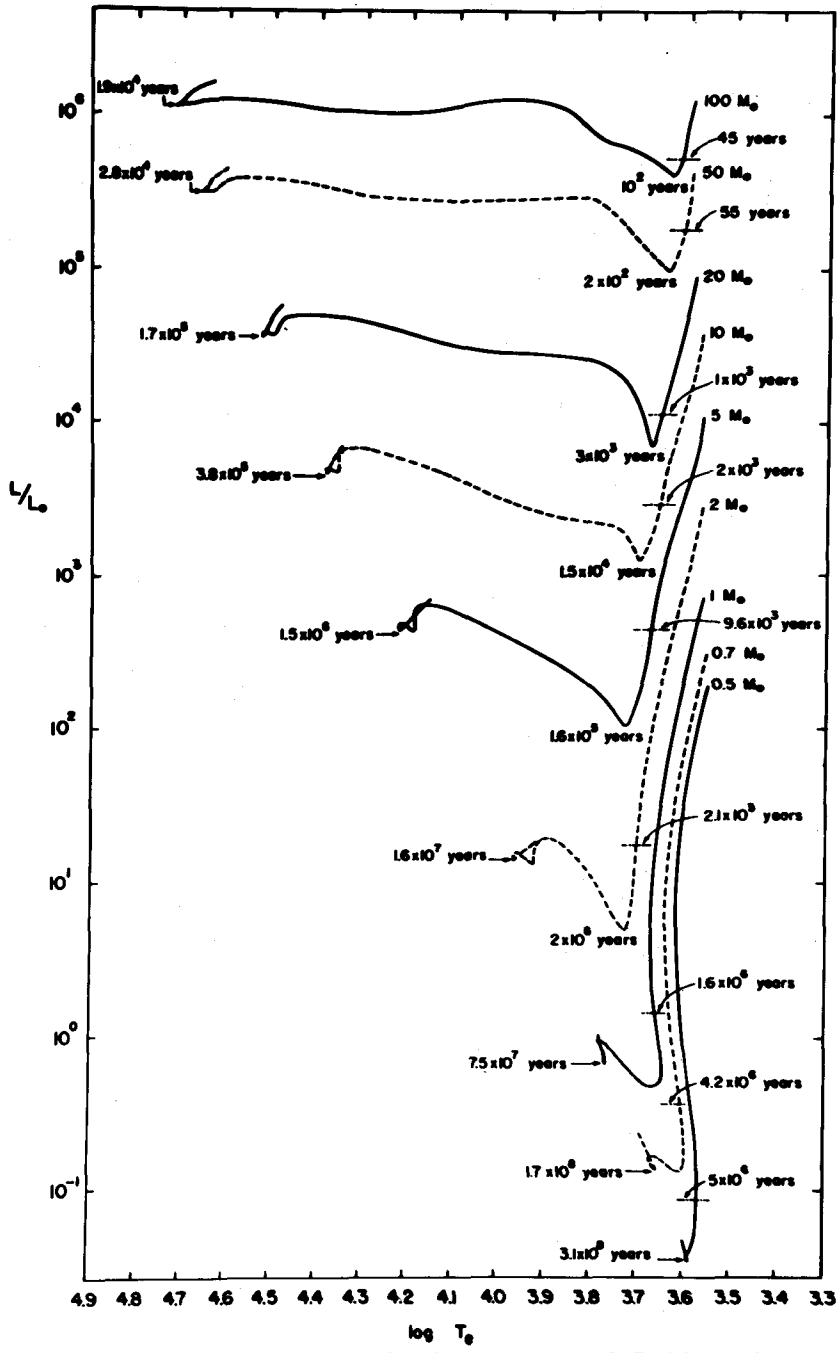

Fig. 4. Evolutionary tracks for stars of 0.5-100 solar masses.

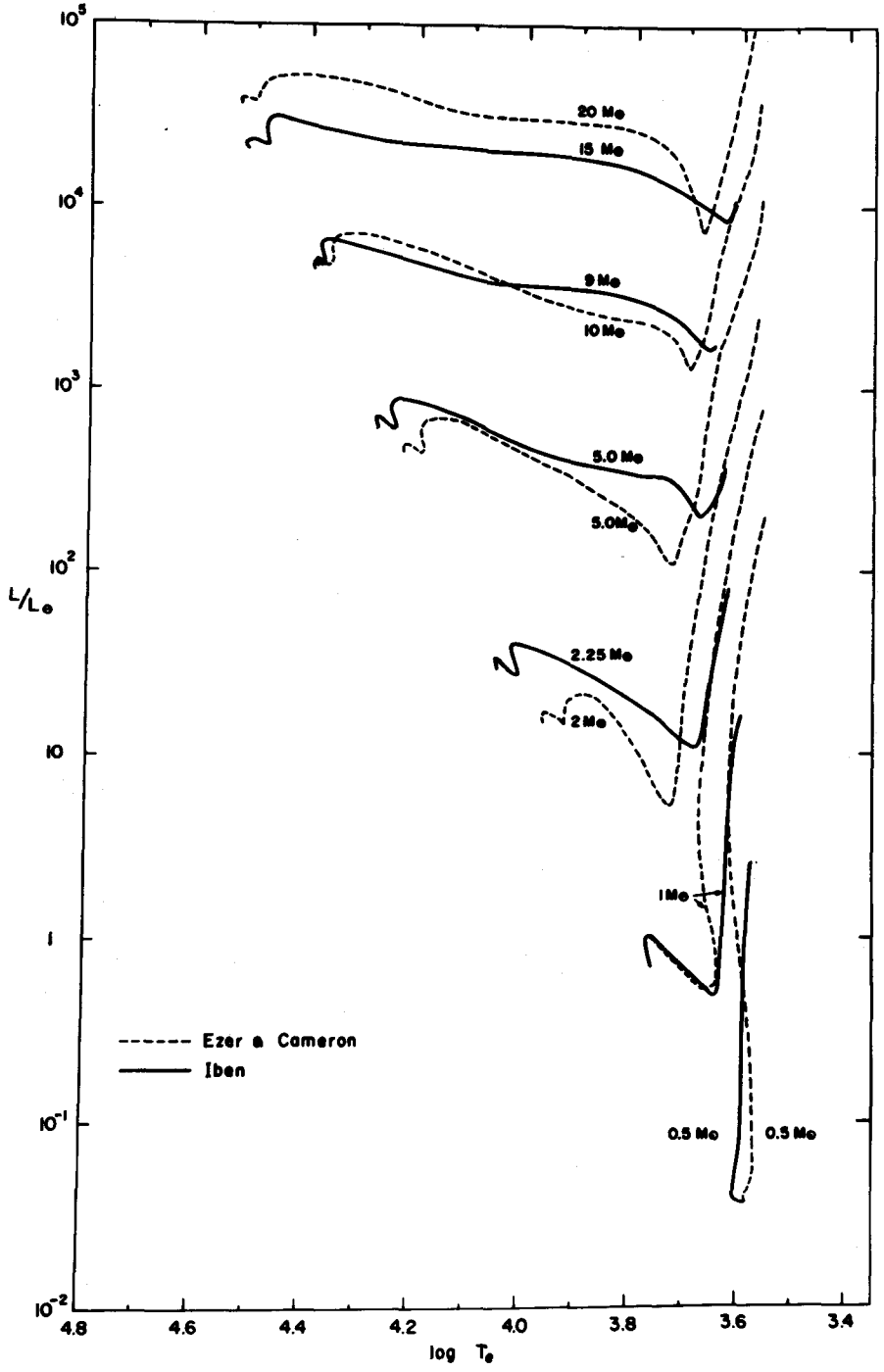

Fig. 5. Comparison with evolutionary tracks of Iben.

lower-mass stars. The stars of 0.2 to 0.4 solar masses evolve down onto the main sequence, but the 0.1 solar mass star evolves directly into a white dwarf without burning hydrogen at all. This mass is slightly above the limit calculated by Kumar for contraction to a white dwarf without hydrogen burning.

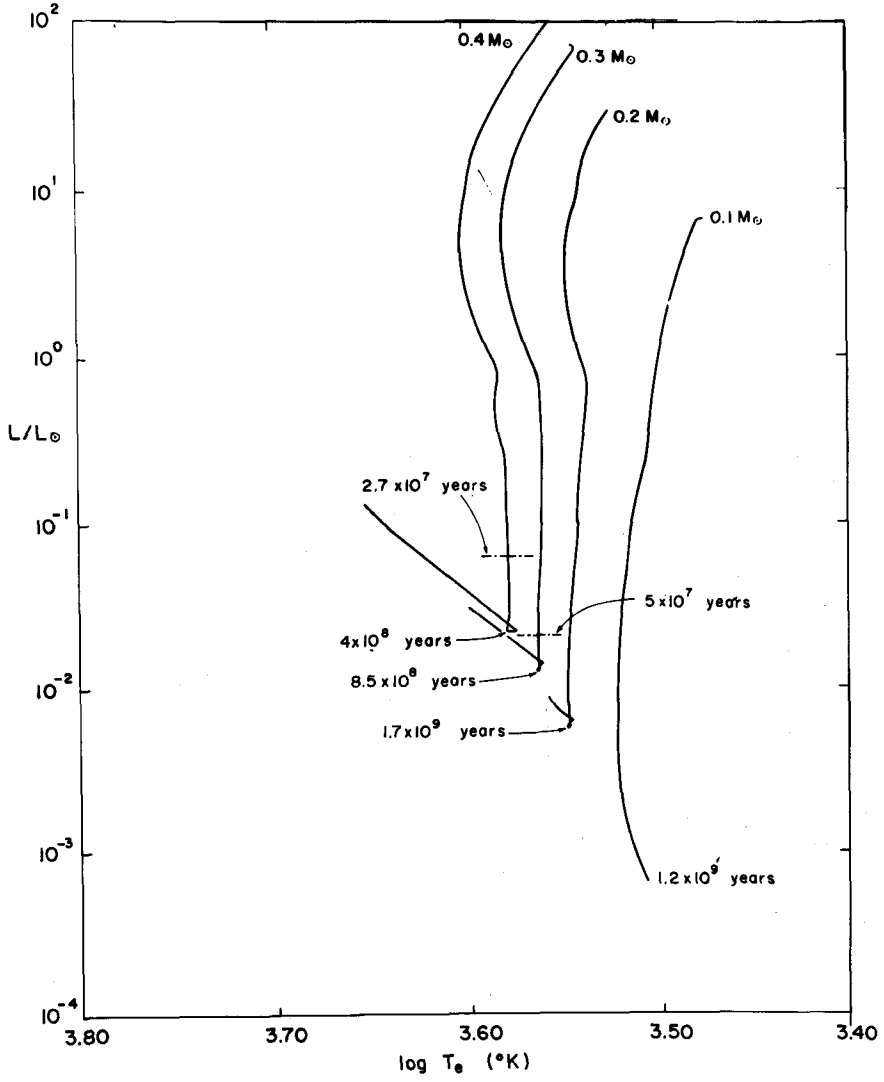

Fig. 6. Evolutionary tracks for low mass stars.

Now let us see what results are obtained when we take angular momentum into consideration. We can assume that given a cloud on the threshold of collapse, it is under sufficient magnetic control so that its angular velocity is roughly equal to the angular velocity which it would have if it were in synchronous rotation about the galactic center. This value is about 10^{-5} radians/sec. There has been considerable discussion about possible mechanisms for removing angular momentum from collapsing gas clouds. However, for the given density and angular velocity, it can be shown that the amount of twist undergone by the collapsing cloud is quite small until its radius has decreased by at least a factor of 10 (Cameron 1962). The cloud is now approaching the condition, described by Pneuman and Mitchell (1965), under which the rate of ohmic dissipation of the trapped interstellar magnetic field becomes relatively large. Thus the magnetic field in the collapsing cloud fragments tends to decrease until it is down to the galactic level.

Under these conditions, there would be virtually no transport of angular momentum out of the cloud into the surrounding medium; the cloud fragments form by collapsing with a constant angular momentum per unit mass. This implies that a cloud fragment of about one solar mass would not form a star at all, but would collapse into a pure disk. The radius of such a disk is very sensitive to the angular momentum per unit mass of the fragment, but it will be of the order of tens of astronomical units. A uniform sphere which is uniformly rotating and which collapses tends to form a disk which is also uniformly rotating and which has a rather flat density distribution throughout its central region. However, an axially-condensed disk could also form under the same set of conditions. Since fragmentation is likely to involve some sort of density gradient increasing toward the center of the fragment, it is likely that the result would be an axially-condensed disk in which the mass density per unit area varies as $1/R$.

The amount of matter at the center of such a disk is too small to form a body in hydrostatic equilibrium, so the main problem to consider in the formation of a disk of this

sort is how it is dissipated. We must keep in mind that the disk is formed violently; that is, it is undoubtedly formed with a great deal of initial turbulence. The decay of the magnetic field back toward the galactic level in the late stages of collapse indicates that magnetic effects are probably so small as to be negligible, so we must deal with hydrodynamic effects. The question as to whether the turbulence can cause the dissipation of the disk was discussed by Von Weizsacker (1944), Kuiper (1949) and ter Haar (1950). Much of this discussion has subsequently been forgotten (perhaps unjustifiably) because it was pointed out that if the angular momentum per unit mass is increasing outward in the disk, such a situation would result in the stabilization of laminar flow against the onset of turbulence. However, Von Weizsäcker pointed out that particles in elliptical orbits can have their relative positions reversed as a result of the revolution, so that retrograde eddies can be set up without any violation of the laws of celestial mechanics. In fact, the turbulence which is violently initiated during the formation of a disk is likely to result in fairly large retrograde eddies. The principal physical question (for which there is not yet a good quantitative answer) is then whether the turbulent viscosity associated with an eddy system of this sort will be able to dissipate the disk. If so, mass is driven toward the center to form a star, thereby releasing energy and at the same time transporting sufficient angular momentum outwards to drive the edge of the disk outwards and to concentrate the angular momentum toward the edge.

The cooling time for these disks, assuming black body radiation, is proportional to $1/T^3$, where T is the temperature; for typical cases this means that cooling to temperatures of the order of 2000° K will occur in only a few months throughout most of the inner parts of the disk. To get down to temperatures of a few hundred degrees will take a few years at most. Consequently, the probability of observing a disk of this sort is rather small, in view of the short time scale involved.

When the temperature falls below 1500° K solid particles will begin to condense. Colgate has pointed out that if any electric fields are present, turbulence in gases of

this sort will tend to separate charges. That is, turbulent energy is being converted to electrostatic energy. We can consider the equation $1/2\rho V_T^2 = E^2/8\pi$, where V_T is the turbulent velocity and E is the electric field strength, as an approach condition because electrical breakdown in the gas is reached long before equality is reached. That means that an additional significant dissipation mechanism in the disk will be the resulting lightning flashes. However, these electric forces are very significant in terms of the formation and accumulation of chondrules. This is an idea first suggested by Whipple which I have been developing recently, and it seems to be very promising.

Once a star is on the Hayashi track, it will develop a hot corona, causing a strong solar wind which blows away the remainder of the gas in the disk. During this phase the star may well be in a state similar to that described previously by Low; namely, there is a rather ordinary reddish star, surrounded by a great deal of nebulosity and particles which absorb much of the radiation from the star and re-radiate it farther in the infrared. This may indeed be an observable phase.

REFERENCES

Cameron, A. G. W., Icarus **1**, 13 (1962).
Gaustad, J. E., Astrophys. J. **138**, 1050 (1963).
Kuiper, G. P., Astrophys. J. **109**, 308 (1949).
Parker, E. N., Astrophys. J. **145**, 811 (1966).
Pneuman, G. W. and Mitchell, T. P., Icarus **4**, 494 (1965).
ter Haar, D., Astrophys. J. **111**, 179 (1950).
von Weizsacker, C. F., Z. Astrophys. **22**, 319 (1944).

DISCUSSION

M. Harwit: If we take the present star formation rate to be of the order of one star per year in the galaxy, then there should be a reasonable number of Hayashi-phase objects around. If the stars in the brightest stages, which only

last about 100 years, are uniformly distributed, we should probably find one within about a kiloparsec. But what should one look for? How would a 3, 000° K Hayashi-phase object differ from a 3, 000° K star? I suppose one might look for them in regions where star formation seems to be active.

A. G. W. Cameron: If these stars always form in clusters, then one would expect to find several in a given region. However, if formation is taking place in the environs of the initial collapsed cloud, there may still be sufficient interstellar grains in the remaining gas to obscure this process significantly. One can follow Low's suggestion that we consider those cases where the spectral energy distribution shows an irregular hump about where it would be expected for a 3, 000°K object, plus a longer tail in the far infrared.

M. Harwit: Another way we might recognize a very young star which is just flashing up into becoming a 0 star would be to look for some of the Kardashev lines--the very high-order transitions in atomic hydrogen--which would arise from the region of ionized hydrogen. These lines would be found in conjunction with the double-humped curve caused by the dust obscuration.

N. Woolf: If we have some doubt as to what happens to the angular momentum of the disk in the case of collapse from the interstellar medium, we do know that similar disks must arise in the case of mass transfer between close binary stars. In the case of ϵ Aurigae, where we see an eclipse by what appears to be a disk, Low has looked for infrared emission but has not observed any.

A. G. W. Cameron: However, in that particular case the gas is at a rather high temperature.

P. Thaddeus: Would you comment on the mode of ionization, produced by any source whatsoever, offsetting the turbulent growth of electrical fields?

A. G. W. Cameron: The principal sources of ionization that one may expect to find in the disk would be radioactive isotopes such as K^{40} or Al^{26}. The level of ionization attained in the nebula would not be grossly different from what is presently produced in the terrestrial

atmosphere by cosmic rays. Since the turbulent separation of fields is a process which seems to work for clouds in the atmosphere, I doubt that ionization would prevent the growth of the fields to the breakdown point in the nebula.

H. Spinrad: The Hayashi tracks presumably impose a boundary to a forbidden region on the right-hand side of the H-R diagram, and post-main sequence evolution runs into the same barrier, the position of which depends on the opacity sources. With such opacity sources, then, one would never see a red star in the sky.

A. G. W. Cameron: That is why I emphasize that one has to look for additional sources of opacity. The inclusion of opacity sources such as water or carbon compounds would allow the Hayashi boundary to move to the right a bit.

13

INFRARED OBSERVATIONS OF COMET 1965f*

E. E. Becklin and J. A. Westphal

I. INTRODUCTION

On September 18, 1965, K. Ikeya and T. Seki independently discovered a cometary object of about eighth magnitude. Early observations indicated that this comet, 1965f, was a member of the 1882 II family of sun-grazing comets and might well become visible in daylight as it neared the sun on October 21.

Infrared measurements were started October 6 with the 24-inch reflector at Mount Wilson. This comet was successfully observed on ten days before and on nine days after perihelion in wavelength windows centered at 1.65, 2.2, 3.4, and 10μ. The last observation was obtained on November 1. The comet-Earth distance varied less than 10 percent from the mean value of 1 a.u. during the full observing period. During the first and last parts of these periods, the measurements were taken before sunrise, while from October 16 until October 26 the data were obtained in daylight near transit of the comet.

---

* This article is reprinted with the permission of the Astrophysical Journal.

II. THE EQUIPMENT

Infrared measurements were made with two separate photometers mounted on opposite arms of the 24-inch reflector at Mount Wilson. This telescope, an f/16 bent cassegrainian, has hollow declination axes and a rotatable flat mirror which allows equipment to be mounted on each arm of the fork mounting and to be illuminated by a simple rotation of the "bending" flat. On those days when the comet was nearest the sun it was necessary to mask the eastern half of the telescope tube to prevent sunlight from illuminating the primary mirror.

The photometer and detector used for the 10-μ measurements were similar to those described by Westphal, Murray, and Martz (1963). The photometer used for the 1.6-, 2.2-, and 3.4-μ measurements is optically similar, though physically rather different. The detectors used in the shorter wavelengths were PbS cells cooled with liquid nitrogen. Each detector was mounted in a separate Dewar with a cooled band-pass filter to isolate the appropriate atmospheric window. Observations were made in windows at 1.5-1.8 μ, 2.0-2.4 μ, 3.0-3.8 μ, and 8.4-13.5 μ.

III. THE OBSERVATIONS

Table I is a record of the usable observations obtained from 1965f. Standard stars (Johnson 1964; Low and Johnson 1964) were observed to obtain absolute flux calibrations in all wavelength regions. Extinction was measured by observing stars or, with a diaphragmed telescope, the sun at various hour angles. The total extinction correction was less than 40 per cent for even the most extreme hour angles.

Figures 1-4 illustrate the observed absolute intensities in each wavelength region with respect to distance R from the sun. These intensities were observed in a 40" diameter circular area located on the head of the comet to yield maxi-

TABLE I

Perihelion, October 20.2

Date (U. T.)	1.65 μ	2.2 μ	3.4 μ	10 μ
October:				
6		X		
7		X		
8		X		
9		X	X	X
10		X	X	
12	X	X	X	X
14	X	X	X	X
16	X	X	X	
17		X	X	X
18		X	X	X
23	X	X	X	X
24	X	X	X	X
25			X	X
26	X	X	X	X
27	X	X	X	X
28	X	X	X	X
29	X	X	X	X
30	X	X		
November:				
1	X	X		

mum flux. During twilight observations this area was observed to be well centered on the starlike nucleus. The size of the error bars is, in most cases, due to uncertainty in the extinction correction.

The flux from the tail was observable for several days near perihelion. Figures 5 and 6 illustrate the normalized flux from the tail on two days for two and three wavelengths. These data resulted from scanning westward in right ascension from the nucleus with the 40" diaphragm. Figure 7 shows the tail at 3.4 μ on October 16 and 23. Flux profiles for various declination scans across the tail are also shown. The signal-to-noise ratio of these scans always exceeded 10:1; thus the sharp differences shown are real and not instrumental.

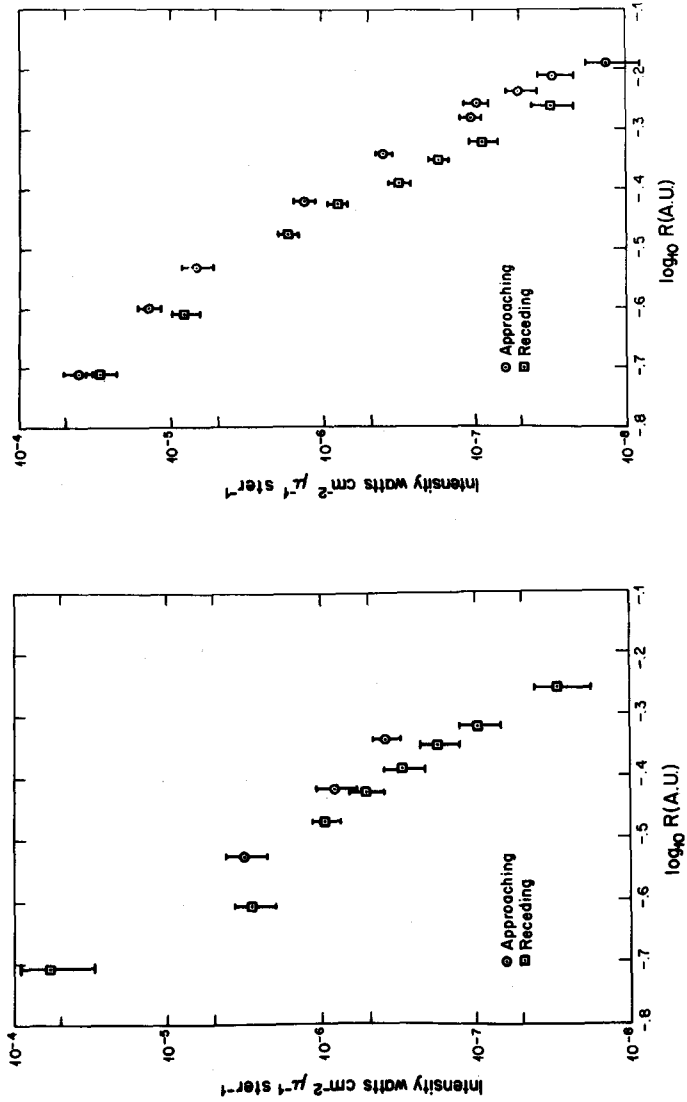

Fig. 1. Intensity at 1.65μ, measured in an area 40'' in diameter centered on the head of comet 1965f, displayed with respect to $\log_{10}$ of the comet-sun distance. The distance from earth to the comet was essentially constant.

Fig. 2. Same as Fig. 1 with intensity at 2.2μ.

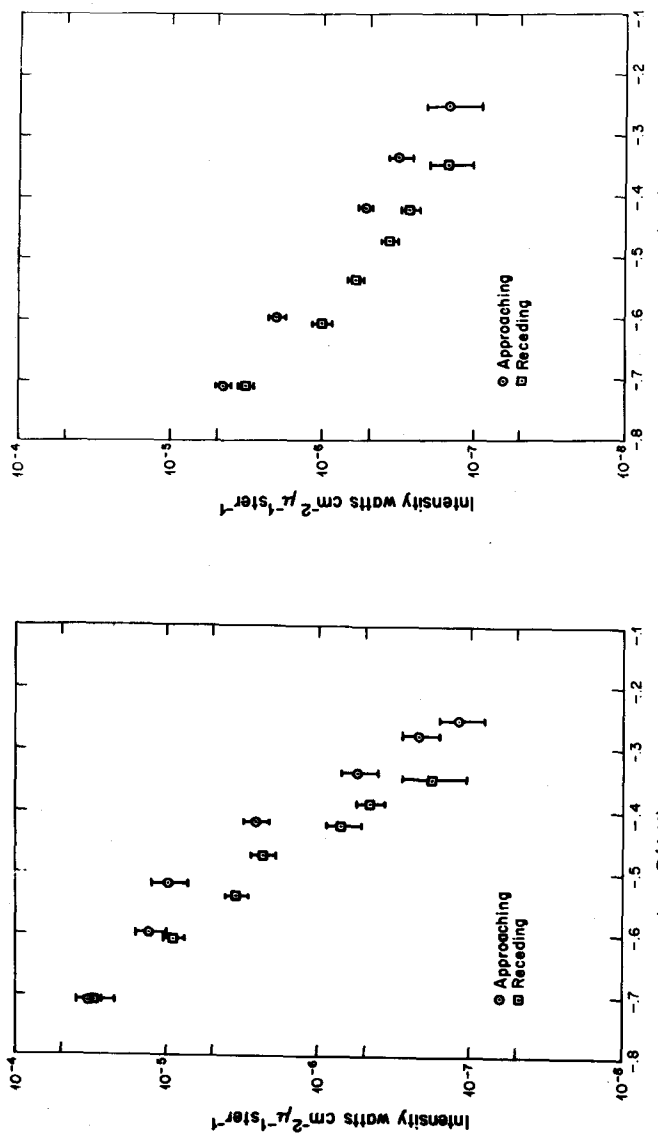

Fig. 3. Same as Fig. 1 with intensity at 3.4μ.

Fig. 4. Intensity at 10μ, measured in an area 30" in diameter centered on the head of comet 1965f, displayed with respect to $\log_{10}$ of the comet-sun distance. The distance from earth to the comet was essentially constant. The intensity values have been corrected to those that would have been measured in a 40" area by use of Fig.15.

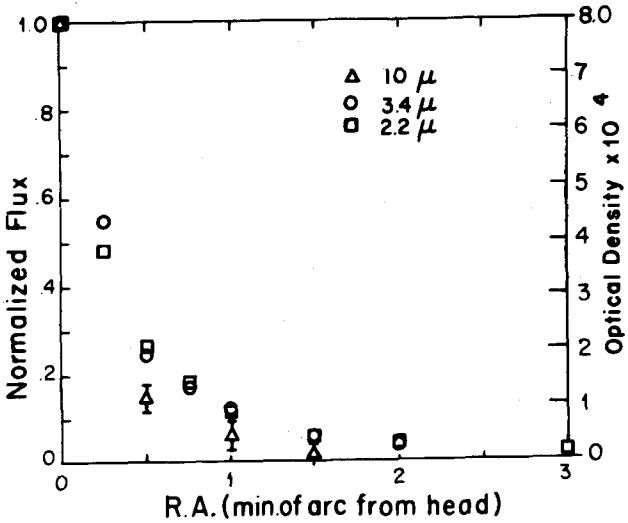

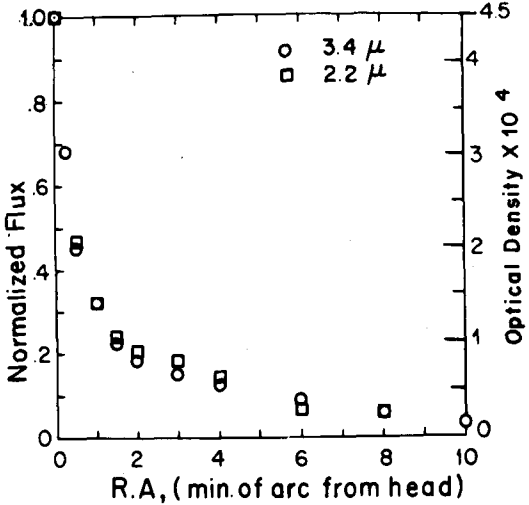

Fig. 5. Fluxes measured in the tail of comet 1965f at 0.195a.u. from the sun as the comet approached perihelion. The flux has been normalized at the head for each profile. The equivalent optical density, assuming clean iron particles, is shown on the right scale.

Fig. 6. Fluxes measured in the tail of comet 1965f at 0.195a.u. as the comet receded from the sun. The flux has been normalized at the head for each profile. The equivalent optical density, assuming clean iron particles, is shown on the right scale.

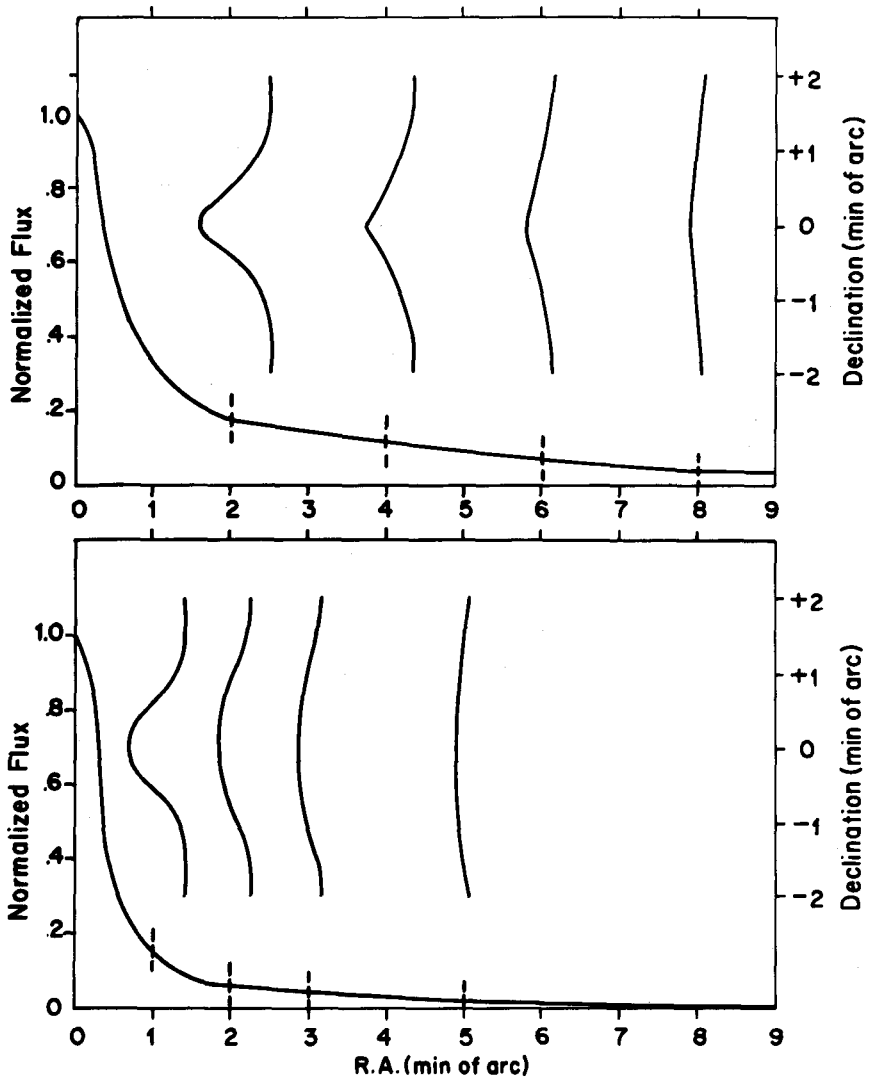

Fig. 7. The 3.4-μ flux from the tail of comet 1965f shown in the lower graph as the comet approached the sun on October 16, 1965, at a solar distance of 0.295 a.u. and in the upper graph on October 23, 1965, at a solar distance of 0.195 a.u. as the comet receded from the sun. The normalized flux along a right ascension profile is shown on the left, the declination profiles with the same flux scale at each of several locations along the tail with the declination scale on the right.

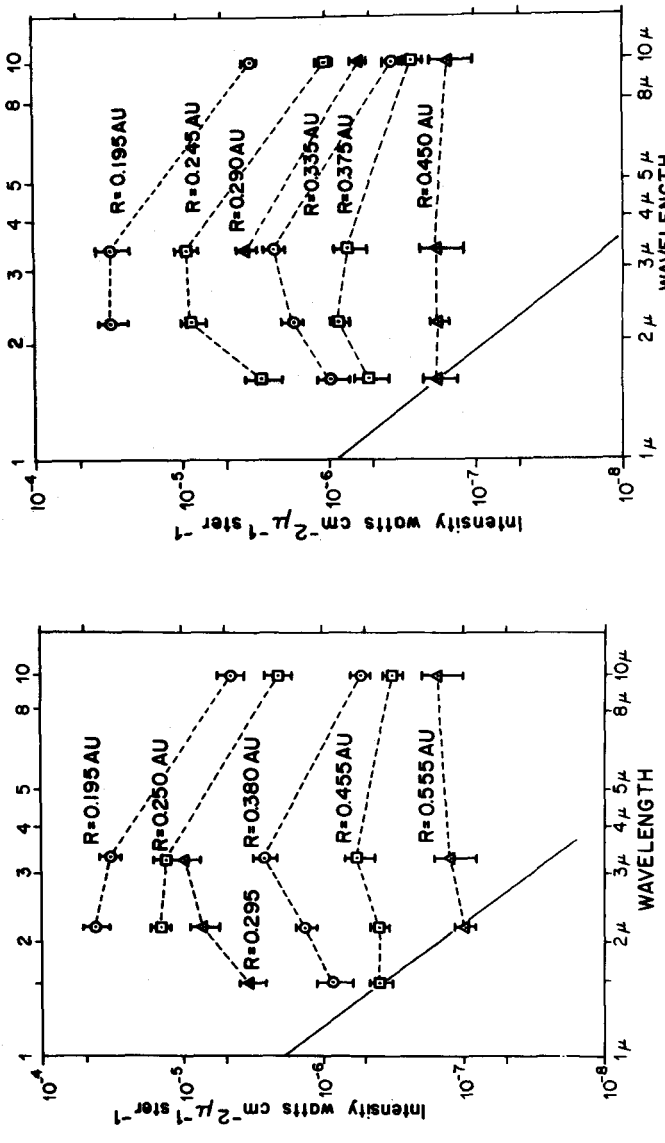

Fig. 8. Intensities measured about the head of comet 1965f displayed for each wavelength at various comet-sun distances as the comet approaches the sun. The slope of the solar spectrum is shown by the solid line on the left.

Fig. 9. Intensities measured about the head of comet 1965f displayed for each wavelength at various comet-sun distances as the comet receded from the sun. The slope of the solar spectrum is shown by the solid line on the left.

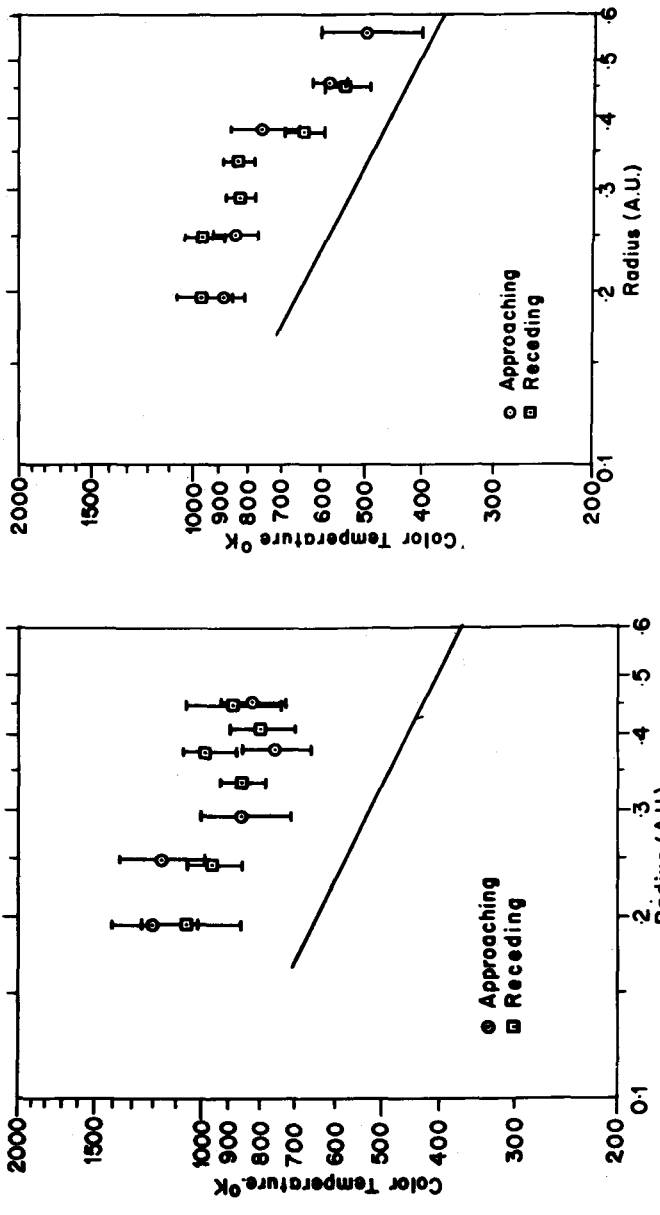

Fig. 10. The color temperatures calculated from the 2.2-and 3.4-μ intensities assuming a constant emissivity. The solid line shows the temperature reached by a black (or gray) conducting sphere due to solar heating.

Fig. 11. The color temperatures calculated from the 3.4-and 10-μ intensities assuming a constant emissivity. The solid line shows the temperature reached by a black (or gray) conducting sphere due to solar heating.

IV. COLOR TEMPERATURES

Figure 10 shows the color temperatures of the cometary head derived from the 2.2- and 3.4-μ data, corrected for solar reflection, assuming that all of the flux at 1.65 μ is reflected sunlight. The emitting material is assumed gray Also plotted is the equilibrium temperature for a black or gray conducting sphere assuming solar heating. Figure 11 illustrates a similar set of data derived from the 3.4- and 10-μ fluxes. The color temperature 1' from the nucleus along the tail on October 18 was essentially the same as that measured on the head. The effect of line emission or absorption on the above color temperatures can be estimated in the 2.2-μ region from spectra obtained on October 11 and 19, 1965 (D. McCammon and G. Neugebauer, private communication). The results show that line emission or absorption is less than 10 per cent of the continuum. The observed continuous spectrum in this region has a distribution which is consistent with the above color temperature.

V. DISCUSSION

The color temperature derived from both the 2.2-3.4-μ and 3.4-10-μ observations indicate a temperature higher than that which would be reached by a solar-heated gray body. However, the solar equilibrium temperature will agree with the color temperatures if it is assumed that the emissivity at 0.5 μ is about 4 times larger than the average emissivity from 2 to 10 μ. If the emissivities in the infrared decrease with increasing wavelength, as they do for those natural materials which have low-infrared emissivities, then the emissivities at 2.2, 3.4, and 10 μ must be in a ratio of about 2:1:1.

Of the materials observed to be present in this comet at perihelion (Dufay, Swings, and Fehrenback 1965), iron has approximately the above emissivity ratios. The emissivity of iron is given in Table II. Figures 12 and 13 illustrate the 2.2-3.4-μ and 3.4-10-μ color temperatures with the assump-

TABLE II

Emissivity of Iron (After Coblentz 1911)

$\lambda(\mu)$	ϵ	$\lambda(\mu)$	ϵ	$\lambda(\mu)$	ϵ
0.55	0.45	3.0	0.15	8.0	0.06
1.0	.35	4.0	.10	10.0	.05
1.5	.28	5.0	.08	12.0	.04
2.0	0.22	6.0	0.07	14.0	0.04

tion that the radiating material is clean iron in particle sizes large enough to radiate as bulk iron. The equivalent equilibrium temperatures are also plotted. The 3.4-10-μ temperatures in Fig. 13 appear somewhat low, suggesting that the emissivity at 10 μ is somewhat higher than that of clean iron. A small coating of oxide or other "black" material would selectively increase the apparent emissivity at longer wavelengths.

Since the effective emissivity of an electrically conducting particle is a function of the particle size to emitted wavelength ratio, the derived emissivity ratios might also be explained by assuming a distribution of particle sizes.

Of course it is not possible to rule out an internal heat source, although it would have to operate in each particle separately for the color temperature to remain the same in the tail where the density is about ten times lower than in the head.

Figure 14 shows the mean optical density τ_R in a region centered on the comet head as a function of distance R from the Sun. If $\tau_R \ll 1$ we have

$$\tau_R = \frac{I_{3.4}(R)}{\epsilon_{3.4} B_{3.4}[T(R)]}$$

where $I_{3.4}$ is the measured intensity, $\epsilon_{3.4}$ is the emissivity of iron, and $B_{3.4}[T(R)]$ is the Planck function at a temperature determined by the 2.2- and 3.4-μ intensities (see Fig. 12).

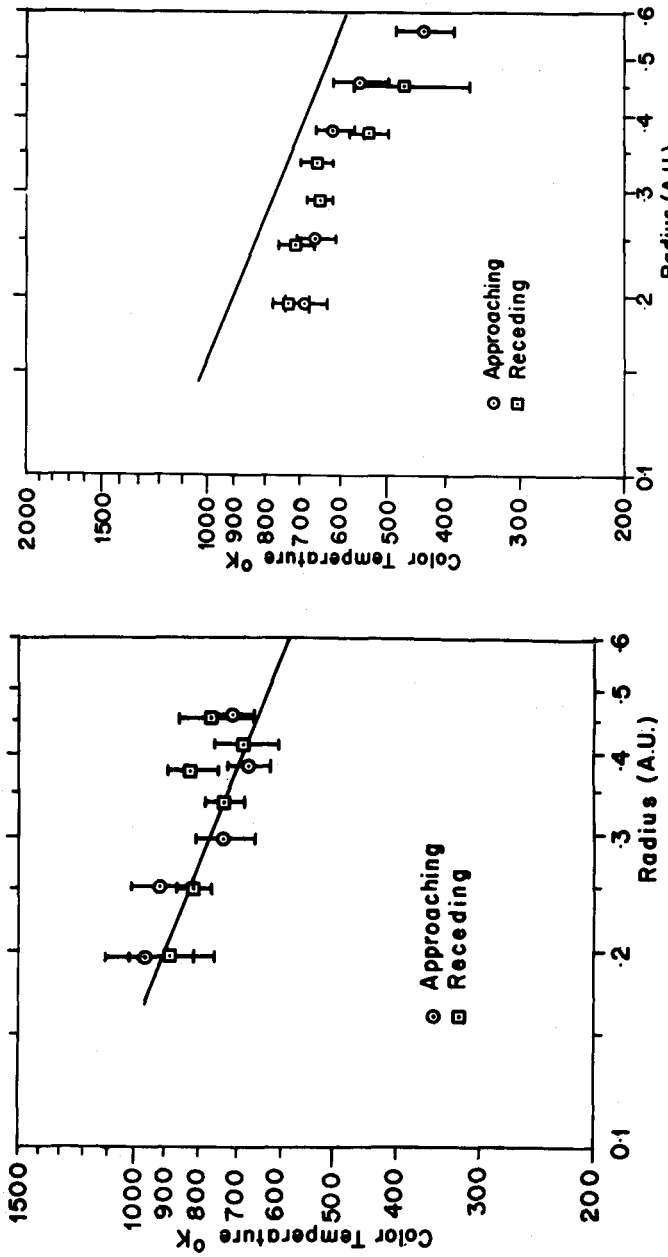

Fig. 12. The color temperatures calculated from the 2.2-and 3.4-μ intensities assuming an emissivity like iron. The solar line shows the temperature reached by an iron sphere due to solar heating.

Fig. 13. The color temperatures calculated from the 3.4-and 10-μ intensitites assuming an emissivity like iron. The solid line shows the temperature reached by an iron sphere due to solar heating.

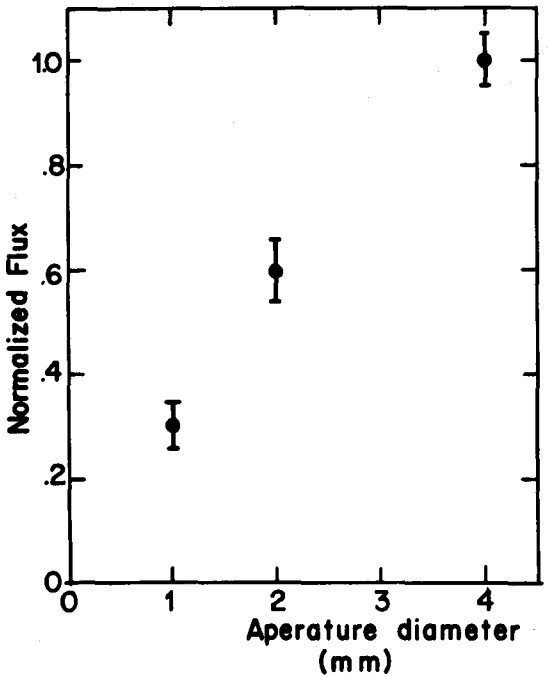

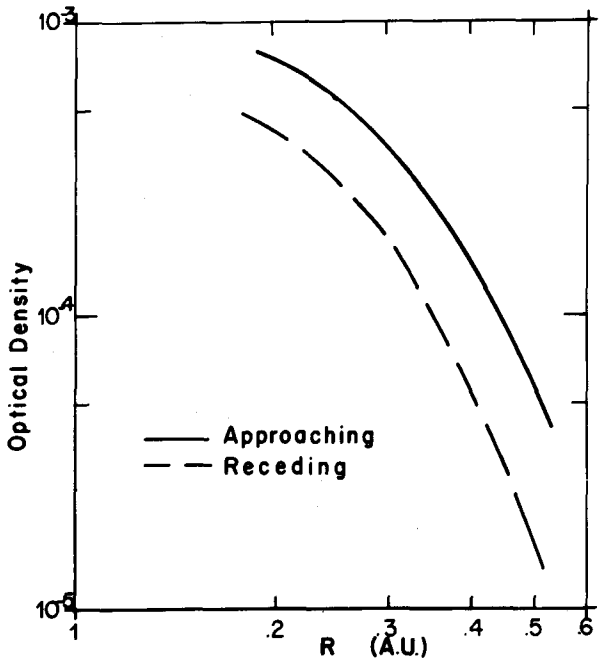

Fig. 14. The optical density of a 40" area around the head of comet 1965f, assuming iron emissivities.

Fig. 15. The relationship of flux and observing aperture size at 2.2μ on October 8, 1965.

The optical density may also be calculated from the reflected sunlight observed at 1.65μ, if one assumes that the particles have albedos similar to iron, are large with respect to the scattered wavelength, and scatter like a Lambert surface. The optical density calculated from the 1.65-μ data under these assumptions and that derived from the thermal data agree within experimental error.

The agreement of these independent measurements of optical density depends strongly on the use of the above emissivity ratios. For example, a gray material with an $\epsilon = 0.8$ results in a disagreement in optical density of more than a factor of 10.

It should be noted that the functional relationship between the optical density and the distance to the sun is about the same for both the approaching and the receding cases. This is consistent with the following assumptions about the processes taking place in the comet: (1) The measured thermal energy was coming from particles which were eroded off of a "solid" nucleus. (2) Over the period of observations the loss of material was small compared to the total material in the nucleus. (3) The velocity of the particles away from the nucleus was large enough so that the mean instantaneous optical density in the region of observation was determined by the instantaneous "boiling" rate. Each of these assumptions can be looked at more closely in terms of other information we have about the comet.

Figure 15 shows the measured flux from the head at 2.2 μ as a function of aperture diameter on October 8, 1965. The flux is seen to be proportional to aperture diameter within experimental error. If the particles are being generated uniformly and escaping with a uniform velocity distribution, then the calculated integrated particle density would be linear with radius from the nucleus.

The optical density data displayed in Fig. 14 show that in passing within 1 $R_\odot$ of the sun the nucleus lost only about $\frac{1}{2}$ of its surface area. This suggests that when the comet is farther from the sun the material lost is small compared to the total material in the nucleus.

A minimum velocity of the particles away from the nucleus can easily be calculated under the third assumption.

The particle velocity must be large enough so that in the time between observations the particles will travel at least the distance to the edge of the aperture. If we take the time $\sim 5 \times 10^4$ sec and projected aperture $\sim 1.5 \times 10^4$ km, then the velocity of expansion must be of the order of or greater than 0.3 km/sec. This can be compared to the following known velocities: (1) The development of the tail shown in Fig. 6 after perihelion requires a velocity of at least 3 km/se (2) Spherical halos from the nucleus of Halley's comet in 1910 had expansion velocities less than 1 km/sec (Bobrovnikoff 1931). (3) The two parts of this comet observed after perihelion were separating at about 0.03 km/sec (Pohn 1965).

It is interesting to note that, from the calculated optical density two days before and two days after conjunction with the sun, it may be concluded that the surface of the nucleus was reduced by a factor of about 2. This implies that the physical radius was reduced by about 30 per cent and the mass was reduced by about 65 per cent.

VI. SUMMARY

Observations in the infrared of comet 1965f have shown that the color temperature changes with distance to the sun in about the way expected from solar heating. For solar-heated particles, the ratio of emissivities between the visible and the infrared must be about 4.

The color temperature measured in the tail is essentially the same as that measured in the head.

If one assumes that the emissivity decreases smoothly with increasing wavelength then the emissivity ratio from 2.2 to 3.4 μ is about 2:1 and that from 3.4 to 10 μ is about 1:1.

We would like to thank Drs. G. Neugebauer, G. Münch, and B. C. Murray for valuable discussions.

REFERENCES

Bobrovnikoff, N. T., Pub. Lick Obs. **17**, Part 2 (1931).
Coblentz, W. W., NBS, Scientific Paper 152, p. 213 (1911).
Dufay, J., Swings, P., and Fehrenback, Ch. Astrophys. J. **142**, 1698 (1965).
Johnson, H. L., Bol. Tonantzintla y Tacubaya Obs. **3**, 305 (1964).
Low, F. J. and Johnson, H. L. Astrophys. J. **139**, 1130 (1964).
Pohn, H., I.A.U. Circular No. 1937, 1965.
Westphal, J. A., Murray, B. C., and Martz, D. E., Appl. Opt. **2**, 749 (1963).

DISCUSSION

M. Harwit: Actually, all that is necessary is that the material have an imaginary component to the index of refraction, and almost any dirty type of material will have this. Consequently, one wouldn't expect to have pure dielectrics there, which is what you were trying to throw out.

J. A. Westphal: Yes, but you must have a substance that has an emissivity four times greater in the visible than it does in the infrared. You cannot start out with something which has an emissivity in the infrared of .5, for example, since the emissivity cannot be greater than 1 in the visible. All dielectric materials or dirty materials have high emissivities in the infrared to start with. Silicates, for example, have emissivities of .8 or so.

E. P. Ney: Almost any metal will have the characteristics you require.

J. A. Westphal: This is true of the poorly conducting metals such as iron, cobalt, nickel, lead, zinc, tin and so forth.

L. Aller: Yet, you pointed out that iron didn't quite work because at 10 microns the emissivity was too low.

J. A. Westphal: This can be corrected by having 10% of the

system as dirt. This is not too difficult to accept, particularly if these particles are glued together in the head. Spinrad has pointed out to me that afterwards the comet developed some gaseous emission features; apparently there was in fact some gaseous material involved, which may also be the glue.

W. Sinton: Do you have any explanation for the fact that the tail was visually much brighter after the encounter?

M. Harwit: This is quite common; the reason is that the dust grains that come off have very low velocities with respect to the comet's head and take about a month to move away. When the comet passes close to the sun a great deal of this material is released from the matter that constitutes the comet's head.

J. A. Westphal: But this mechanism should also apply to the iron grains as well, and yet we observed a decrease of a factor of 2. This seems to be somewhat of a paradox.

M. Belton: If these cometary grains are responsible for the zodiacal light, what will be the effect of these high temperatures?

M. Harwit: Once the grains leave the comet's head, the light pressure on them changes their effective gravitational attraction with respect to the sun so that they come off with positive total energies. Therefore they will drift out of the solar system. For nearly parabolic comets, almost none of the debris stays behind to become part of the zodiacal dust.

14

THE DRY MASSIVE MODEL OF THE ATMOSPHERE OF VENUS

Patrick Thaddeus

Although considerable effort has been devoted to their detection, no resonant lines due to polar molecules have ever been observed in the radio spectrum of Venus. Instead, a continuing decline of brightness temperature with increasing frequency, beginning at about $\lambda = 2$ cm ($\nu = 15$ GHz) is found, which suggests some non-resonant source of atmospheric opacity which increases with frequency.

The dry, massive model of the Venus atmosphere dates from Barrett's (1961) suggestion that the microwave opacity of the atmosphere might be due to collision-induced absorption in CO_2 or other non-polar molecules—an effect which depends on the square of the density and in consequence only becomes appreciable at a pressure of several tens of atmospheres. This model is inspired by the near-infrared spectroscopy to the extent that, as far as atmospheric gases are concerned, it makes do with what is observed (for all practical purposes only CO_2), considering in addition only spectroscopically inert molecules such as N_2 which would escape detection. One then seeks to discover under what physical conditions such constituents can account for two of the most basic properties of the atmosphere: the microwave and infrared opacities.

In particular, this model takes the low amount of atmospheric water vapor derived from the spectroscopy at its face value, and it of course assumes that the high microwave temperature of Venus is of a thermal origin. A high Rosseland mean opacity in the thermal infrared of at least 50-100 is then required to prevent radiative bleeding away of the heat from the lower atmosphere, irrespective of whether the lapse rate is maintained by a true greenhouse mechanism, with sunlight reaching the ground, or by adiabatic heating due to the general circulation, as discussed by Goody and Robinson (1966).

It is evident from the scattering and polarization properties of the Venus atmosphere, and the limb darkening in the thermal infrared, that some sort of particulate matter is present, but the dry, massive model rests in part on the realization that quite a small amount of dust or ice crystals can account for these observations--far less than is needed to provide the requisite microwave and infrared opacities of the deep atmosphere. On the other hand, the situation considered by Goody and Robinson, with dust furnishing a massive infrared opacity in the lower atmosphere, is clearly a variant of the dry, massive model as long as the microwave opacity is still provided by induced absorption in CO_2.

Figure 1 shows how well the dry, massive model accounts for the microwave opacity and hence the microwave brightness as a function of frequency. The radio observations shown are those reported prior to the spring of 1966 and refer to the unresolved disk of the planet. The theoretical curve for the unresolved disk shown in Fig. 1 is calculated on the basis of a cloud-top temperature of 250°K, an average ground temperature of 675°K, and a dielectric constant of 3.75 for the ground, as found by interplanetary radar (Carpenter 1966). The atmosphere is assumed to be isothermal above the clouds, and to possess an adiabatic lapse rate from the ground to the cloud tops. The microwave induced absorption coefficient α used in the calculation is that found by Ho, Kaufman, and Thaddeus (1966) from laboratory studies of model CO_2-N_2 atmospheres:

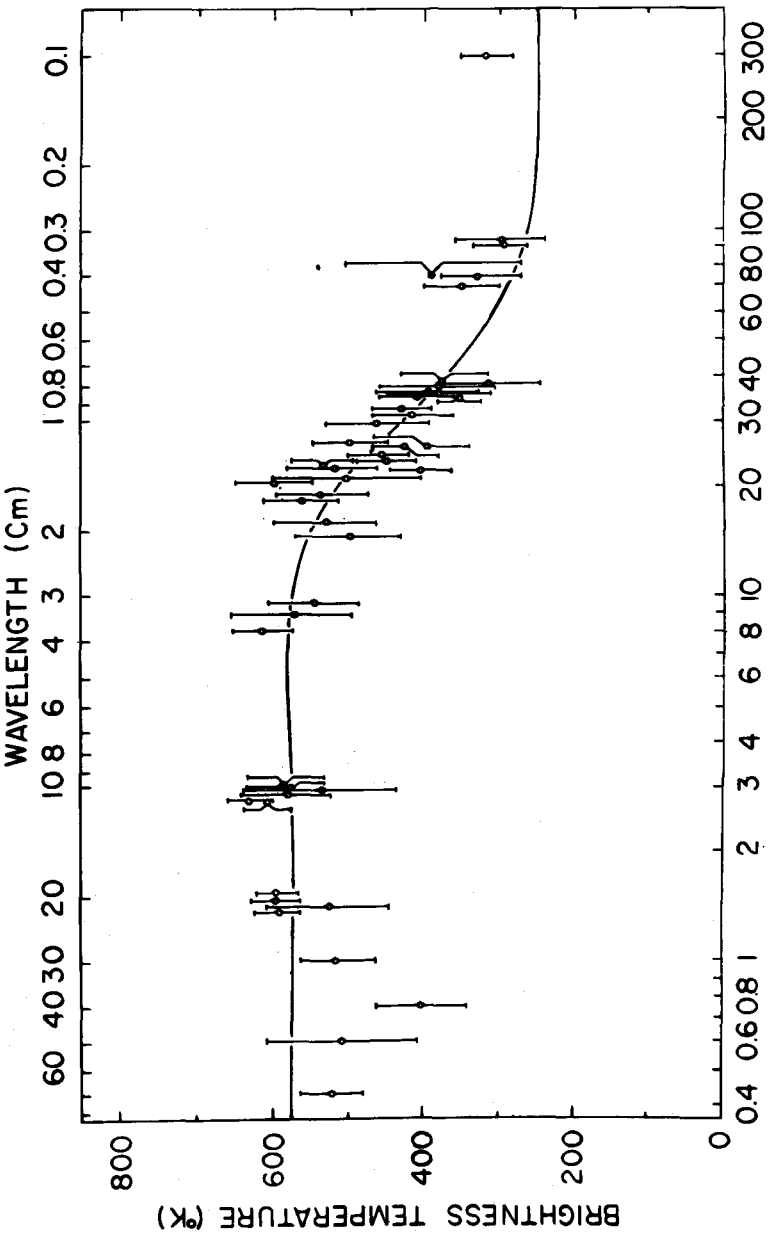

Fig. 1. Radio observations of the unresolved disk of Venus

$$\alpha = P^2 \bar{\nu}^2 (273/T)^5 (15.7\, f_{CO_2}^2 + 3.90\, f_{CO_2} f_{N_2} + 0.085\, f_{N_2}^2) \times 10^{-8} \mathrm{cm}^{-1} \quad (1)$$

where P is the pressure in atm, $\bar{\nu}$ is the frequency in wave numbers, T is the Kelvin temperature, and f_{CO_2} and f_{N_2} are the molar fractions of CO_2 and N_2. Further details of the calculation and the laboratory measurements are given in the paper by Ho, Kaufman and Thaddeus, while this and other models of the radio spectrum have been considered by Barrett and Staelin (1964).

The slight decline in the observed microwave brightness at long wavelengths shown in Fig. 1 may in part be an effect of surface roughness, which is not included in the theoretical calculation. Such an effect is also predicted by the dry, massive model if the lapse rate is substantially subadiabatic near the ground. In any case, since the blackbody intensity of radiation falls off as the inverse square of the wavelength, while sidelobe and interference problems are more serious than at shorter wavelengths, these recent long wavelength observations cannot as yet be given the same weight as those made over the last ten years in the range $\lambda = 21 - 3$ cm.

On the basis of equation (1), the theoretical spectrum shown in Fig. 1 applies to any $CO_2 - N_2$ atmosphere, but with the best-fit ground pressure a function of the fraction of CO_2. Figure 2 shows this relationship. If CO_2 is a minor constituent of the atmosphere as Chamberlain's (1965) analysis of the near-infrared rotation-vibration bands suggests, then the dry, massive model requires a ground pressure of several hundred atmospheres to satisfy the radio observations, but note that if CO_2 is the dominant constituent [as indicated by the most recent infrared work of Belton, Hunten and Goody (1967)] then a pressure as low as 20 atm suffices.

This would seem to be about all that can be learned from radio observations which do not resolve Venus, leaving aside the microwave phase effect, which in my view is such a difficult observation, and one so liable to systematic uncertainties, that it must at this time be given a low weight

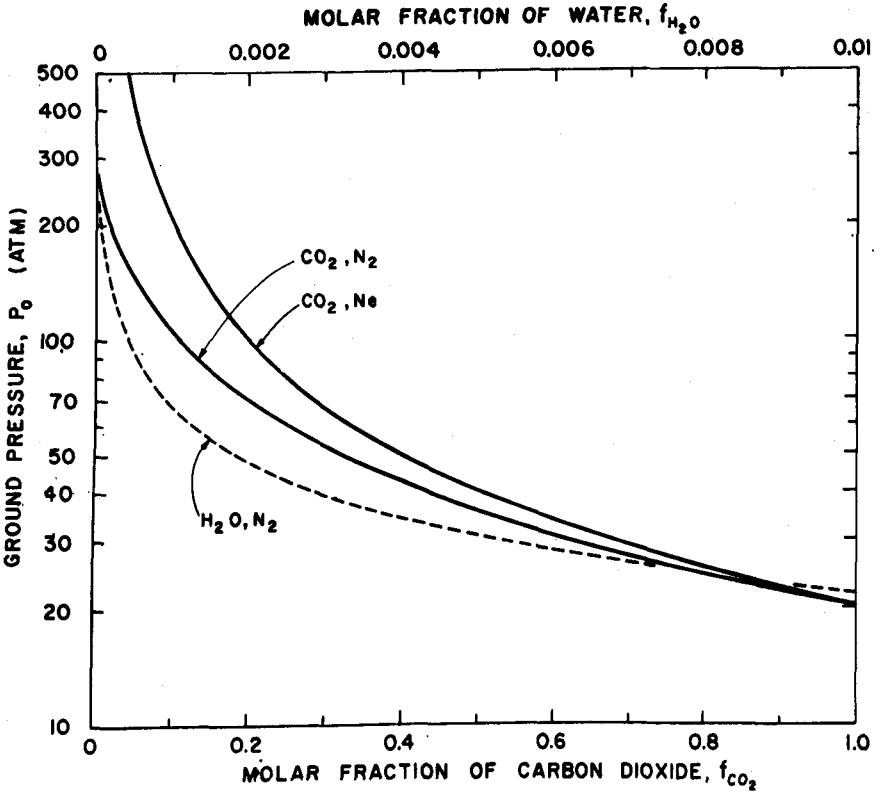

Fig. 2. The ground pressure on Venus as a function of atmospheric composition if pressure-induced absorption is the source of the microwave opacity.

in the over-all analysis. It is true that the simple model shown in Fig. 1 does not provide the vertical atmospheric opacity at $\lambda = 3.8$ cm required to explain the observed radar cross sections at the highest frequencies (Evans, Ingalls, Rainville, and Silva 1966). However, another degree of freedom in our model—say an isothermal or subadiabatic layer near the ground and a somewhat higher ground pressure—will give a good account of these and all the other radar observations to date, while actually somewhat improving the fit to the passive radio data shown in Fig. 1, as mentioned above. If sunlight does not reach the ground, and the circulation in the lowest scale height of the

atmosphere is inhibited by (for example) topographical features, then the existence of such a layer is very plausible.

Let us now turn to the important question of whether the high requisite infrared opacity is provided by the dry, massive model. Several years ago Plass and Stull (1963) calculated the transmittance due to the allowed infrared transitions of CO_2, and it can easily be shown from their work that the Rosseland mean opacity due to allowed transitions alone of the dry, massive atmospheres discussed above is considerably less than 50. As in the microwave region, however, induced transitions contribute broad absorption bands whose width depends on the duration of a collision rather than the interval between collisions, and is thus independent of pressure. The contribution of such transitions to the Rosseland mean opacity can be particularly effective, and I therefore suggested several years ago, on the basis of the strongest induced bands observed in the laboratory, that the dry, massive model might by itself furnish the requisite mean opacity of 50-100 (Thaddeus 1965). Solomon elsewhere in this volume describes calculations which he has recently done in collaboration with R. E. Danielson, based on all the observed induced transitions in CO_2 and N_2, which strongly support this idea.

It should be borne in mind, however, that the laboratory data at high pressure are usually taken over quite short path lengths, and that weak induced bands which can make a significant contribution to the Rosseland mean opacity over paths of tens of kilometers might so far have escaped detection. In this event, the calculations of Solomon and Danielson may only represent a lower limit to the mean infrared opacity of the dry, massive atmosphere.

Mr. John Moore, for his doctoral research in the Physics Department at Columbia (the work is actually being done at Lockheed Electronics, Plainfield, New Jersey), has constructed a high pressure, high temperature infrared White cell which should shed some light on this question, and will in any case provide good laboratory opacities to compare with the theoretical calculations. The path length

of this instrument is about 40 meters, and it can attain a pressure of 200 atm and a temperature of 600°K. It is designed to operate over the spectral range 1 - 20 microns.

REFERENCES

Barrett, A. H., Astrophys. J. **133**, 281 (1961).

Barrett, A. H. and Staelin, D. H., Space Sci. Rev. **3**, 109 (1964).

Belton, M. J. S., Hunten, D. M., and Goody, R. M., in The Atmospheres of Venus and Mars, edited by J. C. Brandt and M. B. McElroy (Gordon and Breach, New York, 1967).

Carpenter, R. L., Astron. J. **71**, 142 (1966).

Chamberlain, J. W., Astrophys. J. **141**, 1184 (1965).

Evans, J. V., Ingalls, R. P., Rainville, L. P., and Silva, R. R., Astron. J. **71**, 902 (1966).

Goody, R. M. and Robinson, A. R., Astrophys. J. **146**, 339 (1966).

Ho, W., Kaufman, I. A., and Thaddeus, P., J. Geophys. Res. **71**, 5091 (1966).

Plass, G. N. and Stull, V. R., J. Geophys. Res. **68**, 1355 (1963).

Thaddeus, P., Advances in the Astronautical Sciences **19**, 201 (1965).

15

OPACITY OF THE VENUS ATMOSPHERE

P. M. Solomon

The infrared opacity for several model atmospheres assuming various mixtures of CO_2 and N_2 has been calculated by Danielson and Solomon (1966, 1968). It has been found that collision-induced transitions are extremely important sources of opacity which have previously been neglected in models of the greenhouse effect.

If the temperature of Venus is 600° K at the surface then a minimum harmonic mean optical depth of 50-100 is required to maintain the difference between the surface and the expected black body temperature of 230° K. Whether or not there is any infrared opacity in clouds composed of water vapor as proposed by Sagan and Pollack (1967, 1968) is largely irrelevant to the greenhouse problem since such clouds cannot exist at a high temperature. Whatever the source of radiative opacity is, it must at least exist in the atmosphere at the temperatures generating the radiation.

The opacity for a model containing 10 atmospheres of CO_2 and no H_2O, in the spectral range $200\mu > \lambda > 2\mu$, is given in Fig. 1. Collision-induced transitions have been neglected in this case and even though the optical depth is extremely great in the centers of all the permitted bands (including the "hot" bands), there are huge windows which make the mean transmission practically infinite. Obviously permitted transitions alone are not sufficient to solve the problem.

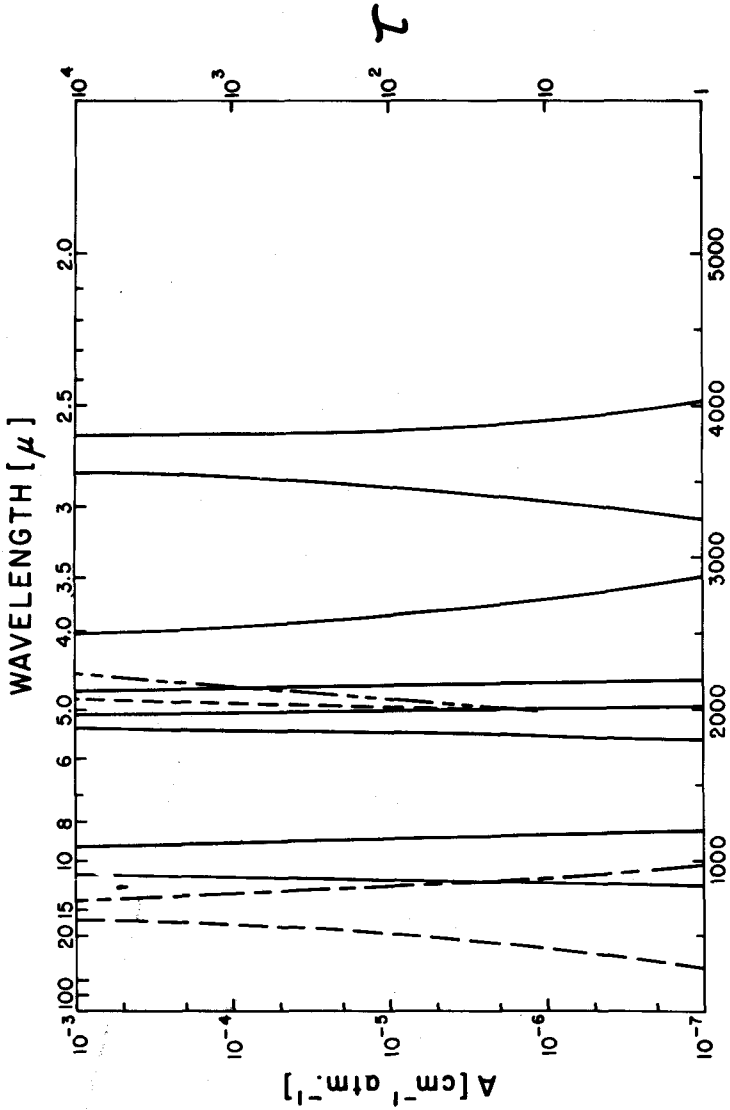

Fig. 1. Calculated optical depth as a function of wavenumber for the permitted bands of CO_2, in a model at 600° K, with a surface pressure of 10 atmospheres.

A large amount of information on the characteristics of collision-induced bands has been obtained in the laboratory and many of the results presented here are based on the experiments of H. L. Welsh and his collaborators at the University of Toronto. The collision-induced rotational band of N_2 measured at a temperature of 300° K (Bosomworth and Gush, 1965) is presented in Fig. 2. It can be seen that the band is much wider than would be indicated by the regular rotational levels, and that there are no spaces between the lines; the band is effectively a continuum. As a result of an analysis of the shape of this band we have found that the line profile for the high frequency end can be fitted quite accurately by an exponential. Figure 3 gives the experimental results for the collision-induced Fermi resonance bands of CO_2 centered at 1280 and 1380 cm^{-1} (Gaizauskas 1955). These bands are extremely important since this is the location of one of the main "windows" in the atmosphere of Venus which cannot be filled with permitted bands of either H_2O or CO_2. One of the most interesting properties,

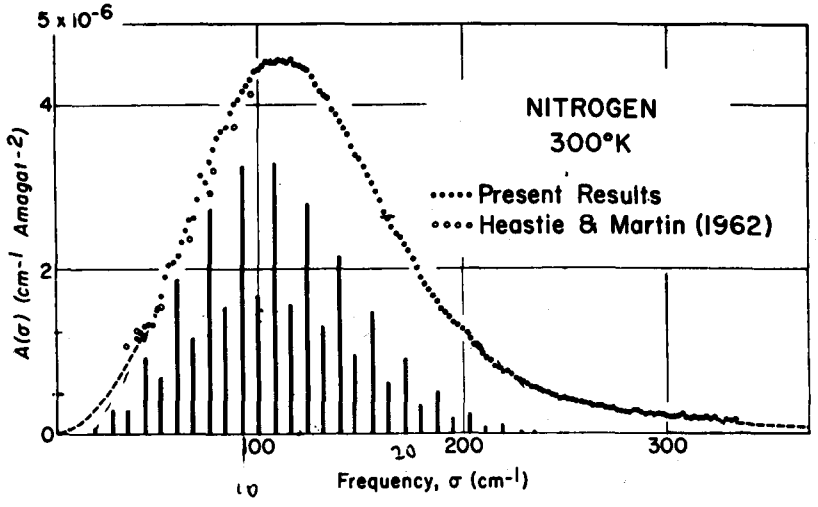

Fig. 2. Experimental absorption profile of collision-induced rotational bands of nitrogen (Bosomworth and Gush).

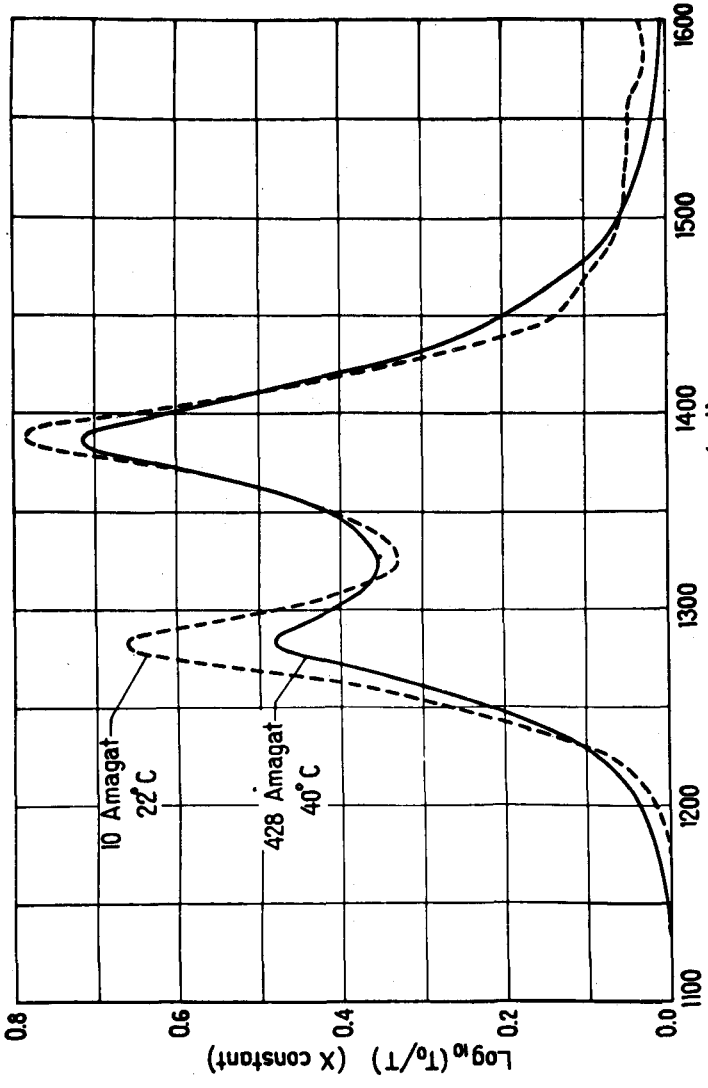

Fig. 3. Experimental absorption profile of the collision-induced Fermi-resonance bands of CO_2.

demonstrated in this case, is that the width of the band is independent of the density. This is completely opposite to what would be expected from pressure broadening of regular bands.

As Thaddeus mentioned in the previous paper, the width of the band is determined by the duration of the collision. Due to the short time that the molecules are in collision there is a large uncertainty in the energy of the molecular levels during the transition. Thus the energy levels completely overlap and the result is a true continuum. Since the collision time $\Delta t \sim T^{-1/2}$ we take the width of the band to be proportional to $T^{1/2}$ where T is the temperature. This has been verified experimentally for the hydrogen bands at temperatures up to about 300° K. The strength of the absorption band is determined by the number of collisions which is proportional to the square of the density or more generally

$$\tau_\nu = \rho_a \rho_b \alpha_\nu l$$

where ρ_a is the density of the molecule undergoing the transition, ρ_b is the density of the perturber, l is the path length and α_ν is the absorption coefficient.

Using the characteristics of the bands discussed above we have calculated the opacity for a model at 600° K, taking account of all known collision-induced bands of N_2 and CO_2 including the simultaneous transitions in both molecules. The results are presented in Fig. 4 for 10 atmospheres of CO_2 and 90 atmospheres of N_2. According to this model there is only one large gap left in the atmosphere but this is filled by the permitted CO_2 bands. When the effects of permitted and collision induced bands are combined we obtain an opacity as shown in Fig. 5. The black body curve for 600° K peaks at about 800 cm^{-1} and it can be seen that there are no gaps near the maximum.

The Rosseland mean opacity $\bar{\tau}$ has a value of 50 for the $10CO_2$ - $90N_2$ model. If a small fraction of water vapor is included then the required pressure goes down substantially. The calculated $\bar{\tau}$ for a $10CO_2$ - $40N_2$ model is approximately 30 but will exceed the required 50 with the addition of

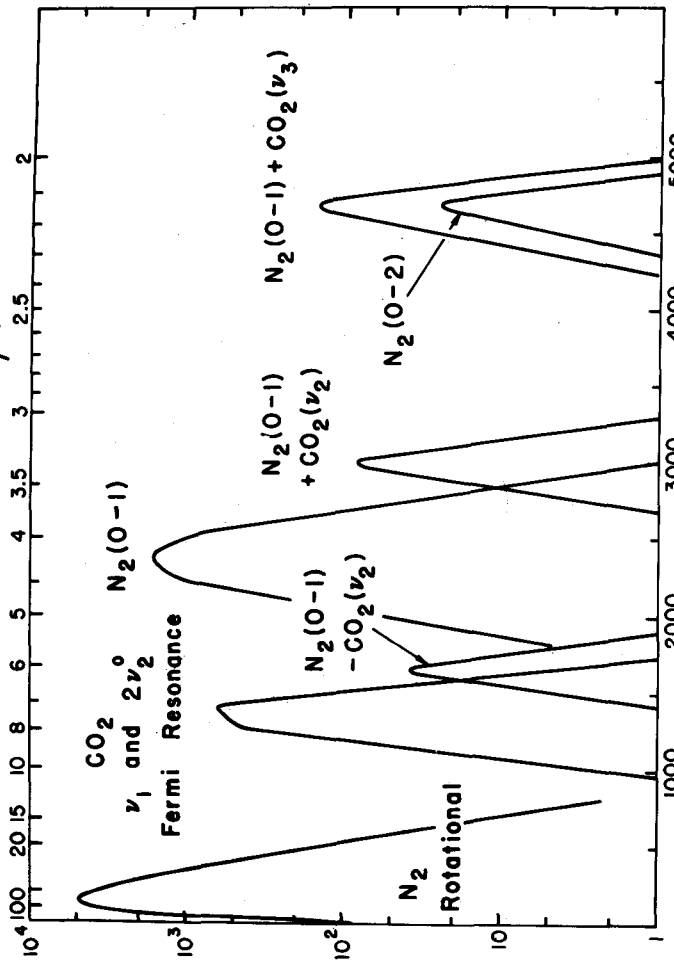

Fig. 4. Calculated optical depth for collision-induced bands in a model atmosphere with a surface pressure of 10 atmospheres of CO_2 and 90 atmospheres of N_2 at 600°K.

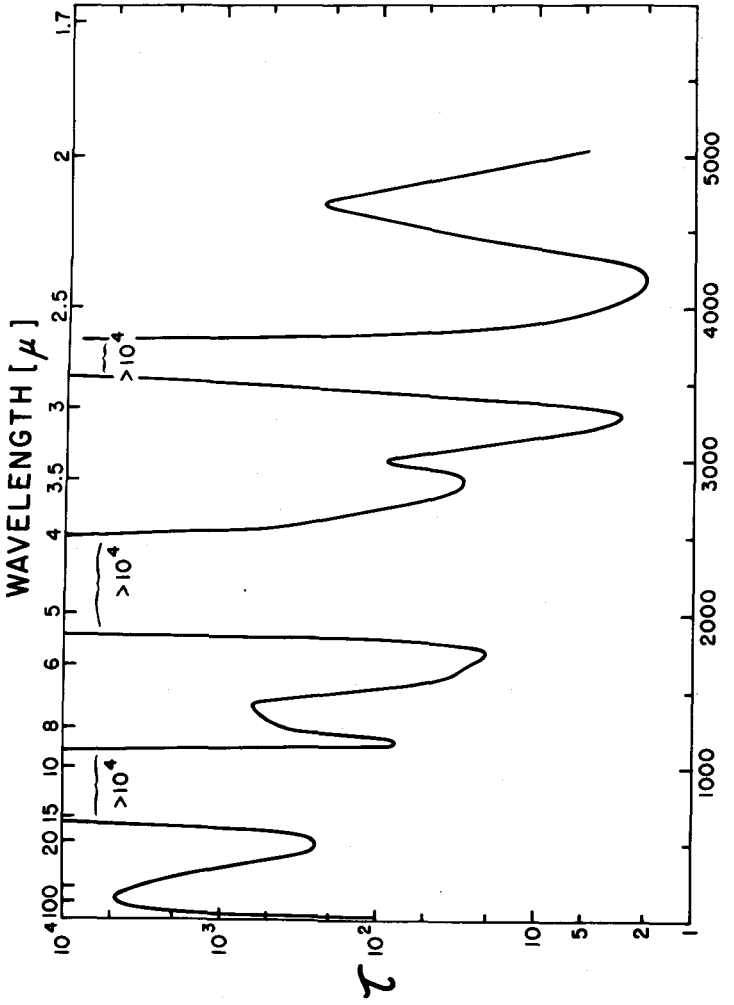

Fig. 5. Calculated optical depth for collision-induced and permitted bands for 10 atmospheres of CO_2 and 90 atmospheres of N_2. For this model $\bar{\tau} = 50$.

some H_2O. In addition the higher the ratio of CO_2 abundance to N_2 the lower the pressure necessary to account for the greenhouse effect. This is in agreement with Thaddeus' s results in the microwave region. We can conclude that if the atmosphere has a CO_2 pressure greater than 10 atmospheres and/or an N_2 pressure greater than 20 atmospheres then collision-induced transitions will be very effective and must be included in any attempt to explain the high surface temperature of Venus.

(Note Added October 24, 1967)

The preliminary findings of the Soviet Venus experiment indicate a surface pressure of approximately 20 atmospheres, almost all CO_2. In view of the calculations discussed above we can conclude that at this pressure the collision-induced bands of CO_2 including the rotational band and the Fermi resonance band will be very important in accounting for the observed temperature of 550° K. However in order to obtain a Rosseland mean optical depth of 50 there must either be a small amount of water vapor on the order of 10^{-3} - 10^{-4} by volume or dust in the atmosphere providing a small background continuous opacity to fill in the gaps which appear when nitrogen is removed from the model.

REFERENCES

Bosomworth, D. R. and Gush, A. P., Can. J. Phys. 43, 751 (1965).

Danielson, R. E. and Solomon, P. M., Astron. J. 71, 382, (1966).

_____, Submitted to Astrophys. J. (1968).

Gaizauskas, V., PhD. Thesis, University of Toronto, 1955.

Sagan, C. and Pollack, J. B., J. Geophys. Rev. 72, 20 (1967).

_____, this volume (1968).

Thaddeus, P., this volume (1968).

DISCUSSION

P. Thaddeus: It appears at first glance that these induced transitions violate spectroscopic stability. What they are doing is robbing opacity from some nearby lines. For example, if one takes the 4.3 micron line alone and spreads the opacity over the 1 to 20 micron region, then for three atmospheres of CO_2 the absorption coefficient over this region would be 1 cm^{-1}. In other words, 10 km would give an opacity which would be of the order of 10^6. The point is that there is an enormous amount of opacity locked in the two allowed rotational-vibrational transitions. Therefore, any collision-induced perturbation which shifts even a small amount of this opacity into all of these innumerable forbidden transitions can result in an enormous opacity.

P. M. Solomon: This is right; it is the width of the band that is significant.

16

THE CLOUDS AND ATMOSPHERE OF VENUS

Carl Sagan and Janes B. Pollack

We would like to show how a quite different model, arrived at in a very natural way without any ad hoc assumptions, helps explain a wide variety of observables about Venus including the microwave spectrum and the infrared opacity.

Sinton, Moroz and Strong have obtained a set of albedo measurements of Venus—both absolute and relative albedos—in the visible and in the near infrared. We have tried to match these observations theoretically. In solving the radiative transfer equation we have been able to show that in problems which involve fluxes rather than intensities the Schuster-Schwarzschild approximation for anisotropic nonconservative scattering is good to within a few percent. The important point is that the clouds of Venus scatter strongly and anisotropically with a large forward lobe; any attempt to solve the transfer equation which neglects this effect will not be able to reproduce the observations. This radiative transfer solution is then combined with Mie theory calculations for ice and liquid water.

Strong and co-workers have also done some laboratory simulations involving substances which could conceivably be constituents of the clouds. They find that only ice particles of a given size distribution are able to match the Venus spectrum. Both theory and observations are shown in Figs. 1 and 2, in which the balloon data are compared with a set of

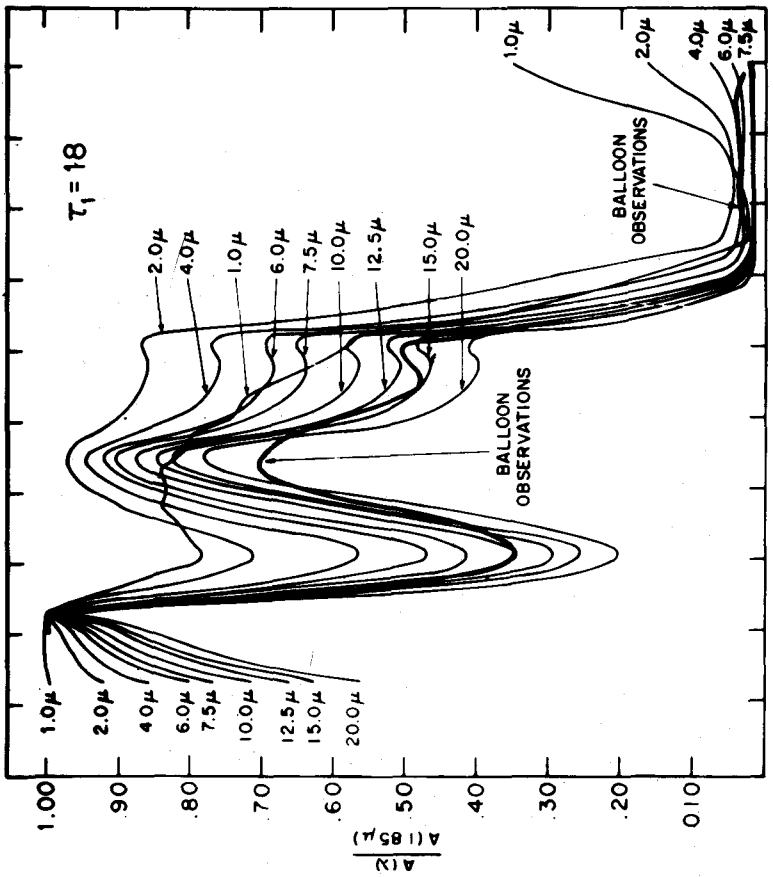
$\tau_1 = 18$
2.0μ
4.0μ
1.0μ
6.0μ
7.5μ
10.0μ
12.5μ
15.0μ
20.0μ
BALLOON OBSERVATIONS
1.0μ
2.0μ
4.0μ
6.0μ
7.5μ
BALLOON OBSERVATIONS
1.00
.90
.80
.70
.60
.50
.40
.30
.20
.10
A(λ) / A(1.85μ)
1.6
1.8
2.0
2.2
2.4
2.6
2.8
3.0
3.2
3.4
λ (μ)

Figure 1

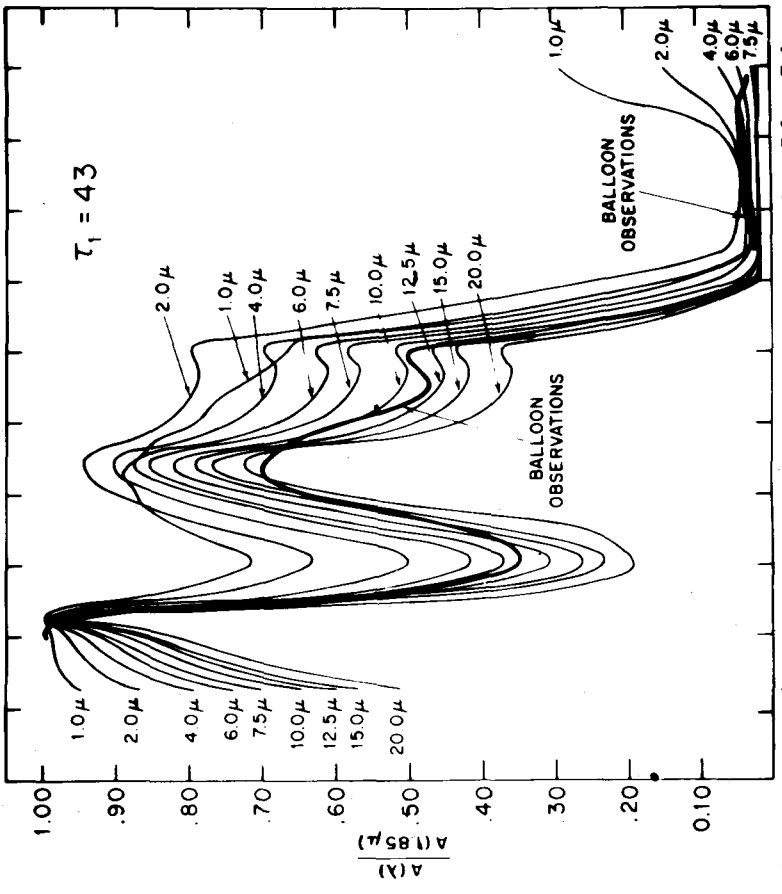
$\tau_1 = 43$
2.0μ
1.0μ
4.0μ
6.0μ
7.5μ
10.0μ
12.5μ
15.0μ
20.0μ
BALLOON OBSERVATIONS
BALLOON OBSERVATIONS
1.0μ
2.0μ
4.0μ
6.0μ
7.5μ
1.00
.90
.80
.70
.60
.50
.40
.30
.20
0.10
A(λ) / A(1.85μ)
1.6
1.8
2.0
2.2
2.4
2.6
2.8
3.0
3.2
3.4
λ (μ)

Figure 2

theoretical curves for ice with different particle radii and for a given interaction optical depth τ_1 in the clouds [Sagan and Pollack, (1967)]. The range of possible values of τ_1 as obtained from the visual and near infrared observations is between 18 and 43; in Fig. 2 we see the theoretical curves obtained if we adopt the upper limit of optical depth. It is our contention that it is very unlikely that there is any other material besides ice with sufficiently high cosmic abundance that could also have the appropriate absorption and scattering properties to reproduce the observations. The reflectivity depends on the variation of the imaginary part of the refractive index with wavelength; this variation is quite complicated for ice and is unlikely to be duplicated by other materials—even liquid water gives a markedly different reflection spectrum.

Given the thickness of the clouds from the interaction optical depth, we can easily compute the amount of ice to within a factor of two or three; we thus obtain a value of about 10^{-2} gm/cm^2-column of ice. Moreover, we can show from the saturation physics that at the observed temperatures of the clouds there must be super-cooled water droplets formed at the bottoms of the clouds. Then the amount of of water vapor above a 700°K surface required to maintain 10^{-2} gm/cm^2-column of condensed water at a temperature of 230 or 240°K turns out to be tens to a few hundred gms/cm^2-column. The ground pressure with this model will be on the order of tens of atmospheres.

This model is able to account for many of the observations. It helps to explain the microwave spectrum; 0.1 gm/cm^2-column of water droplets happens to reproduce the spectrum quite nicely, as Sagan and Giver showed in 1961. The model reproduces the 8-mm phase effect, the amplitude of which is attenuated from the surface phase effect amplitude [Pollack and Sagan, (1965)]. It reproduces the microwave limb darkening as observed in the 19-mm channel of Mariner II [Pollack and Sagan, (1967)]. Since we are only concerned with relative intensities and with the peak brightness temperatures per scan, the principal uncertainites in the Mariner II results are not critically involved in these deductions.

The model also explains the infrared limb darkening at 10 microns [Pollack and Sagan, (1965)]. Here the physics is simplified because at 10 microns the anisotropy of the scattering has been reduced substantially, which is not the case in the region of 1 micron. Our model accounts for the polarization-phase curve in the visible and near infrared. This curve is obtained by plotting degree of polarization vs. phase angle and is based on the observations of Lyot and Dollfus. In Figs. 1 and 2 it was seen that to reproduce the balloon observation data at a few microns wavelength required particle sizes several microns. As with any size distribution of particles falling according to the Stokes-Cunningham equation, the smaller particles will remain above. Since multiple scattering depolarizes, in making polarization measurements we will preferentially sample the small particle sizes. Here ice crystals of a few microns in diameter match the observations. Finally, as we will shown in detail elsewhere, a greenhouse effect due to atmospheric CO_2 and the amount of water vapor necessary to explain the ice clouds also explains the high surface temperature without involking pressures larger than a few tens of bars.

The role of the clouds is not a major one. If the clouds of Venus were suddenly removed, we would be looking down to optical depth 1 in the atmosphere, which is at a temperature of about 325 to 350° K in our model. Thus the clouds shield that temperature from our view. Figure 3 shows a typical set of transmissivity curves for different values of τ_1. Because the clouds are strongly anisotropically scattering and the absorption coefficient is low, visible light penetrates the clouds. There is 10-20% transmission, as on an overcast day on the earth. On the other hand, in the infrared the transmission drops substantially because the absorption coefficient of the clouds has gone up, and the scattering is now more isotropic. As a result there is relatively little light coming through the clouds longward of one to two microns.

The major uncertainty in this model has to do with the observation of water vapor. Tens to hundreds of gms/cm^2-column of water vapor below the clouds should be detected if we could look below the clouds. Strong, from balloon

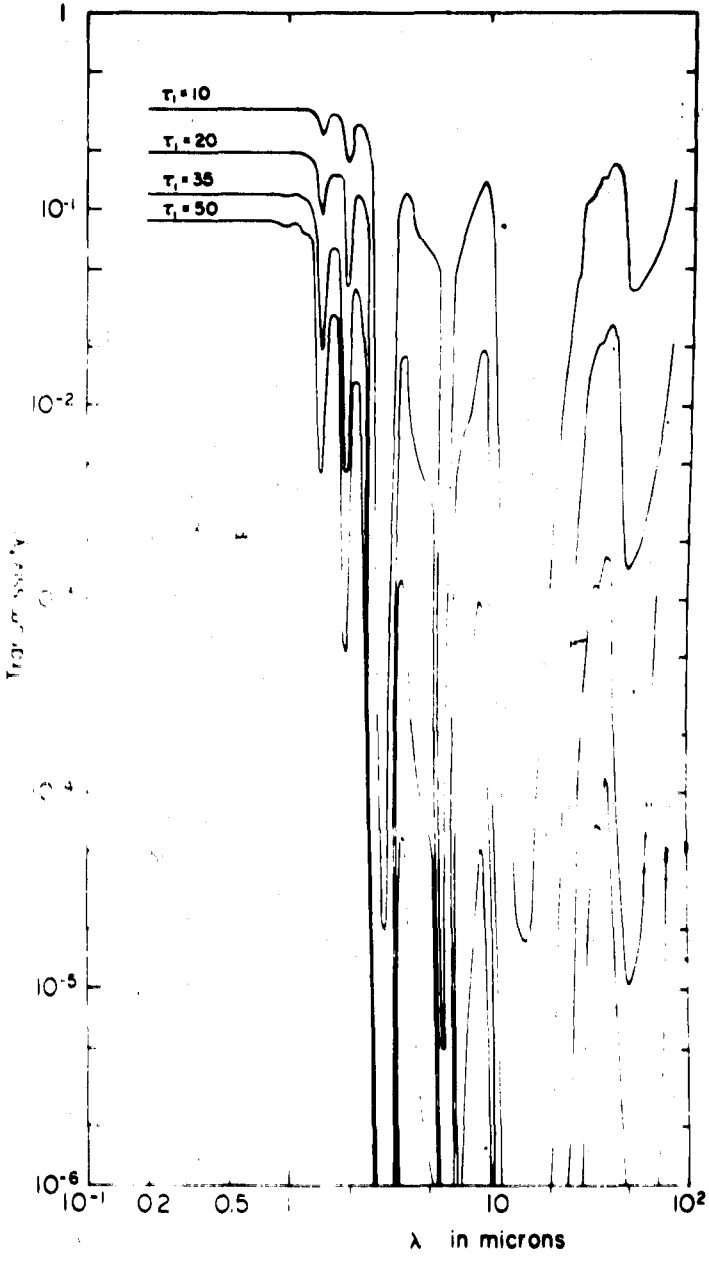
1
$\tau_1 = 10$
$\tau_1 = 20$
$\tau_1 = 35$
$\tau_1 = 50$
10^{-1}
10^{-2}
10^{-5}
10^{-6}
10^{-1}
0.2
0.5
10
10^2
λ in microns

Figure 3

altitudes, has measured a certain amount of water vapor on Venus. If this is the amount of water vapor above the clouds, then there is no difficulty. However, if Strong's observations refer to substantially larger optical depths, or even worse if as Spinrad finds there are no water vapor lines visible on plates which have adjacent CO_2 bands indicating high rotational temperatures, then there is a contradiction, and there does not appear to be any simple way of getting out of the dilemma*.

We should also consider some of the difficulties involved in other models of the atmosphere of Venus. If we believe Chamberlain's value for the CO_2 abundance, then as Thaddeus showed a surface pressure of 200 to 300 atmospheres is required. Thaddeus has also suggested that such pressures would account for the infrared opacity, although Solomon has suggested that a factor of 3 or 4 less in pressure would give the same opacity provided there is a small amount of water vapor. We maintain that these pressures are inconsistent with observations. One such observation is the limb darkening measured by Mariner II at 19 mm. We have tried to explain the limb darkening using the pressure-induced CO_2-N_2 opacity source for various surface temperature distributions ranging from a strong longitudinal temperature gradient from dark inside to bright side to a purely isothermal surface at 600° K. In none of these cases were we able to gain agreement with the observed limb darkening [Pollack and Sagan, (1967)]. On the other hand, the water droplet clouds provide a very natural and quantitative (to within observational error) explanation of the limb darkening.

Our recent calculations of model non-gray Venus atmospheres show that convective equilibrium is to be expected. For an adiabatic atmosphere, the lapse rate is approximately given by

$$\frac{\partial T}{\partial z} = -\frac{g}{c_p \eta} \qquad (1)$$

* Note added in proof: The recent discovery of water vapor by Belton and Hunten (1966), confirmed by Spinrad and Shawl (1966), tends to alleviate this difficulty. We emphasize that the theoretical water line formation problem is still unsolved.

where c_p is the specific heat at constant pressure, g is the acceleration of gravity, and η is some parameter which takes into account the latent heat involved in the condensation. For the earth's atmosphere, where water does condense out over a sizeable part of the atmosphere, η is on the order of 1.6. For an adiabatic atmosphere, we also have the Poisson relation between temperature and pressure, where γ is the ratio of the specific heats:

$$\frac{p}{p_0} = \left(\frac{T}{T_0}\right)^{\eta\gamma/(\gamma-1)} \qquad (2)$$

c_p and γ depend somewhat on pressure and temperature; this can be allowed for in such calculations. Since we have such an enormous atmospheric depth, it is improbable that there is any constituent which is condensing out over the whole atmosphere or even over a significant fraction of it. Therefore η must be about 1. Those people who believe there is very little water vapor in the atmosphere must certainly agree with this.

The pressure and temperature at the cloud tops are roughly known from a variety of arguments. The most recent spectrometric values at cloud top pressures, in agreement with past polarimetric values, are around 0.1 atm; the cloud top temperature is about 210° K. We also have an idea of the mean surface temperature from the microwave observations; it is about 700° K. We can derive, using Eqs. 1 and 2, what the pressure ought to be at the surface. It turns out that we cannot get a pressure of 100 or 200 atmospheres in this manner. It is only possible if there is some isothermal region or some material condensing out; both of these are unlikely.

The situation has improved considerably over a few years ago, when there was no model which satisfactorily explained the infrared and microwave opacities. Now we have two models, and both can't be right. It is possible that the truth lies somewhere in between; that is, there isn't as much water vapor as we think and there isn't as high a pressure as Thaddeus and Solomon have proposed. Within the next few years we may actually learn the answers to these questions.

REFERENCES

Belton, M. J. S. and Hunten, D. M., Astrophys. J. 146, 307 (1966).

Pollack, J. B. and Sagan, C., Astrophys. J. 150, 327 (1967).

_____ Icarus 4, 62 (1965).

_____ J. Geophys. Res. 70, 4403 (1965).

Sagan, C. and J. B. Pollack, J. Geophys. Res. 72, 469 (1967).

Spinrad, H. and Shawl, S. J., Astrophys. J. 146, 328 (1966).

DISCUSSION

G. Field: What is the decisive observation concerning the difference between these models?

P. M. Solomon: I think that the problem can be settled from the ground, or at least from balloons, on the basis of high resolution work in the region of 3 microns. Although the inclusion of the isotopic bands will fill it up somewhat, there will be a definite minimum around 3 microns according to our model, but not according to Sagan's model.

C. Sagan: Our model also predicts a 3 micron reflectivity minimum, due to OH absorption (See Figs. 1 and 2). A key discriminant would be the experiment that didn't work on Mariner II, the one designed to measure the water resonance line at 13.5 mm. The ground-based limit to the depression below the continuum in the vicinity of that line is roughly 10°K. But the amount of water vapor in the well-mixed adiabatic atmosphere we are talking about gives a depression also roughly 10°K. If the signal-to-noise ratio for ground-based or spacecraft observations can be improved, this measurement can be made unambiguously

P. Thaddeus: The important question is what role the clouds play. Are they thin clouds, or are they clouds which significantly affect the opacities? That is where we differ. Thin clouds will satisfy the observed polarization, infrared albedos, et cetera.

The calculation of the surface pressure is full of

uncertainties. The cloud top pressure is by no means a well-known number. We did the calculation using all of the different estimates of the cloud top pressure and temperature. We obtained values of the ground pressure ranging from 5 to 300 atmospheres. The profile is not necessarily adiabatic--the isothermal region might continue into the clouds, or there could be a subadiabatic lapse rate.

C. Sagan: In order to have a sub-adiabatic lapse rate, there must be some condensation. But your model is the one that doesn't want condensation.*

W. M. Sinton: I have made observations which have a bearing on this argument. I have measured a temperature of about 230 ° K at 3.75 and 3.5 microns. According to the pressure broadened N_2-CO_2 model, the opacity is not large enough to prevent seeing a substantially higher temperature at the wavelengths.**

---

* Note added in proof: For pure ice clouds, the range of τ_1 is between 18 and 43—as in Figs. 1 and 2; these are not thin clouds. If we try to explain the high visible albedo by some other, underlying, clouds—say, dust clouds—and the infrared spectra by a thin ice cloud, we run into difficulties: the near infrared single scattering albedo of ice is generally quite high, the underlying dust cloud will therefore make a significant contribution to the total reflectivity, and the reflectivity will not match the observed value.

** Note added in proof: The ice cloud model, on the other hand, does provide such opacity (See Fig. 3).

17

INTERFEROMETRIC SPECTRA OF PLANETS

J. Connes and P. Connes

For the last two years, we have been developing a technique for obtaining planetary spectra using Fourier transform spectroscopy. This research is being done in collaboration with the Jet Propulsion Laboratory.

We will not go into the experimental details of this method. These were fully described at the Bellevue Conference on Instrumental Spectroscopy (April 1966) and will be published by the Journal de Physique, Supplement issue, 1967. The first results have been given by J. and P. Connes, (1966). In these two publications the various spectral traces given here are also reproduced with more complete explanations.

The major difficulty is that if one wants to get an accurate, high-resolution spectrum by Fourier spectroscopy over an extensive spectral range, one has to measure both the path difference and the intensity with greater accuracy than was at first realized. The path difference problem was solved by a special technique in which the path difference is varied in a stepwise manner by stopping the interferometer at each point at which an interferogram sample is desired, integrating the light output during the stopping time, and then moving quickly to the next point. The entire process is done under servo control. It can be shown that

the path difference at each of our points is accurate to a fraction of an angstrom.

The intensity measurement problem is not an especially difficult one for laboratory sources, but is quite troublesome in astronomical measurements because of turbulence problems. One approach is to vary the integration time according to the total intensity of the source. This can be rather easily done, and does compensate for the effects of variations in atmospheric transmission as well as for pure scintillation. But it does not compensate for the much more troublesome problems which arise from a fluctuating optical beam which is moving across non-uniform receiver surfaces and non-uniform optical mirrors or beam splitting plates. The solution which we finally adopted, and which we now consider to be fully satisfactory, involves a modulation of the path difference itself. This produces a sine-wave transform interferogram instead of the usual cosine wave and completely eliminates the average level in the interferogram, the variations of which are the major cause of trouble in this work.

Another factor that helped to produce good results was our insistence on a rather lengthy testing program; we measured a large number of well-known emission or absorption laboratory spectra. In addition, we required a fast method of computation, involving the rapid transmission of the data to a computer so that some results would be available before the next night of observing. Last spring, when observing Mars from Haute Provance, we accomplished this in a rather clumsy manner: we would stop observing at about 6 a.m., then rush the interferogram tapes to the Marseilles Airport. The first available plane took the tapes to Orly Airport near Paris; from there the tapes were taken by car to the Meudon computer. We could then have a reasonable fraction of the computation done before the next night, so that we had the opportunity to correct anything that had gone wrong.

We had a much better procedure for our more recent measurements. We used a telephone-line transmission in which the tapes were reproduced at the output. We did not get the full spectrum because the computation would have

been quite lengthy, but we could compute a small portion within two hours. All of our measurements were made using filters which isolate on the order of one or two thousand wave numbers in the near infrared. Our procedure was to compute a small fraction of the signal near the expected peak and two fractions outside the band-pass. This gave us an idea of the signal-to-noise ratio, from which we could decide whether it was worthwhile to increase the resolution.

Now let us look at some of our experimental tests. An interferogram of a monochromatic line—a potassium line at 1.25μ in the near infrared—was recorded, and the transform was computed (Fig. 1). The resolution is about 0.1 cm^{-1}. This is the maximum resolution that our instrument can give at present, and it is fully adequate for planetary or stellar work. The lower part of Fig. 1 gives a comparison of the theoretical and experimental line shapes. The secondary maxima that appear are due to the apodization function that we used, and they could undoubtedly be made even smaller.

Figure 2 shows, for the same resolving power, the shape of our experimental function and what would be produced by a perfect grating or a perfect Fabry-Perot interferometer. It is clear that this method will give extremely clean instrumental line shapes, provided one measures the path difference accurately. An absorption spectrum test is shown in Fig. 3. We used methyl iodide for which there exist several accurate laboratory spectra. The diagram illustrates two separate tracings, in order to show what is reproducible. The resolution here is of the order of 0.15 cm^{-1}. Also in the diagram are two noise traces taken outside the filter band-pass, indicating that the noise is less than 10^{-2}, and also that the mean level is actually zero. Thus the zero level is accurately determined, and we can obtain absorption depths. We consider such precautions as taking several spectra to check the reproducibility and measuring noise traces to insure that the intensity is zero as absolutely essential. Without them, one can be considerably misled as to the true accuracy of the computed spectrum.

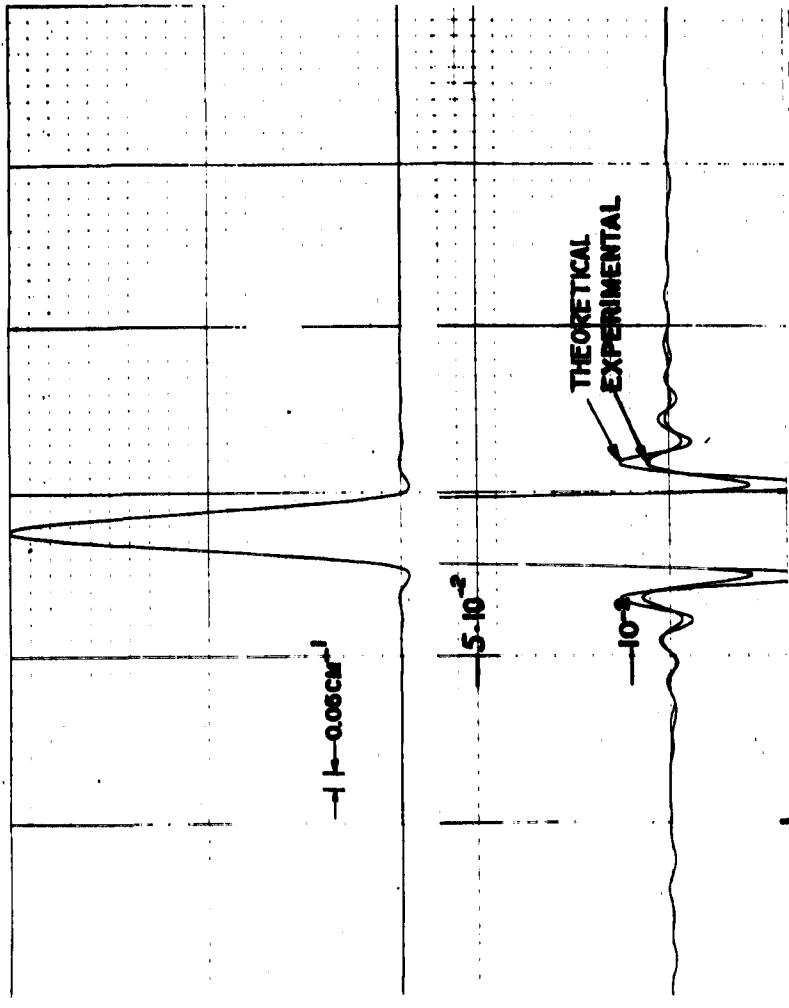

Fig. 1. Transform of interferogram of 1.25μ potassium line and comparison of theoretical and experimental line shapes. The resolution is about 0.1 cm^{-1}.

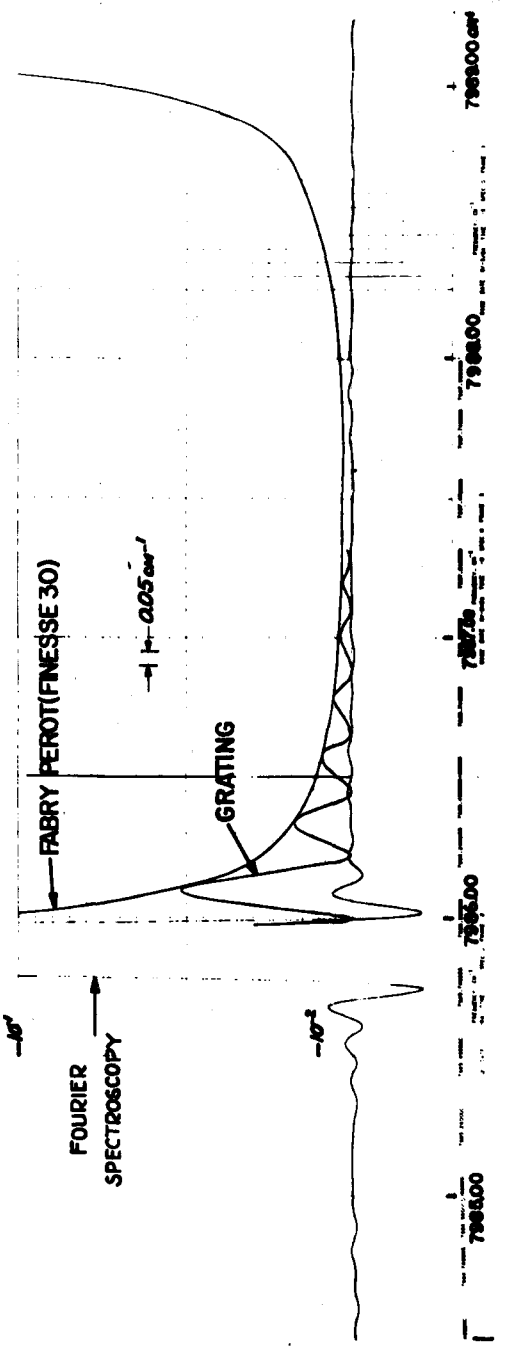

Fig. 2. Comparison of experimental line shape with those produced by a grating and Fabry-Perot interferometer.

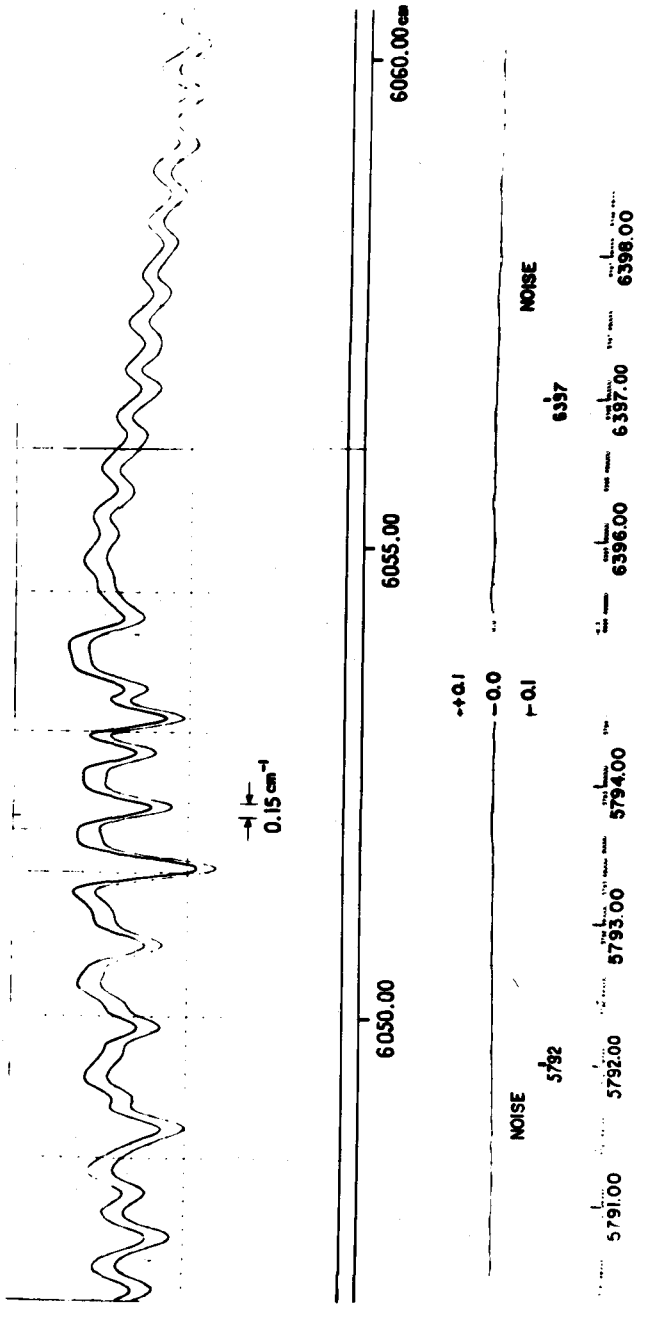

Fig. 3. Two tracings of absorption spectrum of methyl iodide. Two noise traces are shown indicating the noise level. The resolution is approximately 0.15 cm^{-1}.

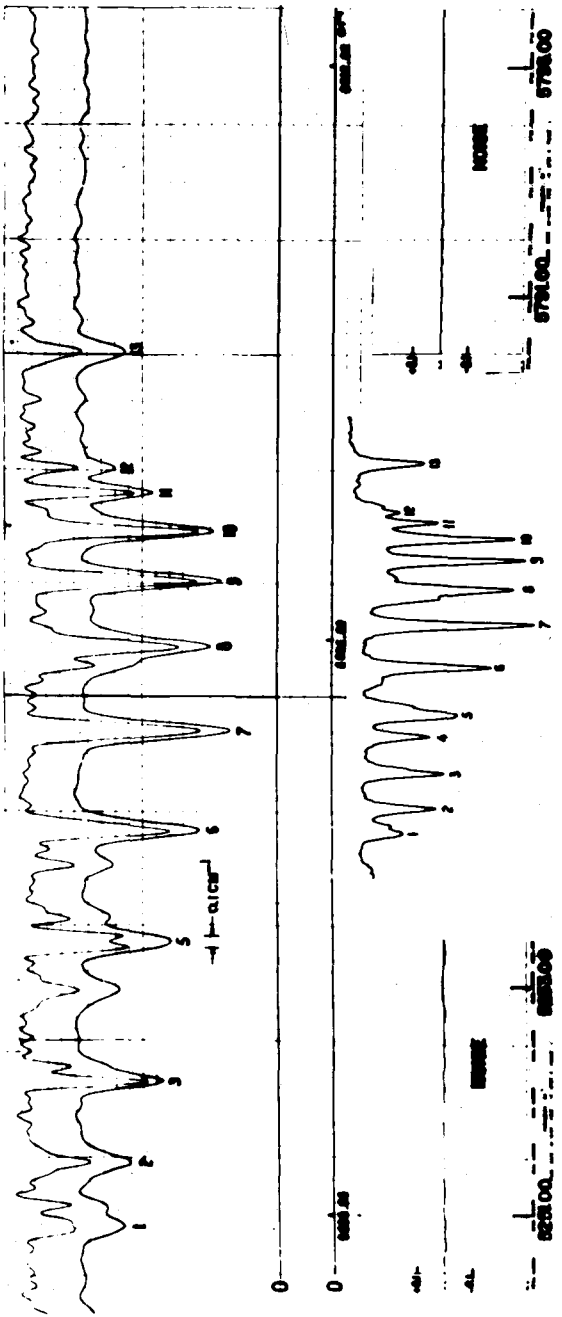

Fig. 4. A portion of the solar spectrum in the near infrared. The features result mainly from telluric methane. The upper trace has been computed without any apodization. The lower insert shows the same band recorded with a grating spectrometer.

Our first astronomical test was to take a solar spectrum (Fig. 4). The resolution is again 0.1 cm^{-1}; the features shown are mainly from a telluric methane band. The two traces were computed from the same interferogram using different instrumental line shapes. In fact, for the upper trace there is no apodization at all. It can be seen that not putting in any apodization gives some increase in resolving power, but it also produces many spurious ripples. The best results are obtained when several computations are made, using several different accurately-known instrumental line shapes, and they are compared. The lower trace shows the same band, with comparable resolution recorded by a grating spectrometer.

Figure 5 shows our first planetary spectra, consisting of two tracings of a CO_2 band on Venus, recorded in September 1964 at the 36-inch telescope of Steward Observatory, on Kitt Peak. A comparison with the best Venus spectrum across the same spectral region (obtained by Kuiper, 1963) with the 82-inch telescope at the McDonald Observatory and reproduced by the lower trace) shows that we are just resolving the structure of the CO_2 band, the outline of which is shown by Kuiper. The instrument was at that time far from its present state of completeness, and we have since improved our results.

In the spring of 1965, we obtained spectra of Mars using the 75-inch telescope at Haute Provence, France. The reproducibility between the two Mars spectra (Fig. 6), which were taken on two different nights, is extremely good. We have plotted the difference between the two Mars traces expanded by a factor of ten (lower trace). It can be seen that the difference is purely random noise; the peak difference is about 1%, which means a signal-to-rms noise ratio of 400 for each of the two traces. Although the signal-to-noise ratio was very good, we were not satisfied with the results. We would have much preferred to get ten times the resolution, and a smaller signal-to-noise ratio. We were not able to do so because the turbulence problem had not been solved at that time.

It is only for Jupiter, in January 1966, that we have fully realized the possibilities of the method. Figure 7

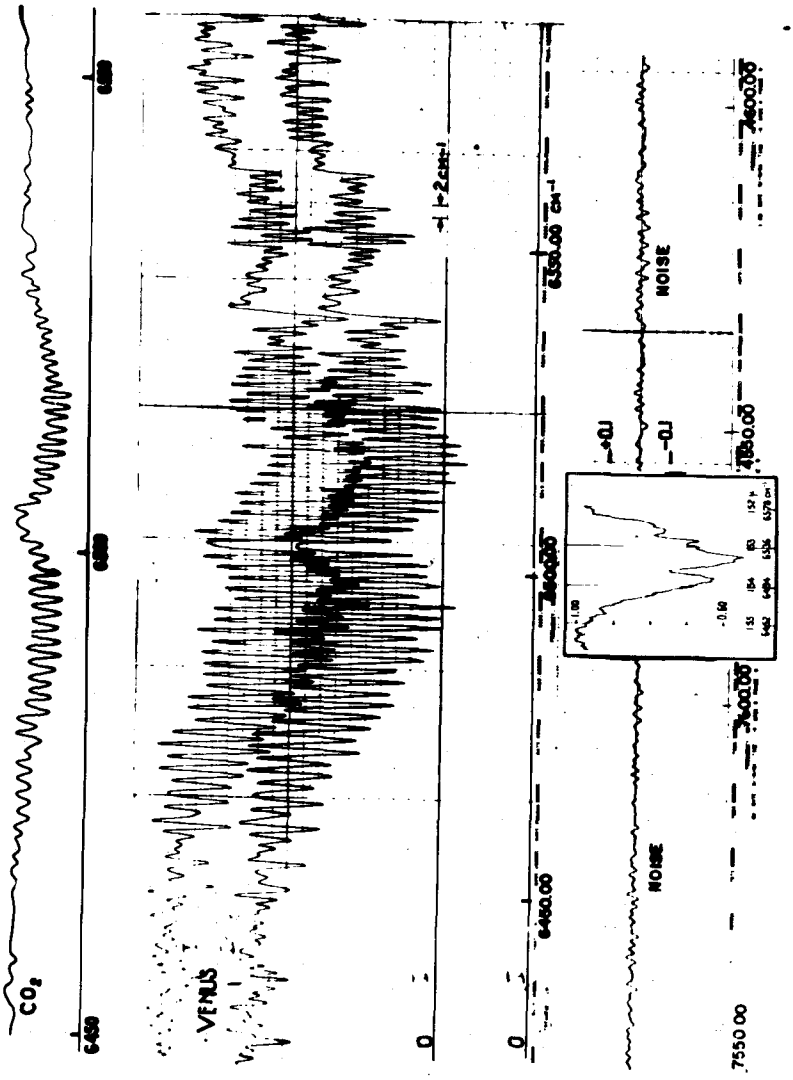

Fig. 5. Spectrum of a CO_2 band produced in the atmosphere of Venus. The spectrum shown in the box below is one obtained by Kuiper in the same spectral region.

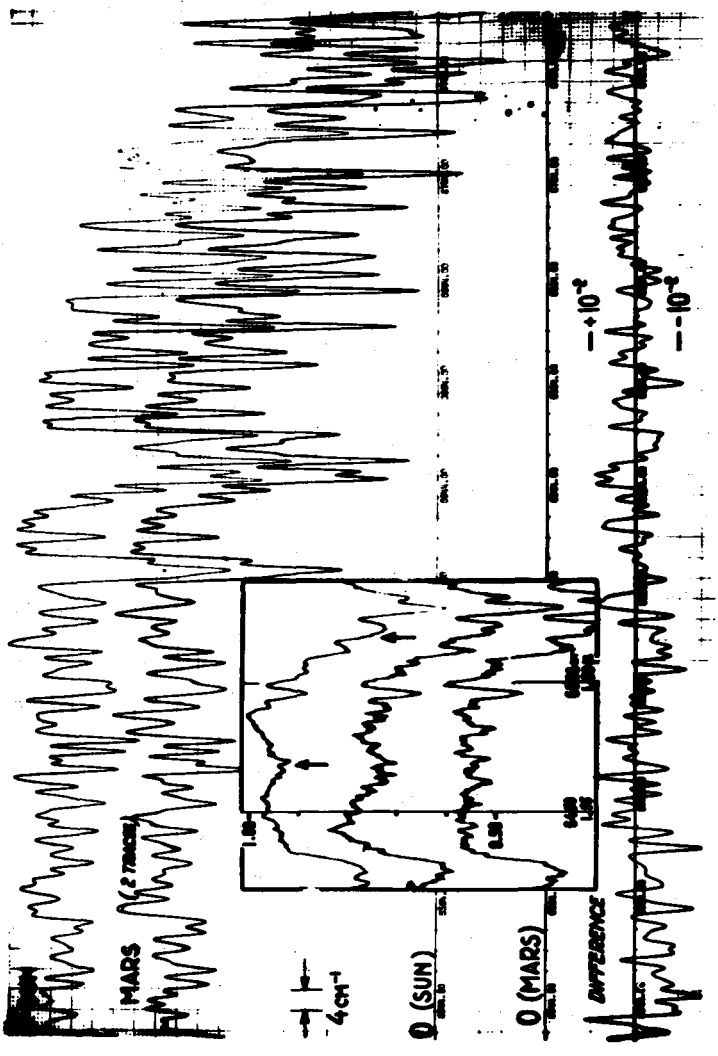

Fig. 6. Two tracings of the spectrum of Mars. The difference between the two tracings is shown at bottom. For comparison, the best Mars spectra (obtained by Kuiper) are shown in the box; the corresponding spectral region is located between the two arrows,

shows two Jupiter spectra obtained by Kuiper in 1963 (upper traces); they were so far the most detailed Jupiter spectra in the region around 1 to 2 microns. A slightly less detailed spectrum obtained by Moroz (1962) is also shown (lower trace). We also present, for comparison purposes, one of our own spectra with artificially reduced resolution which approximately matches the appearance of the other spectra (Fig. 8). The resolution in all three spectra is about 30 cm^{-1}

Figure 9 shows a 100 cm^{-1} portion of our best Jupiter spectrum. Again there are two independent traces; this is essential to the determination of signal-to-noise. The resolution is about 0.3 cm^{-1}. A lunar spectrum was also taken at the same resolution, and is used as a check (the absorption lines are due mainly to terrestrial CO_2). This last spectrum can be used to give a further estimate of the resolution by comparing it (Fig. 10) with the Michigan Atlas solar spectrum. It can be seen that our resolution on the Moon, and hence on Jupiter, is only slightly greater than that of the Michigan spectrum.

We have now enough results to warrant the construction of a specialized telescope for this kind of work. By "specialized telescope," we mean an inexpensive light collector of low accuracy. It is a waste to use a regular high accuracy optical telescope for these measurements. We do not require resolution on the planet; all that is needed is to collect the maximum possible amount of light from the whole planet and focus it on a very small infrared receiver. For this purpose, something on the order of twenty to thirty seconds of arc accuracy is sufficient, at least within the PbS receiver sensitivity range.

We have already begun some preliminary work on the construction of such a telescope, aiming at a 4 meter-aperture. We hope to install it at Meudon Observatory. This is perhaps not the ideal place for infrared work, but it is very close to the computer. The data transmission problem could be solved by a reasonably good runner who should cover the distance in ten or twenty seconds, according to the exact location of the instrument.

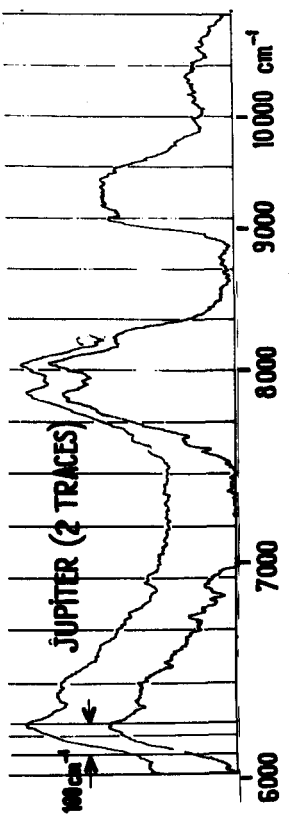

Fig. 7. Infrared spectra of Jupiter obtained by Kuiper (upper two traces) and Moroz (lower trace). The resolution is about 30 cm^{-1}.

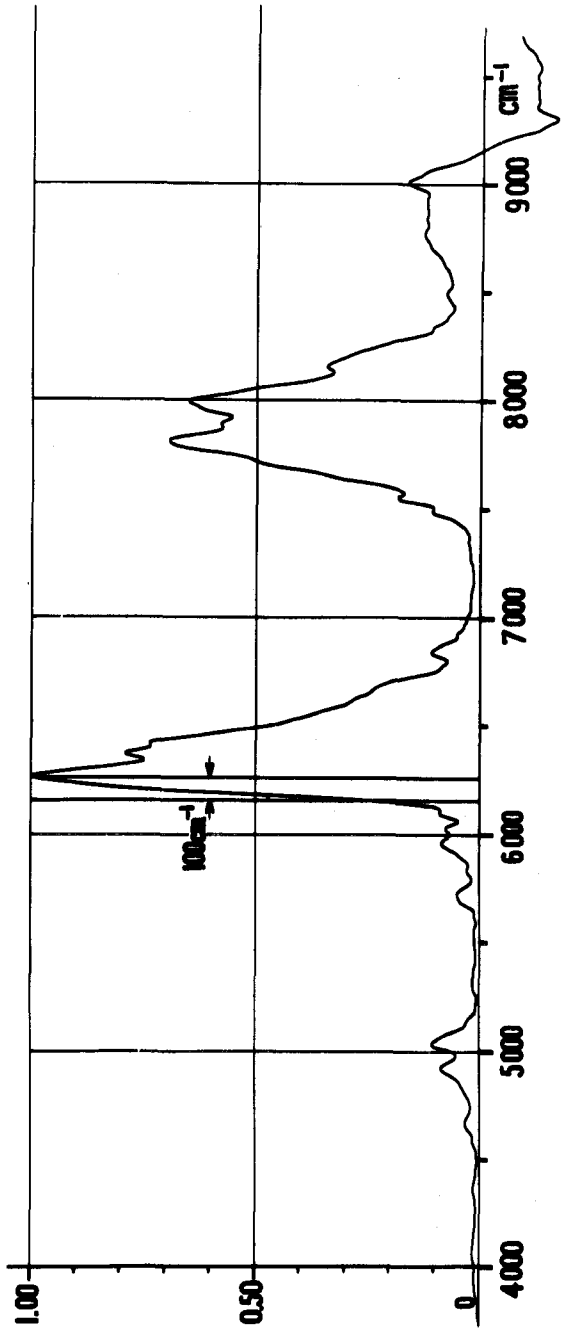

Fig. 8. Spectrum of Jupiter obtained by authors, with resolution artificially reduced to 30 cm^{-1} to match those of Fig. 7.

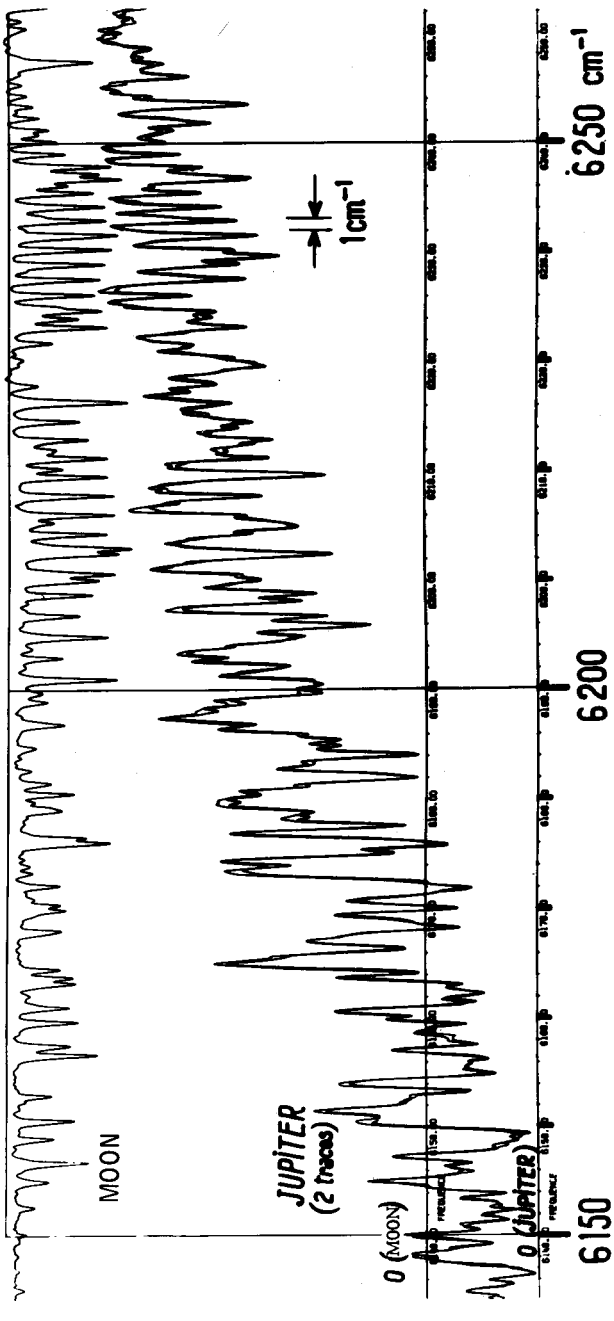

Fig. 9. Portion of best Jupiter spectrum obtained by authors. A lunar spectrum is shown for comparison. The resolution is about 0.3 cm^{-1}.

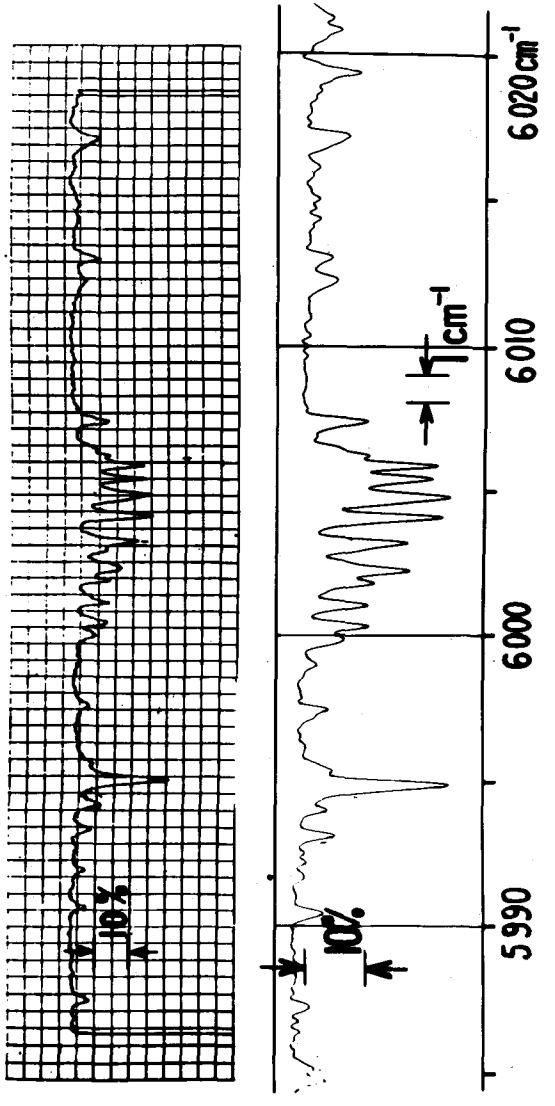

Fig. 10. Comparison of lunar spectrum (lower trace) with Michigan Atlas solar spectrum (upper trace). The spectral region is the same as that of Fig. 4.

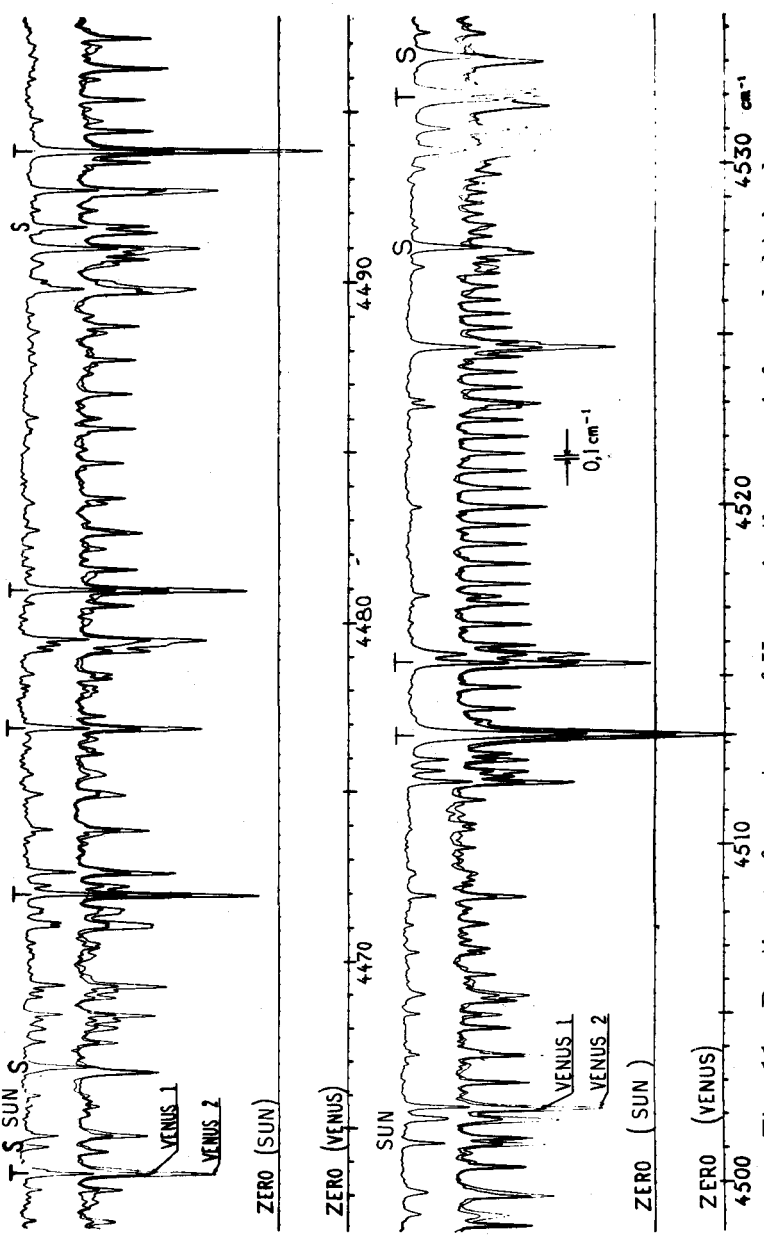

Fig. 11. Portions of spectrum of Venus in the near infrared obtained in June-July 1966. The resolution is 0.08 cm^{-1}. Telluric and solar lines are indicated by the letters T and S, respectively. Venus 1 was recorded with the planet near the meridian; Venus 2 was recorded with Venus at a lower elevation.

NOTES ADDED IN PROOF (FEBRUARY 1967)

It may be of interest to mention here a few recent results. A new interferometer with increased maximum path difference (up to 2 meters) has been built by J. Pinard at Bellevue; the expected theoretical resolution of 5×10^{-3} cm^{-1} has been demonstrated on emission spectra in the near infrared. The instrument was described at the Bellevue conference on instrumental spectroscopy. It is hoped that it will produce absorption laboratory spectra and solar spectra with the same resolution.

The first instrument has since been used to record the near infrared spectrum of Venus in the three atmospheric windows at 8000, 6000 and 4200 cm^{-1}; this was done from Haute Provence again in June - July 1966. The resolution is 0.08 cm^{-1}. A sample of the results is given by Fig. 11; two independent spectra of Venus are superimposed. Venus I has been recorded near the meridian and Venus II at lower elevation in early morning; it shows increased intensity for all the telluric lines, a few of the most intense of which are marked T. A solar spectrum is also given; note the Doppler shift (about 0.15 cm^{-1}) for all solar lines (marked S). The Venusian lines are due to a relatively weak CO_2 band.

The complete spectra will be published in atlas form by the Journal des Observateurs. A preliminary analysis by Kaplan and Benedict has revealed the presence of HCl and HF in the atmosphere of Venus (Connes, Connes, Benedict, and Kaplan, 1967).

REFERENCES

Connes, J. and Connes, P., J. Opt. Soc. Am. **56**, 896 (1966).
Connes, P., Connes, J., Benedict, W. S., and Kaplan, L. D., Astrophys. J. **147**, 1230 (1967).
Connes, J., Connes P., Maillard J. P., Jour. Phys., C2, **28**, 120, (1967).
Pinard, J. Jour. Phys. C2, **28**, 136 (1967).
Kuiper, G. P., Mem. Soc. Roy. Sci. Liege **7**, 269 (Physics of Planets, Eleventh International Astrophysics Colloquium).
Moroz, V. I., Astron. J. **5**, 827 (1962).

DISCUSSION

G. Neugebauer: What was the scan time?
P. Connes: In most cases, we tried to spend between two and three hours on an interferogram. In the case of the Jupiter spectra, each of the two traces represents the average of three independent interferograms. So the total time was rather large—perhaps about fifteen hours for both traces. One of the main advantages of our process is that it enables one to use long scan times, which are unavoidable if one wants to get the maximum amount of data.
G. Field: You implied that to get spatial resolution would be a difficult problem. What is the basic difficulty?
P. Connes: It is very difficult, because the spectral resolution is limited by the total amount of energy. If you wish to use only ten percent of the planet's light, you will get a resolution which will be ten times worse. To get the same kind of spectral resolution and good spatial resolutions as well would require a much larger telescope.

18

MODELS OF THE ATMOSPHERE OF JUPITER

B. D. Savage and R. E. Danielson

I. INTRODUCTION

Several low resolution infrared spectra of Jupiter were obtained during the second flight of Stratoscope II (Danielson 1966). These spectra are shown in Figs. 1 to 5. The large absorption feature centered at 2.25 μ was attributed to the collision induced 1-0 band of H_2 although some absorption due to strong combination bands of NH_3 and CH_4 is expected in this wavelength region. The smaller absorption features at 0.85, 0.99, 1.15, 1.37, and 1.7 μ were identified as CH_4 bands and the large feature near 3.0 μ was interpreted as due to ν_1, ν_3, and $2\nu_4$ bands of NH_3.

Crude estimates of the amount of NH_3 required to form the 3μ feature yielded very large abundances (of the order of 10^4 cm-atm). On the other hand, as discussed in section III, the lack of any prominent absorption in the Stratoscope spectra at 1.51 μ suggested much smaller NH_3 abundances (of the order of 20 cm-atm). These values are not only discrepant with each other, but also with the presently accepted value of 7×10^2 cm-atm for the NH_3 abundance determined in the photographic infrared. (A summary of abundance, temperature, and pressure measurements on Jupiter is discussed in section II.) One possible means of reconciling this discrepancy is to assume

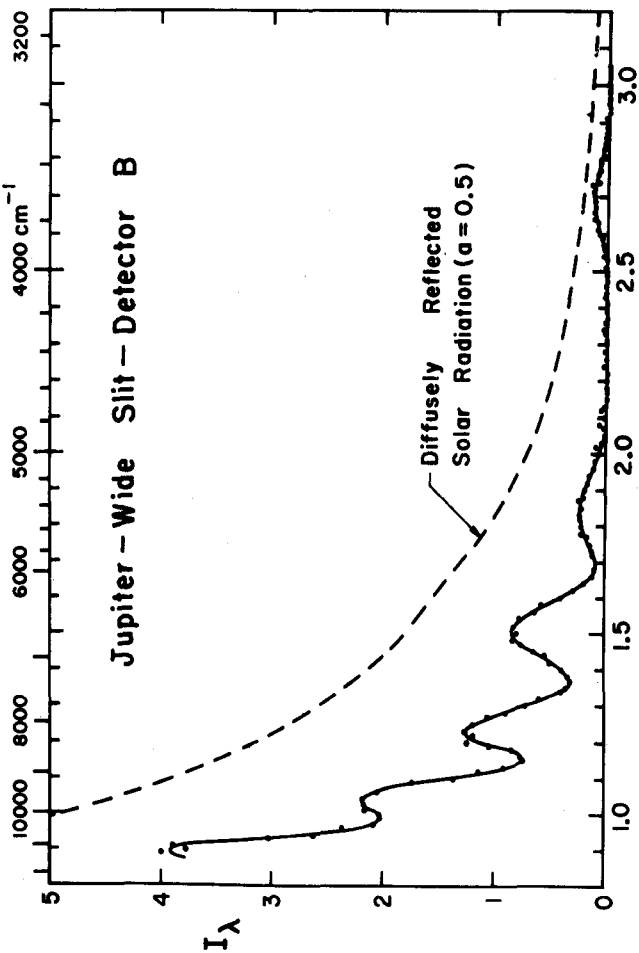

Fig. 1. The absolute intensity spectrum of Jupiter derived from detector B and the wide entrance slit. The intensity of a perfectly diffusing screen (having an albedo of 0.5) held normal to the sun's radiation at Jupiter's distance is shown for comparison. The units of I_λ are 10^3 ergs/cm^2 sec ster μ. (See Danielson (1966) for a description of the spectrometer.)

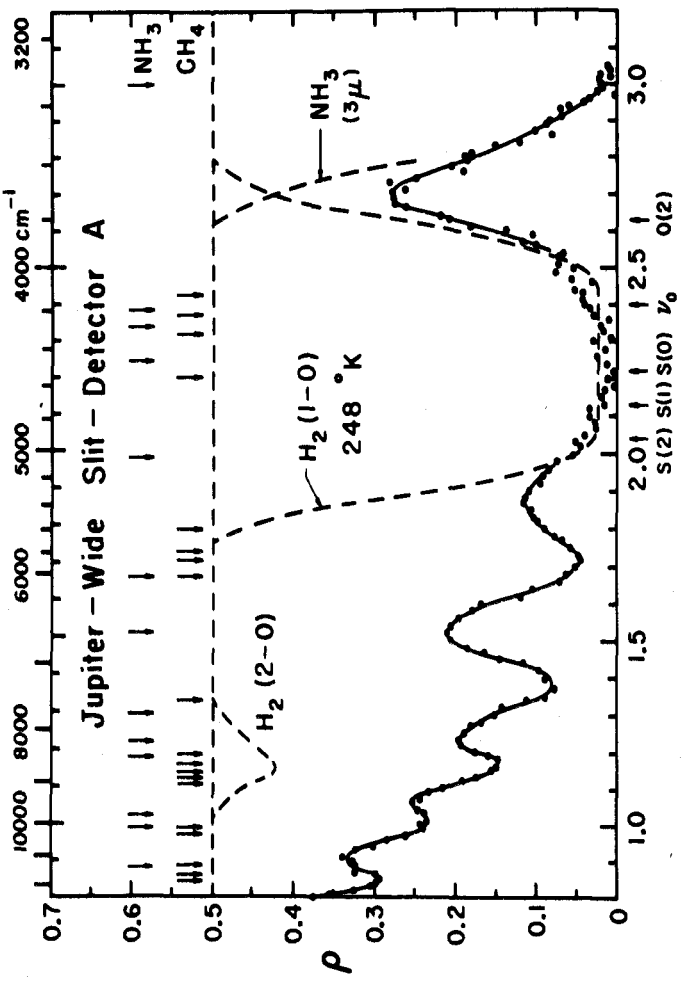

Fig. 2. The ratio of the observed intensity of Jupiter (as derived from detector A and the wide entrance slit) to the brightness of a perfectly diffusing screen (having an albedo of unity) held normal to the sun's radiation at Jupiter's distance. The bands of CH_4 and NH_3 which have been observed in the laboratory are shown along with the positions of the lines in the 1-0 band of H_2.

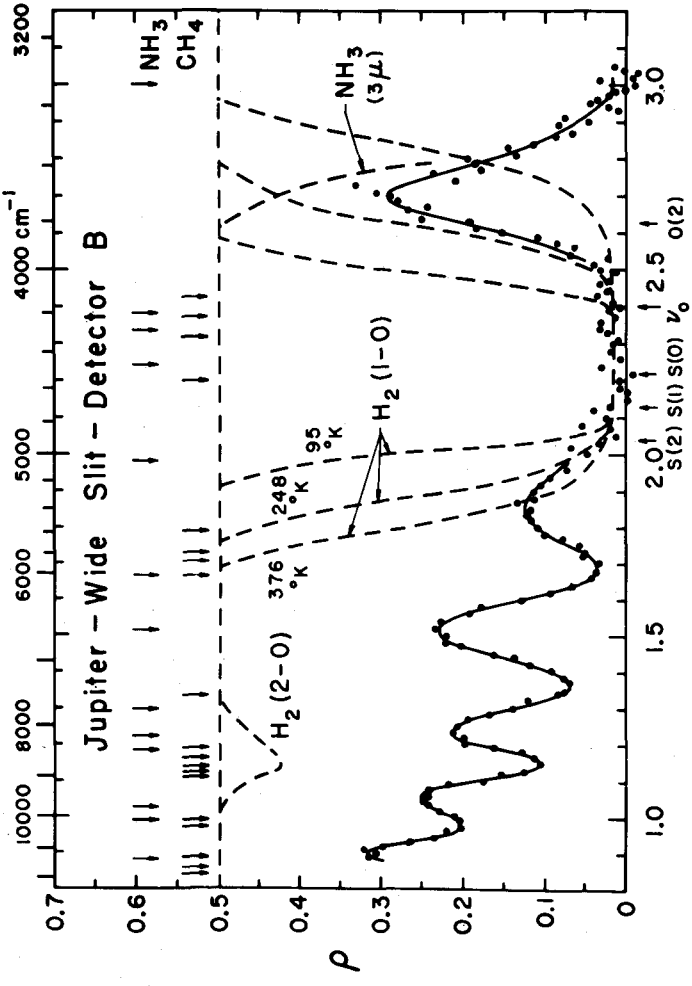

Fig. 3. The ratio of the observed intensity of Jupiter (as derived from detector B and the wide entrance slit) to the brightness of a perfectly diffusing screen (having an albedo of unity) held normal to the sun's radiation at Jupiter's distance. The bands of CH_4 and NH_3 which have been observed in the laboratory are shown along with the positions of the lines in the 1-0 band of H_2.

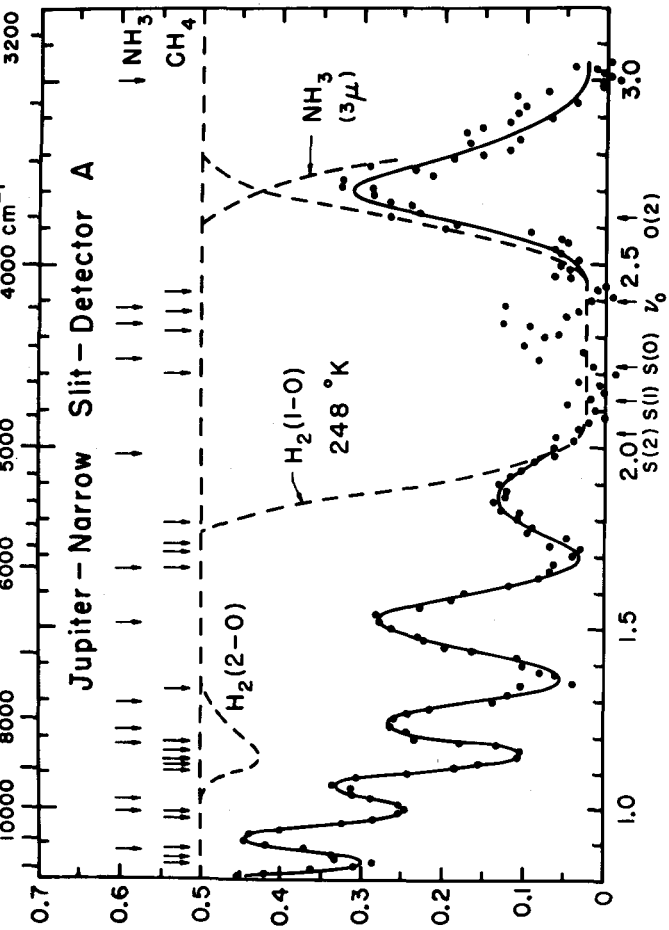

Fig. 4. The ratio of the observed intensity of Jupiter (as derived from detector A and the narrow entrance slit) to the brightness of a perfectly diffusing screen (having an albedo of unity) held normal to the sun's radiation at Jupiter's distance. The bands of CH_4 and NH_3 which have been observed in the laboratory are shown along with the positions of the lines in the 1-0 band of H_2.

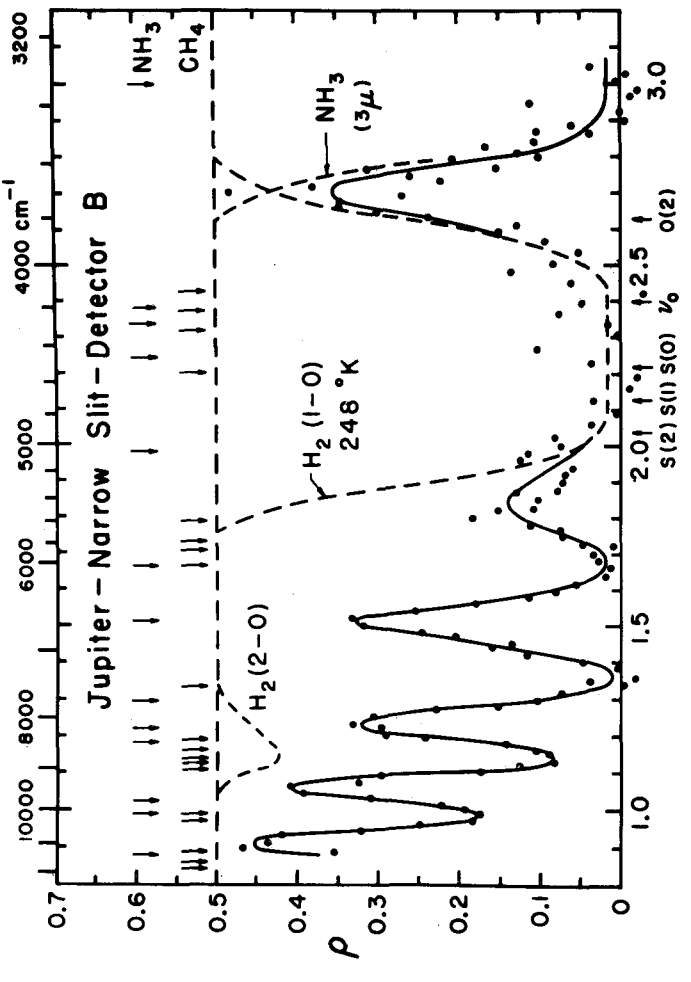

Fig. 5. The ratio of the observed intensity of Jupiter (as derived from detector B and the narrow entrance slit) to the brightness of a perfectly diffusing screen (having an albedo of unity) held normal to the sun's radiation at Jupiter's distance. The bands of CH_4 and NH_3 which have been observed in the laboratory are shown along with the positions of of the lines in the 1-0 band of H_2.

that the effective reflecting level of the infrared radiation is different at 0.7, 1.5, and 3.0μ due to the variation of the scattering parameters of the Jovian clouds with wavelength.

In order to explore this discrepancy and to gain some insight into the structure of Jupiter's atmosphere, simple Jovian model atmospheres were constructed. These models were based on the assumption that the opacity in the far infrared (which is characteristic of Jupiter's thermal emission) is primarily due to collision-induced rotational and translational transitions in H_2 as suggested by Trafton (1967). These models are presented in section IV and their application to Jupiter's atmosphere is discussed in section V and VI.

II. ABUNDANCE, TEMPERATURE, AND PRESSURE MEASUREMENT ON JUPITER

The abundance estimates for the atmosphere of Jupiter have generally assumed that the sunlight is reflected by a sharply defined layer which is the same for all wavelengths. Kuiper (1952) estimated that the CH_4 abundance was 1.5×10^4 cm-atm by comparing spectra of Jupiter with room temperature laboratory spectra in the wavelength interval from 0.6 - 0.9μ. Similarly, Kuiper (1952) estimated from the 0.654μ band that the NH_3 abundance was 7×10^2 cm-atm. From the same band, Dunham (1952) estimated the NH_3 abundance to be 500-1000 cm-atm. These NH_3 and CH_4 abundances have apparently been confirmed by the recent work of Owen (1965b).

The abundance of H_2 has been estimated to be 5 km-atm (Zabriskie 1962) and 27 km-atm (Spinrad and Trafton 1963) from the observed quadrupole lines. These estimates have been increased by Rank, Fink, and Wiggins (1966) on the basis of the curve of growth of the H_2 quadrupole lines derived from laboratory measurements and because of revised line strengths. The H_2 abundances derived from this curve of growth are given in Table I where the amount of H_2 given by Rank, Fink, and Wiggins (1966) has been divided by π in order to account for the double traversal and the secant effect averaged over the slit. The straight average of these

TABLE I

The Abundance of H_2 Above the Reflecting Level as Determined From the S(1) Quadrupole Line. The Amount of H_2 Given by Rank, Fink, and Wiggins (1966) has been Divided by π to Account for the Double Traversal and Secant Effect.

Observation	Equivalent Width (m Å)	So Laboratory 150° K (cm^{-1}/km-amagat)	Abundance above reflecting level (km-atm)
3-0 band			
Kiess, Corliss and Kiess (1960)	80	.0014	150
Spinrad and Trafton (1963)	40	.0014	40
Spinrad and Trafton (1963)	28	.0014	21
4-0 band			
Spinrad and Trafton (1963)	8	.000097	90

abundances is 75 km-atm which is within the abundance limits of 30-80 km-atm suggested by Field, Somerville, and Dressler (1966). Stecher (1965) derived an upper limit of 10.6 km-atm H_2 by interpreting the ultraviolet reflectivity as Rayleigh scattering by pure H_2 above a black cloud layer. Stecher notes that 200 km-atm of helium would also explain the observations, as well as a mixture of H_2 and He.

Spinrad and Trafton (1963) have estimated that the total pressure at the reflecting level in Jupiter is less than 2.8 atm based on an upper limit (set by instrumental broadening) to the widths of lines in the 6190Å band of CH_4. If one assumes that the pressure broadening coefficient of 0.15 cm^{-1}/atm measured by Rank, Fink, and Wiggins (1966) for the 1.66μ $3\nu_3$ CH_4 band is applicable to the 6190Å band, the upper limit to the pressure at the effective reflecting level is reduced to approximately 1.4 atm. If He is more abundant than H_2, this upper limit will be modified depending on the relative broadening efficiencies of H_2 and He.

Thornton and Welch (1963) have measured a radio

temperature of 144 ± 23° K near 8 mm, and Low (1965) has obtained 153 ± 15° K near 1 mm using a very sensitive Ge bolometer. Radio measurements near 3 cm (summarized by Owen 1965a) average somewhat higher (~170° K), but these may contain some contribution from Jupiter's non-thermal radiation.

Wildey, Murray, and Westphal (1965) have obtained 129° K as the 8-14μ temperature of the center of the disk. This is in good agreement with 132 ± 6° K obtained by Low (1965) from 7.5 - 13.5μ. Recently Low (1966) has measured the brightness temperature from 17.5 - 25μ and has obtained 150 ± 5° K for a wide equatorial band and 130° K for the poles.

Spectroscopic temperatures of ~120° K (Spinrad 1964) and ~170° K (Zabriskie 1962) have been estimated from the H_2 quadrupole lines. Owen (1965a) has derived a rotational temperature of 200 ± 25° K from the 3 ν_3 band of CH_4.

The observed temperatures are significantly higher than the 105° K effective temperature predicted from the bolometric albedo of 0.45 and solar radiation (Taylor 1965). In fact, Low (1966) has shown that the total energy Jupiter receives from the sun is less than the observed radiation between 10 and 25μ. Therefore, as discussed by Low (1966), an internal source of energy is implied.

III. NH_3 AND CH_4 ABUNDANCE ESTIMATES FROM THE STRATOSCOPE SPECTRA

Laboratory absorption data on NH_3 and CH_4 from 1.0 - 1.7μ have been published by Kuiper (1964). Figure 6 shows a comparison between the observed spectrum of Jupiter and that predicted from the laboratory data assuming that the total amount of NH_3 and CH_4 traversed by the infrared radiation was 2×10^3 cm-atm and 4×10^4 cm-atm, respectively. The values approximately correspond to the generally accepted abundances (7×10^2 cm-atm NH_3 and 1.5×10^4 cm-atm CH_4) above the reflecting level. It is evident that the predicted absorption, particularly in the 1.5μ region, is much larger than observed. The comparison between the laboratory data and the observations is uncertain because (among other reasons) the laboratory data were obtained at 300°K

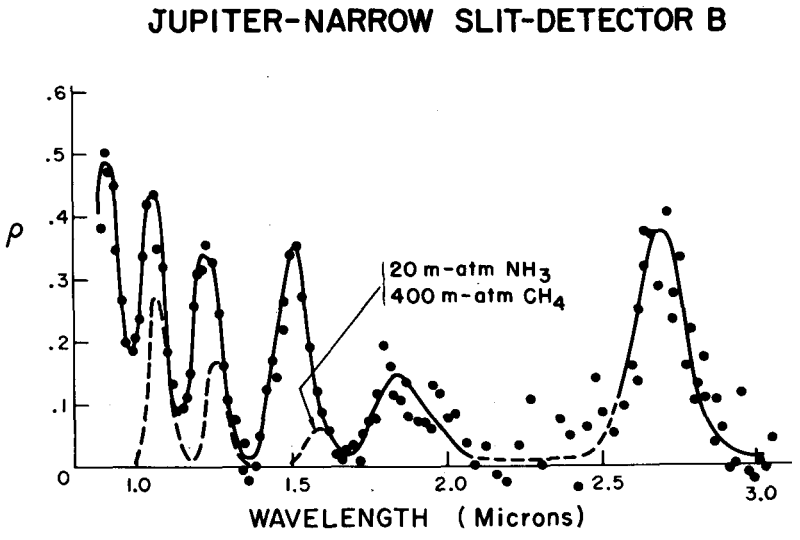

Fig. 6. Observed spectrum of Jupiter (solid line) and spectrum predicted from laboratory data (dashed line) assuming that the total amount of NH_3 and CH_4 traversed by the radiation is 2×10^3 cm-atm and 4×10^4 cm-atm, respectively.

while the relevant temperature of Jupiter's atmosphere is probably about 150° K, and because the relevant pressure in Jupiter's atmosphere is probably somewhat different from the laboratory data. However the discrepancy, which has also been pointed out by Moroz (1962), appears larger than might be expected from these uncertainties.

Figure 7 indicates a similar comparison between the observations and 50 cm-atm NH_3 and 8000 cm-atm CH_4. As was the case in Fig. 6, the instrumental profile of the spectrograph was applied to the laboratory data. The agreement between the observed and predicted absorptions is now very much better if a small wavelength shift is allowed. Although this shift (zero at 1.0 μ, 0.02 μ at 1.25 μ and 0.03 μ at 1.5 μ), is somewhat larger than the estimated accuracy of the wavelength calibration (Woolf, Schwarzschild, and Rose 1964), it cannot be excluded because the spectra of Jupiter were obtained shortly after

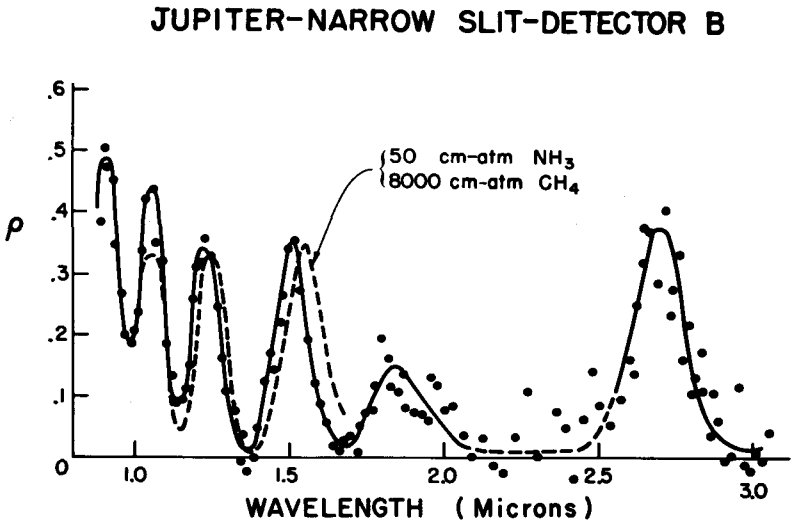

Fig. 7. Observed spectrum of Jupiter (solid line) and spectrum predicted from laboratory data (dashed line) assuming that the total amount of NH_3 and CH_4 traversed by the radiation is assumed to be 50 cm-atm and 8000 cm-atm, respectively.

the balloon reached altitude when the spectrometer may still have been approaching thermal equilibrium.

Thus it appears from the 1.0 - 1.7μ spectra that on the order of 50 cm-atm NH_3 and 8×10^3 cm-atm of CH_4 is traversed by the radiation in these wavelengths. If a discrete reflecting level is assumed, the abundance of NH_3 and CH_4 above this level is $\sim$20 cm-atm and $\sim 3 \times 10^3$ cm-atm, respectively, allowing about a factor of three for the double traversal and for secant effects. It must be emphasized, however, that the uncertainties of the above estimate are such that one can only conclude that the observed amount of NH_3 is at least an order of magnitude smaller than the generally accepted value of 7×10^2 cm-atm derived from the photographic infrared and that the observed amount of CH_4 appears to be several times smaller than the value of 1.5×10^4 cm-atm derived from the photographic infrared.

On the other hand, the estimated NH_3 abundance required to account for the 3μ absorption in the Stratoscope

spectra ranged from $\sim 4 \times 10^3$ to $\sim 4 \times 10^4$ cm-atm depending on whether the pressure at the reflecting level was 10 atm or 1 atm (Danielson 1966). Anticipating the discussion in Section VI it now appears much more likely that this feature is due to the very strong absorption in solid NH_3 near 3μ. In this interpretation, the 3μ feature is due to a rapid change in the continuum reflectivity of Jupiter's clouds due to a large decrease in $\tilde{\omega}_0$, the single scattering albedo of the NH_3 ice crystals assumed to make up the cloud. Thus the large abundance of gaseous NH_3 previously derived appears to be spurious.

An estimate of the variation of $\tilde{\omega}_0$ with wavelength which is needed to produce the 3μ feature can be obtained by assuming that the scattering phase function is isotropic and that ρ, the radiance factor in Figs. 2 to 5, is equal to p, the normal albedo of Jupiter. Neither assumption is completely valid, but they are adequate for this estimate. The results are shown in Fig. 8. No data on the single scattering albedo of NH_3 crystals is available. However, Reding and and Horning (1951) have measured the transmissions of a

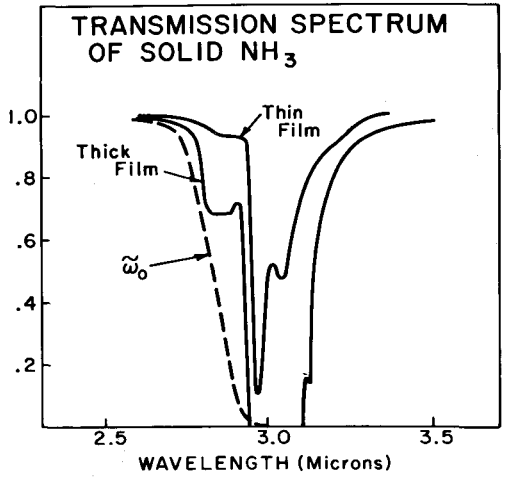

Fig. 8. A comparison of the transmission of "thick" and "thin" films of solid NH_3 with the single scattering albedo, $\tilde{\omega}_0$, required to explain the 3μ feature.

"thick" and "thin" film of solid NH_3. These transmissions are also shown in Fig. 8. Although no precise comparison between the single scattering albedo of crystals and the transmission of films can be made, one would expect them to have a similar variation with wavelength. While the two sets of data in Fig. 8 do not agree exactly, they are satisfactorily similar.

Solid NH_3 exhibits weaker absorptions at 2.28μ and at 2.03μ (Reding and Horning 1951), which may contribute to the large feature centered at 2.25μ. There should also be some absorption in solid NH_3, near 1.5μ, but no data is available.

IV. ATMOSPHERIC MODELS

Simple model atmospheres have been calculated based on three restrictions. First, following Trafton (1967), the collision-induced rotational and translational absorption by molecular hydrogen is assumed to be the principal source of opacity in the infrared wavelengths in which Jupiter radiates. Second, the 17.5 - 25μ temperatures as measured by Low (1966) are used to restrict the range of effective temperatures employed in the calculations. Third, we have assumed that C, N, O, Ne, Si, and S have abundance ratios deep in Jupiter's atmosphere similar to those observed in the sun, but that the H/He and H/C ratios are adjustable parameters.

Figure 9 shows the absorption coefficients of the collision-induced transitions in H_2 is given by Trafton (1967) along with the values of B_ν for temperatures of 130° K and 160° K. For each of the above temperatures (130° and 160°), the Rosseland mean opacity was computed for the three different assumed abundances given in Table II. In Model I, the solar abundances of Goldberg, Müller, and Aller (1960) supplemented by data from B stars given by Aller (1961) are assumed. In abundance Model II, we assume that all elements with $Z \geq 3$ are enriched by a factor of 10 relative to H_2 and He while in Model III, all elements with $Z \geq 2$ are enriched by a factor of 10 relative to H_2. In all of the

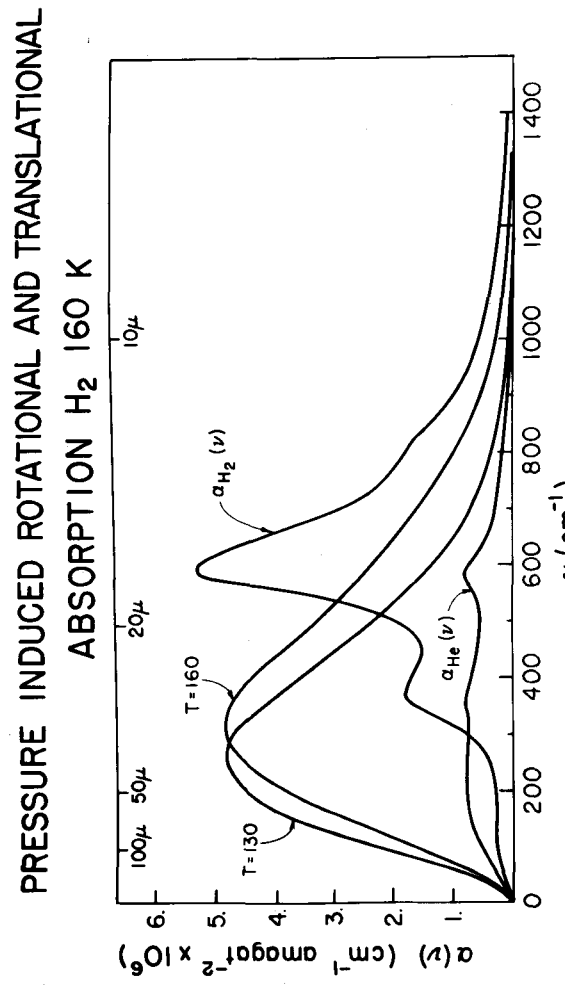

Fig. 9. Collision-induced absorption coefficients as given by Trafton (1967) for equilibrium H_2 at 160° K. The total absorption coefficient for H_2 - He_2 mixtures is

$$K(\nu) = \alpha_{H_2}(\nu)\,\rho_{H_2}^2 + \alpha_{He}\rho_{He}\,\rho_{H_2}$$

Also shown are black body curves for T = 130 and 160° K.

models, C, N, O, Si, and S are assumed to be completely reduced (Lippincott, Eck, Dayhoff, and Sagan 1967).

TABLE II

Relative Abundances (by number) Assumed in the Model Atmospheres. For Each of the Abundance Models, Atmospheric Models have been Calculated for Effective Temperatures of 130 and 160° K. Also listed are the Mean Molecular Weights.

Species	Models I (130) I (160)	Models II (130) II (160)	Models III (130) III (160)
	(Solar abundances)		
H_2	0.757	0.076	0.076
He	0.240	0.024	0.240
CH_4	6×10^{-4}	6×10^{-4}	6×10^{-4}
NH_3	1.7×10^{-4}	1.7×10^{-4}	1.7×10^{-4}
H_2O	14×10^{-4}	14×10^{-4}	14×10^{-4}
Ne	7.6×10^{-4}	7.6×10^{-4}	7.6×10^{-4}
SiH_4	0.5×10^{-4}	0.5×10^{-4}	0.5×10^{-4}
H_2S	0.3×10^{-4}	0.3×10^{-4}	0.3×10^{-4}
μ	(2.5)	(2.9)	(3.7)

From Fig. 9 and the recent measurements of Low (1966) from 17.5 - 25μ (400 - 570 cm^{-1}), we may estimate the likely range of effective temperatures of Jupiter. We note that the absorption coefficient due to self-induced collisional transitions in H_2 is considerably higher from 400 - 570 cm^{-1} than at the smaller wavenumbers at which the maxima occur for B_ν (130° K) and B_ν (160° K). Conversely, for He induced transitions, the opacity near the maximum of B_ν is slightly greater than from 400 - 570 cm^{-1} In the latter case, the assumption of a grey atmosphere is rather good and one would expect that the effective temperature of Jupiter would be close to the temperature measured by Low (1966) in the 400 - 570 cm^{-1} window. On the other hand, if the opacity is due to self-induced collisional transitions in H_2, one would expect that these measured temperatures would be somewhat smaller than the effective temperature. Therefore, it seems likely that the effective temperatures of Jupiter are equal to or larger than those measured in the vicinity of 20μ. Since the measured values by Low (1966)

equal 130° K at the poles and about 150° K at the equator, we have adopted effective temperatures of 130° K and 160° K in our models. These temperatures bracket the likely range of effective temperatures to be found on Jupiter.

For each assumed abundance and effective temperature, the Rosseland mean absorption coefficient was computed. For models I and II, this results in a mean absorption coefficient $\bar{\alpha} \approx 0.8 \times 10^{-6}$ cm^{-1} amagat^{-2} and for model III, $\bar{\alpha} \approx 1.6 \times 10^{-6}$ cm^{-1} amagat^{-2}. Note that $\bar{K}\,[\mathrm{cm}^{-1}] = \bar{\alpha}\,\rho_{H_2}^2$.

For the upper radiative region, τ, the optical depth of the geometrical level for which the overlying abundance of H_2 is W_{H_2} is approximately given by:

$$\tau \approx \frac{\bar{\alpha}}{2H} W_{H_2}^2 \tag{1}$$

where the scale height H is defined by:

$$H = \frac{RT_{eff}}{\mu g} \tag{2}$$

and where μ is the mean molecular weight, R is the gas constant, g is the acceleration due to gravity, and T_{eff} is the effective temperature.

The simple Eddington approximation to radiative transfer in a grey atmosphere is employed until the lapse rate becomes adiabatic. Below that level, the temperature-pressure relationship is assumed to be adiabatic. The effects of phase changes in NH_3 and H_2O were taken into account following the procedures outlined by Lasker (1963). The effects of these phase changes are rather unimportant for the range of abundances used in these models. Only for much larger NH_3/H_2 and H_2O/H_2 abundance ratios such as those assumed by Gallet (Wildt, Smith, Salpeter, and Cameron 1963) is the atmospheric structure significantly altered by phase changes.

The resulting models are shown in Figs. 10 to 15. In these graphs the solid curves give the abundance W (in cm-atm) of each constituent above a given geometrical level as a function of the temperature at that level. The solid curves also give the partial pressure (in atmospheres) of each non-condensing constituent. For condensable

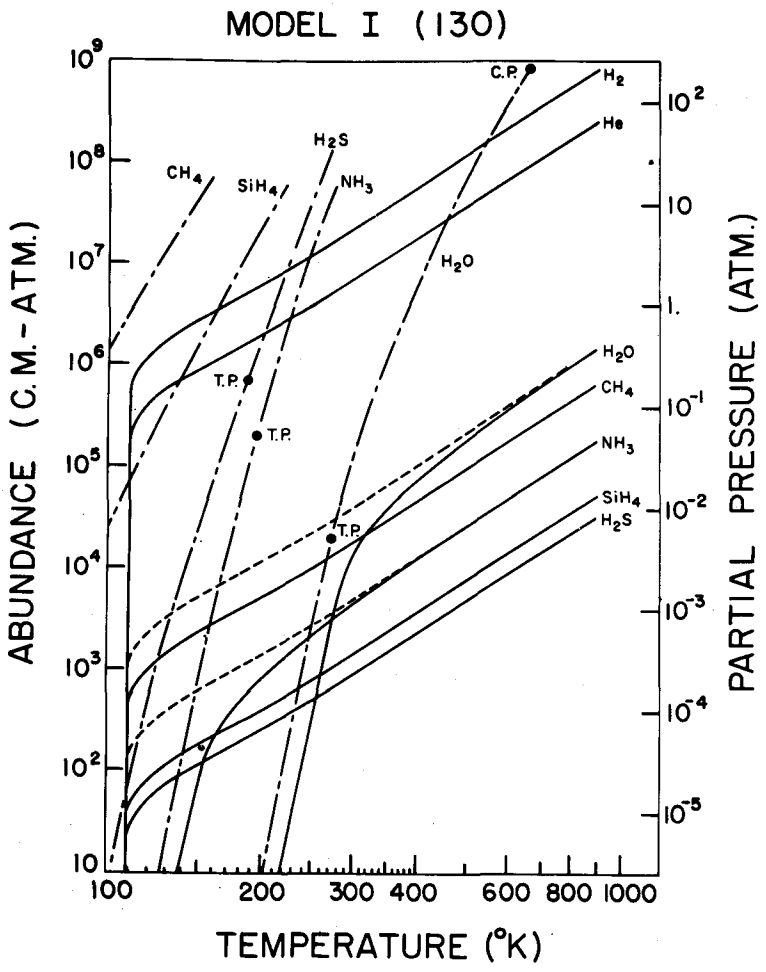

Fig. 10. Model I (130) - The abundances (in cm-atm) of H_2, He, H_2O, CH_4, NH_3, SiH_4, and H_2S above a given geometrical level as a function of the temperature of that level (solid curves). The solid curves also give the partial pressure (in atmospheres) of each non-condensing constituent. The long-short dashed curves are saturation vapor pressure curves with triple points (T.P.) indicated. All these curves are for abundance model I (i.e., Solar Abundances) and Te = 130° K.

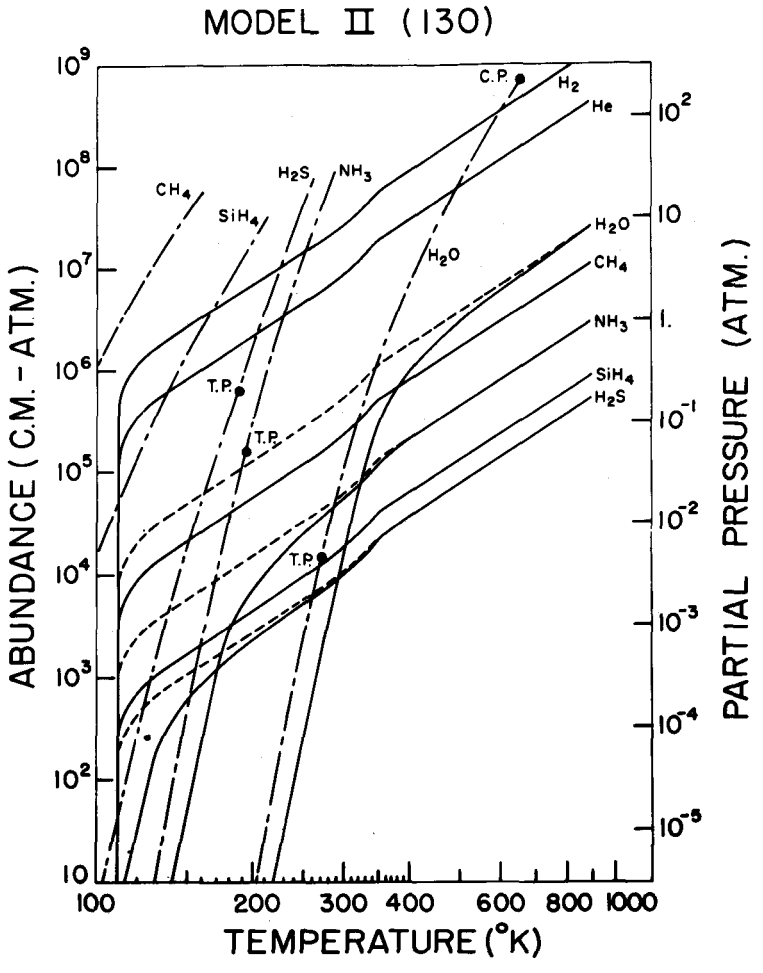

Fig. 11. Model II (130) - The abundances (in cm-atm) of H_2, He, H_2O, CH_4, NH_3, SiH_4, and H_2S above a given geometrical level as a function of the temperature of that level (solid curves). The solid curves also give the partial pressure (in atmospheres) of each non-condensing constituent. The long-short dashed curves are saturation vapor pressure curves with triple points (T.P.) indicated. All these curves are for abundance model II (elements with $Z \geq 3$ enriched by a factor of 10 relative to H_2 and He).

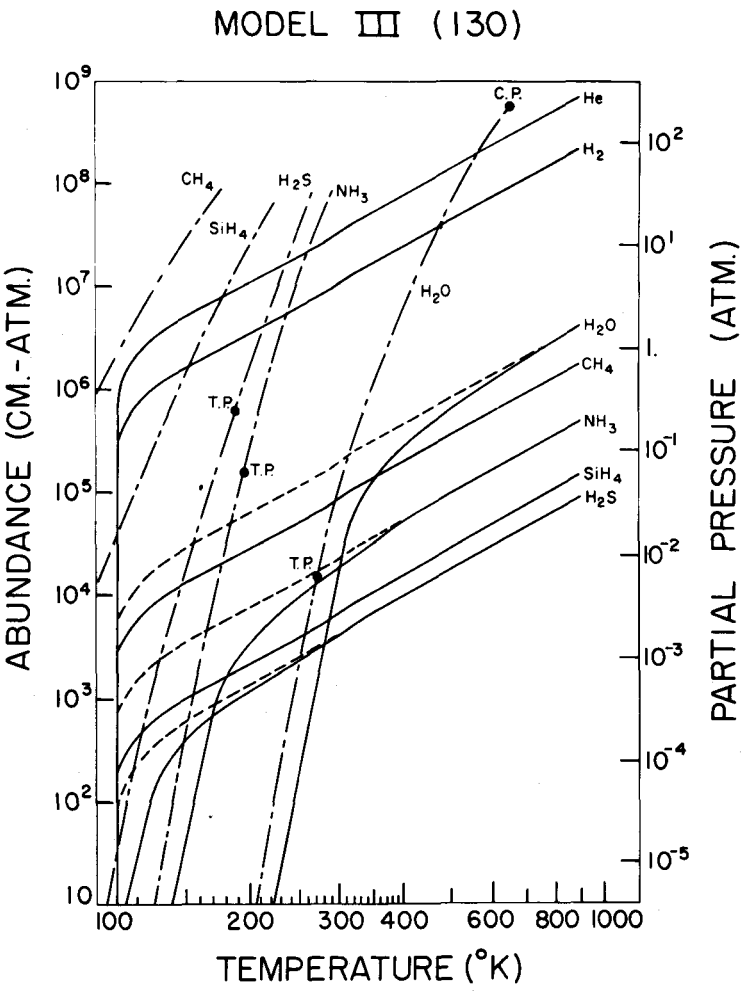

Fig. 12. Model III (130) - The abundances (in cm-atm) of H_2, He, H_2O, CH_4, NH_3, SiH_4, and H_2S above a given geometrical level as a function of the temperature of that level (solid curves). The solid curves also give the partial pressure (in atmospheres) of each non-condensing constituent. The long-short dashed curves are saturation vapor pressure curves with triple points (T.P.) indicated. All these curves are for abundance model III (all elements with $Z \geq 2$ enriched by a factor of 10 relative to H_2).

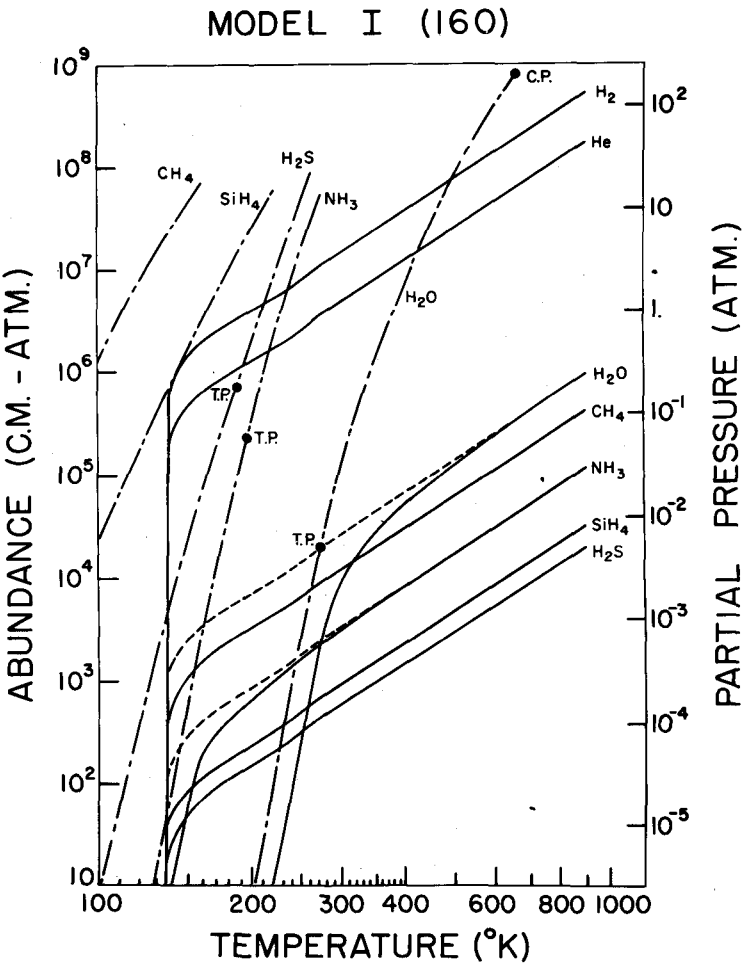

Fig. 13. Model I (160) - The abundances (in cm-atm) of H_2, He, H_2O, CH_4, NH_3, SiH_4, and H_2S above a given geometrical level as a function of the temperature of that level (solid curves). The solid curves also give the partial pressure (in atmospheres) of each non-condensing constituent. The long-short dashed curves are saturation vapor pressure curves with triple points (T.P.) indicated. All these curves are for abundance model I (i.e., Solar Abundances) and Te = 160° K.

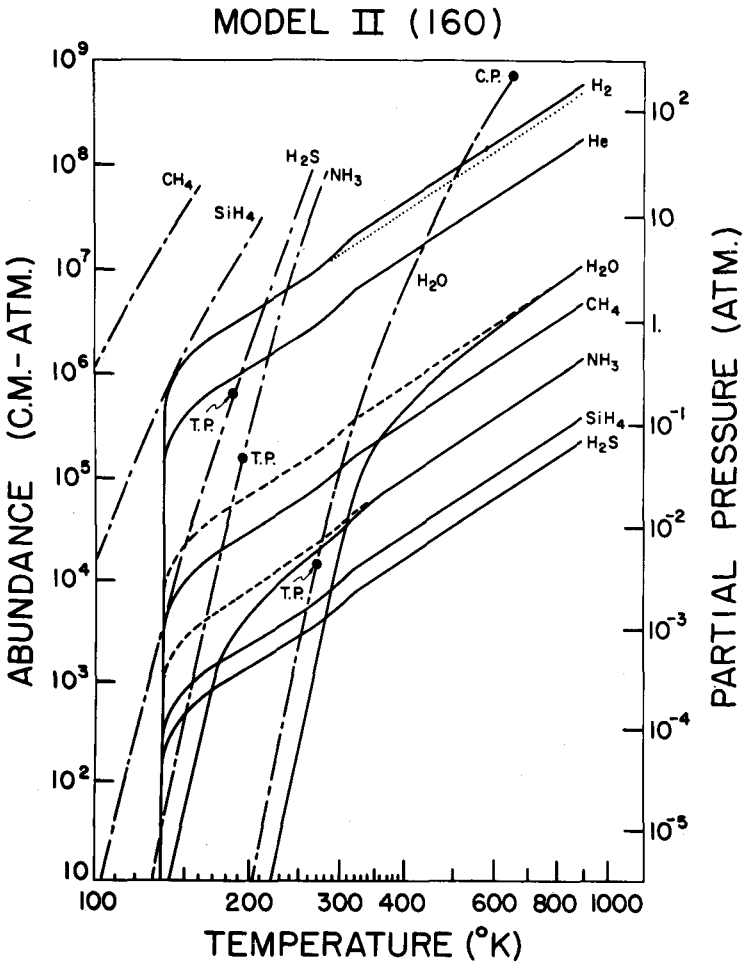

Fig. 14. Model II (160) - The abundances (in cm-atm) of H_2, He, H_2O, CH_4, NH_3, SiH_4, and H_2S above a given geometrical level as a function of the temperature of that level (solid curves). The solid curves also give the partial pressure (in atmospheres) of each non-condensing constituent. The long-short dashed curves are saturation vapor pressure curves with triple points (T.P.) indicated. All these curves are for abundance model II (all elements with $Z \geq 3$ enriched by a factor of 10 relative to H_2 and He) and Te = 160° K.

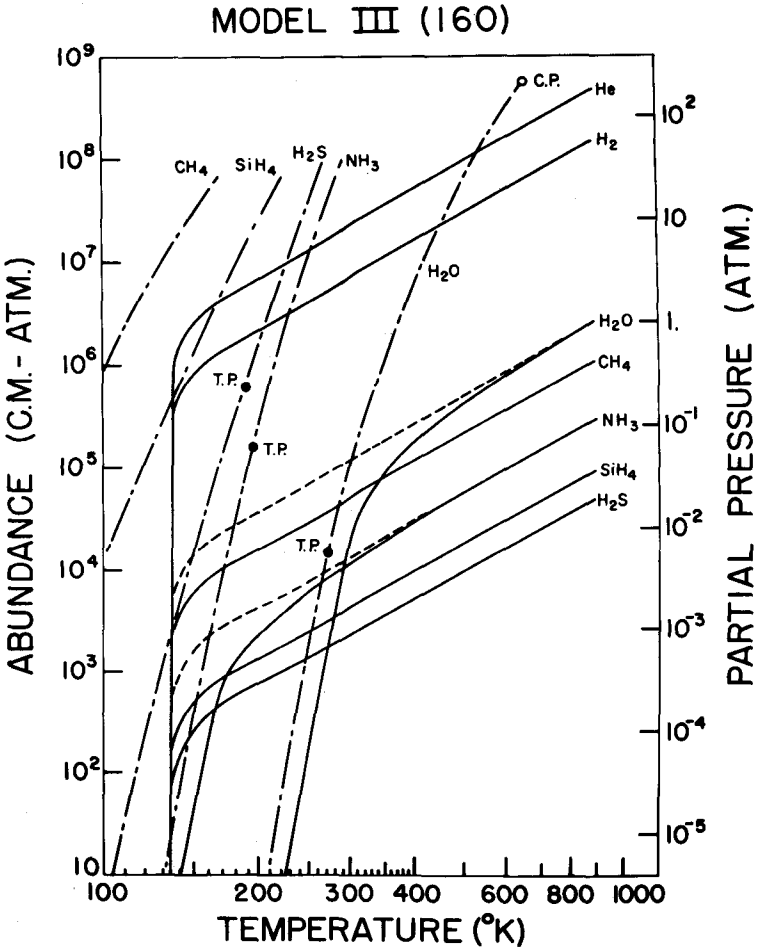

Fig. 15. Model III (160) - The abundances (in cm-atm) of H_2, He, H_2O, CH_4, NH_3, SiH_4, and H_2S above a given geometrical level as a function of the temperature of that level (solid curves). The solid curves also give the partial pressure (in atmospheres) of each non-condensing constituent. The long-short dashed curves are saturation vapor pressure curves with triple points (T.P.) indicated. All these curves are for abundance model III (elements with $Z \geq 2$ enriched by a factor of 10 relative to H_2) and $Te = 160°$ K.

constituents like H_2O, NH_3, and H_2S, the partial pressure is given by the dashed curves until they intersect the saturation vapor pressure curves (long-short dashed curves). At lower temperatures, these constituents are assumed to be saturated, i.e., the partial pressure is given by the saturation vapor pressure curves.

The effect of including the opacity of NH_3 on the thermal structure of these models is minor. This is because the amount of NH_3 which can exist in the upper radiative regions ($T \lesssim 160°$ K) is limited by the NH_3 vapor pressure curve. It can be shown that the contribution to the total Rosseland mean opacity of the amount of NH_3 which can exist above the 160° K level ($\sim$ 180 cm-atm) is small. In the deeper layers ($T \gtrsim 160°$ K), the contribution of NH_3 to the total Rosseland mean opacity begins to become important. But in these regions the atmosphere is convecting and a change in the opacity in such regions does not significantly modify the thermal structure.

V. ANALYSIS OF THE ABUNDANCE MODELS IN TERMS OF A SINGLE CLOUD LAYER

The models given in Figs. 10 to 15 predict the abundance (in cm-atm) of H_2, He, CH_4, H_2O, NH_3, SiH_4, and H_2S as a function of temperature (i.e., as a function of depth in the atmosphere). If the assumption of a well defined reflecting level (e.g. cloud top) is valid, the model which most nearly describes the observations could be determined by comparing the observed abundances of H_2, NH_3, and CH_4 with the predicted abundances. However, it is quite possible that the cloud scattering properties are such that no well-defined reflecting level exists. In this case, the observed abundances cannot be simply interpreted (Chamberlain 1965). Nevertheless, we shall begin by considering discrete reflecting layers.

Figures 16 and 17 show the predicted ratios of the CH_4 and NH_3 abundances as a function of temperature in the atmosphere. Also indicated is the CH_4 to NH_3 abundance ratio of about 21 observed in the wavelength interval from

0.6 - 0.9 μ as well as the CH_4 to NH_3 ratio of roughly 160 which is suggested by Fig. 7 in the 1.0 - 1.7μ region. Table III gives the values of $T_{reflection}$, the temperature at the geometric level where $W_{CH_4}/W_{NH_3} = 160$ and the predicted abundances above this level. Table IV gives similar values for $W_{CH_4}/W_{NH_3} = 21$.

Considering the order of magnitude accuracy of the abundances derived from Fig. 7, none of the predicted abundances given in Table III are sufficiently discrepant to rule out any of the models except, perhaps, Model I (160). The best agreement is obtained by models I (130) and III (160). For these models, $T_{reflection}$ equals 140° K and 148° K, respectively, and the NH_3 sublimation temperatures are 150° and 160° K, respectively. Thus, if the abundances in the

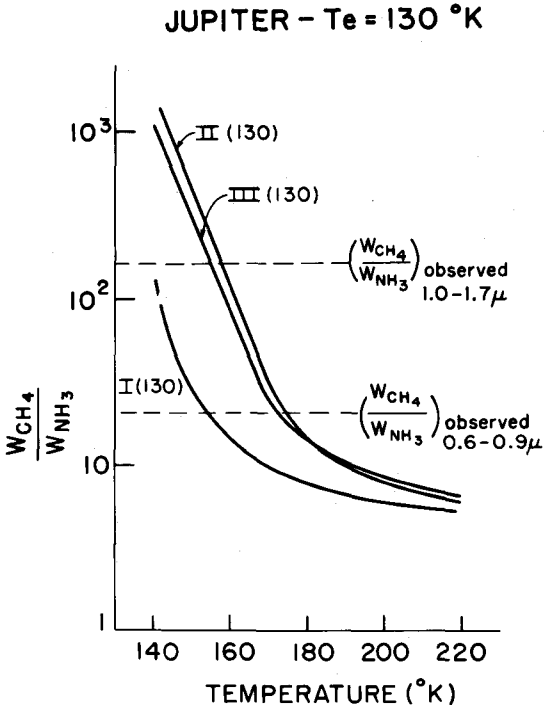

Fig. 16. Predicted ratio of CH_4 and NH_3 abundances above a geometrical level as a function of the temperature of that level for models with Te = 130° K.

1.0 - 1.7μ wavelength interval are to be explained in terms of a discrete reflecting level coinciding with a cloud top, models I (130) and III (160) require that the cloud top temperature be $\sim$ 144° K. Since the adiabatic lapse rate in these models is about 3° K/km, this would be consistent with the presence of an NH_3 crystal cloud layer above the sublimation level having a thickness of a few kilometers.

In the case of the photographic infrared abundance measurements (which may be uncertain by a factor of two), Table IV indicates that models I (130) and I (160) predict CH_4 and NH_3 abundances which are many times smaller than the accepted values of 1.5×10^4 cm-atm and 7×10^2 cm-atm, respectively. Model II (130) is in marginal agreement while models III (130), II (160), and III (160) are in fairly good agreement. For the latter three models, $T_{reflection}$ averages

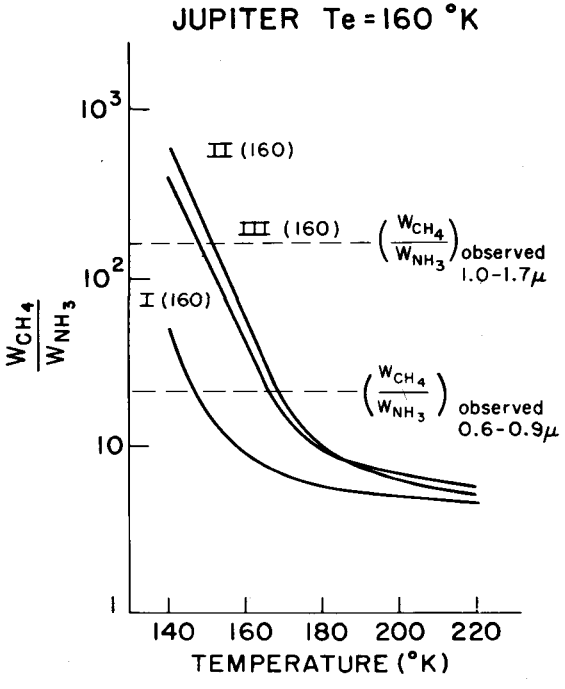

Fig. 17. Predicted ratio of CH_4 and NH_3 abundances above a geometrical level as a function of the temperature of that level for models with Te = 160° K.

about 168° K which is a few degrees higher than the sublimation temperature for these models. Therefore if one assumes, as a first approximation, that the NH_3 clouds do not extend below the sublimation level, one can not explain the existence of a reflecting level having a temperature of $\sim 168°$ K with NH_3 clouds. However, in practice the NH_3 cloud probably extends somewhat below the sublimation level as well as above.

One might attempt to explain the two sets of observed abundances (using model III (160), for example) in terms of a reflecting level in the NH_3 cloud for the 1.0 - 1.7μ radiation which is ~ 6 km higher in the atmosphere than the reflecting level for the radiation in the 0.6 - 0.9μ wavelength interval. Qualitatively, such an effect could occur if the single particle phase function was more forward scattering between 0.6 and 0.9μ than between 1.0 to 1.7μ and if the scattering mean free path was not less in the 0.6 - 0.9μ interval than in the 1.0 - 1.7μ interval. Of course, both the phase function and the mean free path depend on the cloud crystal size distribution and number density, both of which are unknown.

However, even with strongly forward scattering phase functions such as that derived by Deirmendjian (1964) for H_2O droplet clouds at 0.65μ, the photons have been deviated at least 90°, on the average, after 10 scatterings and the majority of emergent photons experience less than 50

TABLE III

Predicted Abundance (in cm-atm) Above the Level at Which the Predicted CH_4 to NH_3 Abundance Ratio Equals the Ratio Observed in the 1.0 to 1.7 μ region. The Temperature ($T_{reflection}$) and pressure ($P_{reflection}$) at the Reflection Level Along With the Sublimation Temperature are Also Listed.

	I (130)	II (130)	III (130)	I (160)*	II (160)	III (160)
W_{H_2}	2.3×10^6	3.3×10^6	1.7×10^6	6.0×10^5	1.4×10^6	7.8×10^5
W_{He}	7.1×10^5	1.0×10^6	5.6×10^6	2.0×10^5	4.4×10^5	2.4×10^6
W_{CH_4}	1.9×10^3	2.7×10^4	1.6×10^4	4.0×10^2	1.1×10^4	5.6×10^3
W_{NH_3}	1.2×10^1	1.7×10^2	1.0×10^2	6.0	6.8×10^1	3.5×10^1
W_{SiH_4}	1.4×10^2	2.1×10^3	1.1×10^3	3.8×10^1	9.0×10^2	4.6×10^2
W_{H_2S}	9.0×10^1	7.3×10^2	4.7×10^2	1.7×10^1	5.2×10^2	2.5×10^2
$T_{reflection}$ (° K)	140	158	155	135	151	148
$P_{reflection}$ (atm)	0.78	1.3	2.8	0.2	0.5	1.2
$T_{sublimation}$ (° K)	150	170	165	143	165	160

*For model I (160) the predicted maximum value of W_{CH_4}/W_{NH_3} is 67. Therefore, the abundances listed for this model are for this maximum ratio.

TABLE IV

Predicted abundances (in cm-atm) Above the Level at Which the Predicted CH_4 to NH_3 Abundance Ratio Equals the Ratio Observed in the .6 - .9 μ Region. The Temperature ($T_{reflection}$) and Pressure ($P_{reflection}$) at the Reflection Level Along With the Sublimation Temperature are Also Listed.

	Models					
	I (130)	II (130)	III (130)	I (160)	II (160)	III (160)
WH_2	3.0×10^6	4.4×10^6	2.3×10^6	1.3×10^6	2.2×10^6	1.3×10^6
WHe	9.5×10^5	1.4×10^6	7.4×10^5	4.5×10^5	6.7×10^5	4.1×10^5
WCH_4	2.5×10^3	3.5×10^4	1.9×10^4	1.0×10^3	1.7×10^4	1.0×10^4
WNH_3	1.2×10^2	1.7×10^3	9.0×10^2	4.8×10^1	8.1×10^2	4.8×10^2
$WSiH_4$	1.9×10^2	2.7×10^3	1.5×10^3	8.0×10^1	1.4×10^3	8.2×10^2
WH_2S	1.2×10^2	1.3×10^3	7.0×10^2	4.7×10^1	8.4×10^2	4.8×10^2
$T_{reflection}$ (° K)	154	174	171	147	168	166
$P_{reflection}$ (atm)	1.04	1.77	3.77	.46	.87	2.1
$T_{sublimation}$ (° K)	150	170	165	143	165	160

scatterings (Moore and Danielson 1968). Therefore if the scattering mean free path in the Jupiter clouds is 100 meters or less (which is characteristic of terrestrial clouds), the average depth of penetration of strongly forward scattering photons cannot be more than a few km deeper than for isotropically scattering photons. Thus, for uniform deep clouds, the increase in the average path length in the cloud of emergent photons with increasing forward scattering is limited. However, in the case of a relatively thin cloud layer, modest changes in the scattering phase function can result in a substantial change in the number of photons which penetrate the cloud layer (Moore and Danielson 1967).

Therefore, it seems more likely to us that the larger abundances observed at shorter wavelengths can be explained in terms of two cloud layers on Jupiter rather than a single cloud layer. Indeed, the presence of at least two cloud layers is suggested by the models given in the previous section. One is a (possibly rather thin) NH_3 crystal cloud layer which will be expected to form above the level (ranging in temperature from 143° K to 170° K in our models) where NH_3 becomes saturated; the second is a (possibly rather thick) H_2O cloud which will be expected to form above the level (having a temperature of roughly 300° K) where H_2O becomes saturated. Also, two of the models [II (130) and III (130)] predict the formation of a H_2S cloud layer high in Jupiter's atmosphere, but we shall not include this third layer in our discussion.

VI. ANALYSIS OF THE ABUNDANCE MODELS IN TERMS OF TWO CLOUD LAYERS

As a first attempt in understanding the wide range of abundance, temperature, and pressure measurements on Jupiter in terms of a two cloud layer model, let us assume that the low NH_3 abundance measured near 1.5μ is a result of essentially all photons at this wavelength scattering off the top of the NH_3 cloud layer. In this idealization, the cloud top temperature is about 145° K since there is about 20 cm-atm NH_3 above the 145° K level in Jupiter's atmosphere (this temperature is rather independent of the model chosen).

Let us further assume that the higher NH_3 abundances measured in the 0.6 - 0.9μ range is due to a significant fraction of the emergent photons at these wavelengths having penetrated to the lower H_2O cloud layer. There is no straightforward way to estimate the temperature of the top of the H_2O cloud since the height of the cloud top will depend, among many factors, on the convective velocities present. However in the two cloud model that we are considering, one can set an upper limit from the fact that no H_2O lines have been observed in the photographic infrared. From the models in section IV, one can see that the amount of gaseous H_2O above the 200° K level is $\sim$ 1 cm-atm while the amount above the 250° K level is $\sim$ 200 cm-atm. The latter amount ($\sim$ 1400 microns precipitable water) should be easily detectable while the former ($\sim$ 7 microns) would be difficult to detect. Therefore, on this basis, the two cloud model requires the H_2O cloud top temperature to be less than 250° K (again, this temperature is quite independent of the model chosen). For the sake of definiteness, we shall rather arbitrarily adopt 200° K.

The amount of NH_3 and CH_4 above the 145° K level is given in Table 5 while the amount above the 200° K level is given in Table 6. From these tables, it seems possible that the abundances observed in the 0.6 - 0.9μ range (7×10^2 cm-atm NH_3 and 1.5×10^4 cm-atm CH_4) can be explained as an average determined by photons that have scattered off the NH_3 cloud layer and by photons that have scattered off the H_2O cloud layer. Considering the

TABLE V

Predicted Abundances (in cm-atm) Above the Level With a Temperature of 145° K. The Pressure (in atm) at This Level is Also Listed.

Model	$W NH_3$	$W CH_4$	$W H_2$	P (atm)
I (130)	2.0×10^1	2.0×10^3	2.4×10^6	0.80
II (130)	2.0×10^1	1.9×10^4	2.4×10^6	1.0
III (130)	2.0×10^1	1.2×10^4	1.4×10^6	2.3
I (160)	2.0×10^1	7.5×10^2	9.5×10^5	0.36
II (160)	2.0×10^1	7.0×10^3	1.0×10^6	0.40
III (160)	2.0×10^1	5.0×10^3	6.5×10^5	1.0

accuracy of the observed abundances, only models I (130) and I (160) seem incompatible with this interpretation.

In the two layer model, one would interpret the 200 ± 25°K rotational temperature obtained by Owen (1965a) in the 1.10μ, $3\nu_3$ CH_4 band as the H_2O cloud top temperature. In this interpretation, it is not necessary that a large fraction of incident photons at 1.10μ penetrate to the H_2O cloud since the highest rotational levels producing measurable lines in the band are significantly populated only at the higher temperatures near the H_2O cloud top.

The temperatures of ~ 130°K observed in the 8 - 14μ window are readily understood in terms of the fact that about 1 cm-atm of NH_3 becomes opaque at these wavelengths (Kuiper 1952, p. 380) and that the abundance of NH_3 above the 130°K level is about 1 cm-atm. A similar interpretation for the 8 mm radio temperature has been given by Thornton and Welch (1963).

One might also identify the large temperature suggested by the width of the collision-induced 1-0 band of H_2 shown in Fig. 3 with the top of the H_2O cloud layer. At these longer wavelengths, the scattering phase function is probably somewhat more isotropic than at 1.5μ which (by itself) would lead to slightly less penetration of the NH_3 cloud layer. However, if the NH_3 crystals have dimensions no larger than about 1μ, the scattering mean free path should be considerably longer at 2.5μ than at 1.5μ. Therefore it seems plausible that a sufficiently large fraction of the photons with

TABLE VI

Predicted Abundances (in cm-atm) Above the Level With a Temperature of 200° K. The Pressure (in atm) At This Level is Also Listed.

Model	W_{NH_3}	W_{CH_4}	W_{H_2}	P (atm)
I (130)	7.4×10^2	5.2×10^3	6.4×10^6	2.2
II (130)	6.0×10^3	5.6×10^4	6.0×10^6	2.9
III (130)	3.4×10^3	2.8×10^4	3.5×10^6	5.4
I (160)	6.4×10^2	3.2×10^3	4.0×10^6	1.3
II (160)	4.5×10^3	3.0×10^4	3.7×10^6	1.4
III (160)	2.3×10^3	1.6×10^4	2.1×10^6	3.4

wavelengths $\sim 2.5\mu$ could penetrate to the H_2O cloud layer to produce the width of the observed feature. If this be the case, the presence of the 2.7μ peak in Jupiter's spectrum (Figs. 1 to 5) also sets an upper limit of roughly 200°K to the H_2O cloud top temperature. If the temperature were much higher, the radiation would be absorbed by the strong H_2O band at 2.7μ on the basis of the H_2O abundance predicted by the models in Section IV.

Following the reasoning in the preceding paragraph, one is tempted to interpret the large absorption feature at 3.0μ as due to absorption by gaseous NH_3 above the H_2O cloud. Indeed, the amount of NH_3 above this cloud in models II (130), II (160), III (130), and III (160) (which ranges from 2.3×10^3 to 6×10^3 cm-atm and cloud top pressures ranging from 1.4 to 5.4 atm) is not impossibly discordant with the amount of NH_3 ($\sim 2 \times 10^4$ cm-atm at a cloud top pressure of 2 atm) needed to explain this feature if one considers the uncertainty in the latter estimate. However, the preceding discussions of photon penetration has assumed that $\tilde{\omega}_0 \approx 1$ where $\tilde{\omega}_0$ is the single particle albedo. But, as discussed in Section II, the strong absorption band in solid NH_3 will reduce $\tilde{\omega}_0$ to values much less than unity in the vicinity of 3μ. This has the result that virtually no photons near 3μ will penetrate to the H_2O cloud layer; practically all should be absorbed in the NH_3 cloud. Thus, it seems much more plausible to attribute the 3μ feature to absorption by <u>solid</u> NH_3 than by gaseous NH_3.

One can also explain, at least qualitatively, the large H_2 abundances determined from the 3-0 and 4-0 quadrupole lines if, as suggested for the NH_3 and CH_4 abundances, the H_2 abundances are an average determined by photons that scatter off the NH_3 cloud and by photons which emerge after having scattered off the H_2O cloud. One might also explain the low H_2 abundance ($\lesssim$ 10 km-atm) obtained from the ultraviolet reflectivity measurements of Stecher (1965) if one identifies this abundance with the amount of H_2 above the NH_3 cloud. From Table V and excluding models I (130) and I (160) by previous considerations, one can see that models II (160) and III (160) are in agreement with this abundance measurement.

The abundance determined by Stecher (1965) was derived on the assumption of completely absorbing clouds which requires that the NH_3 cloud be strongly absorbing in the ultraviolet. But pure solid NH_3 has no appreciable absorption between 2000 and 3000 Å (Dressler and Schnepp 1960) and therefore "dust" in Jupiter's atmosphere is required in order to understand the ultraviolet observations. Indeed the presence of a significant amount of dust in the atmosphere of Jupiter (probably as absorbing nuclei of the cloud crystals) is implied by the visible albedo of 0.76 (Harris 1961, p. 370). It is known (Allen 1964, p. 122) that the absorption mean free path due to dust in the earth's atmosphere increases strongly with decreasing wavelength and therefore it seems plausible that the presence of dust in the NH_3 cloud could cause it to appear black shortward of 3000 Å.

The observed upper limit of 1.4 atmospheres for the 6190 Å CH_4 band (see Section II) sets one more constraint on our models. If the observed upper limit refers (as assumed for the abundances) to some average of the pressure at the NH_3 cloud top and at the H_2O cloud top, reference to Table VI indicates that model II (160) provides the best agreement with the pressure measurements.

Indeed, abundance model II (160) probably provides the best overall agreement with the observations. The NH_3, CH_4, and H_2 abundances given by this model are in satisfactory agreement with the observations considering the

uncertainty in the measurements, the qualitative treatment of reflection and transmission of the two cloud layers, and the probability that the effective temperature varies from the equatorial to the polar regions. The occultation measurement of Baum and Code (1953) would favor the large He content of models III (130) and III (160). However, the uncertainty in the scale height (6.2 - 12.5 km) plus the uncertainty in the stratospheric temperature (100 - 130°K) where the occultation is assumed to have occured, leads to values of the mean molecular weight ranging from 2.6 to 6.7. The mean molecular weight of 2.9 for models II (130) and II (160) also falls within this range.

In summary, it appears to use that a two cloud model of the type discussed above is a promising "next step" after the single cloud top model in understanding the widely varying abundances and temperatures observed on Jupiter. Although model II (160) appeared to provide the best agreement with the observations, detailed calculations of photon reflection and transmission in cloud layers will be required before a unique model of Jupiter's atmosphere is possible.

ACKNOWLEDGEMENTS

This work was supported, in part, by Project Stratoscope of Princeton University sponsored by NSF, ONR, and NASA.

One of us (B.D.S) wishes to acknowledge support from a National Aeronautics and Space Administration Traineeship.

Note added in proof: After this paper was completed, we became aware that SiH_4 is not expected to occur in significant quantities in Jupiter's atmosphere. As pointed out by Greenspan and Owen (Science, 156, 1498 (1967)), the equilibrium for the chemical reaction

$$SiH_4 + 2H_2O \rightleftharpoons SiO_2 + 4H_2$$

is such that virtually all the SiH_4 will be converted into SiO_2 in spite of the large quantity of H_2 present. Thus the SiH_4 curves in Figures 10-15 should be ignored.

REFERENCES

Allen, C. W., Astrophysical Quantities (Athlone Press, London, 1964), 2nd Edition.
Aller, L. H., The Abundances of the Elements (Interscience, New York, N. Y., 1961).
Baum, W. A. and Code, A. D., Astrom. J. **58**, 108 (1953).
Chamberlain, J. W., Astrophys. J. **141**, 1184 (1965).
Danielson, R. E., Astrophys. J. **143**, 949 (1966).
Deirmendjian, D., Appl. Opt. **3**, 187 (1964).
Dressler, K. and Schnepp, O., J. Chem. Phys. **33**, 270 (1960).
Dunham, T., The Atmospheres of the Earth and Planets, edited by G. P. Kuiper (University of Chicago Press, Chicago, 1952), 2nd Edition, Chap. 11.
Field, G. B., Somerville, W. B., and Dressler, K., Ann. Rev. Astronomy Astrophys. **4**, 207 (1966).
Goldberg, L., Müller, E. A., and Aller, L. H., Astrophys. J. Suppl. **5**, No. 45, 1 (1960).
Harris, D. L., "Planets and Satellites," in The Solar System, edited by G. Kuiper and B. Middlehurst (University of Chicago Press, Chicago, 1961), Vol. 3, p. 272.
Kiess, C. C., Corliss, C. H., and Kiess, H. K. Astrophys. J. **132**, 221 (1960).
Kuiper, G. P., The Atmospheres of The Earth and Planets, edited by G. P. Kuiper (University of Chicago Press, Chicago, 1952), Chap. 12.
_____, Mem. Soc. Roy. Sci. Liege **9**, 365 (1964)
Lasker, B. M., Astrophys. J. **138**, 709 (1963).
Low, F., Lowell Observatory Bull. **7**, No. 128, 184 (1965).
_____, Astron. J. **71**, 391 (1965).
Lippencott, E. R., Eck, R. V., Dayhoff, M., and Sagan, C., Astrophys. J. **147**, 753 (1967).
Moore, D. and Danielson, R. E. (to be published).
Moroz, V. I., Soviet Astron.—AJ **5**, 827 (1962).
Owen, T. Astrophys. J. **141**, 444 (1965)a.
_____, Astrophys. J. **142**, 782 (1965)b.
Rank, D. H., Fink, U., and Wiggins, T. A., Astrophys. J. **143**, 980 (1966).
Reding, F. P. and Horing, D. F., J. Chem. Phys. **19**, 594 (1951).

Spinrad, H., Appl. Opt. **3**, 181 (1964).
Spinrad, H. and Trafton, L.M., Icarus **2**, 19 (1963).
Stecher, T. D., Astrophys. J. **142**, 1186 (1965).
Taylor, D. J., Icarus **4**, 362 (1965).
Thornton, D. D. and Welch, W. J., Icarus 2, 228 (1963).
Trafton, L. M., Astrophys. J. **147**, 765 (1967).
Wildey, R. L., Murray, B. C., and Westphal, J. A., J. Geophys. Res. **70**, 3711 (1965).
Wildt, R., Smith, H. J., Salpeter, E. E., and Cameron, A. G. W., Phys. Today **16**, 19 (1963).
Woolf, N. J., Schwarzschild, M., and Rose, W. K. Astrophys. J. **140**, 833 (1965).
Zabriskie, F. R. Astron. J. **67**, 168 (1962).

INDEX

Albedo,
of Venus, 183, 192
of Jupiter, 222
Alpha Orionis, see Betelgeuse
Ammonia (NH_3) in atmosphere of Jupiter, 211-223, 227-242
Angular momentum, in star formation, 133, 141-142
Arcturus, 63, 66
B stars, interstellar extinction of, 2, 6, 10
Becklin's object, 50-51
Betelgeuse (α Orionis), 10, 31, 34, 48-50, 66, 75
Bolometers, 45, 78, 103, 219
Carbon dioxide (CO_2)
collision-induced absorption by, 165-169, 173-180, 189, 192
in atmosphere of Venus, 165-170, 173-181, 187, 189, 192, 200-201
in stellar spectra, 55, 62
Carbon hydride (CH) in stellar spectra, 59-62
Carbon monoxide (CO) in stellar spectra, 29-37, 55-59, 62 66
Carbon stars, 30-38, 47
Cepheus, interstellar extinction in, 6-7
χ Cygni, 21, 28, 33, 34, 59-62, 67
Chromosphere,
solar, 77-78
stellar, 47-48
Clouds
in atmosphere of Jupiter, 237-242
in atmosphere of Venus, 183-192
interstellar, 115-117, 131-132, 141-142
Cluster diameter method, 4, 6
Collision-induced absorption
by carbon dioxide, 165-169, 173-180, 189, 192
by molecular hydrogen, 217, 223-225, 239
by nitrogen, 165-169, 175-177
Color difference method, 1-4
Color excess, 2, 5
Comet 1965f (Ikeya-Seki), 147-163
color temperatures of, 155-158
emissivity of, 156-158, 161-163
infrared emission from, 148-155
opacity of, 157-160
Cosmic background radiation, 97, 101-103
Cyanogen (CN), interstellar absorption by, 103-108
Cygnus source (NML Cygnus), 16, 27, 30, 35-38, 48-51, 70-75

Deuterium burning, 136

Electric fields, in protostars, 142-145
Emissivity
in Comet 1965f, 156-158, 161-163
of iron, 157
Extinction curves, 2-4

Fourier spectroscopy, 193-195

Germanium bolometer, 45, 78, 103, 219
Greenhouse effect, 166, 173, 180, 187

Hayashi phase, 134, 136, 143-145
Helium
in H II regions, 110-112
in atmosphere of Jupiter, 218, 227-233

H-R diagram, 46, 137
Hydrogen
  H^- opacity, 29, 47, 84, 87, 89, 135
  H I regions
    cyanogen in, 105-107
    infrared emission from, 116-127
    properties of, 115, 128
  H II regions, 116, 128
    and cyanogen, 105, 108
    infrared emission from, 109-112
  molecular (H_2),
    in interstellar clouds, 119-127
    in Jupiter, 217-219, 223-233, 239-241
    in Mira, 63-66
    in stars, 84-87, 133
    infrared spectrum of, 119-120
Hydroxyl (OH) in M stars, 36-38

I magnitudes, 14-15, 19
IC418, 110-112
Ice, in atmosphere of Venus, 183-187, 192
Ikeya-Seki, see Comet 1965f
Infrared detectors, 14, 43-45, 78-80, 93
Infrared emission
  from Comet 1965f, 148-155
  from H I regions, 116-127
  from H II regions, 109-112
  from interstellar grains, 132-133
  from interstellar shock waves, 115-129
  from planetary nebulae, 110-113
Infrared spectra
  of Jupiter, 200-205, 211-216, 220-221
  of Mars, 200, 202
  of quasars, 41, 51-53
  of stars, 22-38, 50-51, 55-75
  of Venus, 207-210
Infrared spectrometers, 23-24
Interferometers, 55, 193-197, 210
Interstellar absorption by CN, 103-108
Interstellar clouds, 115-117, 131-132, 141-142
Interstellar extinction, 1-11
Interstellar grains, 132-133
Interstellar shock waves, 115-129
Iron
  emissivity of, 157
  in Comet 1965f, 156-157

Jupiter
  atmosphere of, 211-242
    ammonia in, 211-223, 227-242
    clouds in, 237-242
    helium in, 218, 227-233
    methane in, 211-221, 227-235, 238-242
    molecular hydrogen in, 217-219, 223-233, 239-241
    opacity of, 217, 223, 225
    silicon hydride in, 227-233, 242
    water vapor in, 227-233, 237-242
  infrared albedo of, 222
  infrared spectra of, 200-205, 211-216, 220-221
  temperature of, 218-220, 223-226, 234-236, 239-242

K magnitudes, 14-16, 19
Kardashev lines, 144

Lead sulfide (PbS) detectors, 14, 23, 45, 46, 148
Limb darkening
  of sun, 77-81
  of Venus, 187, 189

INDEX

M stars
  an interstellar extinction, 6-11
  infrared spectra of, 25, 28-36, 66
Magnetic fields in interstellar clouds, 131, 141-142
Mariner II, 184, 187, 189
Mars, infrared spectra of, 200, 202
Methane (CH_4) in atmosphere of Jupiter, 211-221, 227-235, 238-242
Microwave measurements of Venus, 166-168
Mira (o Ceti), 25, 29, 33, 34, 63-69, 73, 75
Mira variables, 46, 56, 67, 73-75
μ Cephei, 6-7, 10-11

N stars, infrared spectra of, 30-34, 36, 38
Neon, in H II regions, 109-112
Nitrogen
  collision-induced absorption by, 165-169, 175-177
  in atmosphere of Venus, 165, 168-170, 173, 177-180, 189, 192
NML Cygnus, see Cygnus source
NML Taurus, see Taurus source

O stars, interstellar extinction of, 2, 6, 10
o Ceti, see Mira
Oort constant, 9
Opacity
  of atmosphere of Jupiter, 217, 223, 225
  of atmosphere of Venus, 165-170, 173-181, 189
  of Comet 1965f, 157-160
  of interstellar clouds, 133
  Rosseland mean, 166, 170, 177, 223, 232
  stellar, 83-89, 134-136
Orion, interstellar extinction in, 3, 6, 11

Perseus, interstellar extinction in, 6-8
Photometry, 14-15, 23-28, 42-46, 148
Planetary nebulae, 110-113
Polarization of light
  from M stars, 9
  from Venus, 187
Pressure broadening, see Collision-induced absorption
Protostars, 47, 131-145

Quasars, 41, 51-53

R Andromedae, 71-74
R Leonis, 56-58, 62, 75
R Monocerotis, 48, 50-51
RS Cygni, 26, 30, 34, 35, 59, 61
Rayleigh scattering, 84, 88, 89, 218
Rosseland mean opacity, 166, 170, 177, 223, 232
Rotational temperature of cyanogen, 103-108

S stars, infrared spectra of, 30-34
Shock waves in interstellar matter, 115, 116
Silicon detectors, 14
Silicon hydride (SiH_4), in atmosphere of Jupiter, 227-233, 242
Star clusters, interstellar extinction in, 5-6
Steady state theory of universe, 101
Stellar
  chromospheres, 47-48
  evolution, 136-140
  model atmospheres, 83-89
  opacity, 83-89, 134-136
  spectra, 22-38, 50-51, 55-75
Stratoscope II, 22, 29, 83, 86, 211, 221

Sun
chromosphere of, 77-78
limb darkening of, 77-81
photosphere of, 78, 81
Swan bands, 31
Synchrotron emission, 48

T Lyrae, 59, 61
T Tauri, 50-51
Taurus source (NML Taurus), 16, 26, 27, 30, 35-36, 46, 50, 67-73
3C273, 41, 51-53
Threshold of energy stability, 134, 136
Titanium oxide (TiO)
in model stellar atmospheres, 86
in stellar spectra, 67-72

U Hydrae, 28, 31, 32
UU Aurigae, 59, 61

Vanadium oxide (VO) in stellar spectra, 68-72
Variable extinction method, 4-6
Venus
atmosphere of, 165-171, 173-180, 183-192
carbon dioxide in, 165-170, 173-181, 187, 189, 192, 200-201
clouds in, 183-192
collision-induced absorption in, 165-169, 173-180, 189, 192
ice in, 183-187, 192
nitrogen in, 165, 168-170, 173, 177-180, 189, 192
opacity of, 165-170, 173-181, 189
pressure in, 168, 180, 186, 189-192
water vapor in, 166, 173, 177, 180, 186-189, 191-192
greenhouse effect on, 166, 173, 180, 187
infrared albedo of, 183, 192
infrared spectra of, 207-209
limb darkening of, 187, 189
microwave measurements of, 166-168, 186
temperatures, 166-167, 173-180, 186-190

Water vapor
in atmosphere of Jupiter, 227-233, 237, 242
in atmosphere of Venus, 166, 173, 177, 180, 186-189, 191-192
in Mira, 64, 66, 68
in stellar spectra, 10, 28, 30-36, 55-58, 62, 69, 86-87
in terrestrial atmosphere, 101-103
WZ Cassiopeiae, 26, 30, 31, 34, 35

Y Canum Venaticorum, 26, 28, 31, 32

ζ Ophiuchi, 104-107
Zodiacal light, 91, 99, 163

Brancazio
Cameron

Infrared Astronomy

RECOMMENDED BOOKS

NUCLEOSYNTHESIS

W. D. Arnett, C. J. Hansen, J. W. Truran, and A. G. W. Cameron, editors (1158) 288 pp.

Proceedings of a conference held at the Institute for Space Studies, Goddard Flight Center, NASA, 1965. The seventh in a continuing series of inter-disciplinary meetings on topics in space physics.

CONTENTS: Difficulties with Theories of Nucleosynthesis in Stars. Observational Evidence Concerning Nucleosynthesis. Observations of Abundance Anomalies in Magnetic Stars. Comments on Peculiar A Stars. Abundances in Metallic-Line Stars. On Scandium Production. Thermonuclear Reaction Rates: On the Nucleosynthesis of the S and P Elements. Current Research at Orsay on the Nuclear Formation Cross-Section of Lithium, Beryllium and Boron. Stellar Evolution through Helium Burning. Evolution of a Star of 30 Solar Masses. The Evolutionary State of Peculiar A Stars. The Approach to Supernova Implosion Conditions. Statistical Properties of Nuclei. The Approach to Nuclear Statistical Equilibrium. Equilibrium Composition of Matter at High Densities. The Nuclear Synthesis Conditions of Types I and II Supernovae. Hydrodynamic Implosion Calculations. Neutron Capture Cross Section Measurements. Neutron Cross Section Measurements with Nuclear Devices. Distribution of Neutron-Source Strengths for the s-Process. Calculation of r-Process Abundances. Summary and Impressions. Recent Experiments on Multiple Neutron Capture. Models of Carbon Burning Stars.

INTRODUCTION TO SPACE SCIENCE (Second revised and enlarged edition)

**Written by the staff of the Goddard Space Flight Center, NASA.
Wilmot N. Hess and Gilbert Mead, editors (0145) 1046 pp.**

In view of rapid developments in space science, this second edition contains substantial revisions and additions in the chapters on Ionosphere, Meteorology from Space, the Interplanetary Medium, the Boundary of the Magnetosphere, Interplanetary Dust Particles, Cosmic Chemistry, the Moon, Planetary Atmospheres, Stellar Evolution, and Extragalactic Radio Sources. The chapters on the Shape of the Earth, Man in Space, the Sun, Space Astronomy, and Nucleogenesis have been completely rewritten.

CONTENTS: Part I The Earth and Its Environment: The Earth's Magnetic Field. The Earth's Atmosphere. The Ionosphere. The Earth's Radiation Belt. The Aurora. Meteorology from Space. The Shape of the Earth. Part II Space: The Interplanetary Medium. The Boundary of the Magnetosphere. Cosmic Rays. Interplanetary Dust Particles. Cosmic Chemistry. Orbital Mechanics. Man in Space. Part III The Solar System and Beyond: Origin of the Solar System. The Physics of the Sun. The Moon. Planetary Atmospheres. Planetary Structure. Space Astronomy. Stellar Evolution. Extragalactic Radio Sources. Nucleosynthesis. Author Indexes and Subject Indexes.

**GORDON AND BREACH, SCIENCE PUBLISHERS, INC.
150 Fifth Avenue, New York, N.Y. 10011**

523.
015
012
INF
G|B